PROVENANCE OF GARNET IN THE NEOARCHEAN VERBAARD GRANITOID GNEISS: COMPLEXITY OF CHARACTERIZING GRANITOIDS IN HIGH-GRADE TERRANES

by

THEMBISO OTLADISANG BASUPI

Reg. No: BT14100012

BSc (Geology)

Department Earth and Environmental Sciences,

Faculty of Sciences,

Botswana International University of Science and Technology

basupit@biust.ac.bw, (+267) 72238879

A Thesis Submitted to the Faculty of Sciences in Partial Fulfilment of the Requirements for the Award of the Degree of Master of Science in Geology of BIUST

Supervisor: Professor Rajesh Hariharan

Department of Earth and Environmental Sciences,

Faculty of Sciences, BIUST

rajesh.hm@biust.ac.bw, (+267) 73626281

Signature: _____ Date: 10/10/2018

October, 2018

DECLARATION AND COPYRIGHT

I, Thembiso Otladisang Basupi, declare that this thesis is my own original work and that it has not been presented and will not be presented to any other university for a similar or any other degree award.

Signature.....

This thesis is copyright material protected under the Berne Convention, the Copyright Act of 1999 and other international and national enactments, in that behalf, on intellectual property. It must not be reproduced by any means, in full or in part, except for short extracts in fair dealing; for researcher private study, critical scholarly review or discourse with an acknowledgement, without the written permission of the office of the Provost, on behalf of both the author and the BIUST.

CERTIFICATION

The undersigned certifies that he has read and hereby recommends for acceptance by the Faculty of Sciences a dissertation/thesis titled: Provenance of garnet in the Neoarchean Verbaard granitoid gneiss: Complexity of characterizing granitoids in high-grade terranes, in fulfilment of the requirements for the degree of Master of Science in Geology of the BIUST.

.....

Prof. Rajesh Hariharan

Date: 10/10/2018

Acknowledgements

A special thanks to my supervisor Prof. H. M. Rajesh for offering academic guidance throughout the research period, and also for the patience and support throughout most challenging times of this project. It is simply the help that changed my whole life completely.

I gratefully acknowledge the financial support provided by BIUST throughout the research.

The two examiners provided encouraging, thoughtful and critical comments which helped in producing the present version of the thesis.

Dr. Georgy Belyanin of the University of Johannesburg, South Africa, is thanked for his collaboration in assisting with EPMA-SEM mineral chemical analyses.

Mpho Keeditse, Thuto Mokatse and Jacob Kaavera, are thanked for their company, helpful advices and discussions during the series of field works, as part of the study.

Lastly I thank my family, particularly my lovely wife for being my source of strength, and believing in me, you are the reason I am kept propelled even in the most difficult times.

TABLE OF CONTENTS

Declaration and copyright i
Certification ii
Acknowledgements iii
Table of contents iv
Abstract vi

Chapter 1 Introduction, geologic setting and objectives
1.1. Introduction – significance of Neoarchean granitoid magmatism 1
1.2. Complexity of characterizing granitoids in Archean high-grade terranes 3
1.3. Geologic setting 10
1.3.1. General characteristics of Neoarchean granitoids in the Central Zone 12
1.3.2. Study area 17
1.4. Objectives and approach 19
1.5. Sampling and analytical methods 21
1.6. Outline of the thesis 22

Chapter 2 Field relations
2.1. Introduction 24
2.2. Rock types 26
2.3. Metapelite 29
2.4. Garnet-bearing leucocratic bodies associated with gabbro 33
2.5. Verbaard granitoid 36
2.6. Relative chronology of the rocks 41

Chapter 3 Petrographic characteristics
3.1. Introduction 43
3.2. Metapelite 43
3.2.1. High-Al metapelite and associated leucosomes 44
3.2.2. Low-Al metapelite and associated leucosomes 55
3.3. Verbaard granitoid 62
3.4. Gabbro 75
3.5. Meta-ironstone 76

Chapter 4 Mineral chemical characteristics
4.1. Introduction 78
4.2. Garnet 78
4.3. Biotite 86
4.4. Feldspars 89
4.5. Cordierite and sillimanite 90

Chapter 5 Whole-rock geochemical characteristics
5.1. Introduction 96
5.2. Major element characteristics 96
5.3. Trace and rare earth element characteristics 102

Chapter 6 Discussion
6.1. Introduction 109
6.2. Are the two groups of metapelites an artefact of the extent of partial melting? 109
6.3. Timing of high-grade event(s) and related melting of the metapelites 113
6.4. Compositional variation of garnet in metapelites 117
6.5. Provenance of garnet in the Verbaard granitoid 122
6.6. Petrogenetic characterization of the Neoarchean Verbaard granitoid 126

Chapter 7 Concluding remarks 136

REFERENCES 140

APPENDIX 157

Abstract

Neoarchean granitoids are commonly exposed along Archean high-grade metamorphic terranes, where they occur as granitoid gneisses. A number of issues, including the effect of overprint event(s), can complicate the characterization of these granitoids in Archean terranes. A case study is presented here highlighting the complexity of characterizing Neoarchean granitoid magmatism from the Limpopo Complex high-grade terrane in southern Africa. Neoarchean granitoids occurring within the Central Zone of the Limpopo Complex include the ~2.73-2.64 Ga biotite±amphibole-bearing Alldays granitoid, the ~2.68-2.62 Ga garnet-bearing Singelele leucogranite, the ~2.65-2.63 Ga Avoca granitoid with pyroxene-bearing and pyroxene-absent variants, the ~2.65-2.62 Ga biotite-bearing Verbaard granitoid and the ~2.61-2.58 Ga Bulai granitoid with pyroxene-bearing and pyroxene-absent variants. Of the different granitoids, the Singelele leucogranite and Verbaard granitoid exhibit evidence for anatectic overprint. This study focuses on characterizing the nature of overprint in the Verbaard granitoid. Exposures in the Verbaard area show a conspicuous network of garnet-bearing leucocratic veins overprinting the light greyish biotite-bearing Verbaard granitoid. These leucocratic veins, with more or less straight line outline, do not have any biotite-bearing melanocratic margins, indicating that they formed elsewhere. On the other hand, the garnet-bearing irregular outline leucosomes associated with surrounding metapelites have biotite-bearing melanocratic margins indicating *in situ* formation by partial melting. Detailed mineral chemical characteristics of garnet occurring in the metapelite, associated leucosome, and the Verbaard granitoid, indicate comparable composition,

suggesting common origin. It is argued that the garnet in leucocratic veins overprinting the Verbaard granitoid represent relics from the metapelites, with the leucocratic veins representing segregated melt away from the source region. Of the two types of metapelites found in the study area – high-Al and low-Al metapelites – the distinction between the two is suggested as an artifact of the extent of partial melting, with the high-Al metapelite preserving more of the restitic domains, while the low-Al metapelite preserving more of the leucosomic material. Using rim-core-rim garnet mineral chemical profiles, the leucosomes are suggested as sites of preservation of different stages of garnet formation in the associated metapelites.

Whole-rock geochemical characteristics of carefully sampled garnet-free domains of the Verbaard granitoid indicate that they are similar to low-HREE Archean TTGs. Comparison with experimental melts from a variety of source rocks indicates that the Verbaard granitoid was likely derived from the melting of metabasalts. A comparative exercise with other Neoarchean granitoids from the Central Zone indicates that the compositional characteristics of the Verbaard granitoid are closely comparable to those of the Alldays granitoid. It is suggested that the Verbaard granitoid represents the manifestation of the Alldays granitoid magmatism in the Verbaard area.

Chapter 1

Introduction, geologic setting and objectives

1.1. Introduction – significance of Neoarchean granitoid magmatism

With the Neoarchean (2.8-2.6 Ga) period characterizing a peak in granitoid magmatism (Fig. 1.1; Condie and Aster, 2010) and the transition from commonly gneissic Na-rich granitoids (tonalite-trondhjemite-granodiorites or TTGs; Barker and Arth, 1976; Martin et al., 1983) to relatively undeformed K-rich granitoids (granite-granodiorite-monzogranites or GGMs; Sylvester, 1994; Kemp and Hawkesworth, 2003), the granitoid variants that form part of the Neoarchean felsic crust has been the subject of detailed studies from different Archean terranes (Feng and Kerrich, 1992; Sage et al., 1996; Champion and Smithies, 2003; Kampunzu et al., 2003; Moyen et al., 2003; Whalen et al., 2004; Frost et al., 2006; Jayananda et al., 2006; Shang et al., 2007; Almeida et al., 2010; Huang et al., 2010; Mikkola et al., 2011; Feio et al., 2013; Dey et al., 2014; Jiang et al., 2016; Dall'Agnol et al., 2017; Moreno et al., 2017; Regan et al., 2017). In general, there seems to be a greater proportion of Na-rich granitoids relative to K-rich granitoids in most Archean terranes, with the Neoarchean TTGs seemingly having a different composition compared with their Paleo- and Mesoarchean counterparts (see reviews in Kemp and Hawkesworth, 2003; Condie, 2005; Martin et al., 2005; Laurent et al., 2014; Halla et al., 2017). Among the unique granitoid variants that became relatively prominent in the Neoarchean include the Archean sanukitoids with geochemical characteristics of both Na-rich and K-rich granitoids (Shirey and Hanson, 1984; Stern and Hanson, 1991; Jayananda et al., 1995; Stevenson et al., 1999; Bibikova et al., 2005;

Lobach-Zhuchenko et al., 2008; Halla et al., 2009; Wang et al., 2009; Heilimo et al., 2010; Martin et al., 2010), pyroxene-bearing granitoids (charnockites) (Bohlender et al., 1992; Berger et al., 1995; Frost et al., 2000; Percival and Mortensen, 2002; Laurent et al., 2011; Rajesh, 2012; Milidragovic and Francis, 2014; Bai et al., 2015), and peraluminous leucogranites (Day and Weiblen, 1986; Davis et al., 1994; Champion and Sheraton, 1997; Manya et al., 2007; Vijaya Kumar et al., 2011; Dey et al., 2012; Mikkola et al., 2012; Farina et al., 2015; Frost et al., 2016).

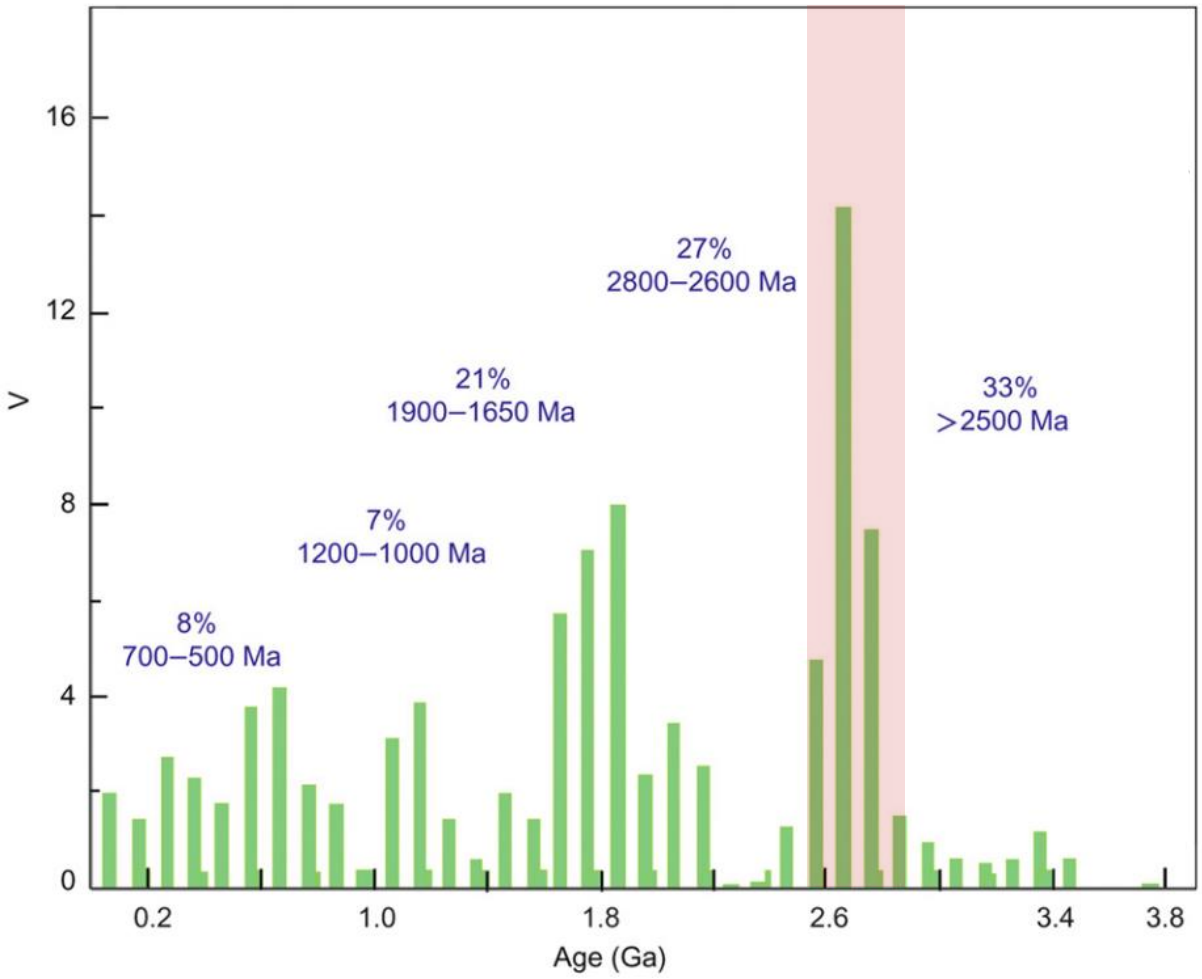


Figure 1.1. Frequency distribution of juvenile continental crust with time in bins of 50 Ma. A major peak in granitoid magmatism occurs in the Neoarchean period (highlighted) [from Condie and Aster (2010)].

While the association of TTGs and sanukitoids are commonly attributed to formation in a subduction setting (Martin et al., 2010; Rapp et al., 2010; Halla et al., 2009; Laurent et al., 2014), K-rich variants such as peraluminous leucogranites arguably provide the least ambiguous examples of granitic rocks generated from remelting of pre-existing crustal rocks, likely in a collision setting (England and Thompson, 1986; Sylvester, 1994; Patiño Douce, 1999; Kemp and Hawkesworth, 2003; Watkins et al., 2007). Although the general nature of the transition from Na-rich to K-rich granitoid magmatism and its likely tectonic expression have been quite well understood now, it has quite different characteristics and absolute durations in different Archean terranes (see reviews in Kemp and Hawkesworth, 2003; Condie et al., 2009; Laurent et al., 2014; Halla et al., 2017). So it is likely that, in detail, it might be more complicated especially if smaller time scales are considered. Archean high-grade terranes are characterized by voluminous and diverse granitoid magmatism in relatively short time spans, and are good candidates to investigate the variants that characterize the Neoarchean granitoid magmatism. However, a number of issues can complicate the characterization of granitoids occurring in Archean high-grade terranes.

1.2. Complexity of characterizing granitoids in Archean high-grade terranes

Before considering the effect of overprint event(s) on granitoids occurring in Archean high-grade terranes, an important aspect, which is often overlooked, is identifying the distribution or extent of individual granitoids. Often it is difficult to map the extent of individual granitoid variants in a given Archean high-grade terrane, as the different granitoids, which formed one after the other, occur interlayered with older supracrustal

rocks (e.g., Fig. 1.2), with both the voluminous and less voluminous ones characterized by their wide distribution (widespread nature) rather than forming single continuous plutons. Thus in a given area within a high-grade terrane the granitoid variants can be tonalite-trondhjemites, tonalite-granodorites or granodiorite-monzogranites, with the Na-rich ones having *TTG-like* composition. But if considered together with occurrences of similar age from other areas of the same high-grade terrane, TTG *sensu stricto* compositions emerge. In such cases, whole-rock geochemistry can be a useful tool to characterize the different granitoid variants.

Overprint event(s) are to be expected in high-grade terranes. Typically granitoids in Archean high-grade terranes are gneissic (e.g., Fig. 1.3a). In less common instances, they can preserve a linear fabric (e.g., Fig. 1.3b) or both. Another conspicuous feature of granitoids occurring in high-grade terranes is migmatitic overprint (e.g., Fig. 1.4a). As is typical of partial melting, the newly formed melt segregates resulting in deformation (e.g., Fig. 1.4b). As the felsic melt moves away from the source region, they can form network of crisscrossing leucocratic/leucogranitic veins in the nearby granitoids (e.g., Fig. 1.5). Peritectic minerals like garnet, related to the melting event or relics from the source rock, can occur in these leucocratic veins (e.g., Fig. 1.5a). When dealing with less volume melts, especially if the overprinting leucocratic veins contain anhydrous minerals like pyroxene (e.g., Fig. 1.5b), the possibility of fluid-related metasomatism should also be considered. Characterization of granitoids showing effects of such overprint event(s) need to be careful, as the newly formed/relic minerals (e.g., garnet, pyroxene) can end up occurring *locally* in the host granitoid.



Figure 1.2. Field photographs illustrating the common occurrence of granitoids in Archean high-grade terranes as bodies interlayered with older supracrustal rocks **(a, b)**. [This and other field images used in this chapter are from the Central Zone of the Limpopo Complex, a typical Archean high-grade terrane. All the field images in this chapter were obtained from the collection of various researchers working in the Limpopo Complex and (originally) based at the University of Johannesburg]

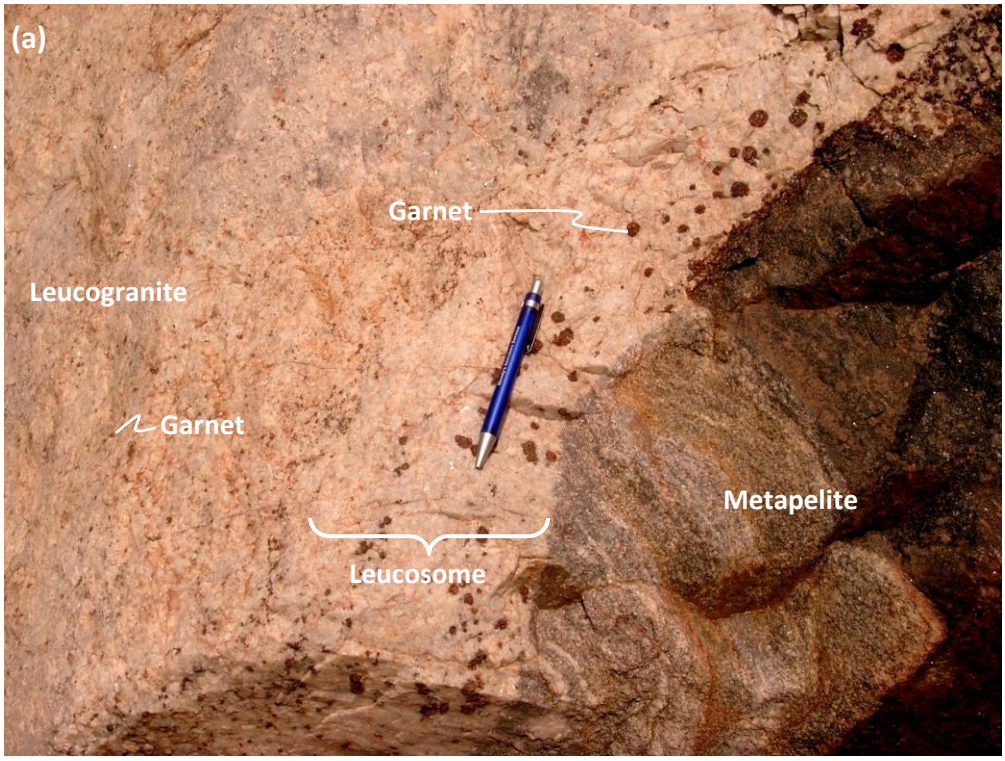




Figure 1.3. Granitoids in Archean high-grade terranes are typically gneissic **(a)**, with less common preservation of a linear fabric **(b)**.



Figure 1.4. Migmatitic overprint **(a, b)** is typical of granitoids occurring in Archean high-grade terranes, with segregation of melt often leading to deformational structures.



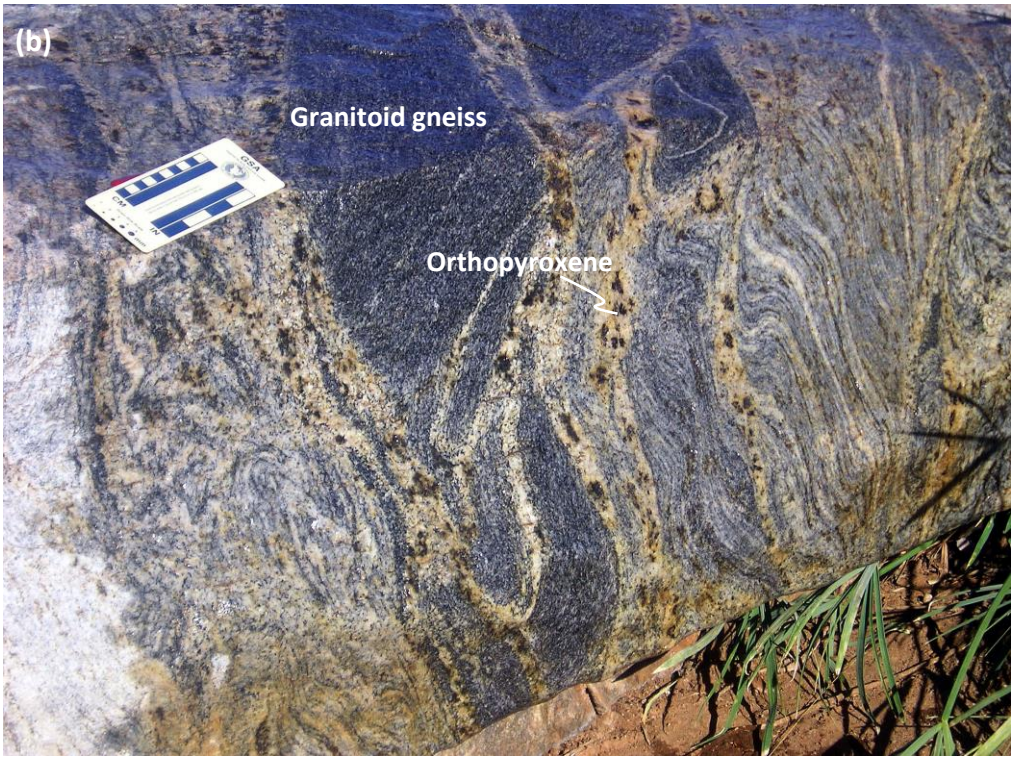


Figure 1.5. Often leucocratic veins related to partial melting and/or fluid-related metasomatism can end up overprinting nearby/associated granitoids in Archean high-grade terranes. **(a)** Garnet-bearing leucosome overprinting an earlier garnet-bearing leucogranite. The garnets in the leucosome are coarser. **(b)** Orthopyroxene-bearing leucocratic/leucogranitic veins overprinting the fabric of the earlier granitoid gneiss.

Such *assimilation* is not just related to overprint events, but can occur in regions of granitoid closer to supracrustal inclusions. In such instances, detailed field mapping is important. For e.g., as shown in Fig. 1.6, garnet only occurs in the particular granitoid within about ~2 m from the enclosed metapelite inclusion, indicating that it was assimilated from the latter. When the terrane is affected by multiple high-grade events, the granitoid can preserve effects of it, in which case the compositional characterization need to be carefully carried out together with mineral chemical data. The present study presents an example of complexity involved in characterizing Neoarchean granitoids occurring in a polymetamorphic terrane – the Limpopo Complex.



Figure 1.6. Garnet occurring in a biotite-bearing granitoid gneiss. Here the garnet only occurs in the granitoid within about ~2 m from enclosed metapelite inclusion, indicating that it was assimilated from the latter.

1.3. Geologic setting

The Palaeoarchaean to Palaeoproterozoic Limpopo Complex is a high-grade (amphibolite- to granulite-facies) metamorphic terrane occurring between the Archean Kaapvaal and Zimbabwe cratons (Fig. 1.7a). It is subdivided into three zones – the Southern Marginal Zone occurring along the northern margin of the Kaapvaal Craton, the Central Zone occupying the central and largest area of the complex, and the Northern Marginal Zone occurring along the southern margin of the Zimbabwe Craton. The three zones are separated from one another and also from the adjacent cratons by kilometre-scale shear/thrust zones (Fig. 1.7a; see reviews in Blenkinsop, 2011; Smit et al., 2011; Van Reenen et al., 2011).

The Central Zone is comprised of a variety of deformed supracrustal rocks (Beit Bridge Complex, with detrital zircons of >3.8 Ga) and minor mafic to ultramafic rocks (~3.35 Ga Messina layered intrusion), which are tectonically interleaved within voluminous granitoid orthogneisses (~3·31-3·28 Ga migmatitic Sand River tonalite-trondhjemite-granodiorite gneisses, and various ~2·73-2·57 Ga granitoid gneisses) (see reviews in Smit et al., 2011; Kramers et al., 2011).

Available structural, metamorphic and geochronological data from different parts of the Central Zone are interpreted to indicate the prominence of two high-grade tectono-metamorphic events, at ~2.72 to 2.61 Ga and ~2.04 to 2.01 Ga, with the Neoarchaean tectono-metamorphic event correlated with the intrusion of voluminous granitoids, while the Palaeoproterozoic tectono-metamorphic event is related to the anatectic intrusions, granitic pegmatites and reactivation along shear zones (Van Reenen et al., 2004, 2008;

Holzer et al., 1998; Kröner et al., 1999; Perchuk et al., 2008; Zeh et al., 2007, 2010; Gerdes and Zeh, 2009). The Palaeoproterozoic event also incorporates metasomatic overprinting (e.g., Rajesh et al., 2014).

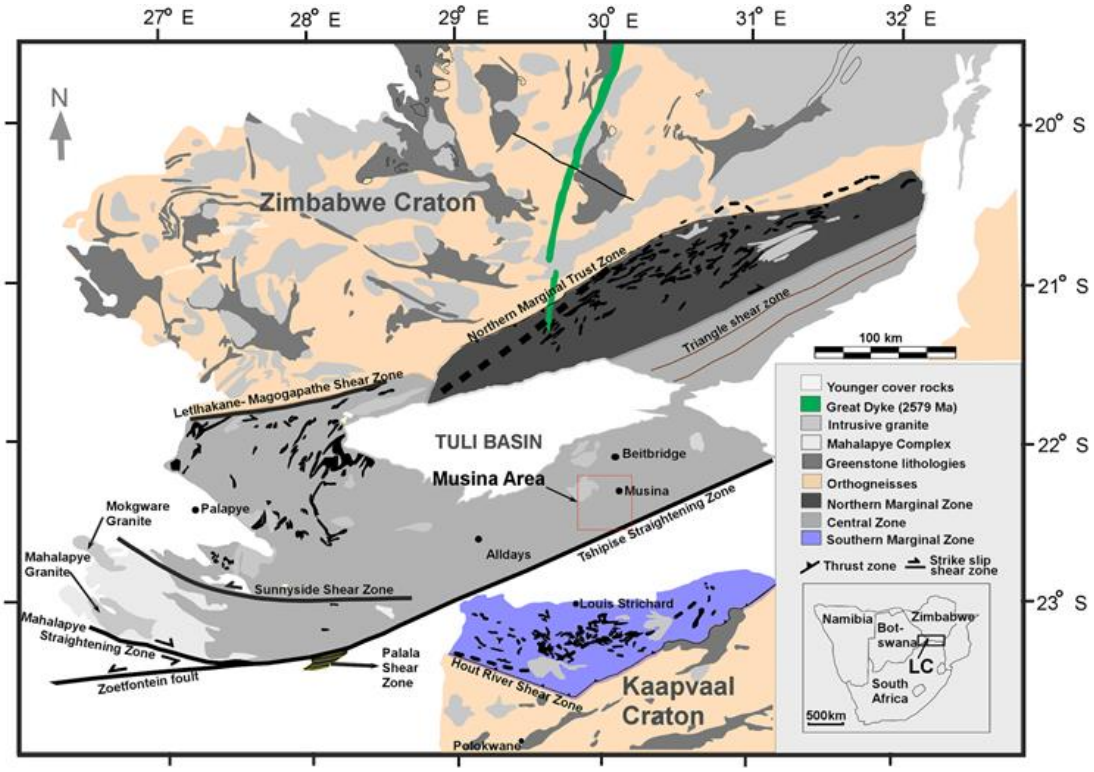


Figure 1.7. (a) Generalized geological map of the Limpopo Complex showing the three zones and adjacent Archean cratons (from Boshoff et al., 2006). The present study area occurs SW of Musina.

In terms of the metamorphic P-T conditions attained, the Neoarchaean metamorphic event reached conditions of ~860 to 900°C and ~8 to 9 kbar (Millonig et al., 2008; Perchuk et al., 2008; Smit et al., 2011); few studies also reported local attainment of ultra-high temperature metamorphic conditions (~1000°C and ~10 kbar) during the Neoarchaean (Tsunogae and Van Reenen, 2006, 2011; Smit et al., 2011; Belyanin et al., 2012) (Fig. 1.7b). The Palaeoproterozoic event is characterized by P-T conditions reaching up to ~800°C and ~5 to 6 kbar around the Messina (now Musina) area (Smit et al., 2011), while P-T conditions of

~680 to 770°C and ~6.5 to 8 kbar are reported from the Venetia-Alldays areas (Zeh et al., 2005; Chudy et al., 2008; Rigby et al., 2008) (Fig. 1.7b).

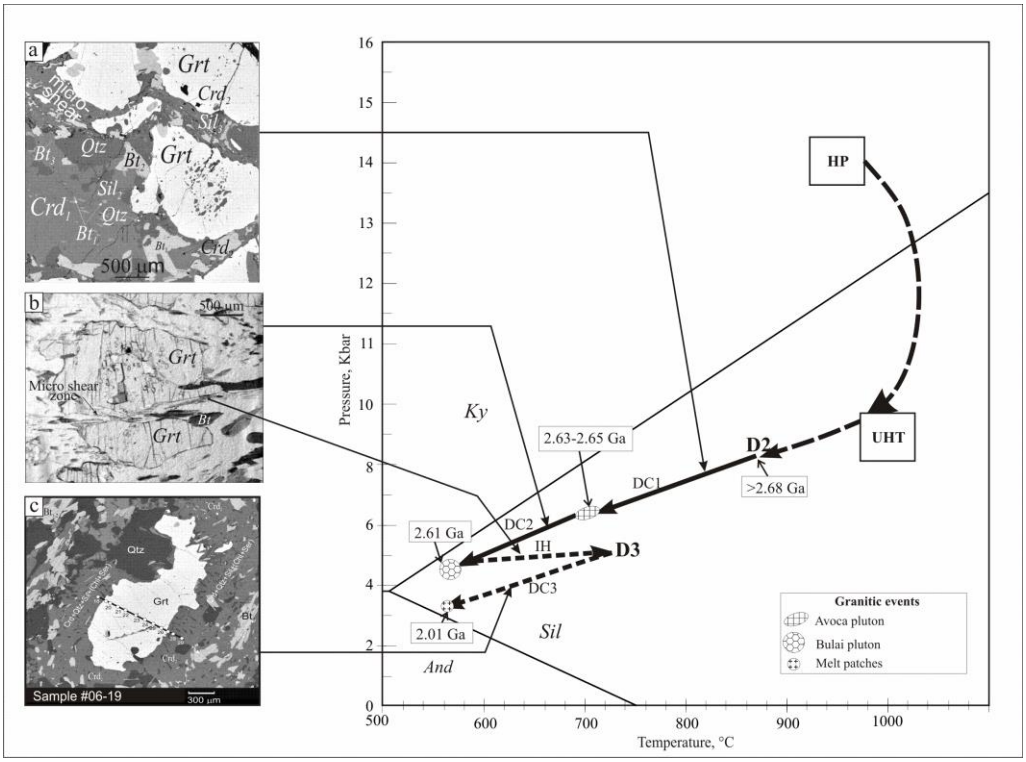


Figure 1.7. (b) D-P-T-t digram that summarizes the currently known Neoarchean-Paleoproterozoic evolution of the Central Zone [from Smit et al. (2011)]. The early (more than 2.68 Ga) high-pressure (HP) and ultrahigh temperature (UHT) events are taken from Tsunogae and Van Reenen (2006). The post-oeak DC1-DC2-IH-DC3 evolution in the interaval ca. 2.68-2 Ga is from Smit et al. (2011). (a) to (c) indicate representative phototmicrographs characteristic of mineral assemblages from different stages of metamorphism. DC – decompression cooling; IH – isobaric heating.

1.3.1. General characteristics of Neoarchean granitoids in the Central Zone

The oldest granitoid in the Musina area, where the present study area (Verbaad section) occurs, is the dark to light grey biotite-amphibole-bearing Sand River granitoid gneiss (Fig. 1.8a), well exposed along the pavements of the Sand River. It is well-banded, migmatitic and contain inclusions of the Beit Bridge Group supracrustal rocks and rocks of the Messina layered intrusion (Fig. 1.8b; Fripp, 1983). Compositionally, it includes dominant tonalites,

and lesser trondhjemites and granodiorites. U-Pb zircon geochronologic studies indicate a crystallization age of ~3.31-3.27 Ga for the Sand River gneiss (Retief et al., 1990; Tsunogae and Yurimoto, 1995; Jaeckel et al., 1997; Kröner et al., 1998, 1999; Zeh et al., 2007; Gerdes and Zeh, 2009; Zeh et al., 2010). A minor leucocratic granitoid gneiss with distinct centimeter-scale layering (termed Dorothy gneiss) occur interlayered with the Sand River gneiss (Hofmaan et al., 1998), and has a U-Pb zircon age of ~3.24 Ga (Kröner et al., 1998).

The oldest reported Neoarchean granitoid is the well-foliated (Fig. 1.8c) and locally layered greyish biotite±amphibole-bearing Alldays granitoid (Brandl, 2002). Compositionally, it include tonalites and granodiorites and to a lesser extent trondhjemites. The Alldays granitoid contains inclusions of older supracrustals (Fig. 1.8d) and rocks of the Messina layered intrusion, and is widely distributed within the Central Zone. It locally contains small grains of assimilated garnet, up to 2 metres from the contact of garnet-bearing supracrustal inclusions such as metapelite (Brandl, 2002). Available U-Pb zircon ages on the Alldays granitoid vary between ~2.73 and 2.64 Ga (2734 ± 4 Ma, 2637 ± 3 Ma: Jaeckel et al., 1997; Kröner et al., 1999).

The garnet-bearing Singelele leucogranite (Söhnge, 1946; Bahnemann, 1973; Fripp et al., 1979) constitutes a long lived Neoarchean magmatic event [~2.68-2.62 Ga; 2681 ± 8 Ma, 2620 ± 8 Ma (U-Pb zircon): Kröner et al., 1999; 2647 ± 12 Ma (U-Pb zircon): Zeh et al., 2007; 2627±3 Ma (U-Pb monazite): Van Reenen et al., 2008]. They are non-layered and exhibit weak foliation (Fig. 1.8e). Like the Alldays granitoid, the Singelele leucogranite contain inclusions of the supracrustal rocks (Fig. 1.8f) and rocks of the Messina layered intrusion, and

is widely distributed within the Central Zone. Unlike the Alldays granitioid, garnet is a rock-forming mineral and is uniformly distributed within the Singelele leucogranite. Application of Pb-Pb step-wise leaching method on garnet from the Singelele leucogranite gave a less precise age of 2602±53 Ma, interpreted to reflect the time of crystallisation of the igneous garnet (Boshoff et al., 2006; Van Reenen et al., 2008). A second-generation garnet-bearing leucosome overprints the Singelele leucogranite locally. Significantly, the garnet grains are coarser in the anatectic overprinted portions compared to the garnet in the leucogranite.

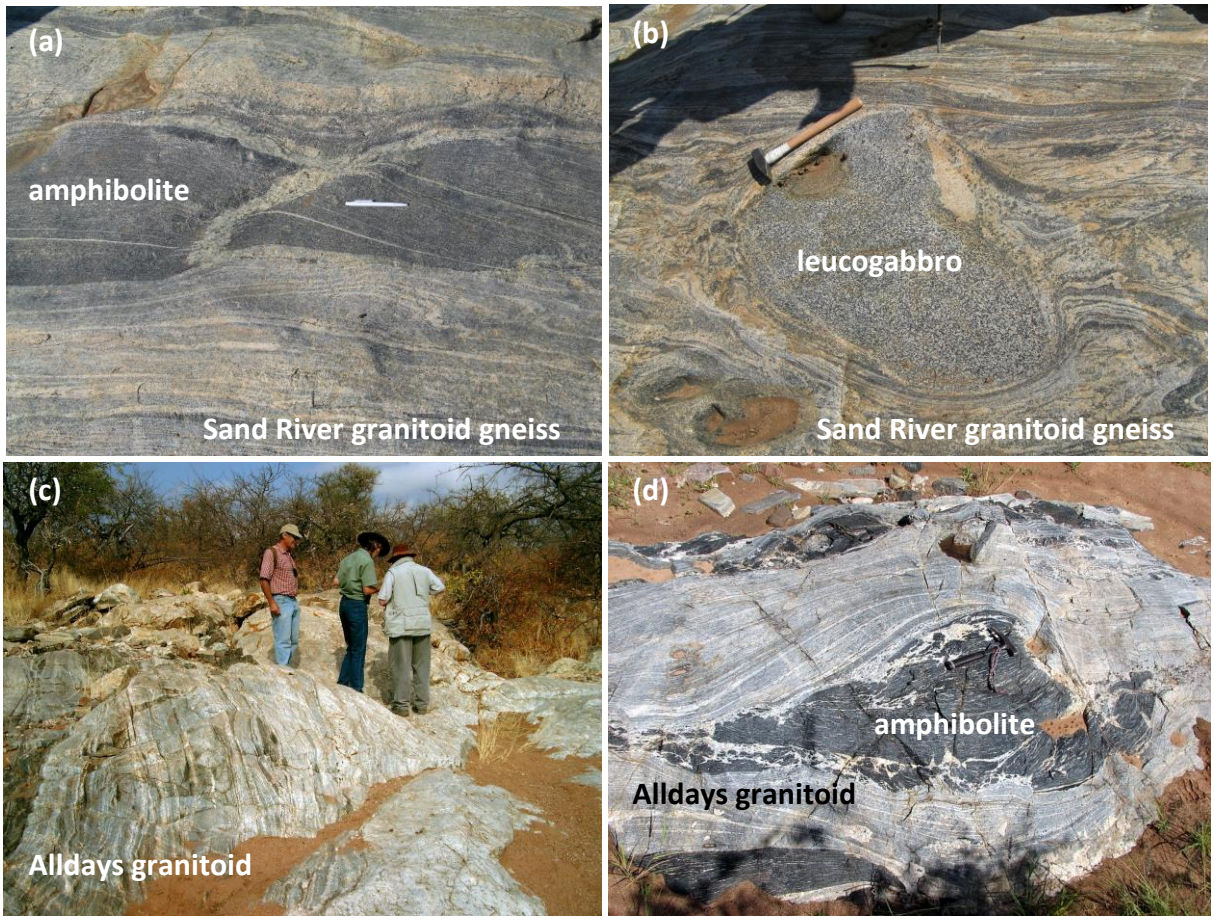


Figure 1.8. Representative field photographs illustrating the mode of occurrence of prominent granitoids in the Central Zone of the Limpopo Complex. **(a, b)** Mesoarchean Sand River granitoid gneiss with inclusions (xenoliths) of earlier mafic rocks, **(c, d)** Neoarchean Alldays granitoid. Inclusion of amphibolite is shown in (d). Hammer for scale in (d) can found to the top corner of the inclusion.

The smallest of the Neoarchean granitoids, the ~2.65-2.63 Ga Avoca granitoid occurs as a ring structure towards the northwestern margin of the Central Zone (Boshoff, 2004; Van Reenen et al., 2008). In spite of its smaller size, the Avoca granitoid preserves a wide compositional spectrum from a pyroxene-bearing TTG core (Fig. 1.8g) to a pyroxene-absent granite rim (Fig. 1.8h). U-Pb zircon geochronological results indicate an age of ~2.63 Ga (2627±5 Ma) for the TTG in the core, while the granite rim has a U-Pb zircon age of ~2.65 Ga (2651±8 Ma) (Boshoff, 2004; Van Reenen et al., 2008). While both the core and rim rocks exhibit a linear fabric, the granite in addition preserves a penetrative foliation, and local occurrence of two-pyroxene-bearing metabasite intercalations and boudins (Fig. 1.8h). The Avoca granitoid intrudes into the Alldays granitoid, which retains no evidence for linear features observed in the Avoca rocks.

Although of similar age to the Avoca granitoid, the ~2.65-2.62 Ga Verbaad granitoid (Jaeckel et al., 1997), the focus of the present study and occurring in the southern portion of the Central Zone, have quite different characteristics. The Verbaad granitoid reported by Jaeckel et al. (1997) at localities exposed along the Sand River southeast and southwest of Musina is a suite of homogenous botite-bearing tonalitic and granodioritic gneiss with a foliation but no compositional layering (see chapter 2 for detailed field images). They often occur interlayered and infolded with the Sand River granitoid gneiss, and locally cut its lithological layering (Jaeckel et al., 1997; Hofmann et al., 1998). An important feature of the Verbaard granitoid is the conspicuous occurrence of a network of garnet-bearing leucocratic veins overprinting the granitoid (see chapter 2 for detailed field images).



Figure 1.8. (continued) , **(e, f)** Neoarchean Singelele leucogranite**, (g, h)** Neoarchean Avoca granitoid, and **(I, j)** Neoarchean Bulai granitoid.

The largest of the Neoarchean granitoids, the ~2.61 to 2.58 Ga Bulai granitoid, is a composite plutonic body consisting of an earlier pyroxene-bearing granitoid and a latter

pyroxene-absent granitoid (Figs. 1.8i, j), towards the northern margin of the Central Zone [Watkeys et al., 1983; 2605±2 Ma, 2572±4 Ma (U-Pb zircon): Barton et al., 1994; Holzer, 1995; 2587.1±0.4 Ma (U-Pb zircon): Kröner et al., 1999; 2612±7 Ma (U-Pb zircon): Zeh et al., 2007; 2606±24 Ma, 2593±17 Ma (U-Pb zircon): Laurent et al., 2011]. The Bulai granitoid contains abundant inclusions of the earlier rocks, including metapelitic Beit Bridge Group rocks and the Singelele leucogranite, the latter containing lenses of the metapelite, indicating that the Singelele leucogranite is earlier than the Bulai granitioid.

1.3.2. Study area

The study of Jaeckel et al. (1997) reported ages (~2.65-2.62 Ga) on a *new variety* of Neoarchean granitoid within the Central Zone and named it the Verbaard granitoid based on the type locality within the Verbaard farm (Verbaard area in Fig. 1.9). Hofmann et al. (1998), which is primarily a field mapping study, reported that the Verbaard granitoid is well exposed within and around the Verbaard farm along the Sand River pavement (Fig. 1.9). After carrying out a preliminary field survey, a well exposed area along the Sand River pavement, within the extents of the Verbaard farm, 10 km SW of Musina town, was selected as the main study area (Fig. 1.9). To characterize the relation of the Verbaard granitoid to the surrounding rock (metapelite), samples from a petrologically and geochronologically well characterized metapelite outcrop (referred as O6-19; Boshoff, 2008; Perchuk et al., 2008; Van Reenen et al., 2008), to the northeast of the Verbaard area was also included as part of the present study. Thus the study area (Fig. 1.9) involves two components – the Verbaard area and the O6-19 outcrop (see Fig. 2.1 in chapter 2 for details).

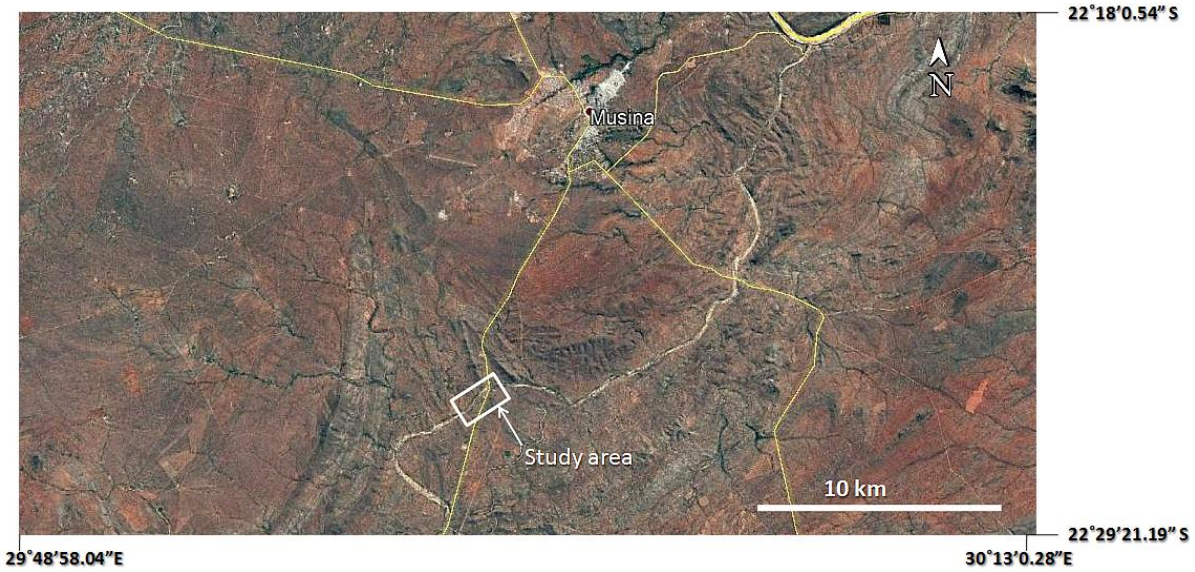


Figure 1.9. Google satellite image showing the location of the study area with respect to the Musina area. Study area involves the Verbaard area and the O6-19 outcrop (both within the rectangle).

The study area forms part of the Musina area, one of the well characterized geological regions in the Central Zone. Musina area exposes all the prominent rock types of the Central Zone, including the Beit Bridge Group supracrustals, Paleoarchean Messina layered intrusion, Mesoarchean Sand River granitoid gneiss, Neoarchean granitoids and Paleoarchean intrusions/metasomatic overprint (Fig. 1.10). Further, although the extent of polymetamorphism in the Central Zone is a topic of continuing debate (e.g., Rigby et al., 2011), the region around Musina, where the study area is situated, is less controversial, with a number of studies presenting structural, metamorphic and geochronologic evidence for polymetamorphism (e.g., Kröner et al., 1999; Van Reenen et al., 2004, 2008; Perchuk et al., 2008; Zeh et al., 2007, 2010; Mouri et al., 2009).

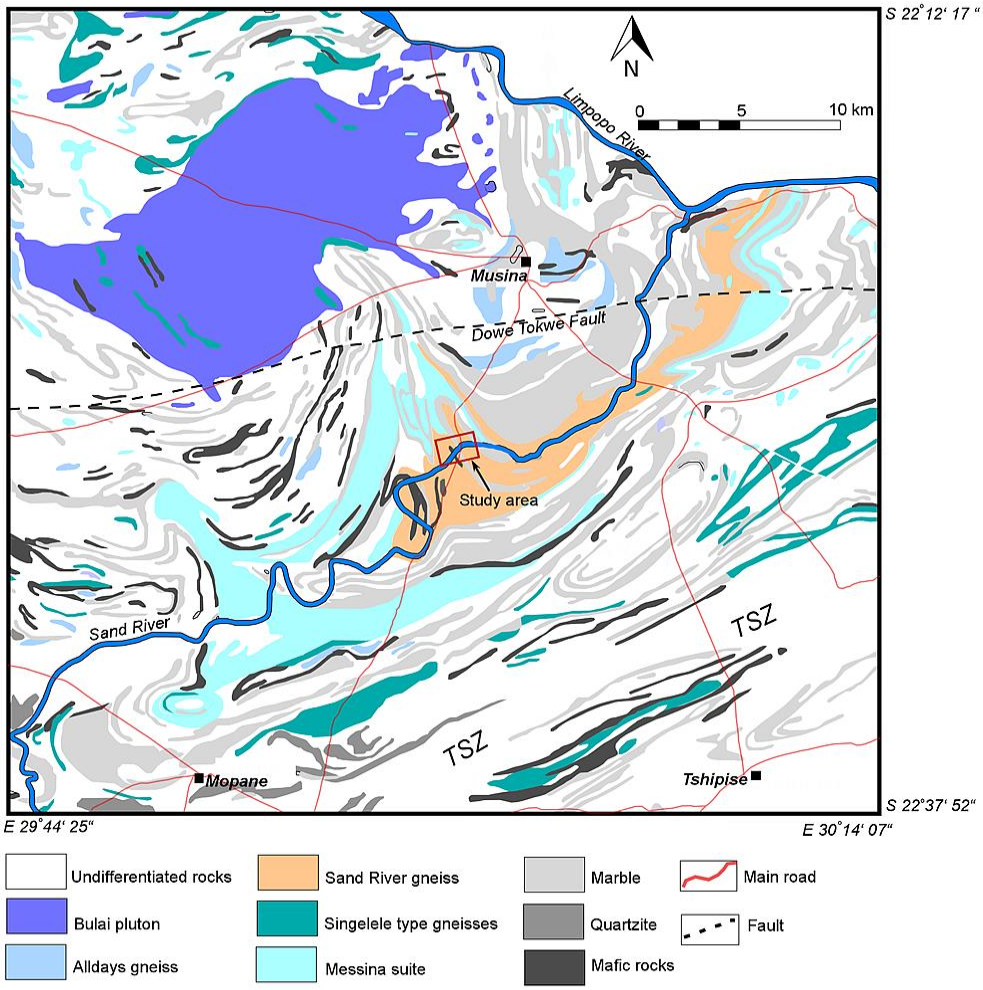


Figure 1.10. Geologic map of the Musina area showing the study area (from Boshoff, 2008 and references therein). TSZ - Tshipise Straightening Zone.

1.4. Objectives and approach

The study aims to characterize and understand the origin of the Neoarchean Verbaard granitoid. Considering the conspicuous occurrence of garnet-bearing leucocratic veins prominently overprinting the granitoid, evaluating the provenance of garnet became the main focus. For the purpose, characterization of metapelite (the surrounding rock) and associated garnet-bearing leucosomes occurring close (Verbaard area) and further away (O6-

19 outcrop) from the Verbaard granitoid were an obvious addendum. After going through the literature on Neoarchean granitoids, especially those from high-grade metamorphic terranes, the following objectives and related approach were laid out.

- Field geologic mapping of the study area to identify, delineate and demarcate the various rock types, understand field relations, including the effect of overprint event(s).

- Petrographic characterization of representative samples collected from the field to identify the minerals present and understand their mutual relations. Complementing the petrographic characterization with backscattered electron imaging helps to understand the mutual textural relation between the different rock forming minerals, and the effect of overprint event(s).

- Mineral chemical characterization of petrographically characterized samples to study the chemical composition of prominent minerals. Detailed mineral chemical profiles on garnet from different modes of occurrences were used to evaluate the provenance of garnet.

- Whole-rock geochemical characterization of petrographically characterized samples, which can give a plethora of information including the possible genetic relation of two rocks (e.g., leucosome associated with metapelite, and leucocratic vein associated with the Verbaard granitoid), and the likely origin of the granitoid.

1.5. Sampling and analytical methods

Since starting the project in 2014, a number of field sessions were carried out in the study area. A detailed geologic map was prepared for the Verbaard area, and was carried out together with a parallel study (Keeditse, 2017) which focused on characterizing the layered ultramafic-mafic rocks occurring in the study area. Sample locations and structural measurements were imported onto a satellite image of the area, on which the georeferenced geologic map was overlain using ArcGIS.

Representative bulk rock samples of the different rock types were collected from the field and transported to the geologic lab at BIUST. Selected samples were cut and polished rock thin sections were prepared at the University of Johannesburg (UJ), South Africa. These thin sections were subjected to detailed petrographic analyses using transmitted light microscopy at the geologic lab in BIUST.

After petrographic study, representative polished rock thin sections were subjected to back-scattered electron (BSE) imaging using a scanning electron microscope (SEM) to understand the textural relation between different rock-forming minerals. The BSE-SEM imaging was carried out at the central analytical facility of UJ. Electron microprobe analyses of minerals in thin sections were carried out using a CAMECA SX100, equipped with four WDS spectrometers which contain TAP, LIF, LLIF, PET, LPET, PC1, PC2 and PC3 crystals, housed at UJ. Analytical conditions were 15 kV accelerating voltage, 20 nA beam current, counting times of 10-20s for most elements, except 50s for F and 30s for Cl, and 1 to 5µm beam spot size were used. The ZAF matrix correction procedure was applied to the data. ZAF

matrix correction accounts for the difference in the intensity of the emitted X-rays. The matrix correction depends on the composition of the specimen and is calculated by the software. Fe^{2+}/Fe^{3+} values were calculated assuming full site occupancy.

Petrographically studied bulk samples were powdered at the rock crushing facility at UJ. Major and trace element contents of powdered rock samples were determined by X-ray fluorescence (XRF) spectrometry at ACME Labs, Canada, on glass beads prepared from powdered whole-rock samples with a sample-to-flux (lithium tetraborate) ratio of 1:10. Volatiles were determined by loss on ignition. Trace and rare earth elements (REE) were analyzed by inductively coupled plasma mass spectrometry (ICP-MS) at ACME Labs. The sample powders were mixed in lithium metaborate flux fusion and the resulting molten bead was rapidly digested in a nitric acid solution. Precision based on replicate analysis of international rock standards (SQ-18, OREAS76A, OREAS45CA, DS8, CSC) are 2-5% (1σ) for most elements and ±10% for U, Sr, Nd, and Ni. More information on the procedure, precision and accuracy of ACME Labs ICP-MS analyses could be found at www.acmelab.com.

1.6. Outline of the thesis

The different chapters of the thesis are structured so that it correlates with the field relations-petrography-mineral chemistry-whole-rock geochemistry approach mentioned above. A brief introduction to the geologic setting of the Musina area and the Central Zone of the Limpopo Complex is given in chapter 1. The thesis commences with first addressing and evaluating the field relations of rocks exposed in the study area (chapter 2). From

chapter 3 onwards, the study focuses on the Verbaard granitoid, associated garnet-bearing leucocratic vein, metapelite and associated leucosome occurring in the study area. Chapter 3 details the petrographic characteristics. Chapter 4 addresses the role of mineral chemical characteristics in addressing the nature of composition of minerals (preserved) in the studied rocks. Whole-rock geochemical characteristics of the rocks are presented in chapter 5. Finally, in chapter 6, the results from different studies are discussed. After characterizing the provenance of garnet occurring within the Verbaard granitoid, the study finally addresses the petrogenetic characteristics of the granitoid, in comparison to information available from other Neoarchean granitoids from the Central Zone. The resulting concluding remarks are given in chapter 7.

Chapter 2

Field relations

2.1. Introduction

Two variants of the Verbaard granitoid – tonalitic and granodioritic – have been reported. Jaeckel et al. (1997) and Kröner et al. (1999) reported respective Pb-Pb zircon ages of 2647 ± 0.4 Ma and 2629 ± 3 Ma for the two variants. The dark-grey tonalitic variant is primarily restricted to Sand River pavement exposures to the southwest of the Verbaard farm (outside the study area) and contains abundant centimetre- to decimetre-scale inclusions of supracrustal gneiss, Sand River granitoid gneiss and amphibolite (Hofmann et al., 1998). No visible evidence of overprint events occur in the tonalitic variant. The light-grey granodioritic variant, which is primarily exposed within and northeast of the Verbaard farm, is characterized by a conspicuous network of anatectic leucocratic veins, and is the focus of the present study.

The study area covers the area within (Verbaard area) and to the northeast [O6-19 outcrop (S 22^{o}26'11.4", E 30^{o}00'33.7")] of the Verbaard farm (Fig. 2.1a). This chapter presents description of field relations between rock types exposed in the study area, where the light-grey granodioritic Verbaard granitoid is well exposed. The geologic map of the Verbaard area is given in Fig. 2.1b. Although a number of rock types occur in the study area, the description given below primarily focuses on the metapelite, associated leucosomes, nearby rocks which exhibit anatectic overprint and the Verbaard granitoid.

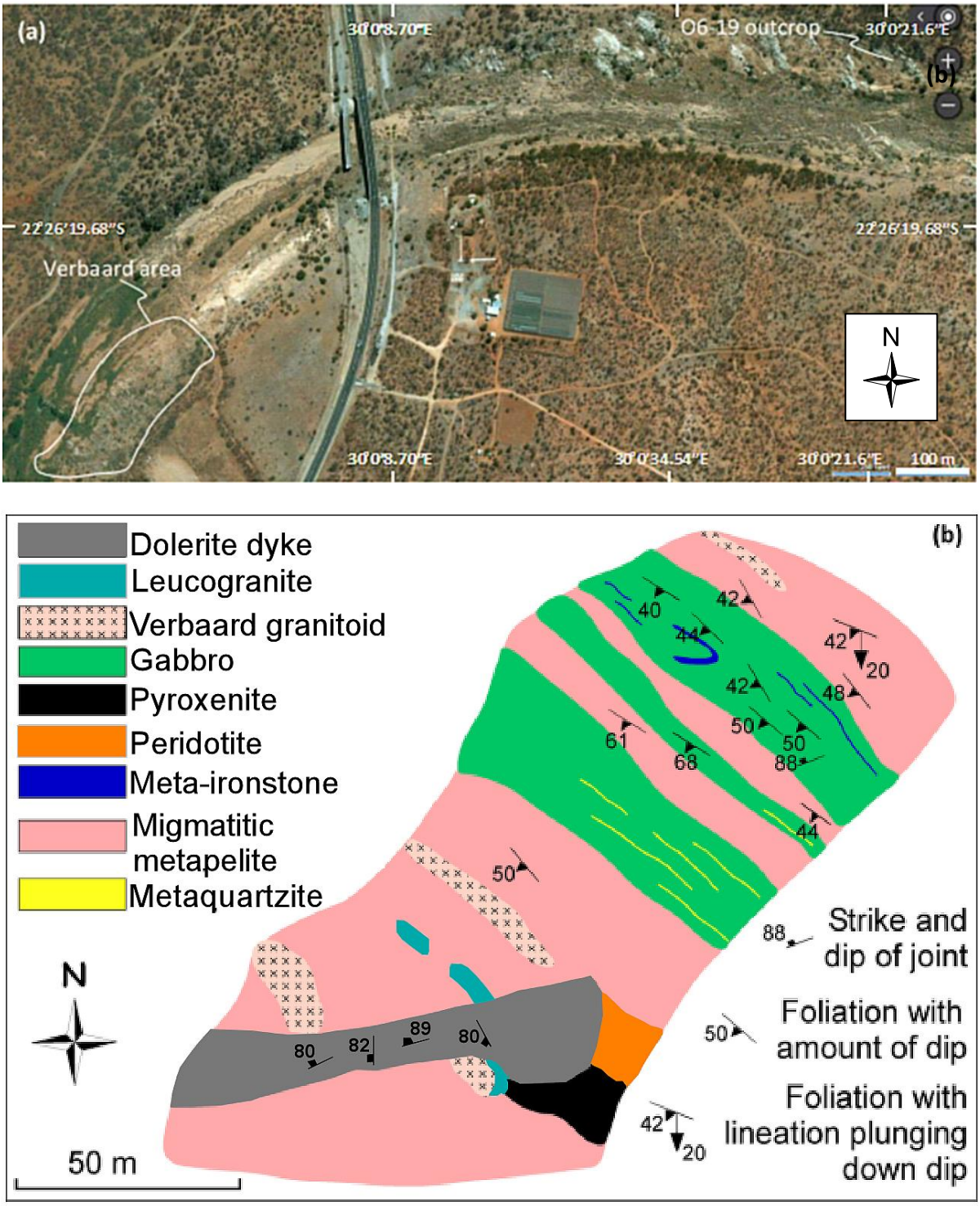


Figure 2.1. (a) Satellite image showing the extent of the study area, with the mapped Verbaard area and outcrop O6-19 to the northeast, and covers the area indicated by the white rectangle in Fig. 1.9. **(b)** Geological map of the Verbaard area showing the occurrence of Verbaard granitoid and its relation to other rock types. In the legend of (b), the rocks are arranged with oldest at the bottom and youngest at the top.

In addition, description on metapelite and associated leucosomes from the O6-19 outcrop [the notation O6-19 follows the terminology used in Boshoff (2008), Perchuk et al. (2008) and Van Reenen et al. (2008)], northeast of the Verbaard area (Fig. 2.1a) is also included. The field relations observed between the rock types of concern to the present study – metapelite, associated leucosomes, Verbaard granitoid – are similar in the mapped Verbaard area as well as in the area with the O6-19 outcrop (together forming the study area).

2.2. Rock types

The study area exposes nine rock types (Fig. 2.1b), which can be lumped into four groups. The oldest group including metaquartzite, metapelite and meta-ironstone form part of the Beit Bridge Group supracrustals. Ultramafic (peridotite, pyroxenite) and mafic (gabbro) rocks form part of the Paleoarchean Messina layered intrusion. Two types of granitoids – the Neoarchean Verbaard granitoid and the Paleoproterozoic leucogranite – occur in the study area. Dolerite dyke constitutes the youngest rock in the study area.

Quartzite occurs as thin layers parallel to the general NW-SE fabric in the area. The layers are widespread and typically restricted to the gabbroic units (Fig. 2.1b). It is relatively impure with visible layering (Fig. 2.2a). The meta-ironstone is a reddish-brown rock (Fig. 2.2b), occurring as banded to massive gneissic units. Its occurrence is restricted to the gabbro and metapelite. Garnet occurs locally, and pyroxene is prominent in the ironstone. Metapelite constitute the dominant rock type in the study area (Figs. 2.1b, 2.2c) and is dealt in detail below under a separate section.



Figure 2.2. Representative field photographs of the various rock types in the study area.

Ultramafic rocks occur as thin layers, parallel to the general trend of the area (Fig. 2.1b). Peridotite either occurs as dark and massive, sub-rounded to lens-shaped discontinuous bodies (~2 m in diameter) (Fig. 2.2d), or as massive continuous exposures. A light olivine greenish appearance at hand specimen scale is distinctive of the serpentinized variant. Pyroxenite occurs as dark, massive exposures (Fig. 2.2e). No garnet or garnet-bearing leucocratic granitic veins occur in the ultramafic rocks. Except for its altered nature (due to serpentinization), peridotite is similar in appearance to the pyroxenite.

Gabbroic rocks dominantly occur as thin- to thick-layers concordant to the general trend of the metapelite (Fig. 2.1b). At hand-specimen scale, the rock appears massive. Elongated bands of gabbroic rocks occur interleaved with the metapelite. Garnet-bearing leucocratic veins locally crisscross the gabbroic rocks (Fig. 2.2f). A number of inclusions occur within the gabbroic rocks, and include meta-ironstone occurring as folded and concordant layers, and metaquartzite occurring as concordant layers. Only the largest ones obvious at the map-scale are shown in Fig. 2.1b.

Like the metapelite, Verbaard granitoid is dealt in detail below in a separate section. Although smaller, relative to the Verbaard granitoid, a number of garnet-bearing leucogranite bodies intrude into the ultramafic rocks and metapelite (Fig. 2.1b). The undeformed leucogranite intrudes into the gneissic Verbaard granitoid (Fig. 2.2g). The leucogranite bodies also lack the garnet-bearing leucocratic veins which are conspicuous of the Verbaard granitoid. An approximately E-W trending dolerite dyke intrudes all the rocks exposed in the ‘southern’ part of the area (Figs. 2.1b, 2.2g, h).

2.3. Metapelite

Two types of metapelite – a darker (Fig. 2.3) and a lighter (Fig. 2.4) variant - occur in the study area. The darker metapelite is best exposed at the O6-19 outcrop (Figs. 2.1a, 2.5). Both the metapelitic variants are migmatitic, defined by alternating leucocratic and melanocratic (restitic) layers. The layers are *closely packed*, with the quartzofeldspathic leucocratic layers (leucosomes) characterized by irregular outline (Figs. 2.3 to 2.5). The occurrence of garnet and biotite is conspicuous in both metapelitic variants, with biotite-rich layers delineating the margins of leucosomes. The lighter metapelite has a greater proportion of leucosomes (Fig. 2.4), while the darker metapelite have more restitic domains (Figs. 2.3, 2.5) than the lighter variant. Sillimanite and cordierite can be observed at hand specimen scale. In general, the size of garnet increases from the restitic domains to the irregular-outlined leucosomes, often forming aggregates in the latter. Leucosomes associated with metapelite at the O6-19 outcrop exposes some of the largest garnet crystals (Fig. 2.6). The leucosomes, considered to be product of partial melting, are generally concordant to the gneissic fabric (Figs. 2.3 to 2.6). Locally, they cross cut the gneissic fabric (Fig. 2.6). With segregation of melt, local discrete shear zones characterized by asymmetric porphyroclasts develop within the rock (Figs. 2.4a, 2.5a). Boudinaging and intrafolial folds are prominent (Figs. 2.3a, 2.4b). Rare wider bands of leucogranite occur (Fig. 2.7a). Unlike the irregular outlined leucosomes, these leucogranite bands have more or less straight outline, and lesser (both size and modal abundance) garnet. These leucogranite bands are similar to the garnet-bearing leucogranite bodies that intrude in the southern part of the Verbaard area (Fig. 2.1b).

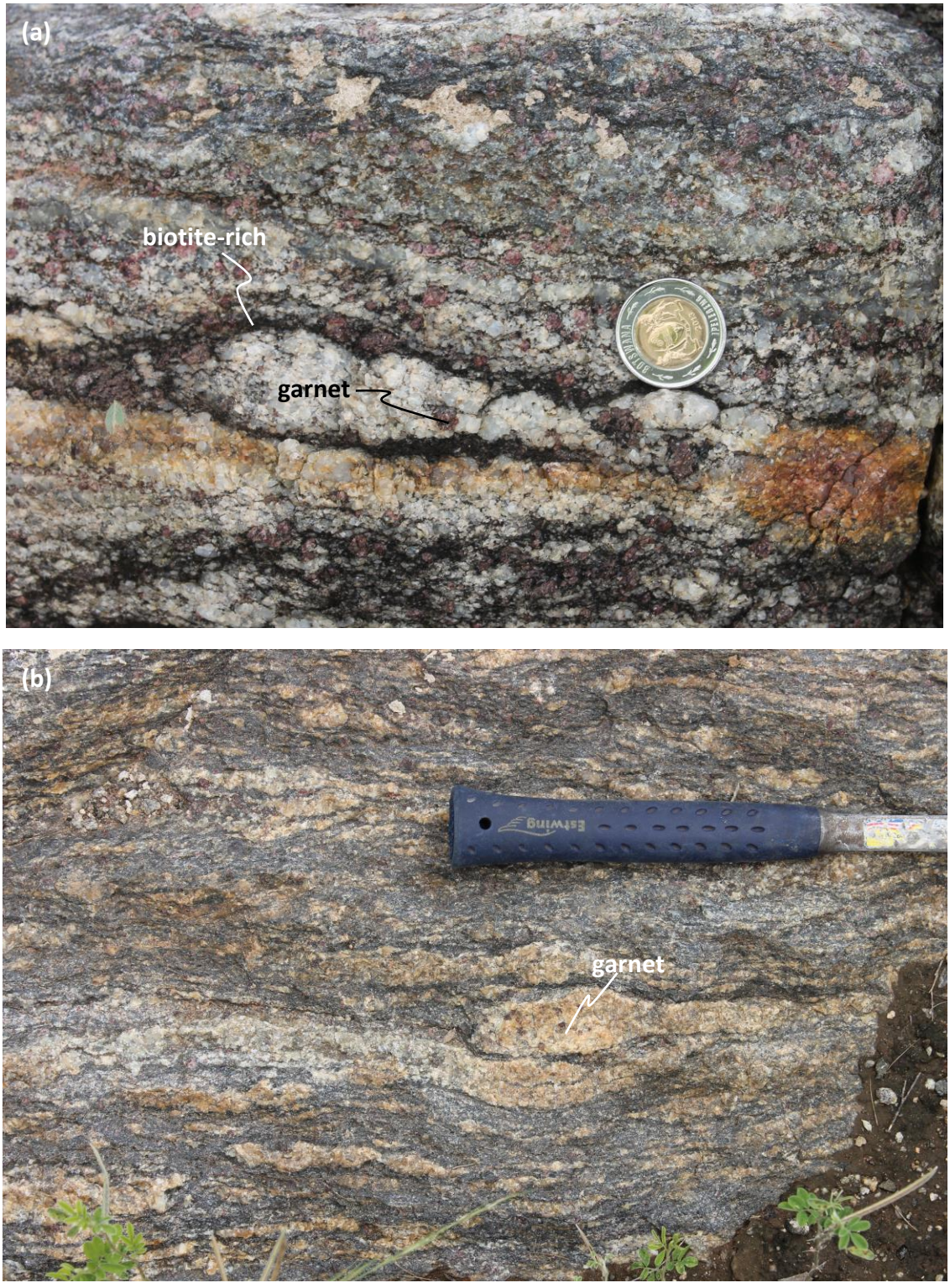


Figure 2.3. (a, b) Representative field photographs illustrating the darker metapelite (with more restitic domains) in the Verbaard area. Outcrop in (b) is on the river pavement. The boudinaging and asymmetric structures seen are part of the deformation related to melt segregation.

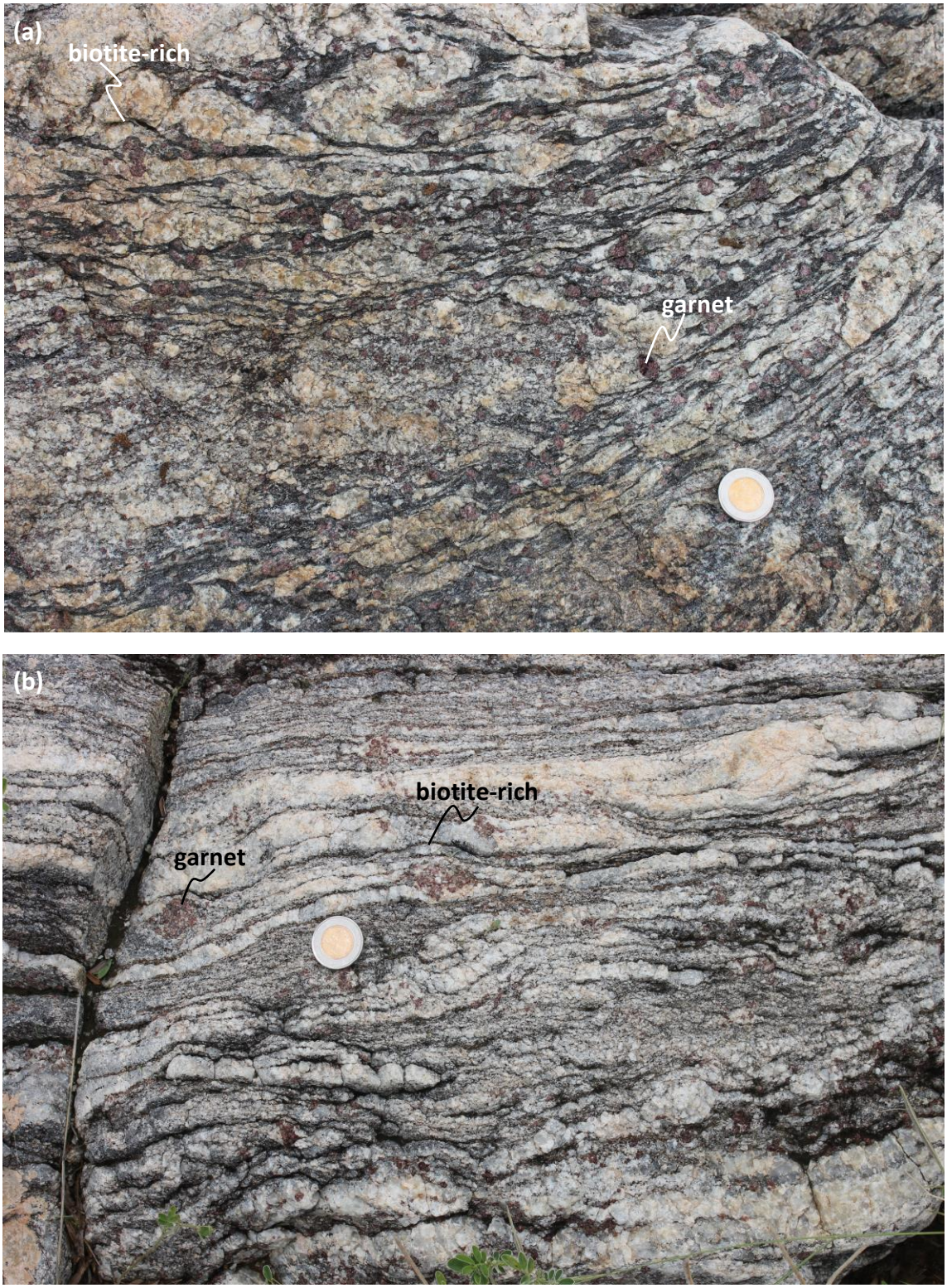


Figure 2.4. (a, b) Representative field photographs illustrating the lighter metapelite (with more leucosomic portion than the darker metapelite) in the Verbaard area. The asymmetric structures including intrafolial folds seen are part of the deformation related to melt segregation.

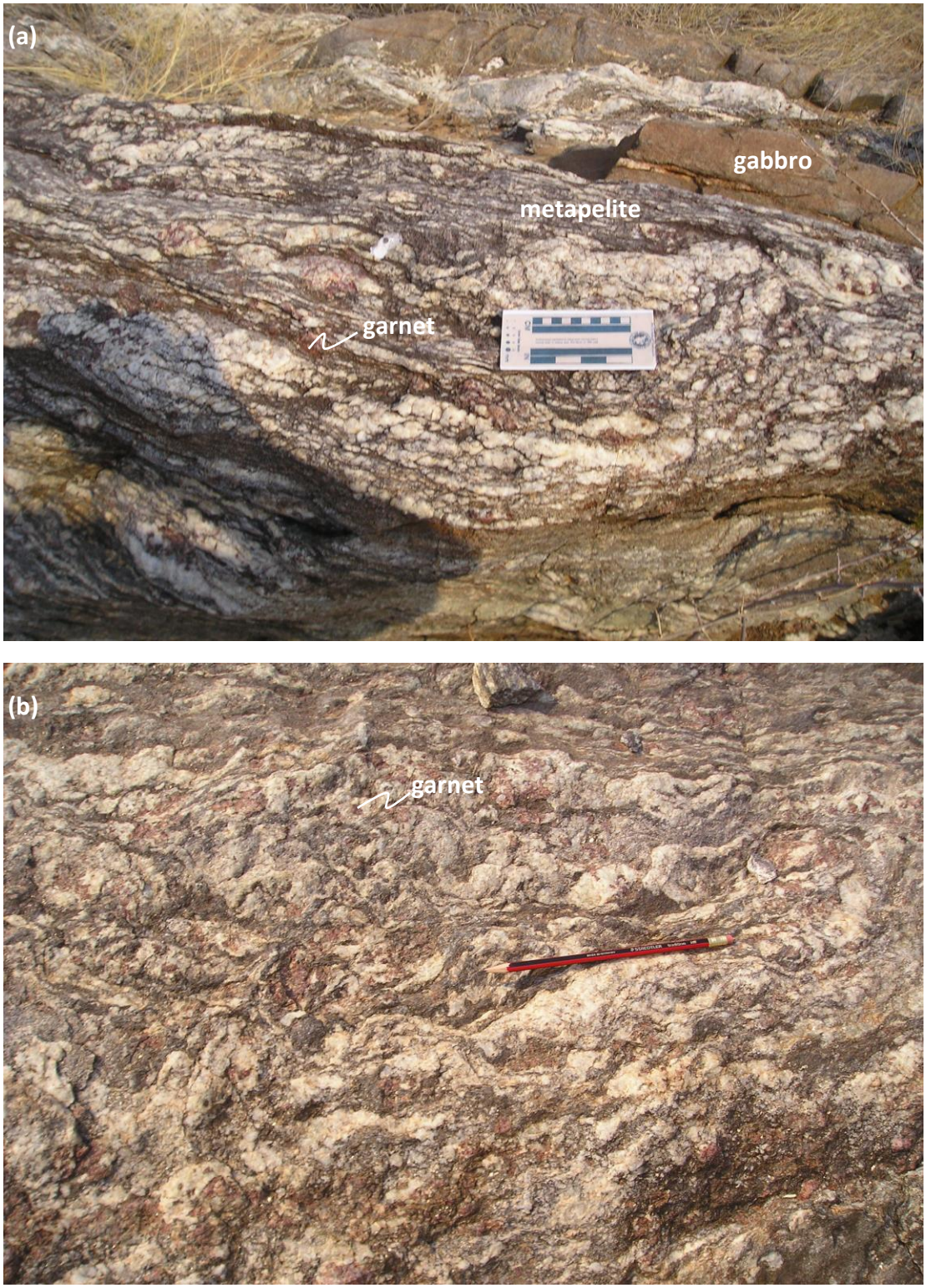


Figure 2.5. (a, b) Representative field photographs illustrating the darker metapelite at the O6-19 outcrop. Exactly similar field relations are observed as in the Verbaard area. The asymmetric structures seen are part of the deformation related to melt segregation.



Figure 2.6. Field photograph of the metapelite occurrence at the O6-19 outcrop. This particular outcrop was sampled for various studies. Notice the large garnet within the discordant leucosome in the metapelite.

2.4. Garnet-bearing leucocratic bodies associated with gabbro

Although garnet occurs locally *within* meta-ironstone and gabbro, garnet-bearing leucosomes or leucocratic veins are seen only overprinting gabbroic bodies occurring associated with the metapelite. In the general case, the contact between gabbro and metapelite is sharp with no garnet occurrence in the mafic intrusive rock (Fig. 2.7b). But locally, garnet-bearing leucosomes or leucocratic veins overprint the gabbroic bodies (Fig. 2.8). Adjacent to metapelite (within cms) leucosomes with patchy irregular outline occur in the gabbro. They do not follow any pre-defined fabric. They have more garnet grains in it (Fig. 2.8a). Leucosomes are generally thicker than the leucocratic veins.



Figure 2.7. (a) Rare wider leucogranite band associated with metapelite in the Verbaard area. **(b)** Contact relation between the garnet-absent gabbro and garnet-bearing migmatitic metapelite.

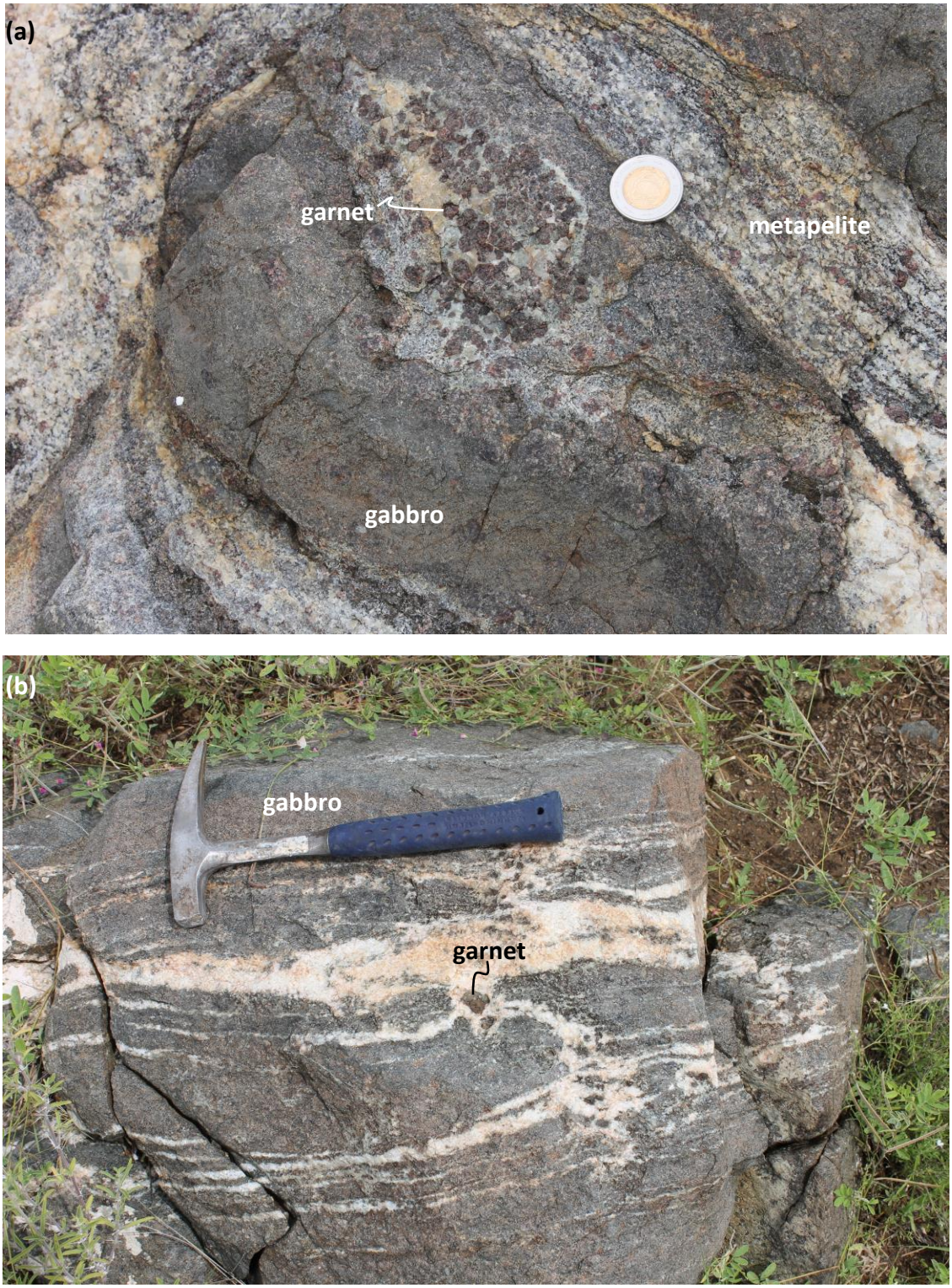


Figure 2.8. Garnet-bearing irregular patchy leucosomes **(a)** and thinner mostly concordant leucocratic veins with more or less linear outline **(b)** overprinting the gabbroic bodies associated with metapelite. Relative to (a) (centimeters), (b) is further away (metres) from the metapelite. Notice the fewer garnet grains in the leucocratic veins in comparison to the leucosomes.

Away from the metapelite (within metres), veins with more or less linear outline (boundary) overprint the gabbro. These veins follow the fabric in the rock. Few garnet grains occur. The thicker leucosomes with irregular patchy outline are characterized by aggregates of large garnet crystals (Fig. 2.8a). In comparison, the thinner mostly concordant leucocratic veins with more or less straight line (less curved) outline have fewer garnet grains (Fig. 2.8b). It should re-emphasized that the term “leucosome” is used in this study as pertaining to melt associated with the restite. Once they leave the source region, the term leucocratic vein is used.

2.5. Verbaard granitioid

A number of light-grey homogeneous biotite-bearing granitoid intrude into the ultramafic rocks and metapelite (Figs. 2.9, 2.10a), mostly, in the southern part of the Verbaard area (Fig. 2.1b). Weathered surfaces are pinkish to brownish (Fig. 2.10). The biotite-defined foliation in the granitioid is generally parallel to the gneissic fabric of the metapelite. No inclusions of surrounding rock were found within the exposed granitoid bodies. The Verbaard granitoid bodies are conspicuous by the presence of a crisscrossing network of garnet-bearing leucocratic veins (Figs. 2.10, 2.11). The leucocratic veins are dominantly concordant to the gneissic foliation (Figs. 2.10, 2.11). Unlike the leucosomes in the metapelite, the leucocratic veins in the Verbaard granitoid are characterized by more or less straight line (less curved) outline. The garnet forms aggregates towards the center of these anatectic leucocratic veins (Fig. 2.12).

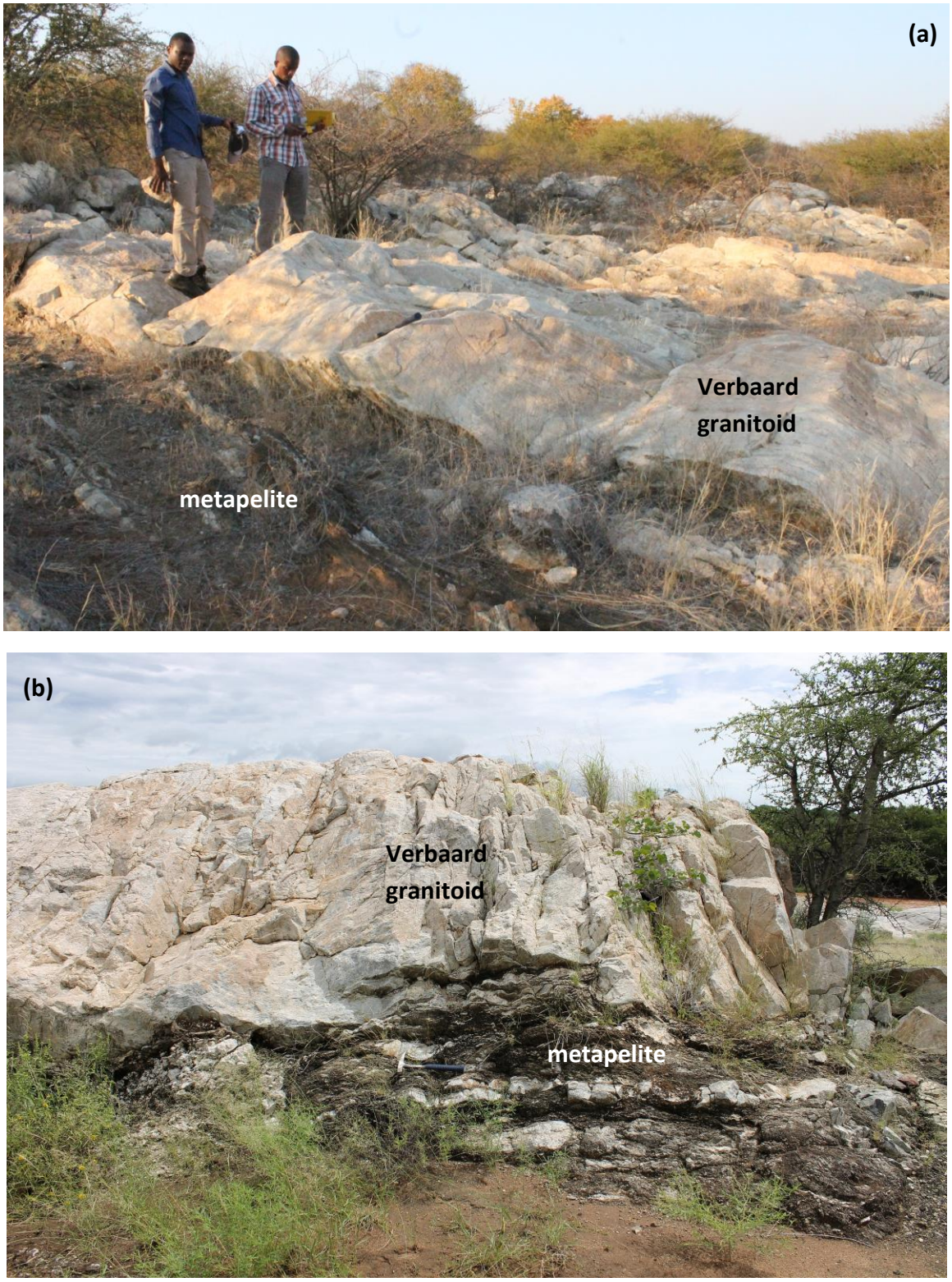


Figure 2.9. (a, b) Field photographs illustrating the typical outcrops of light grey Verbaard granitoid intruding into metapelite in the Verbaard area.



Figure 2.10. (a, b) Weathered surfaces of the light grey Verbaard granitoid are pinkish to brownish. A characteristic feature is the conspicuous network of garnet-bearing leucocratic veins.



Figure 2.11. (a, b) Field photographs illustrating the conspicuous occurrence of a network of garnet-bearing leucocratic veins overprinting the light grey Verbaard granitoid.

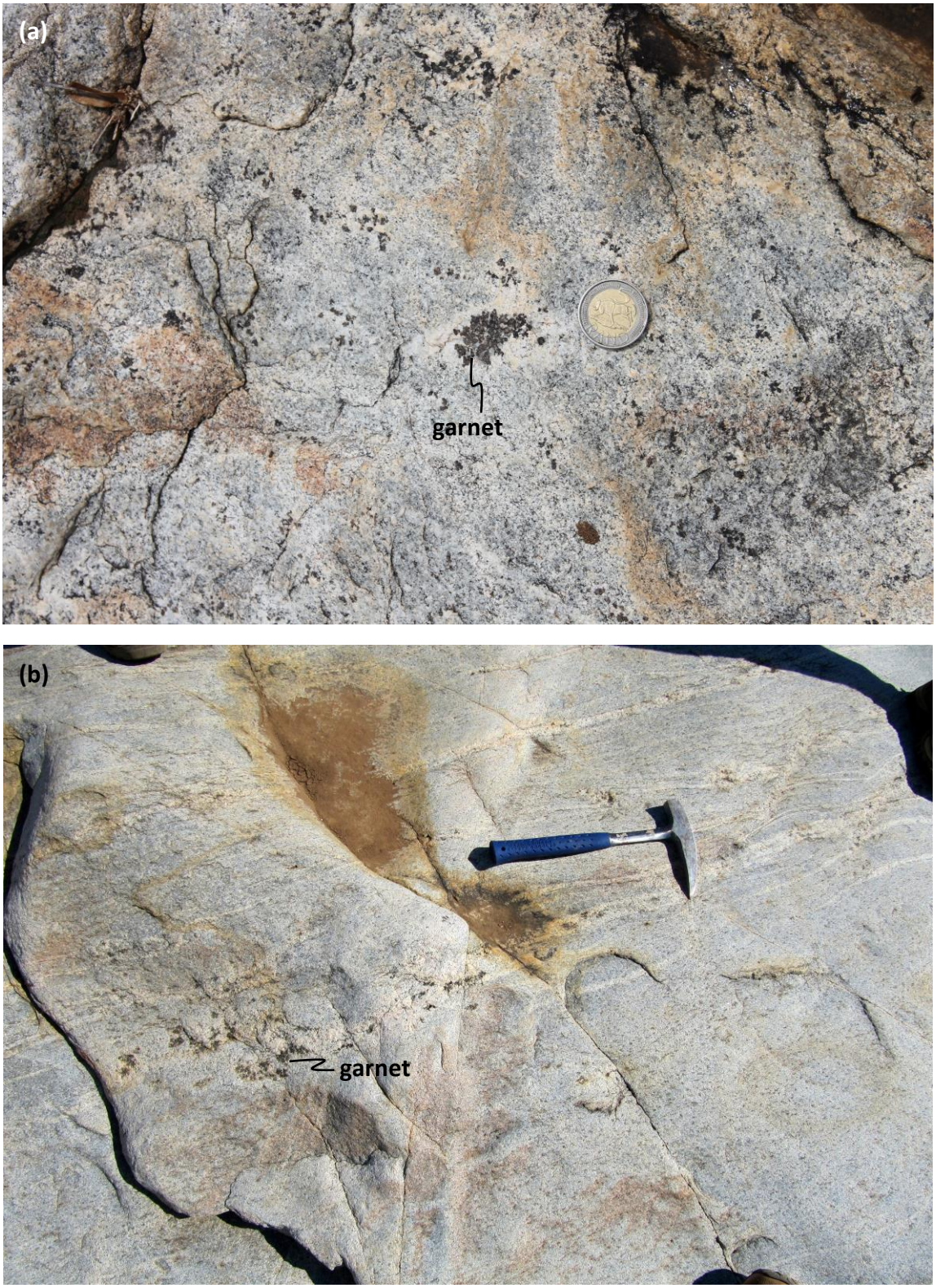


Figure 2.12. (a, b) Garnet forms aggregates towards the center of the anatectic leucocratic veins associated with the Verbaard granitoid.

While the leucosomes in the metapelite are characterized by biotite-rich melanocratic margins, no such margins occur in the leucocratic veins associated with the Verbaard granitoid bodies. The occurrence of Verbaard granitioid outside the mapped area is mostly restricted to isolated exposures along the Sand River pavement (Fig. 2.13). These exposures are also characterized by the conspicuous network of garnet-bearing leucocratic veins overprinting the light-grey Verbaard granitoid (Fig. 2.13). Sampling of Verbaard granitoid for the present study was carried out from exposures like the ones illustrated in Figs. 2.9 to 2.12.

2.6. Relative chronology of the rocks

The Verbaard area exposes all the prominent lithologies (Fig. 2.1b) of the Central Zone of the Limpopo Complex. Based on the field relations, the peridotite, pyroxenite and gabbro, all part of the Paleoarchean Messina layered intrusion, are intrusive into the older Beit Bridge Group supracrustal rocks (meta-quartzite, metapelite and meta-ironstone). The partial melting of the metapelite is later than this, with the available geochronologic evidence (Boshoff, 2008; Van Reenen et al., 2008) arguing for the metapelite to have been subjected to two high-grade events (~2.61 and ~2.02 Ga). The large-garnet bearing leucosome traversing the migmatitic metapelite at O6-19 ouctrop has been dated at ~2.02 Ga (Boshoff, 2008; Van Reenen et al., 2008). The garnet-bearing leucocratic veins overprinting the Neoarchean Verbaard granitoid indicate an anatectic overprint. Kröner et al. (1999) reported an age of 2570 ± 4 Ma from the ~2.63 Ga Verbaard granitoid, and interpreted it as related to the Neoarchean high-grade overprint. The overprint age is within error similar to the age of

high-grade overprint (~2.61 Ga) from the associated migmatitic metapelite. The general lack of deformation structures in the garnet-bearing leucogranite bodies indicates that they are younger than their host rocks, except for the unmetamorphosed dolerite dyke, which represents the last event to occur in the Verbaard area.



Figure 2.13. (a, b) Field photographs illustrating the typical river pavement exposures of the Verbaard granitoid outside the Verbaard area shown in Fig. 2.1b. (b) is a close up of (a). The head of the hammer in (a) can be seen at the bottom of (b).

Chapter 3

Petrographic characteristics

3.1. Introduction

The chapter presents petrographic characteristics of the metapelite, associated leucosomes and the Verbaard granitoid from the study area. Petrographic characteristics of gabbro and meta-ironstone showing local occurrence of garnet are also included to complete the inventory of rocks in the study area with associated/overprinted garnet. Transmitted light photomicrographs form the primary method of characterization of the different rocks. The focus of the detailed photomicrographs given under each sub-section characterizing a particular rock type is on the mineral assemblages and their mode of occurrence, including grain margin outlines. As the metamorphic history of metapelites in the Musina area has been characterized in detail by a number of studies (e.g., Van Reenen et al., 2004; Zeh et al., 2004; Perchuk et al., 2008; Smit et al., 2011), no attempt is made to address the reaction textures (and infer the corresponding reactions) in the metapelite. Metapelite is studied here with the intention of understanding the relation of garnet occurring within it as well as the associated leucosomes to that in the Verbaard granitoid.

3.2. Metapelite

The darker and lighter coloured metapelite in the study area respectively correlates with the two types of metapelites – high-Al and low-Al metapelites – recognized by Boryta and

Condie (1990) from the Musina area (see also chapter 5). Hence, the usages high-Al and low-Al metapelites will be used *hereafter* when respectively referring to the darker and lighter metapelite. The metapelite exposed at the O6-19 outcrop is a high-Al metapelite. Both types of metapelite from the study area have more or less similar mineralogy. But they differ primarily in the constitution (make up/modal abundance) and arrangement of the minerals. This study subdivides metapelites into three domains – restitic, quartzofeldspathic, and leucosomic. The description given below follows this order. Leucosomes associated with metapelites are different from these three domains, and are described last.

3.2.1. High-Al metapelite and associated leucosomes

The high-Al metapelite, with more restitic domains, is characterized by conspicuous biotite-sillimanite-cordierite-dominant layers of varying thickness (~0.01–~0.04 mm) separated by thin (<0.3 mm) quartzo-feldspathic domains (Fig. 3.1). While biotite and sillimanite are prominently aligned parallel to the length of the yellow-brown layers, quartz and feldspar generally occur as elongated grains in the felsic and mafic layers (Figs. 3.1, 3.2).

Cordierite alteration is prominent, with both pinite and sericite variants (Fig. 3.1), giving the yellow-brown color to the aluminous layers. It includes both sillimanite and biotite. Sillimanite is prominently concentrated in the central portion, while biotite occurs in the central and marginal portions (Fig. 3.1). Sillimanite occurs as prismatic and fibrous crystals (Fig. 3.1). In places, long prismatic sillimanite occurs (Fig. 3.1). Different variants of the aluminous layers occur, with the common one having biotite-sillimanite-dominant central

portions (Fig. 3.1). Less common ones include layers with a biotite-dominant central portion and a sillimanite-dominant marginal portion (Figs. 3.2a, b), and layers with both central and marginal portions dominated by sillimanite (Figs. 3.2c to f).

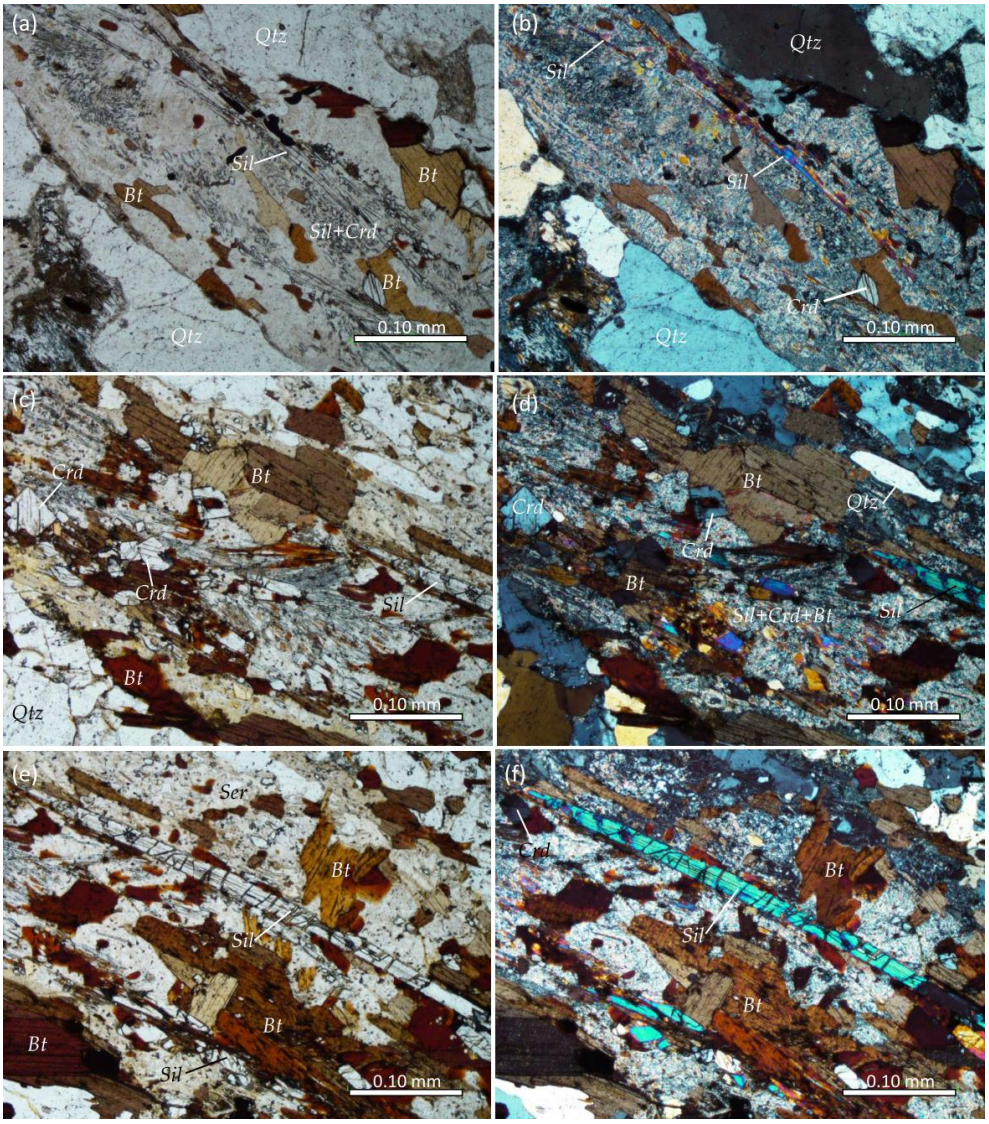


Figure 3.1. Photomicrographs illustrating the conspicuous cordierite-biotite-sillimanite-dominant yellow-brown layers in the high-Al (darker) metapelite. Cordierite exhibit pinite and sericite alteration. Sillimanite primarily concentrates in the central portion, while biotite occurs both in the central and marginal portions. Sillimanite occurs as both fibrous and prismatic needle-shaped crystals dominantly elongated parallel to the length of the layer. Straight line grain margins are prominent in the aluminous layers. Minor felsic minerals occurring in the aluminous layers have lobate rounded grain margins. Crd – cordierite; Bt – biotite; Sil – sillimanite; Qtz – quartz; Kfs – K-feldspar; (a), (c), (e) taken under plane polarized light (PPL); (b), (d), (f) taken under cross-polarized light (XPL).

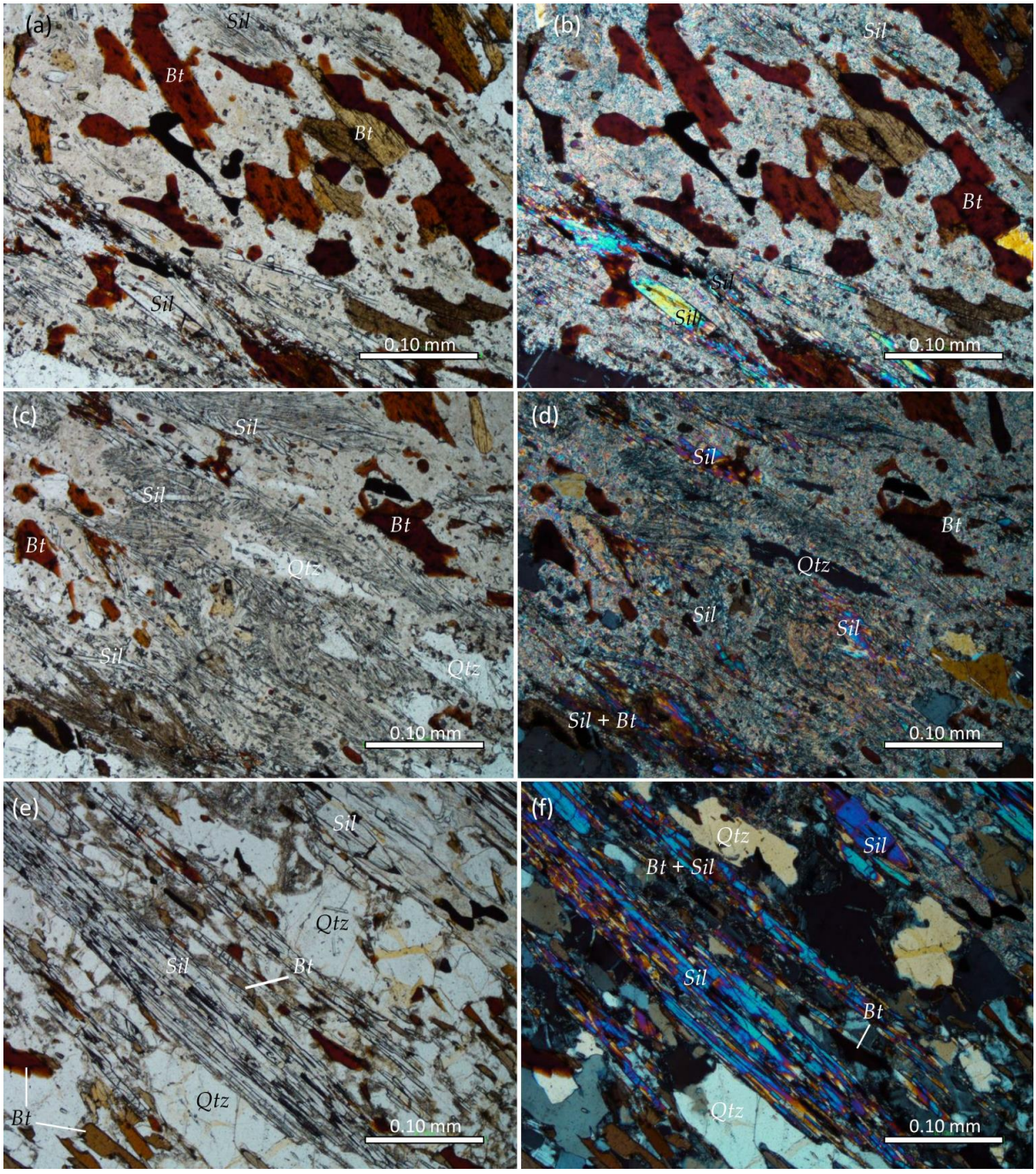


Figure 3.2. Photomicrographs illustrating the less common variants of the aluminous layers in the high-Al metapelite. The common mode of occurrence of the aluminous layer is shown in figure 3.1. Less common variants include layers with biotite-dominant central portion and sillimanite-dominant marginal portion **(a, b)**, and layers with both central and marginal portions dominated by sillimanite **(c to f)**. Minor felsic minerals with lobate rounded grain margins occurring in the aluminous layers are generally elongated parallel to the length of the layer. (a), (c), (e) taken under PPL; (b), (d), (f) taken under XPL.

Minerals with straight grain outline are prominent within the aluminous layers (Figs. 3.1, 3.2). Locally rounded grain margins occur. Minor felsic minerals with lobate rounded grain margins occurring in the aluminous layers are generally elongated parallel to the length of the layer (Figs. 3.1, 3.2). A closer inspection of the mode of occurrence of quartz and feldspar with lobate rounded grain margins in the aluminous layers indicate a transition from more or less patchy occurrence (Figs. 3.3a, b) to thinner elongated grains (Figs. 3.3c, d) to larger grains generally elongated parallel to the length of the layer (Figs. 3.3e, f).

Garnet is locally found associated with the aluminous layers (Fig. 3.4). These garnets are always separated from the biotite-sillimanite-rich layers by alteration associated with cordierite (Fig. 3.4). These garnets can be either oriented discordant to the layer (more or less penetrating into the layer) (Figs. 3.4a, b) or more or less elongated parallel to the length of the layer (Figs. 3.4c to f). Rarely, small garnet crystals are completely surrounded by altered cordierite (Figs. 3.4e, f). The garnet crystals associated with aluminous layers have both straight line and lobate rounded grain margins (Fig. 3.4).

Garnet occurs prominently in the quartzofeldspathic portion/layers and is characterized by their irregular outline (Fig. 3.5). Their occurrence varies from small grains to large porphyroblasts (Fig. 3.5); the larger ones occurring towards the leucosomic portions. They can have straight line as well as lobate rounded grain margins (Fig. 3.5). When present, the inclusions within garnet include quartz, biotite and sillimanite (Fig. 3.5). Alteration is often found adjacent to garnet porphyroblasts, with the alteration veins locally invading the garnet along fractures (Fig. 3.5).

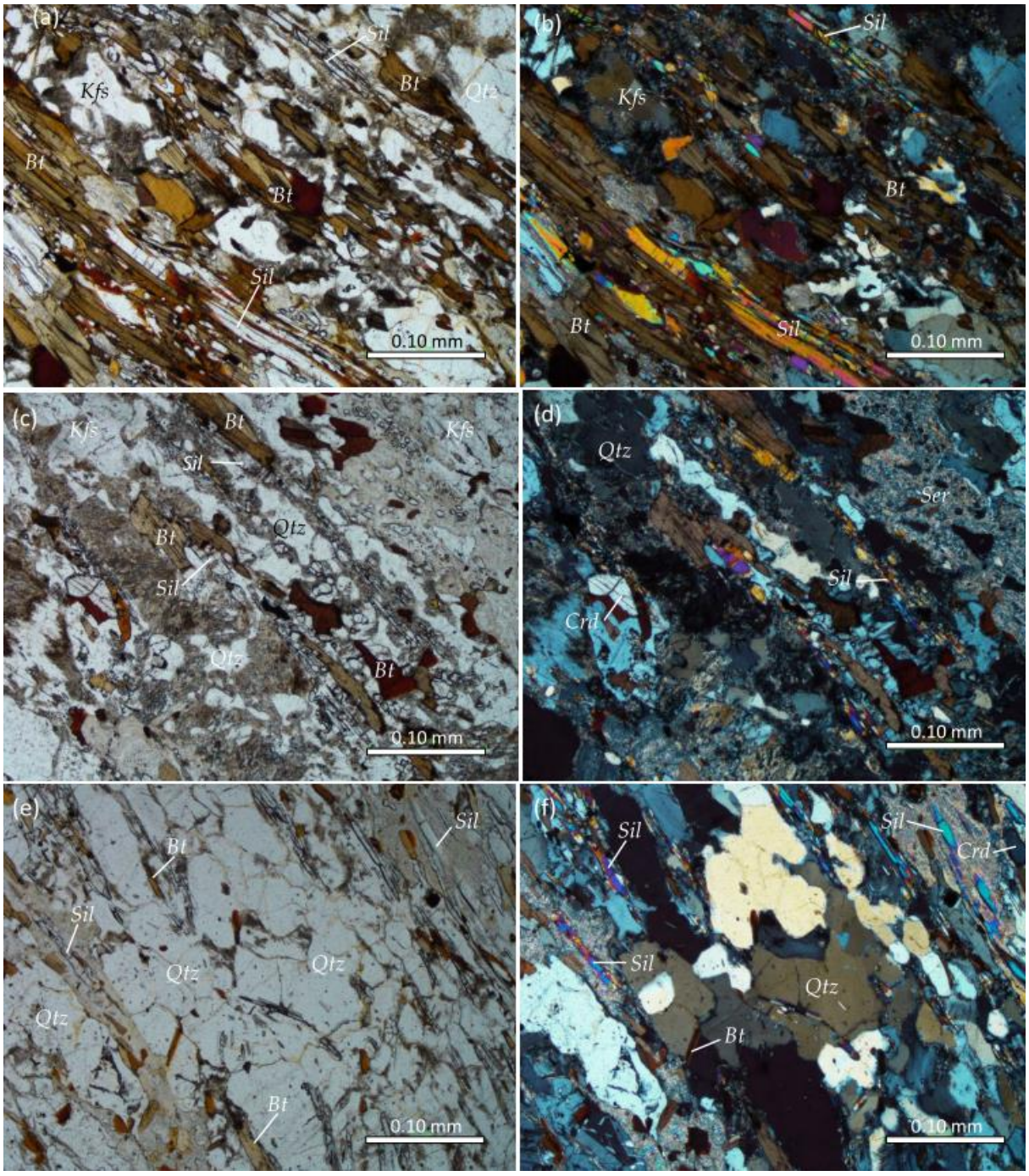


Figure 3.3. Photomicrographs illustrating the mode of occurrence of minor felsic minerals in the aluminous layers in the high-Al metapelite. The felsic minerals (quartz and feldspar) have lobate rounded grain margins. A closer inspection of the mode of occurrence of these felsic minerals indicate a transition from more or less patchy occurrence **(a, b)** to thinner elongated grains **(c, d)** to larger grains generally elongated parallel to the length of the layer **(e, f)**. Pl – plagioclase; Other mineral abbreviations same as those in Fig. 3.1, for this and rest of the figures. Where needed, additional abbreviations are indicated. (a), (c), (e) taken under PPL; (b), (d), (f) taken under XPL.

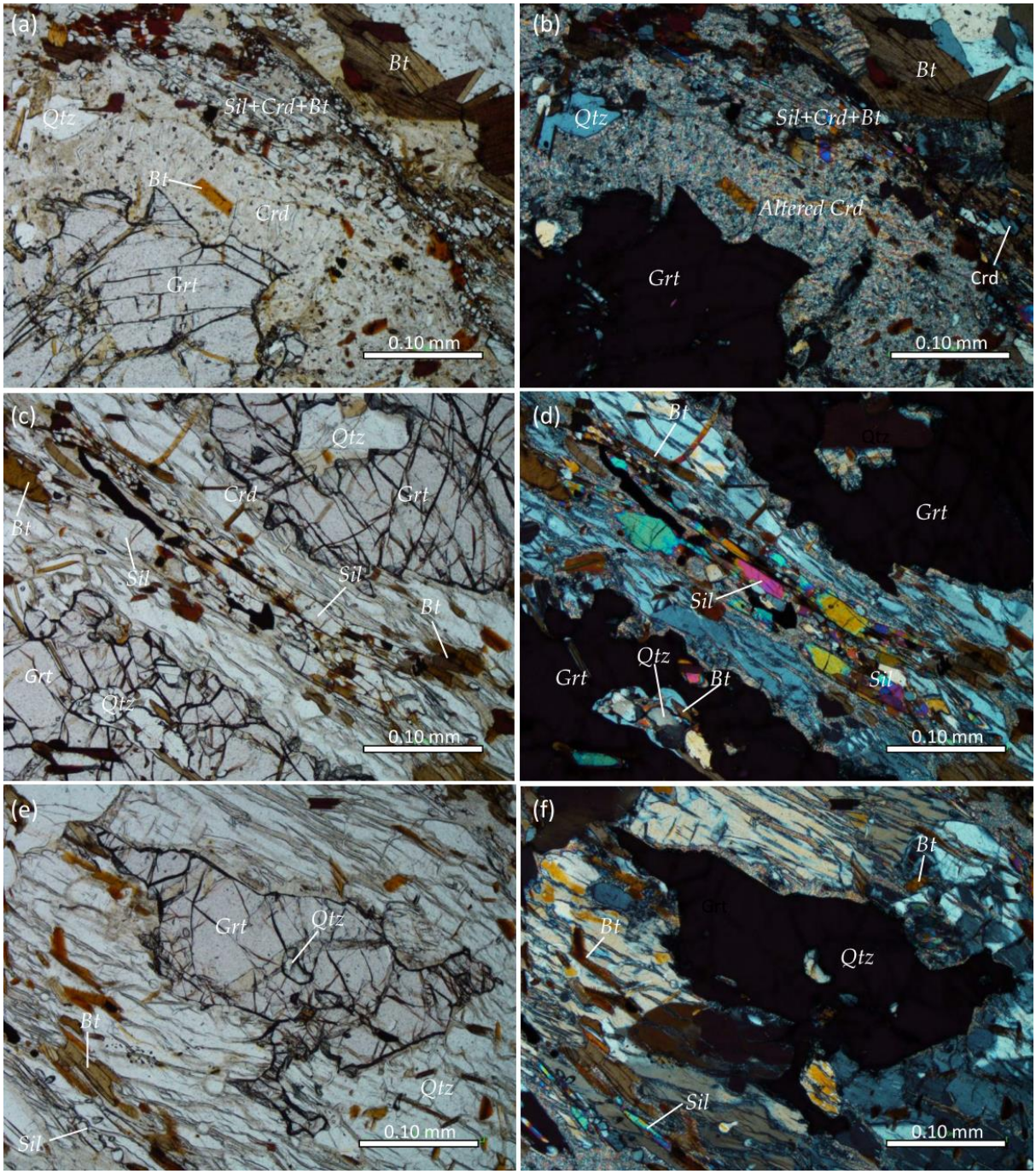


Figure 3.4. Photomicrographs illustrating the mode of occurrence of garnet associated with the aluminous layers in the high-Al metapelite. These garnets are always separated from the biotite-sillimanite-rich layers by alteration associated with cordierite. They can be either oriented discordant to the layer (more or less penetrating into the layer) **(a, b)** or more or less elongated parallel to the length of the layer **(c to f)**. Rarely, small garnet crystals are completely surrounded by alteration associated with cordierite **(e, f)**. Grt – garnet; (a), (c), (e) taken under PPL; (b), (d), (f) taken under XPL.

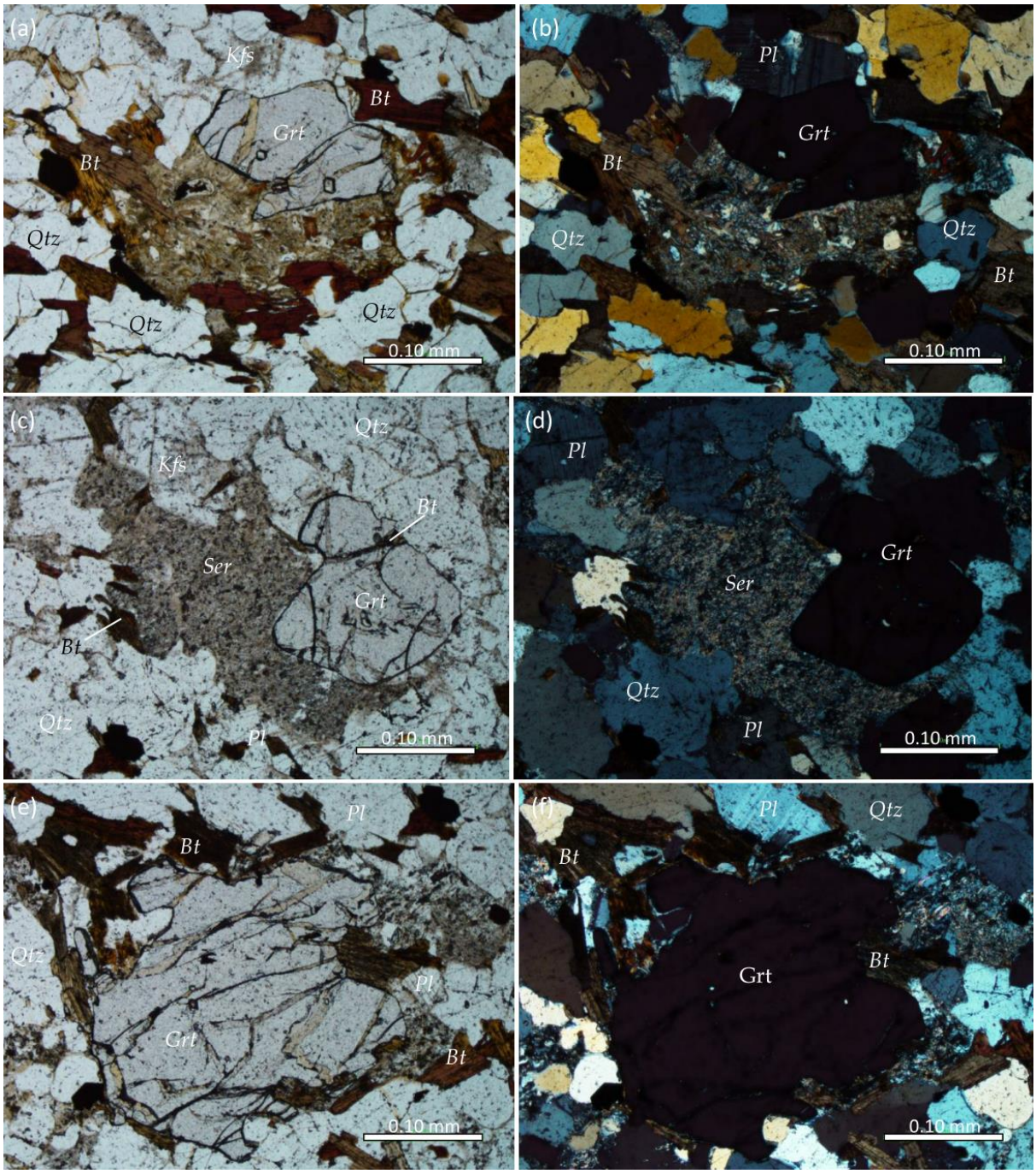


Figure 3.5. Photomicrographs illustrating the mode of occurrence of garnet, which is primarily concentrated in the quartzofeldspathic portion of the high-Al metapelite. Their occurrence varies from small grains to large porphyroblasts. When present, the inclusions within garnet include quartz, biotite and sillimanite. Alteration is commonly often found adjacent to garnet porphyroblasts. Both straight line and lobate rounded grain margins can be observed between the different minerals. The quartzofelspathic portion is primarily made up of quartz and K-feldspar. (a), (c), (e) taken under PPL; (b), (d), (f) taken under XPL.

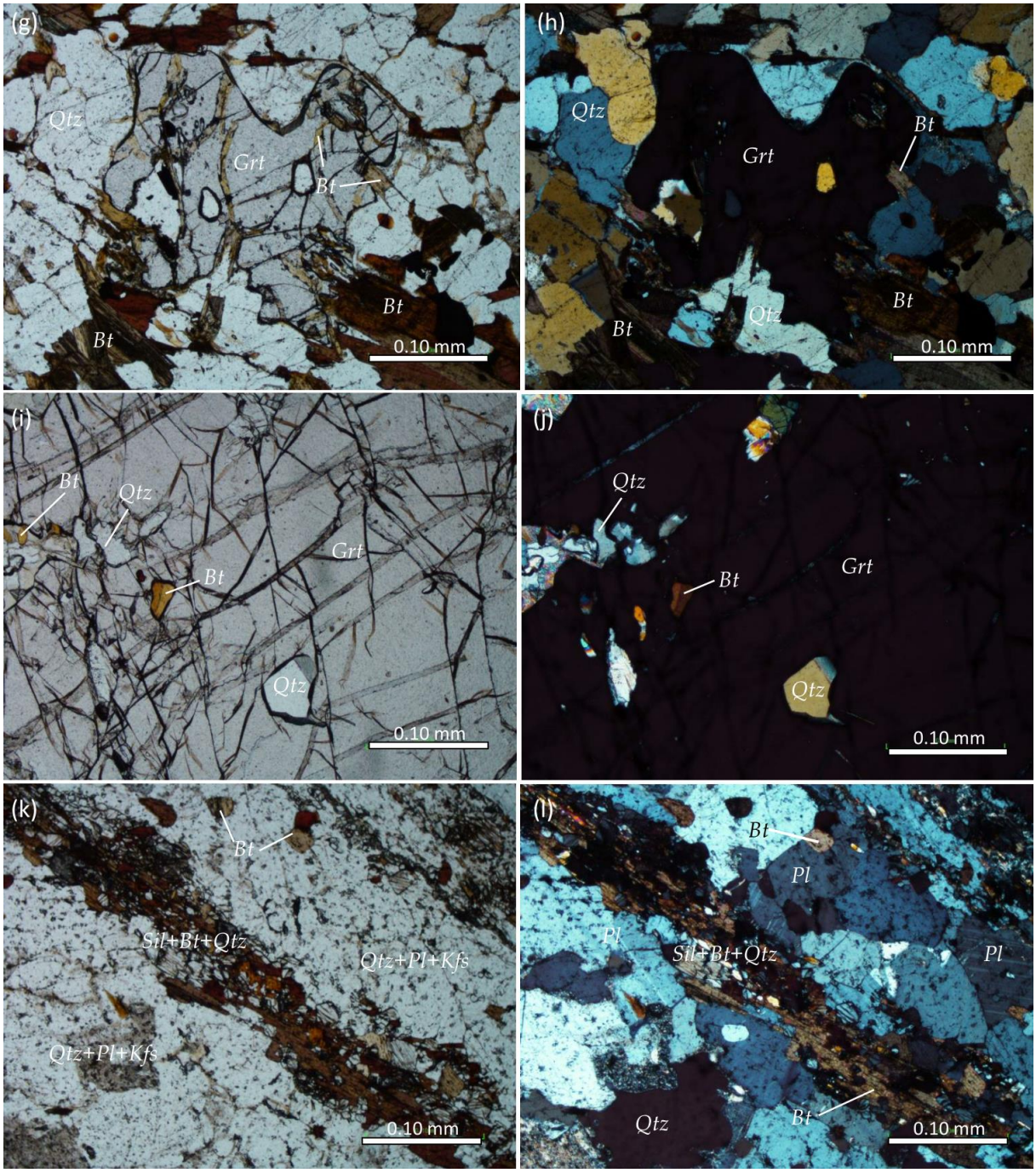


Figure 3.5. continued. Photomicrographs illustrating the mode of occurrence of garnet in the quartzofeldspathic portion of the high-Al metapelite. Larger grains or porphyroblasts **(i, j)** occur towards leucosomic portions. Thin layers of finer-grained biotite and sillimanite occur within the quartzo-feldspathic portion **(k, l)**. In comparison to the thicker biotite-sillimanite-cordierite-dominant layers (Figs. 3.1, 3.2), the thin biotite-sillimanite-rich layers do not contain cordierite. Nearer to the thin biotite-sillimanite-rich layers, polygonal granoblastic texture with straight line grain margins and 120° triple junction is prominent in the quartzofeldspathic portion. (g), (i), (k) taken under PPL; (h), (j), (l) taken under XPL.

Feldspar in the quartzofeldspathic portion/layer is dominantly K-feldspar, with quartz grains exhibiting undulatory extinction (Figs. 3.5, 3.6). Quartz and feldspar grains towards the leucosomic portions are characterized by medium- to coarse-grain size and lobate rounded grain margins (Fig. 3.6).

Thin (<0.05 mm) layers of finer-grained biotite and sillimanite occur within the quartzo-feldspathic portion (Figs. 3.5k, l). In comparison to the thicker biotite-sillimanite-cordierite-dominant layers (Figs. 3.1, 3.2), the thin biotite-sillimanite-rich layers (Figs. 3.5k, l) do not contain cordierite. Nearer to the thin biotite-sillimanite-rich layers, polygonal granoblastic texture with straight line grain margins and 120° triple junction is prominent in the quartzofeldspathic portion (Figs. 3.5k, l). Away from it, lobate rounded grain margins become prominent in the quartzofeldspathic portion (Fig. 3.6). Lobate rounded grain margins are primarily seen between the felsic minerals (quartz-quartz, quartz-feldspar) and their contact with the mafic minerals, especially garnet (Figs. 3.5, 3.6). Similar lobate rounded grain margins characterize the minor felsic minerals seen in the aluminous layers (Figs. 3.1, 3.2). Biotite is the dominant inclusion phase in the quartzofeldspathic portion, occurring in both quartz and feldspar. Quartz and feldspar inclusions occur in each other. Myrmekite and microcline occur locally in the quartzofeldspathic layers, especially towards the leucosomic portions. Minor Fe-Ti oxides are irregularly distributed, but have an affinity with biotite and garnet. Relatively finer-grained biotite-sillimanite rich layers, similar to that shown in Figs. 3.5k and l, characterize the contact with leucosomic material, with the quartzofeldspathic portion medium-grained near the contact.

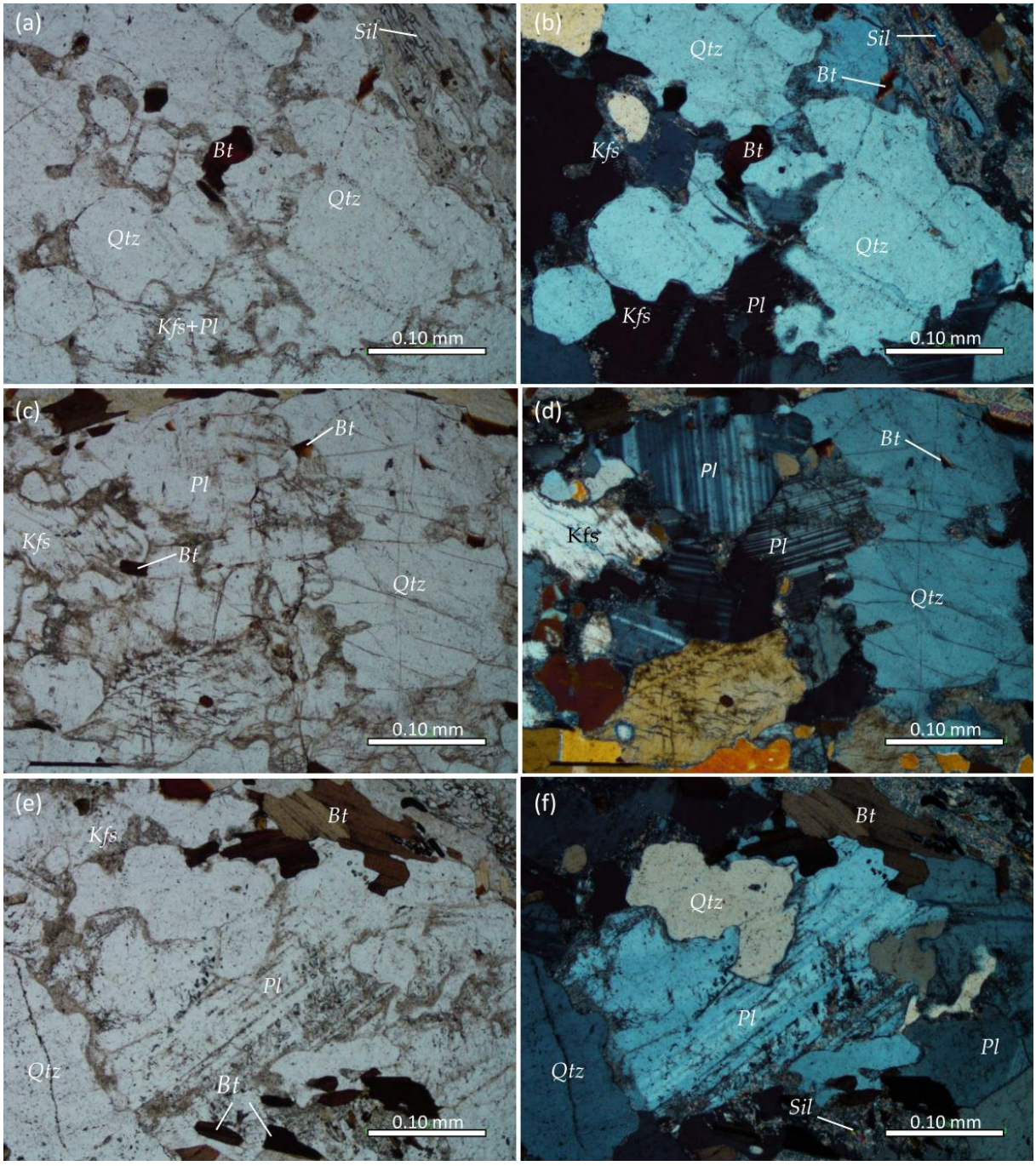


Figure 3.6. Photomicrographs illustrating the mode of occurrence of minerals in the transition zone from the quartzofeldspathic portion to the leucosomic portions associated with the high-Al metapelite. Lobate rounded grain margins are prominent. Notice the medium-grain size in the set of images show on this page, and the coarse-grain size in the set of images shown on the next page. (a), (c), (e) taken under PPL; (b), (d), (f) taken under XPL.

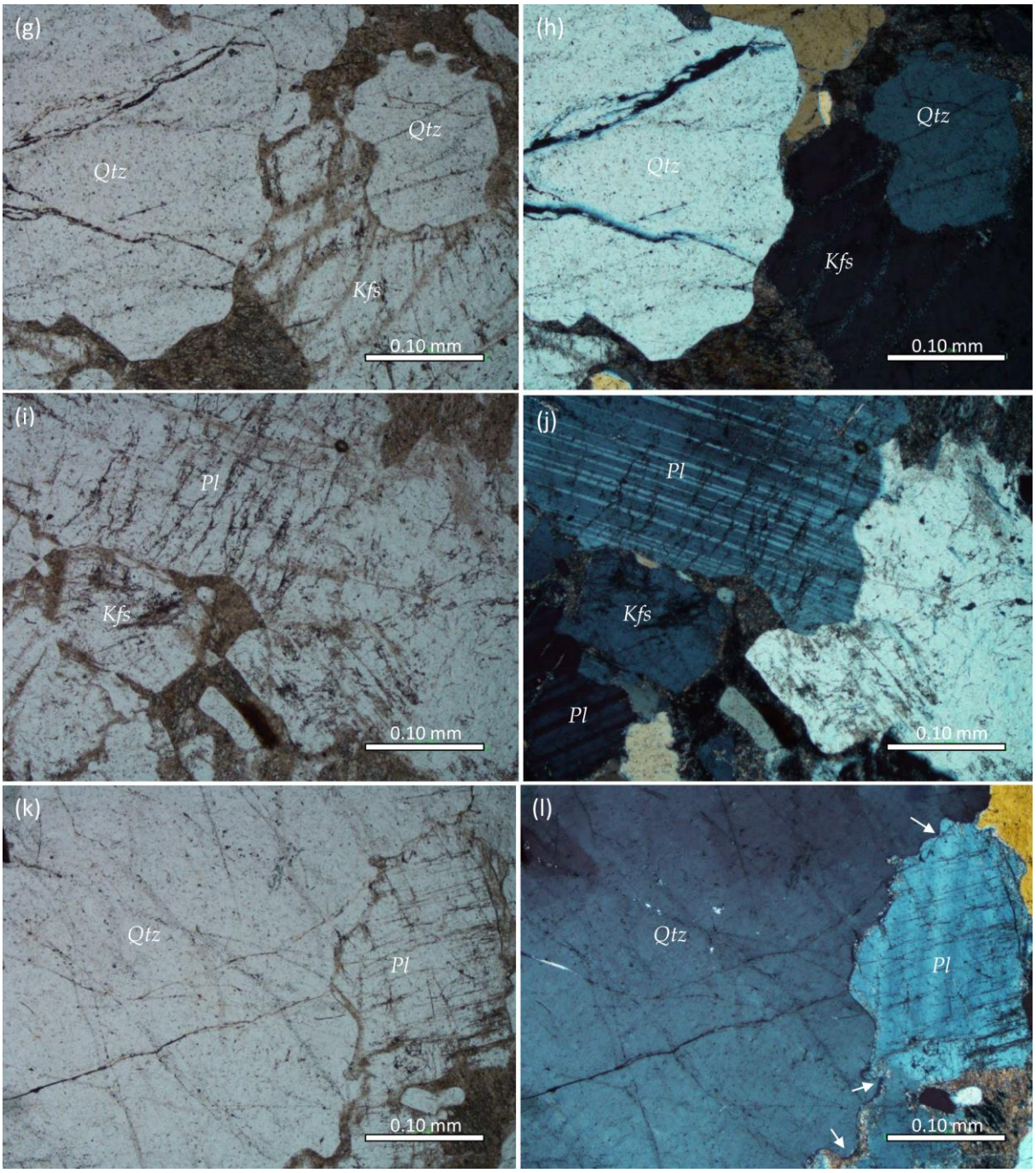


Figure 3.6. continued. Photomicrographs illustrating the mode of occurrence of coarse-grained felsic minerals found towards the leucosomic portions associated with the high-Al metapelite. Lobate rounded grain margins are prominent. Plagioclase starts to become the dominant feldspar. Sericite alteration associated with feldspar can be seen. (g), (i), (k) taken under PPL; (h), (j), (l) taken under XPL.

Regarding the petrographic characterization of the leucosomes associated with the high-Al metapelite, samples from large irregular discordant leucosomes from the O6-19 outcrop (see Fig. 2.1) were used. These leucosomes are characterized by large garnet crystals (Figs. 2.6, 3.7). Unlike the leucocratic layers of the high-Al metapelite, where medium-grained K-feldspar and quartz dominates, the leucosomes are dominated by coarse-grained plagioclase and quartz (Fig. 3.8). Plagioclase is sericitized and quartz commonly shows undulatory extinction. Lobate rounded grain margins between the felsic minerals are conspicuous (Fig. 3.8). Large garnet crystals occur either as rounded grains or as irregular network of grains, both exhibiting prominent lobate grain margins (Figs. 3.7, 3.8). Minor biotite occurs.

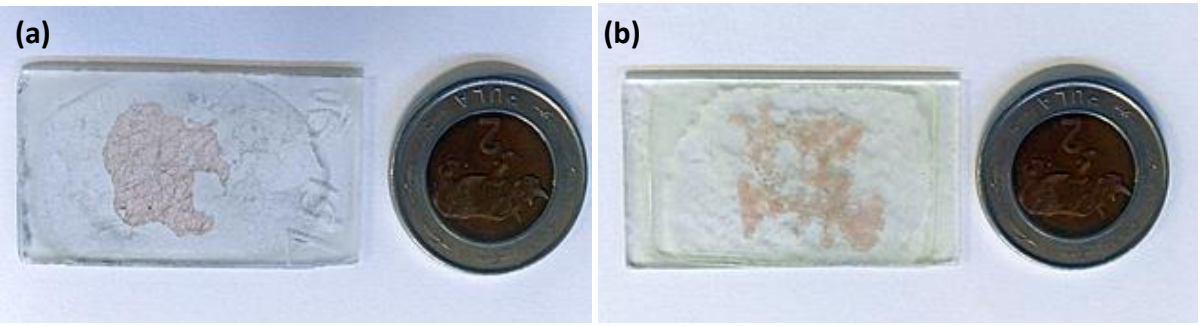


Figure 3.7. Representative images of thin sections made from samples of discordant leucosomes associated with high-Al metapelite at the O6-19 outcrop. The typical mode of occurrence of the large pink garnet grains in the leucosomes is shown. Photomicrographs of part of the garnet in (a) is shown in Fig. 3.8. The 2 pula coin has a 27 mm diameter.

3.2.2. Low-Al metapelite and associated leucosomes

In comparison to the high-Al variant, the low-Al metapelite has more quartzofeldspathic portion. Biotite is the dominant mafic mineral. Aligned biotite and more or less elongated quartzofeldspathic grains define the fabric in the rock (Fig. 3.9).

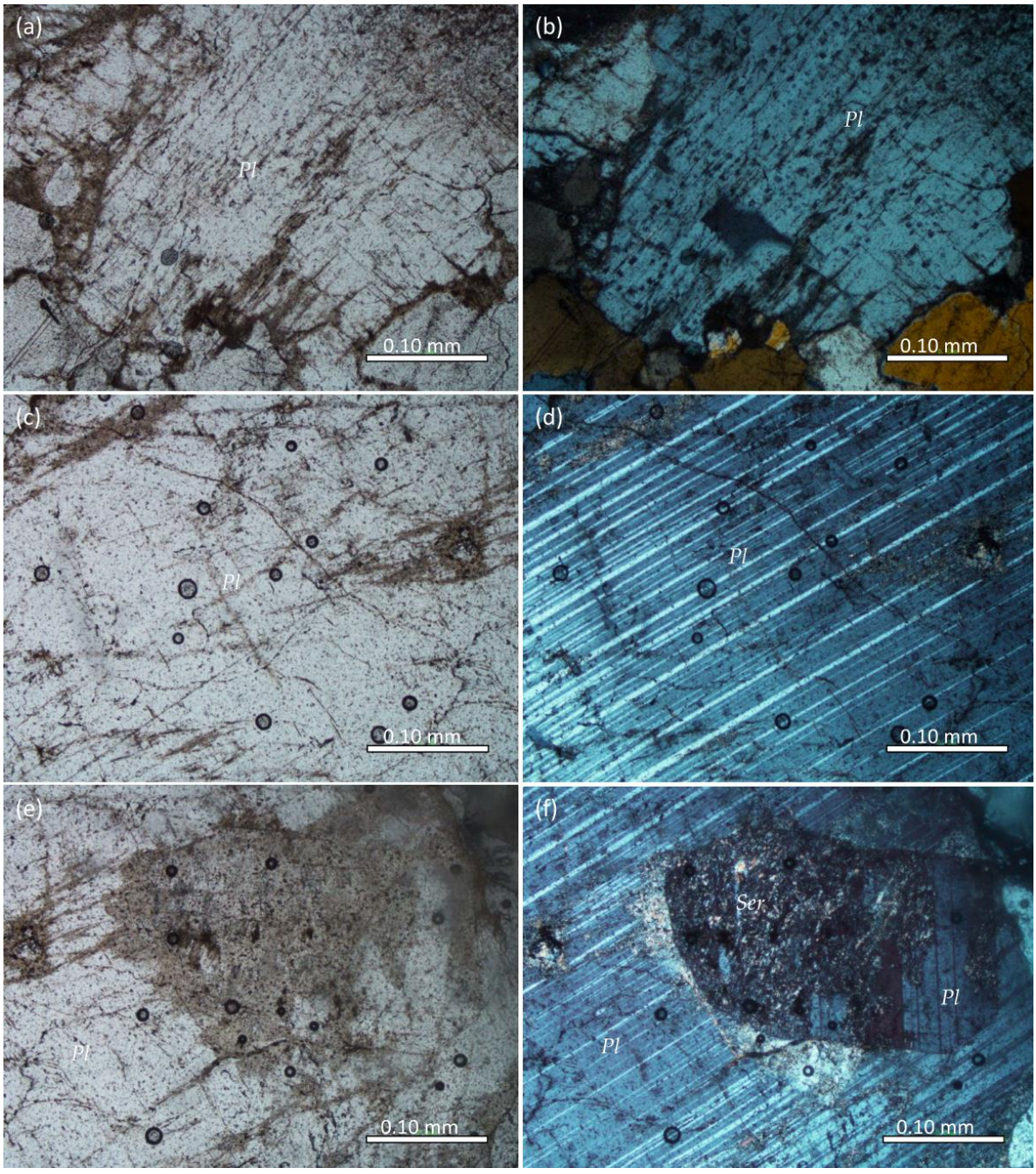


Figure 3.8. Photomicrographs illustrating the mode of occurrence of minerals in the discordant leucosome with large garnet crystals associated with the high-Al metapelite at the O6-19 outcrop. Unlike the metapelite, the dominant feldspar in the leucosomes is plagioclase feldspar. Plagioclase is sericitized. Lobate rounded grain margins are conspicuous. (a), (c), (e) taken under PPL; (b), (d), (f) taken under XPL.

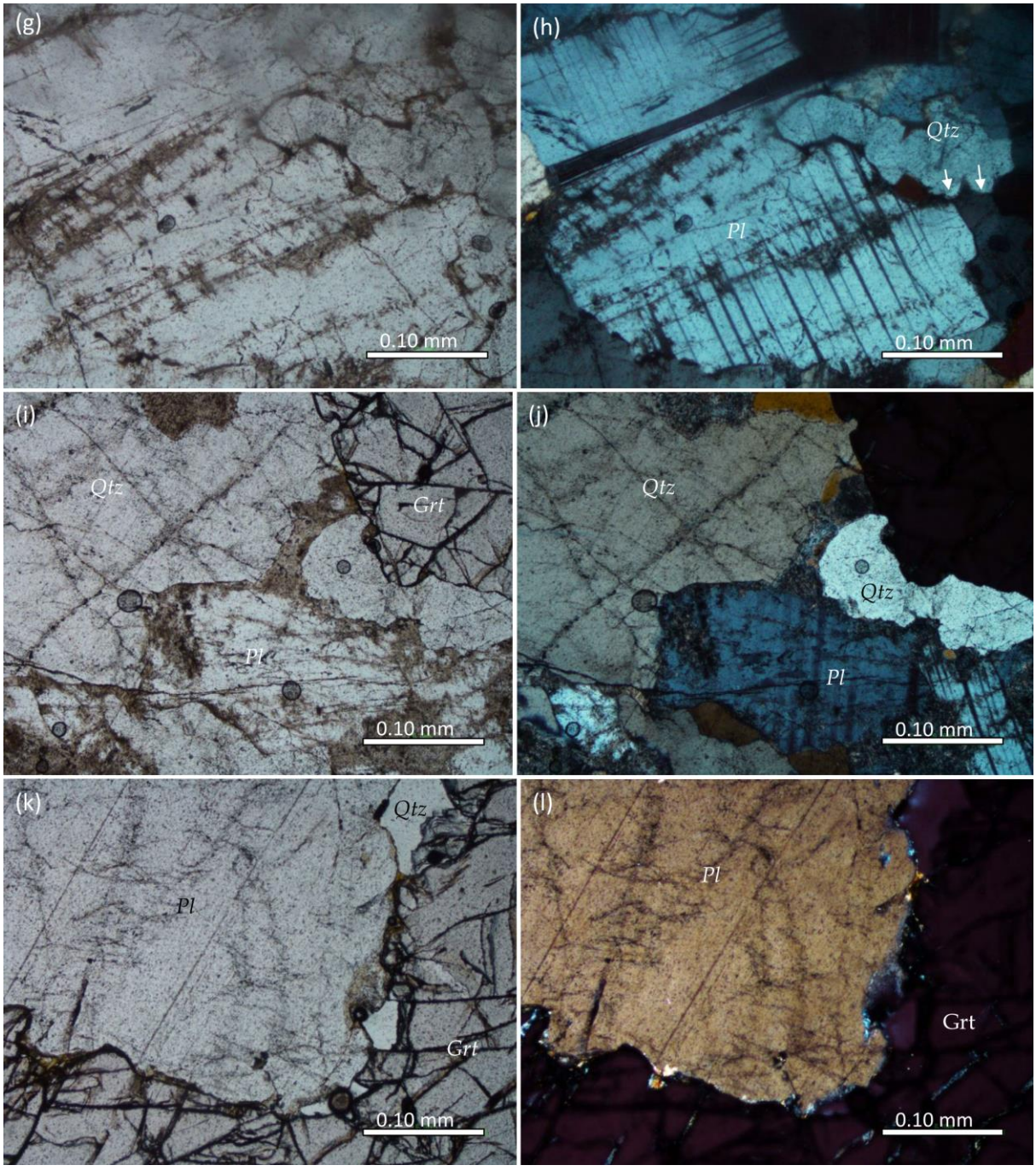


Figure 3.8. continued. Photomicrographs illustrating the mode of occurrence of minerals in the discordant leucosome with large garnet crystals associated with the high-Al metapelite at the O6-19 outcrop. Feldspar is commonly altered (sericitized), while quartz shows undulatory extinction. Lobate rounded grain margins are prominent. The garnet crystal shown in (k, l) is the margin of the garnet shown in full in Fig. 3.7a. The abnormal inference color of feldspar is due to the fact that the concerned thin section was deliberately made thick (see Fig. 3.7a) to avoid losing parts of the large garnet grains during polishing. (g), (i), (k) taken under PPL; (h), (j), (l) taken under XPL.

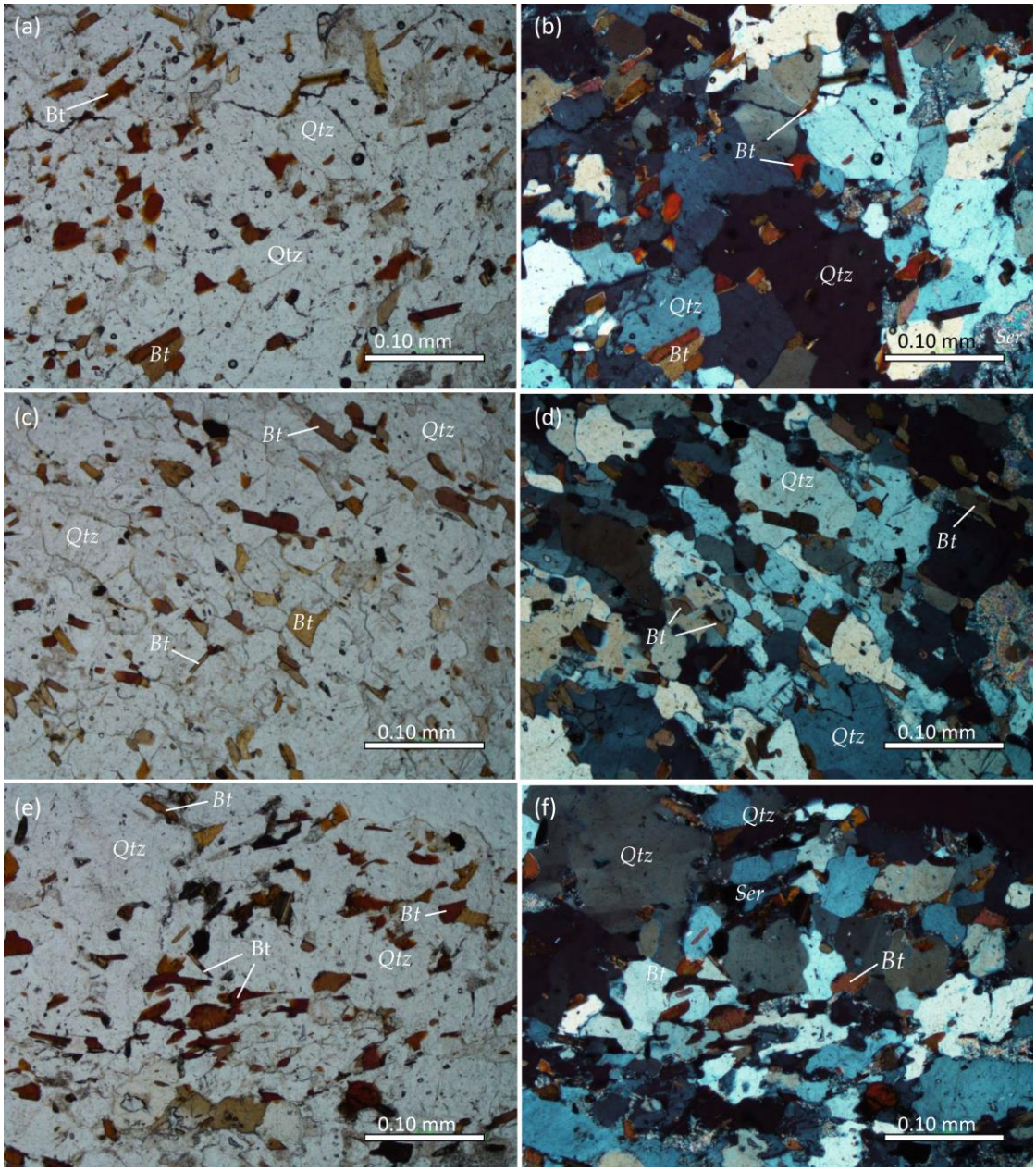


Figure 3.9. Photomicrographs illustrating the mode of occurrence of biotite in the low-Al metapelite. Aligned biotite and more or less elongated quartzofeldspathic grains define the fabric in the rock. In comparison to the high-Al metapelite, there is more quartzofeldspathic portion in the low-Al metapelite. (a), (c), (e) taken under PPL; (b), (d), (f) taken under XPL.

Minor sillimanite and cordierite occur associated with biotite in the quartzofeldspathic portions (Fig. 3.9). Aluminous layers or patches with sillimanite and cordierite occur in the

low-Al metapelite (Fig. 3.10). But unlike the prominent thicker aluminous layers in the high-Al metapelite, the yellow-brown layers/patches in the low-Al metapelite are thinner (<0.05 mm) and are almost devoid of biotite (Fig. 3.10). Cordierite alteration is prominent with pinite and sericite variants, and encompasses sillimanite. Sillimanite dominantly occurs as prismatic crystals and less dominantly as fibrous needle-like crystals. Sillimanite is generally concentrated in the central portion of aluminous layers/patches (Fig. 3.10). When present, biotite dominantly occurs along the margins of aluminous layers. Elongated felsic minerals with lobate grain margins commonly permeate into the thin aluminous layers (Fig. 3.10). Very thin (<0.01 mm) layers of finer-grained biotite and sillimanite occurs locally associated with the cordierite-sillimanite-dominant layers (Figs. 3.10c, d). These layers are thinner than similar layers occurring in the high-Al metapelite.

Like in the high-Al metapelite, garnet is locally associated with the thin aluminous layers/patches in the low-Al metapelite (Figs. 3.10e, f, 3.11). These garnet grains are prominently associated with cordierite alteration, into which they occur either as discordant (more or less penetrating) grains or elongated grains parallel to the length of the layers (Figs. 3.11). Locally, the alteration associated with cordierite can surround the garnet grain (Figs. 3.11e, f). When present, inclusions in garnet include quartz and sillimanite (Fig. 3.11). Both straight and lobate rounded grain margins are shown by garnet grains associated with aluminous layers/patches (Fig. 3.11). Garnet dominantly occurs as porphyroblasts associated with quartzofeldspathic minerals (Fig. 3.12).

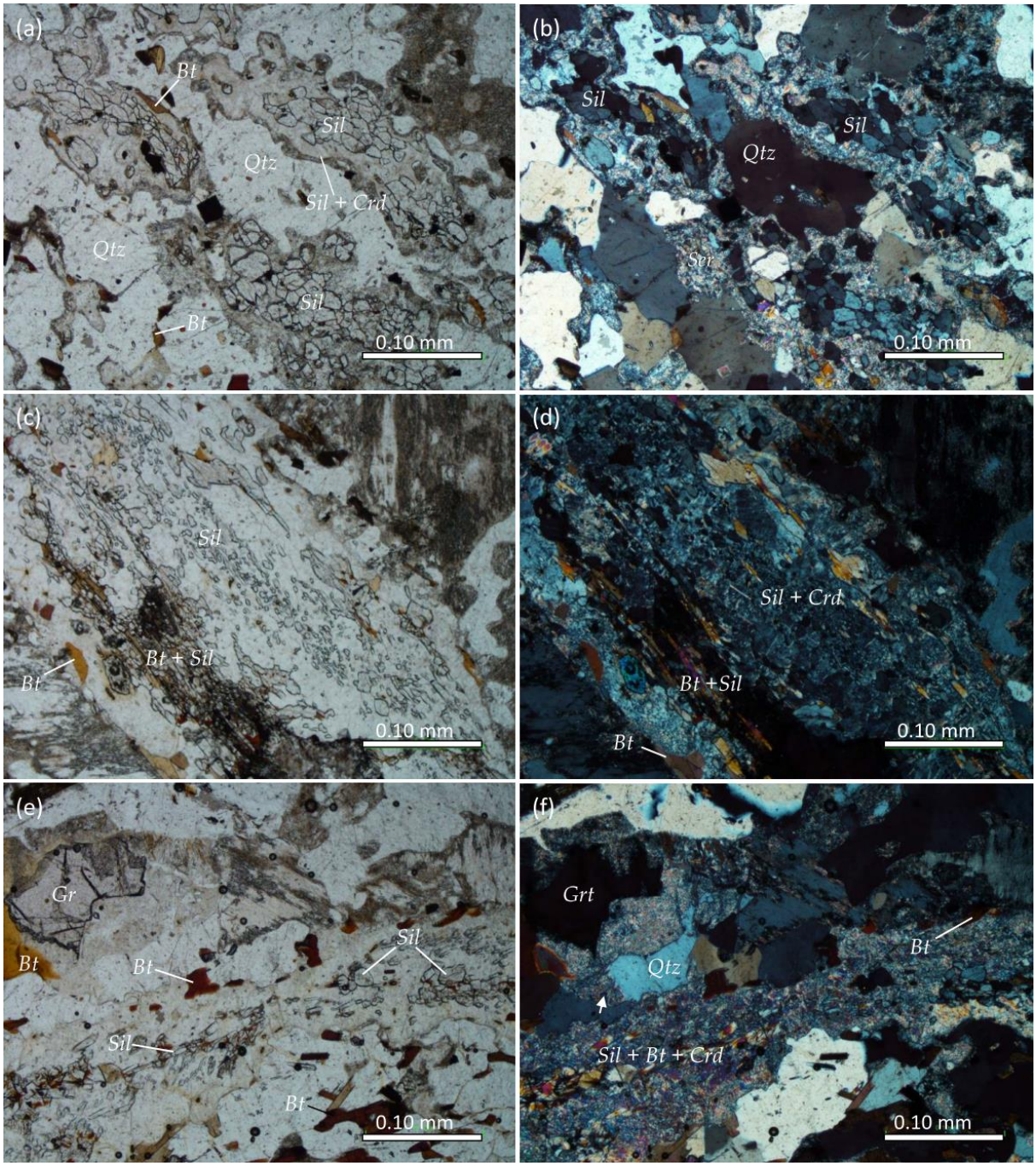


Figure 3.10. Photomicrographs illustrating the mode of occurrence of aluminous layers in the low-Al metapelite. Unlike the thicker layers in the high-Al metapelite (Figs. 3.1, 3.2), the aluminous layers in the low-Al metapelite are thinner and less prominent. Cordierite is altered, forming the yellow-brown layers/patches. Sillimanite is generally concentrated in the central portion of the aluminous layers. Elongated felsic minerals with lobate grain margins commonly penetrate into the thin aluminous layers. Like the high-Al metapelite, layers of finer-grained biotite and sillimanite occur in the low-Al metapelite, but are comparatively thinner **(c, d)**. Garnet is local associated with the aluminous layers. (a), (c), (e) taken under PPL; (b), (d), (f) taken under XPL.

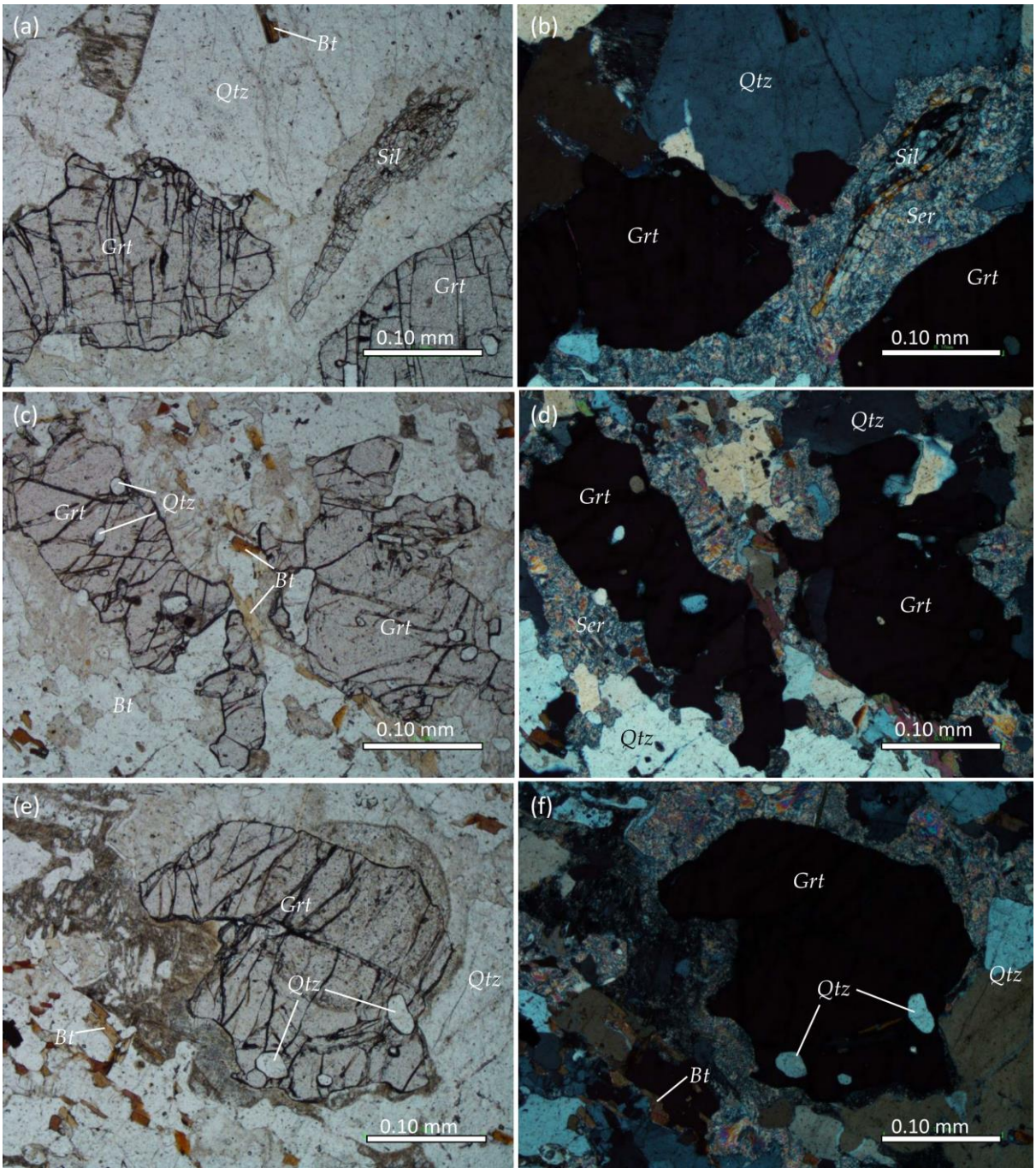


Figure 3.11. Photomicrographs illustrating the association of garnet with aluminous layers/patches in the low-Al metapelite. Cordierite is altered exhibiting both pinite and sericite variants. The garnet grains occur either as discordant (more or less penetrating) grains or elongated grains parallel to the length of the layers. Locally, the alteration associated with cordierite can surround the garnet grain. When present, inclusions in garnet include quartz and sillimanite. Both straight line and lobate rounded grain margins are shown by garnet grains. (a), (c), (e) taken under PPL; (b), (d), (f) taken under XPL.

The garnets range from small irregular commonly elongated grains associated with medium-grained quartz and feldspar. The large garnet porphyroblasts are associated with coarse-grained felsic minerals (Fig. 3.12) towards the leucosomic portions associated with low-Al metapelite. When present, inclusions in these garnets include quartz, biotite and sillimanite (Fig. 3.12). These garnet grains exhibit both straight line and lobate rounded grain margins with the adjacent felsic minerals (Fig. 3.12). In general, garnet is fewer in the low-Al metapelite than in the high-Al metapelite.

Regarding the quartzofeldspathic portion, both K-feldspar and plagioclase feldspar is prominent in the low-Al metapelite (Fig. 3.13). Plagioclase feldspar is dominant than K-feldspar. Quartz typically shows undulatory extinction. The grain size of quartzofeldspathic minerals vary from medium- to coarse-grained, the latter occurring towards the leucosomic portions associated with the low-Al metapelite (Fig. 3.13). Feldspar (sericite) alteration is prominent (Fig. 3.13). Perthite and myrmekite occurs locally (Fig. 3.13). Both straight and lobate rounded grain margins occur, with the latter becoming prominent in the coarse-grained leucosomic portions (Fig. 3.13).

In summary, both high-Al and low-Al metapelites are characterized by three domains – restitic, quartzofeldspathic, and leucosomic. Both restitic domains/layers and quartzofeldspathic domains/layers are medium-grained and can contain minerals like garnet, sillimanite, cordierite and biotite. The quartzofeldspathic domain contains the aluminous minerals in minor proportion. The medium-grained quartzofeldspathic domain grade into a coarse-grained leucosomic portion. The different domains indicate stages of melt

segregation. The leucosomes *sensu stricto* are coarse-grained quartzofeldspathic rocks with irregular outline and with melanocratic margins. It should be emphasized here that the leucosomic portions on the other hand, have no such melanocratic margins.

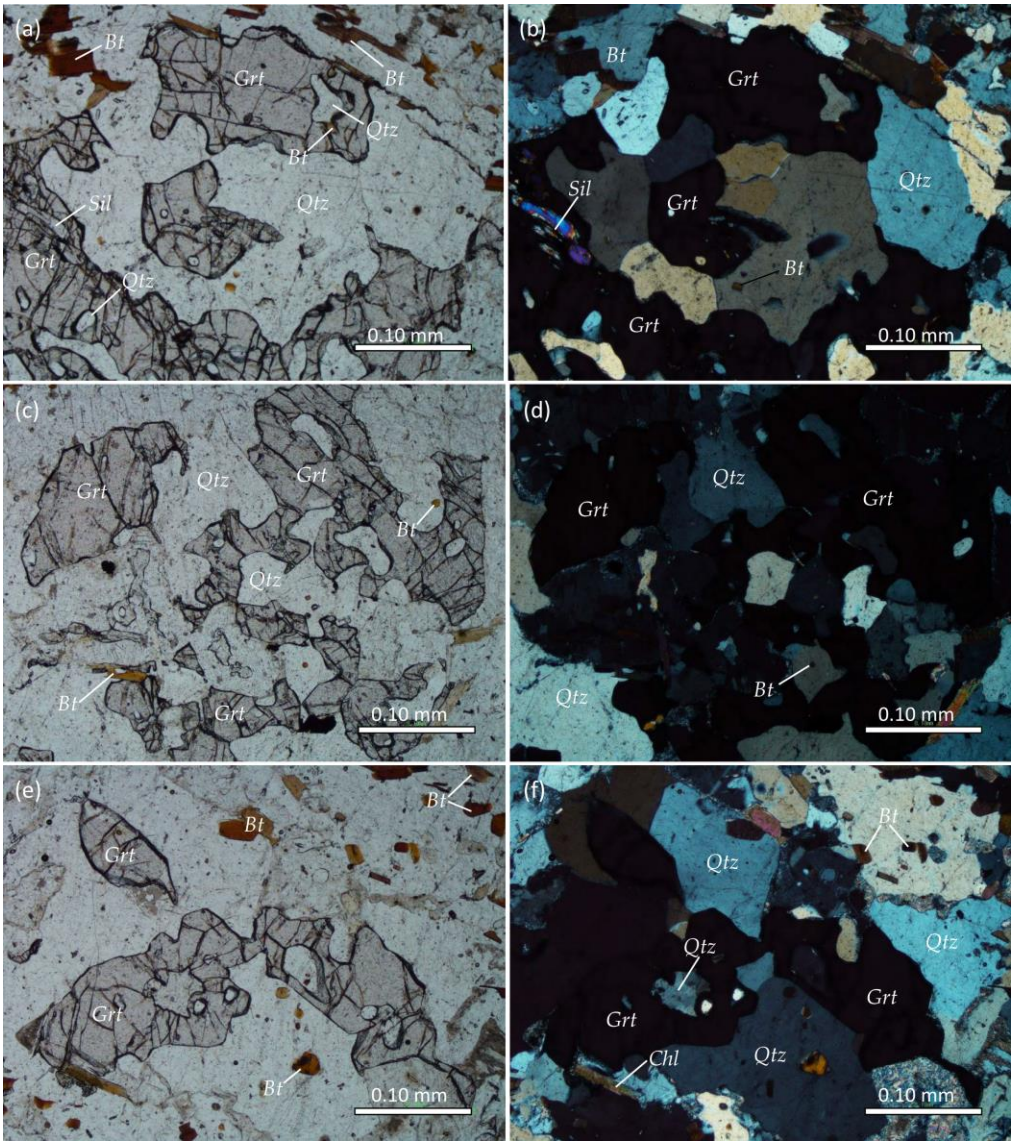


Figure 3.12. Photomicrographs illustrating the dominant mode of occurrence of garnet as porphyroblasts in association with quartzofeldspathic minerals in the low-Al metapelite. Minor association with cordierite alteration can be seen. They range from smaller irregular commonly elongated ones associated with medium-grained quartz and feldspar (images shown on this page), to larger porphyroblasts associated with coarse-grained felsic minerals (images shown on the next page); the latter towards leucosomic portions. When present, inclusions in these garnets include quartz, biotite and sillimanite. (a), (c), (e) taken under PPL; (b), (d), (f) taken under XPL.

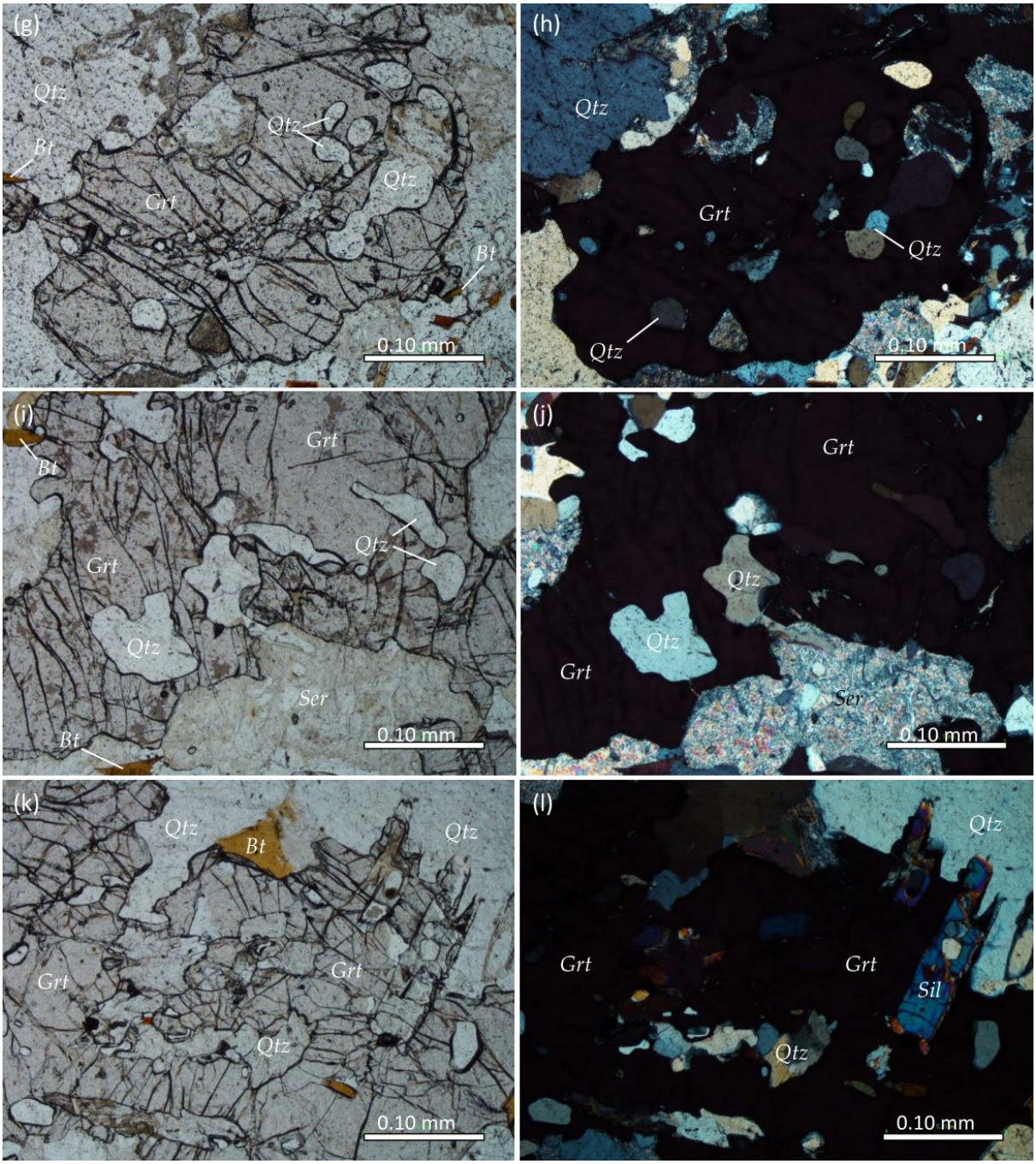


Figure 3.12. continued. Photomicrographs illustrating the mode of occurrence of garnet as large porphyroblasts in association with quartzofeldspathic minerals in the low-Al metapelite. The large garnet grains occur towards the leucosomic portions associated with the low-Al metapelite. (g), (i), (k) taken under PPL; (h), (j), (l) taken under XPL.

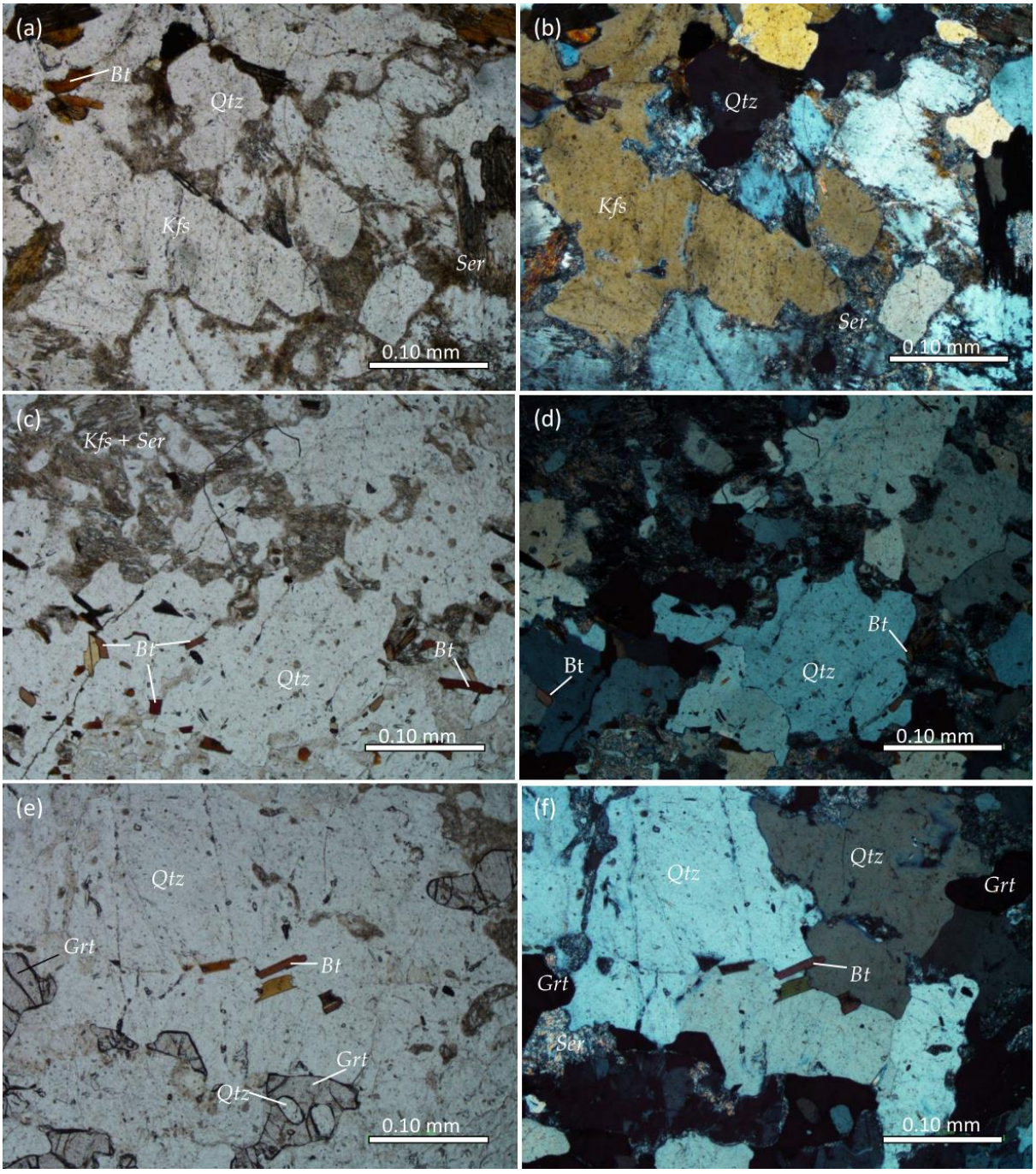


Figure 3.13. Photomicrographs illustrating the mode of occurrence of minerals in the transition zone from the dominantly medium-grained quartzo-feldspathic portion to the coarse-grained leucosomic portion associated with the low-Al metapelite. The low-Al metapelite has more quartzofeldspathic portion than the high-Al metapelite. Both plagioclase and K-feldspar are prominent. Alteration of feldspar is prominent. Both straight line and lobate rounded grain margins occur. (a), (c), (e) taken under PPL; (b), (d), (f) taken under XPL.

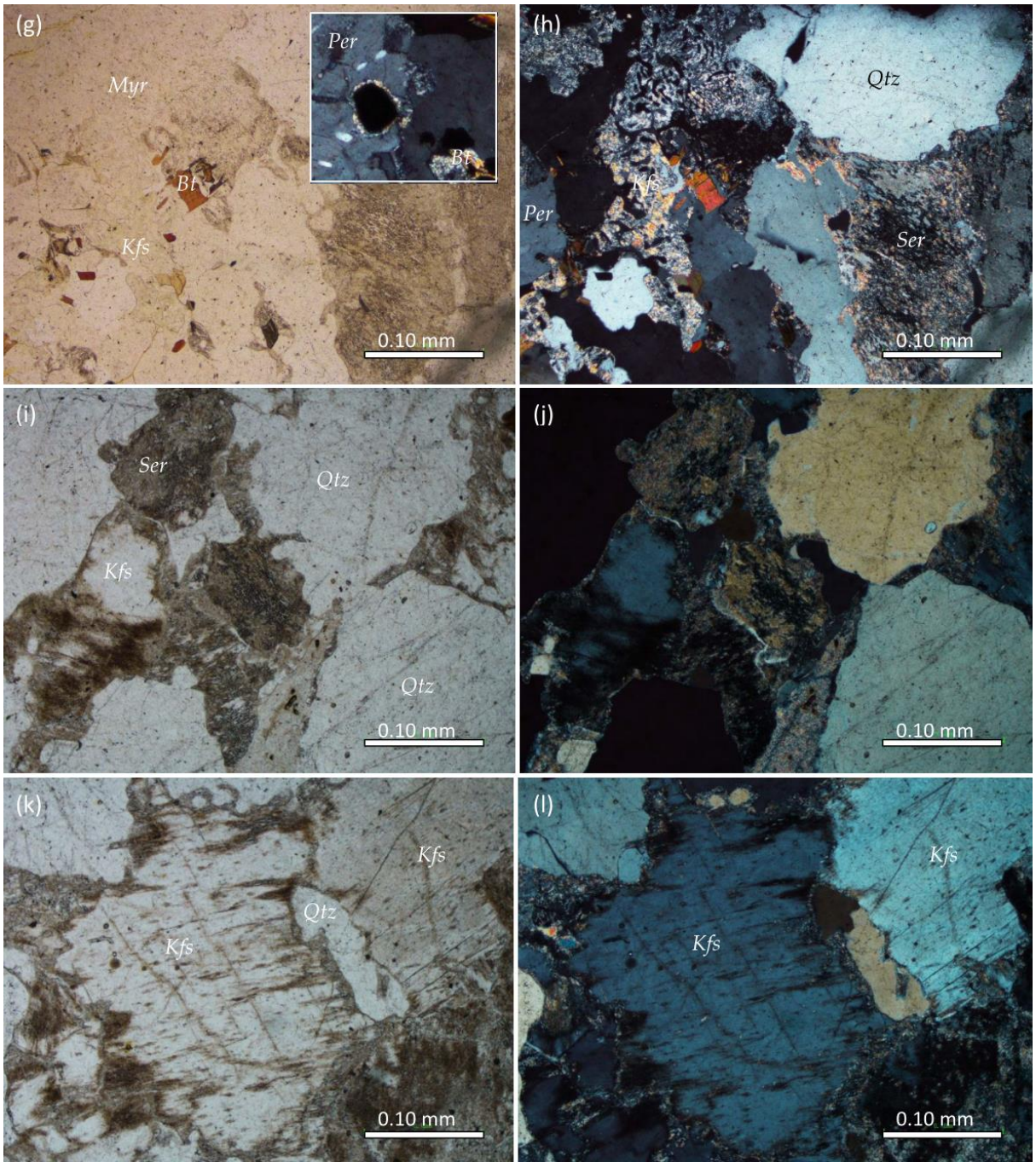


Figure 3.13. continued. Photomicrographs illustrating the mode of occurrence of minerals in the transition zone from the dominantly medium-grained quartzofeldspathic portion to the coarse-grained leucosomic portion associated with the low-Al metapelite. Feldspar alteration is prominent. Perthite and myrmekite occurs locally. Both straight line and lobate rounded grain margins occur. Per – perthite; Inset in (g) showing perthite is taken at the same scale as the main image. (g), (i), (k) taken under PPL; (h), (j), (l) taken under XPL.

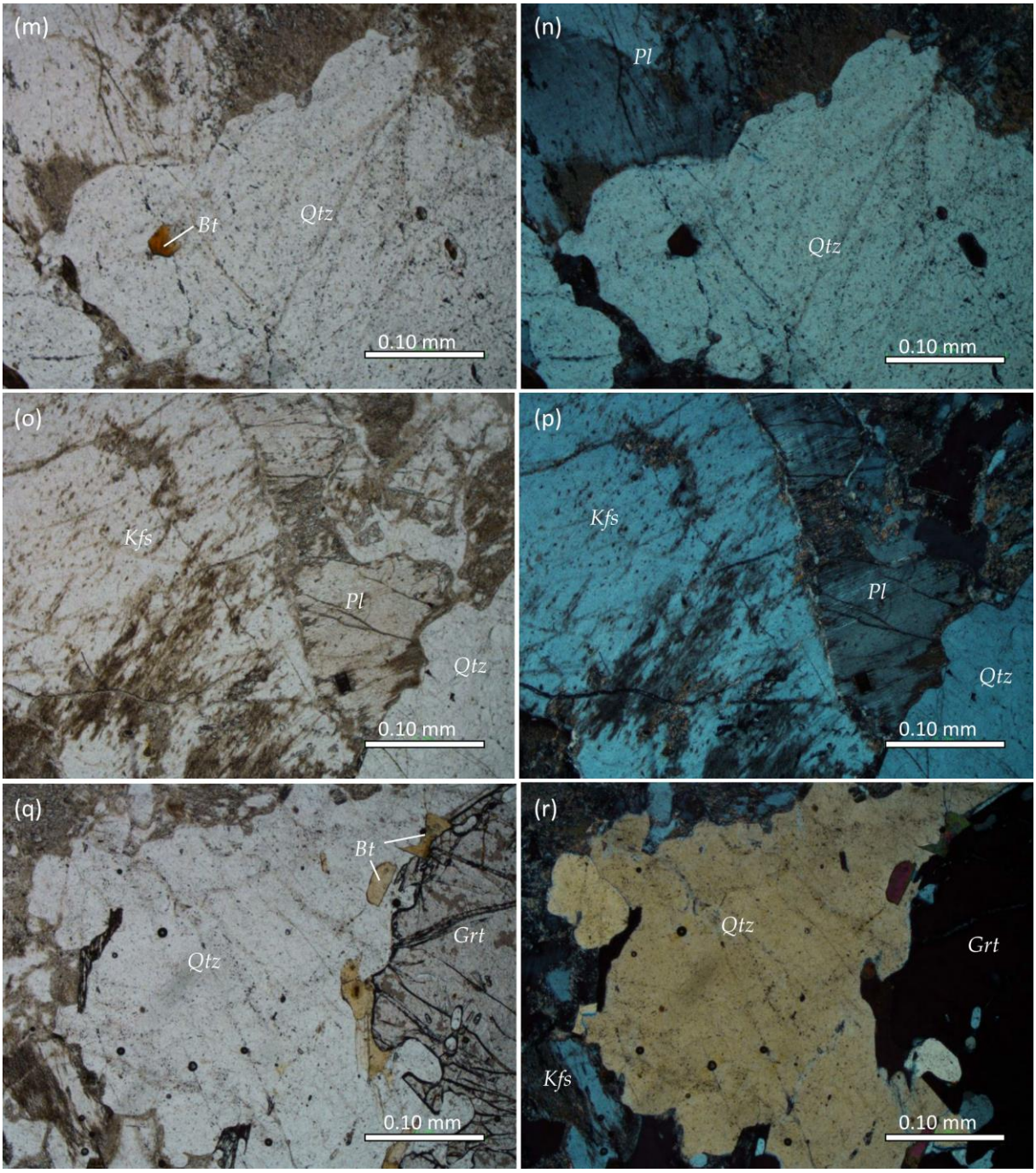


Figure 3.13. continued. Photomicrographs illustrating the mode of occurrence of coarse-grained minerals in the leucosomic portion associated with the low-Al metapelite. Feldspar alteration is prominent. Quartz shows undulatory extinction. Lobate rounded grain margins dominate. Large garnet porphyroblasts occur associated with coarse-grained quartzofeldspathic minerals in the leucosomic portions associated with the low-Al metapelite. (m), (o), (q) taken under PPL; (n), (p), (r) taken under XPL.

3.3. Verbaard granitoid

The Verbaard granitoid is dominantly made up of plagioclase (up to 45 modal %), K-feldspar (up to 20 modal %) and quartz (up to 30 modal %) (Fig. 3.14). Albite twins in plagioclase, perthitic texture and undulatory extinction of quartz are common.

Biotite is the most common mafic mineral, and is commonly interstitial to the felsic minerals (Fig. 3.14). Magmatic texture is obvious in most samples (Fig. 3.14). In some samples, biotite defines a weakly visible gneissic fabric (Figs. 3.14, 3.15). Elongated quartz and feldspar (Figs. 3.15a, b) further enhance the gneissic fabric. Biotite inclusions occur in the felsic minerals (Fig. 3.15). Quartz and feldspar occur as inclusions in each other (Fig. 3.15). Both straight line and lobate rounded grain margins occur (Figs. 3.14 to 3.16), the former prominently associated with the primary magmatic texture. Irregular grain margins protruding into the adjacent grain were observed between quartz-plagioclase, quartz-K-feldspar and quartz-quartz. Close observation reveals that the penetration of the lobate rounded grain margins postdate the preserved straight line grain margins (Figs. 3.14 to 3.16), and are likely related to the anatectic overprint. Alteration of feldspars to sericite is prominent (Fig. 3.16). Minor Fe-Ti oxides occur.

Garnet has two modes of occurrence in the Verbaard granitoid (Figs. 3.16 to 3.18). In addition to the dominant occurrence as large porphyroblasts in leucocratic veins (Fig. 3.18), garnet also occurs locally as small grains in the matrix of the Verbaard granitioid (Figs. 3.16, 3.17). Small garnet grains were only found in a few of the studied Verbaard granitoid samples, and occur either as irregular elongated grains associated with elongated

quartzofeldspathic portions (Figs. 3.17a, b) or as idiomorphic grains (Figs. 3.17c to f). When present, the inclusions include quartz and minor biotite (Fig. 3.17). Larger garnet porphyroblasts occur in the leucocratic veins (Fig. 3.18) and contain more inclusions than the relatively smaller garnet grains in the matrix of the Verbaard granitoid (Fig. 3.17).

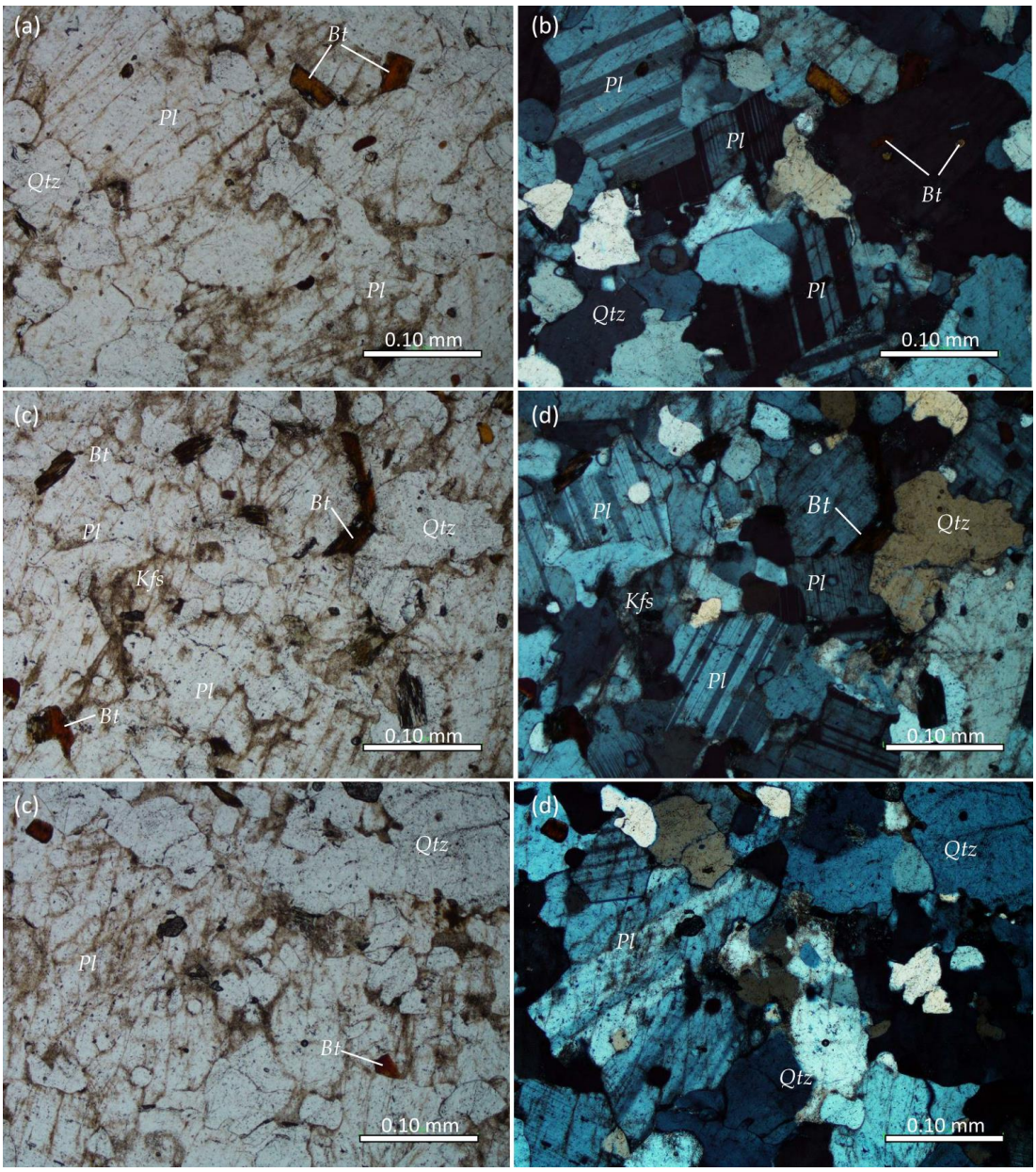


Figure 3.14. Photomicrographs illustrating the mode of occurrence of minerals in the Verbaard granitoid. (a), (c), (e) taken under PPL; (b), (d), (f) taken under XPL.

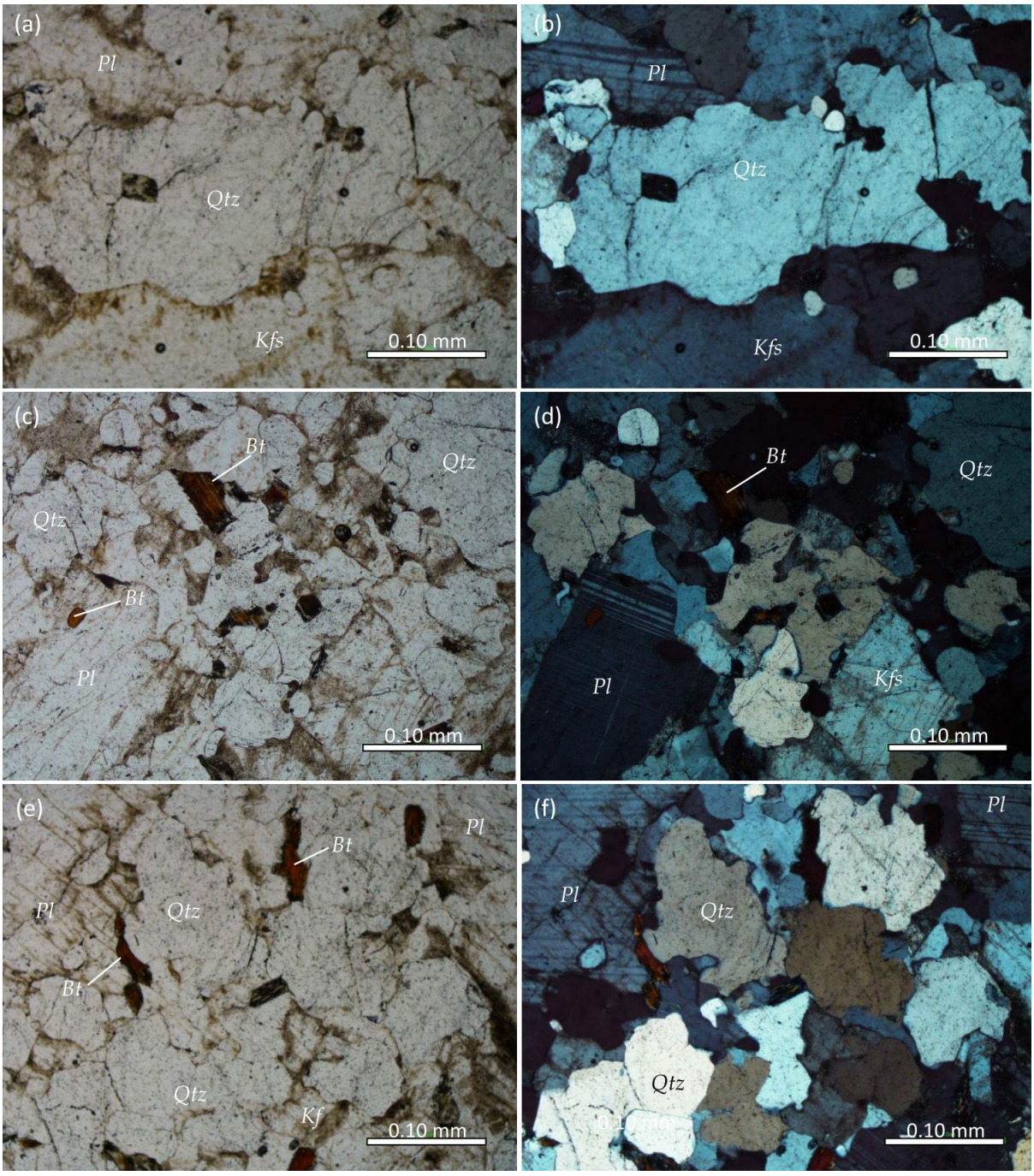


Figure 3.15. Photomicrographs illustrating the mode of occurrence of minerals in the Verbaard granitoid. Locally elongated felsic minerals together with aligned biotite form a feebly visible gneissic fabric. Biotite commonly occurs interstitial to the felsic minerals. Biotite inclusions occur in quartz and feldspar. Quartz and feldspar inclusions occur in each other. Both straight line and lobate rounded grain margins occur. Close observation indicates that the lobate rounded grain margins penetrate the associated straight line grain margins. (a), (c), (e) taken under PPL; (b), (d), (f) taken under XPL.

In comparison to the medium-grained felsic minerals in the Verbaard granitoid, quartz and feldspars in the leucocratic veins are coarse-grained (Fig. 3.18). Perthite and myrmekite occur locally (Fig. 3.18).

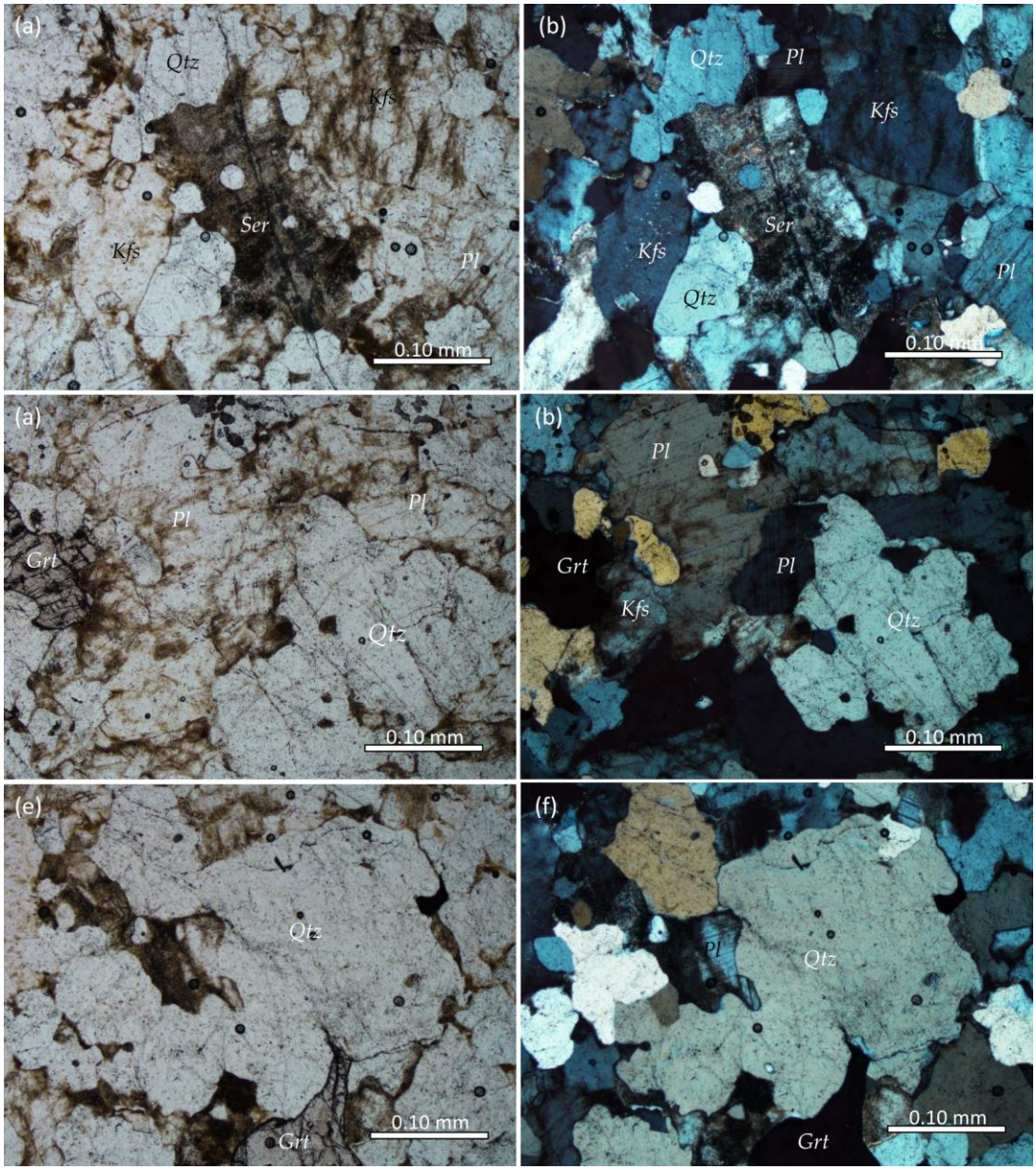


Figure 3.16. Photomicrographs illustrating the mode of occurrence of minerals in the Verbaard granitoid. Alteration of feldspars is prominent. Quartz shows undulatory extinction. Both straight line and lobate rounded grain margins occur. Close observation indicates that the lobate rounded grain margins penetrate the associated straight line grain margins. Small grains of garnet occur in some of the studied Verbaard granitoid samples. (a), (c), (e) taken under PPL; (b), (d), (f) taken under XPL.

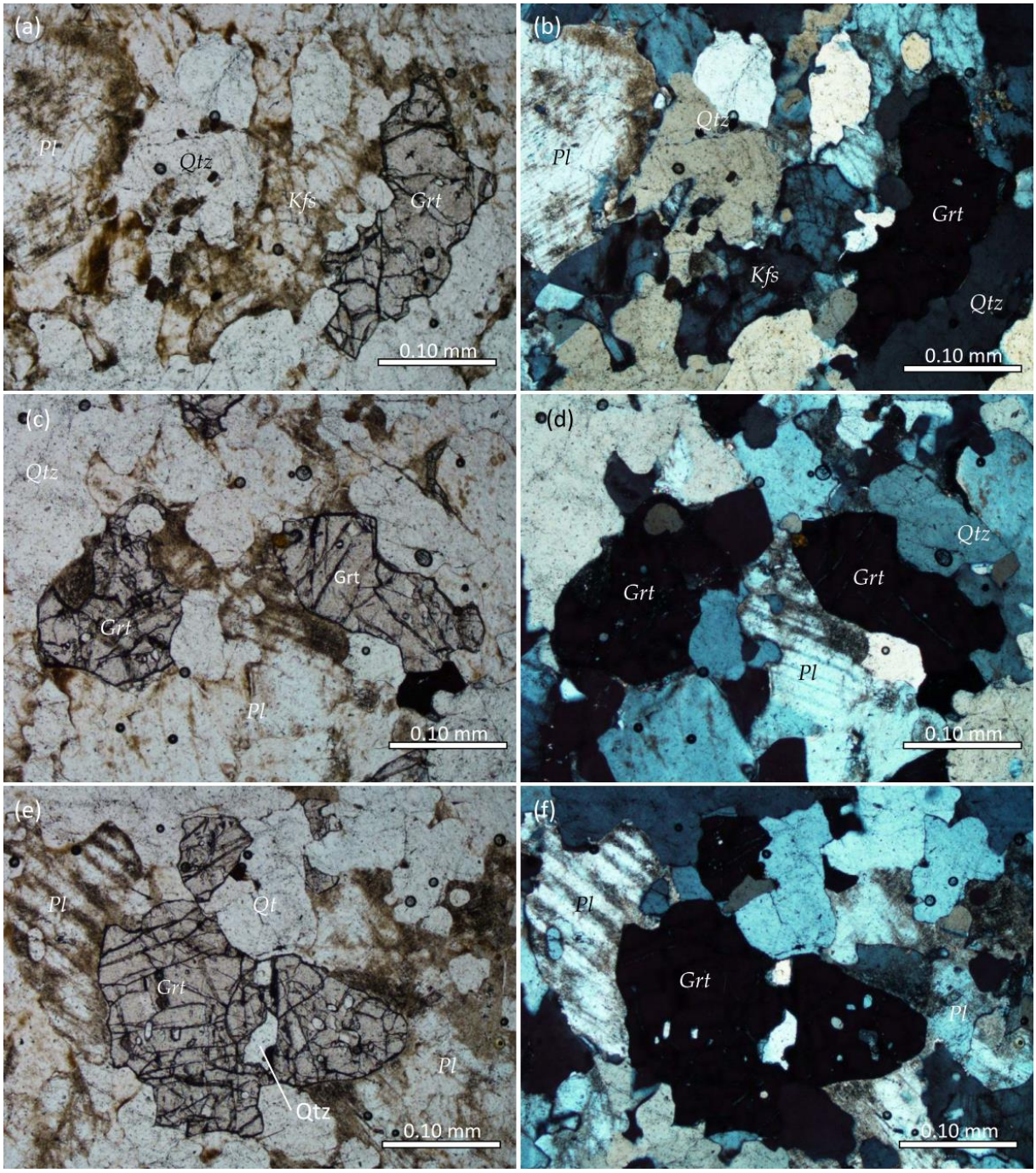


Figure 3.17. Photomicrographs illustrating the mode of occurrence of garnet in the Verbaard granitoid. They occur either as irregular elongated grains associated with elongated quartzofeldspathic portions or as subhedral-anhedral grains. When present, the inclusions include quartz and minor biotite. (a), (c), (e) taken under PPL; (b), (d), (f) taken under XPL.

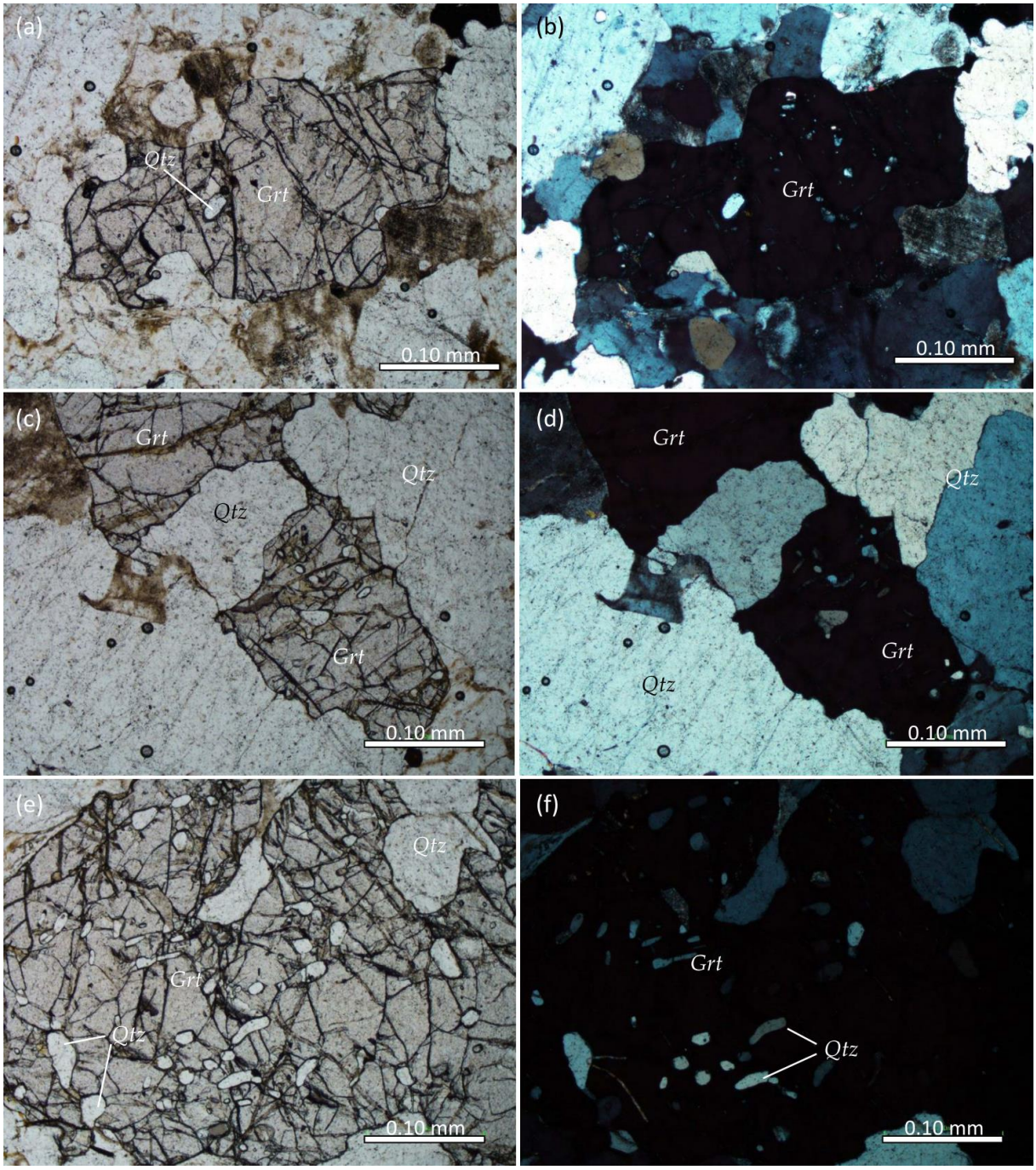


Figure 3.18. Photomicrographs illustrating the mode of occurrence of garnet in the matrix of the Verbaard granitoid **(a to d)** and associated leucocratic veins **(e, f)**. The larger garnet porphyroblasts in (e, f) contain more inclusions than the relatively smaller garnet grains in the matrix of the Verbaard granitoid. (a), (c), (e) taken under PPL; (b), (d), (f) taken under XPL.

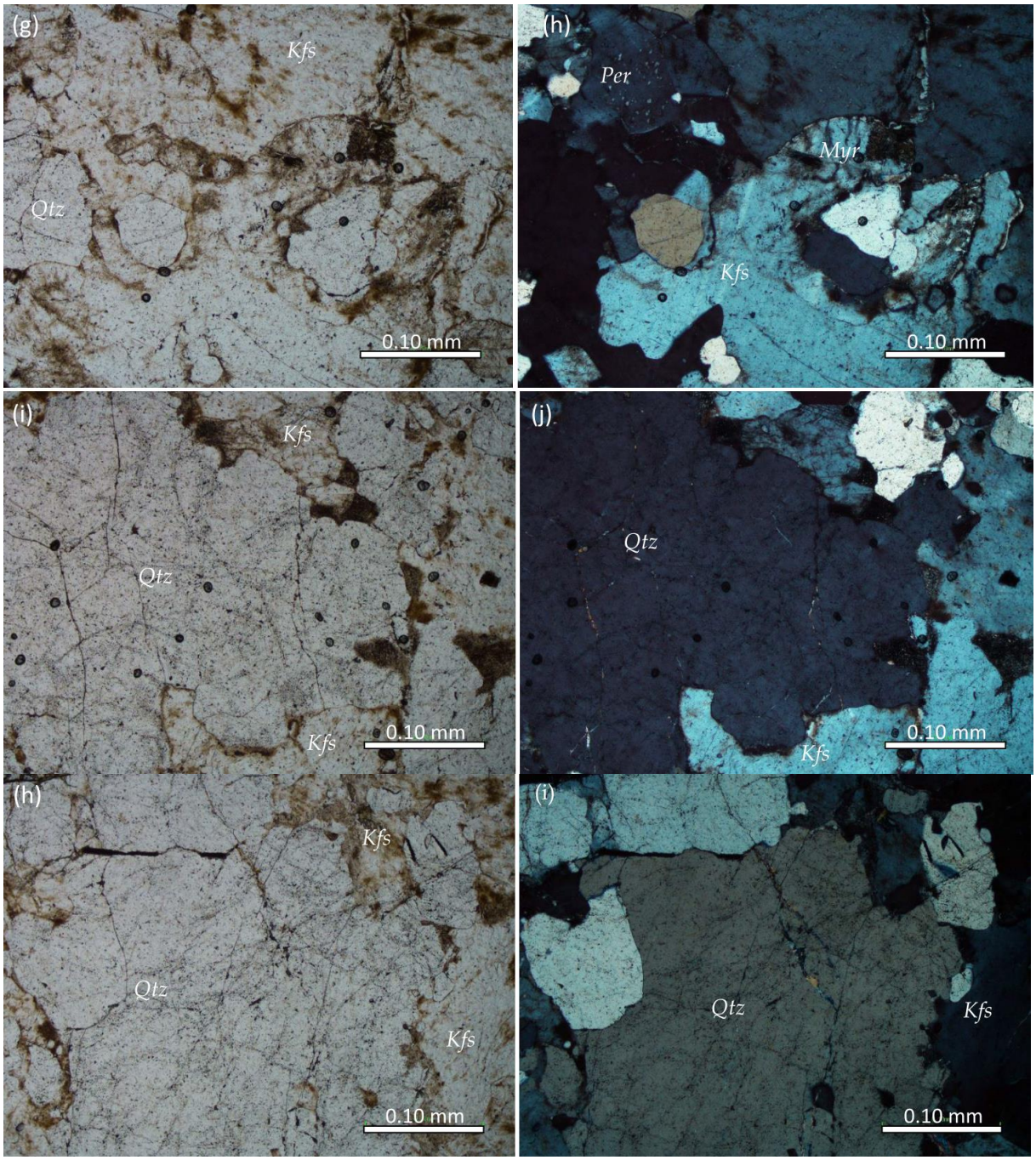


Figure 3.18. continued. Photomicrographs illustrating the mode of occurrence of coarse-grained felsic minerals in the leucocratic veins associated with the Verbaard granitoid. In comparison to the medium-grained felsic minerals in the Verbaard granitioid, quartz and feldspars in the leucocratic veins are coarse-grained. Perthite and myrmekite occurs locally. Myr – myrmekite; (g), (i), (k) taken under PPL; (h), (j), (l) taken under XPL.

3.4. Gabbro

Petrographic characterization of the gabbro is included to highlight the mode of occurrence of garnet associated with it. It should be pointed out that the studied gabbro samples do not contain any visible garnet-bearing leucosomes/leucocratic veins. Gabbro is made up of amphibole (primary magmatic pargasite), orthopyroxene, clinopyroxene and plagioclase, with minor magnetite, ilmenite, pyrite and chalcopyrite (Fig. 3.19). Based on the modal proportions it is an amphibole noritic gabbro. Pyroxene exsolution is common (Fig. 3.19). Alteration is minor, with sericitization of feldspar seen in some samples. Minor biotite and quartz, the latter reaching up to 5 vol.%, were observed locally. Quartz is likely from the assimilation of material from the widespread supracrustal quartzite inclusions within the gabbro layers. Biotite is late occurring along the margins of amphibole, and was observed only in samples collected from a local discrete shear zone.

Garnet occurs locally within the gabbro (Fig. 3.19f). They occur as small grains occurring in the matrix of the gabbro (Fig. 3.19f). These garnet grains do not show any (preferential) association with quartzofeldspathic (melt-related) minerals. It is possible that these small garnets are related to a high-grade metamorphic overprint that affected the gabbro, and not to the anatectic overprint that likely formed garnet in rocks like the Verbaard granitoid and associated leucocratic veins. As garnet occurs along the margins of pyroxene, they could be related, as seen in the meta-ironstone (see section 3.5). The purpose of studying these garnets in the gabbro was to compare them with the small garnet grains that occur within the Verbaard granitoid.

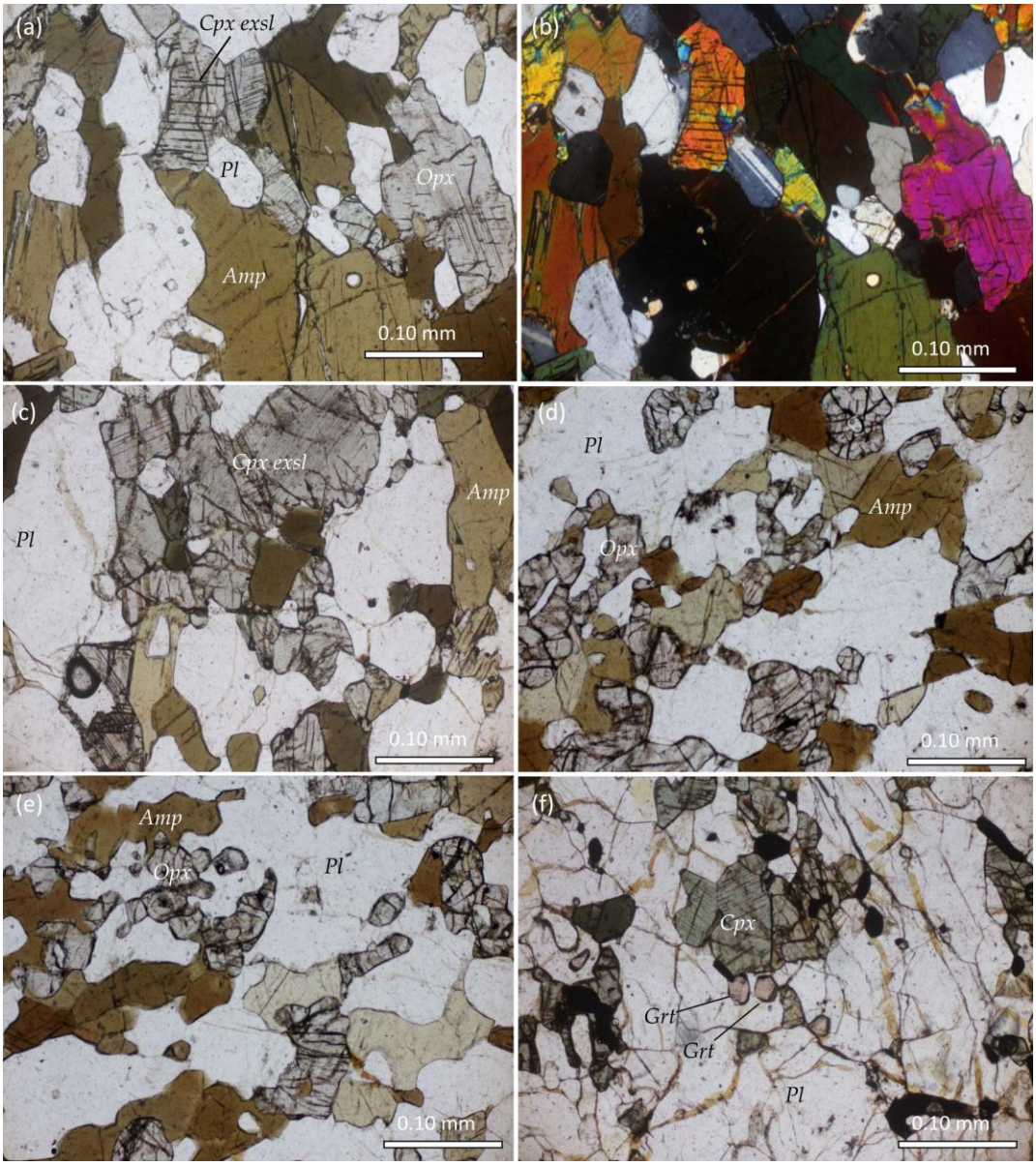


Figure 3.19. Representative photomicrographs illustrating petrographic characteristics of the gabbro. Pyroxenes, amphibole and plagioclase are the dominant minerals. Pyroxene exsolution can be seen. Garnet occurs locally in some samples. Except **(b)**, all the other images taken under PPL. **(b)** – XPL. Opx – orthopyroxene; Cpx – clinopyroxene; Amp – amphibole; exsl – exsolution.

3.5. Meta-ironstone

A passive petrographic study was also carried out on the meta-ironstone with the purpose of understanding the nature of local occurrence of garnet within it. Meta-ironstone

is characterized by alternating coarse-grained quartz-rich layers and conspicuous magnetite-pyroxene-rich layers (Fig. 3.20a). Granoblastic texture is obvious. Although both pyroxenes occur, orthopyroxene predominates (Fig. 3.20b). Magnetite and pyroxenes occur in the quartz-rich layers. Greenish spinel associated with magnetite is widespread in the oxide-pyroxene-rich layers (Fig. 3.20b). Garnet porphyroblasts occur locally and contain inclusions of magnetite and quartz (Fig. 3.20c). In addition, small garnet grains occur along the margin of pyroxenes, and can contain inclusions of pyroxene (Fig. 3.20d). Unlike in the gabbro, both types of garnet exhibit lobate rounded grain margin relations with quartzofeldspathic (melt-like) material (Figs. 3.20c, d).

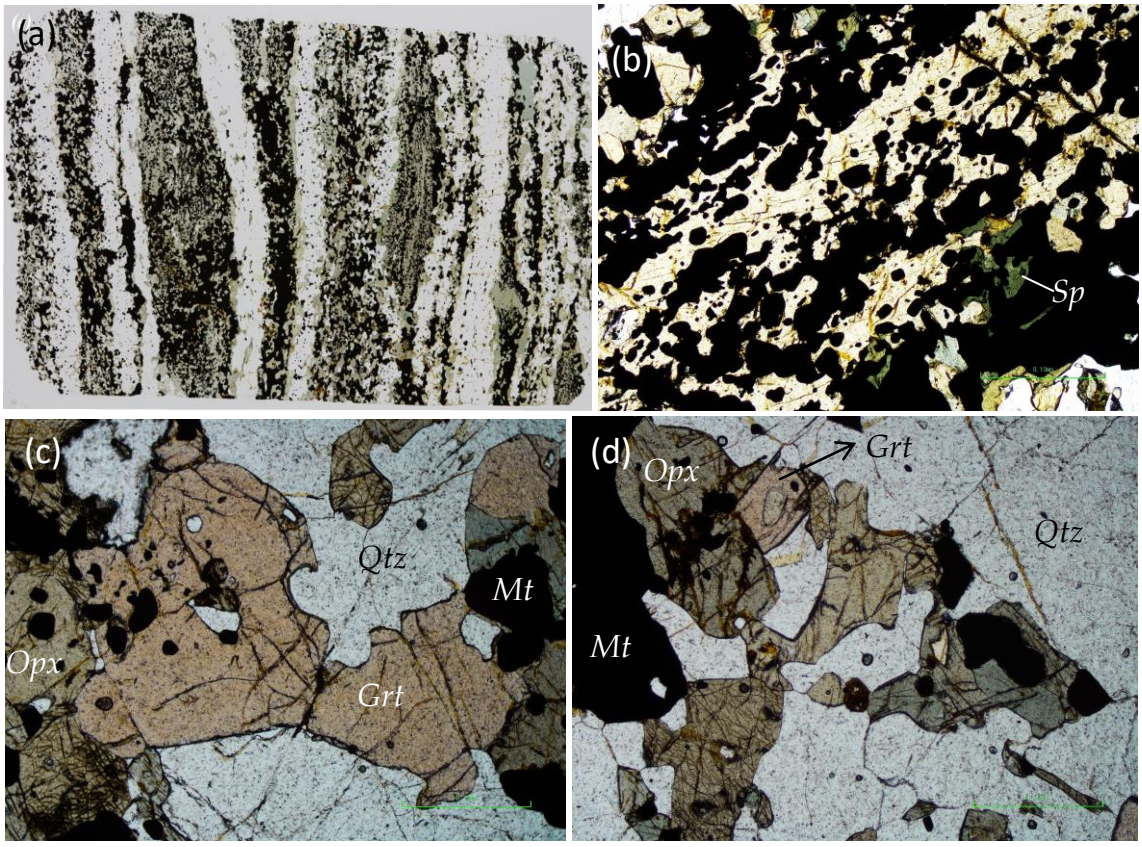


Figure 3.20. Representative image of thin section **(a)** and photomicrographs **(b** to **d)** illustrating the petrographic characteristics of the meta-ironstone from the study area. Sp – spinel; Mt – magnetite.

Chapter 4

Mineral chemical characteristics

4.1. Introduction

This chapter presents chemical characteristics of prominent minerals from the metapelite, associated leucosomes and the Verbaard granitoid from the study area. The main focus is on garnet, followed by biotite and feldspars. Cordierite and sillimanite mineral compositions, where obtained, are included, but are of cursory importance as far as the main focus of the study – to evaluate the provenance of garnet in the Verbaard granitoid. Mineral chemical analyses of garnet from gabbro and meta-ironstone are also presented for comparison. Most electron microprobe analyses of minerals in the rocks are given in tables in the chapter. Mineral chemical data related to microprobe profiling of garnet in leucosome associated with high-Al metapelite at O6-19 is given as appendix material. Representative BSE-SEM images obtained during analyses are included in this chapter. Compositional characteristics of similar minerals from different rocks are presented in a comparative way. As detailed characterization of P-T conditions of metapelites from the Verbaard area has been presented by Perchuk et al. (2008), no attempt in this regard is carried out here.

4.2. Garnet

Large garnet grains with or without inclusions (Fig. 4.1) were targeted for mineral chemical analyses from the metapelites, associated leucosome, the Verbaard granitoid and

associated leucocratic vein. An interesting feature observed while using BSE imaging during mineral chemical analyses was the change in morphology of zircons preserved within or associated with garnet in the different rock types (Fig. 4.1). While zircons in metapelites have irregular rounded morphology (Fig. 4.1a), those in the leucosome associated with the metapelite (Fig. 4.1c), the Verbaard granitoid and associated leucocratic vein start to exhibit subhedral-euhedral outlines.

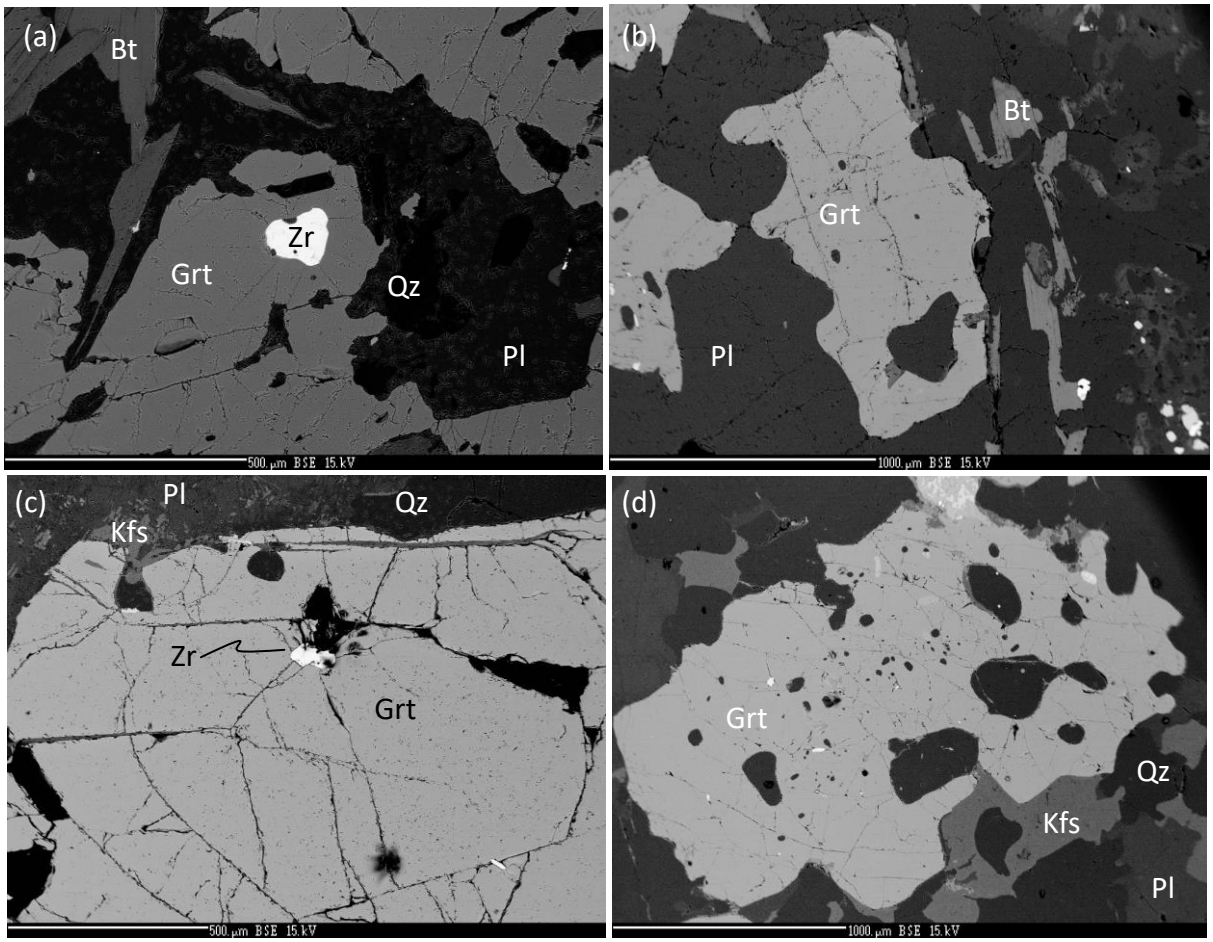


Figure 4.1. Representative BSE images illustrating some of the garnet grains that were subjected to mineral chemical analyses from metapelites **(a, b)**, associated leucosome **(c)** and leucocratic vein associated with the Verbaard granitoid **(d)**. Zr – zircon. While zircons in metapelites have irregular rounded morphology, those in the leucosome and Verbaard granitoid start to exhibit subhedral-euhedral outlines.

Table 4.1. Representative mineral chemical data of garnet in low-Al (LowAl meta) and high-Al (HighAl meta) metapelites from the study area.

Rock	LowAl meta	LowAl meta	LowAl meta	LowAl meta	LowAl meta	LowAl meta	LowAl meta	LowAl meta	LowAl meta	LowAl meta	LowAl meta	LowAl meta
SiO_2	38,63	38,68	38,72	38,32	38,82	38,57	38,50	38,52	38,74	38,64	38,49	38,65
TiO_2	0,00	0,00	0,03	0,00	0,00	0,00	0,00	0,00	0,01	0,01	0,00	0,00
Al_2O_3	21,73	21,66	21,77	21,66	21,82	21,80	21,84	21,72	21,82	21,82	21,72	21,70
Cr_2O_3												
FeO	31,87	31,72	31,70	31,66	31,51	31,34	31,24	31,37	30,99	30,91	30,71	30,93
MnO	1,03	0,99	1,00	0,99	1,04	1,03	1,01	1,00	0,99	0,98	0,99	0,94
MgO	6,86	6,98	7,05	7,02	7,12	7,21	7,29	7,34	7,50	7,64	7,62	7,67
CaO	0,77	0,83	0,80	0,76	0,81	0,78	0,82	0,81	0,77	0,83	0,85	0,87
Na_2O	0,03	0,02	0,04	0,02	0,02	0,05	0,01	0,03	0,02	0,02	0,03	0,00
K_2O	0,00	0,01	0,01	0,01	0,01	0,00	0,02	0,02	0,01	0,00	0,00	0,01
Total	100,92	100,89	101,12	100,44	101,15	100,78	100,73	100,81	100,85	100,85	100,41	100,77
O=12												
Si	3,005	3,007	3,003	2,994	3,007	2,998	2,993	2,993	3,002	2,993	2,994	2,996
Ti	0,000	0,000	0,002	0,000	0,000	0,000	0,000	0,000	0,001	0,001	0,000	0,000
Al(IV)	0,000	0,000	0,000	0,006	0,000	0,002	0,007	0,007	0,000	0,007	0,006	0,004
Al(VI)	1,992	1,985	1,990	1,989	1,992	1,996	1,994	1,984	1,993	1,987	1,987	1,980
Cr	0,000	0,000	0,000	0,000	0,000	0,000	0,000	0,000	0,000	0,000	0,000	0,000
Fe(III)	0,002	0,007	0,004	0,009	0,001	0,004	0,005	0,014	0,004	0,011	0,012	0,018
Fe(II)	2,071	2,055	2,052	2,059	2,040	2,034	2,026	2,024	2,005	1,991	1,987	1,987
Mn	0,068	0,065	0,066	0,066	0,068	0,068	0,067	0,066	0,065	0,064	0,065	0,062
Mg	0,795	0,809	0,815	0,818	0,822	0,835	0,845	0,850	0,866	0,882	0,884	0,886
Ca	0,064	0,069	0,066	0,064	0,067	0,065	0,068	0,067	0,064	0,069	0,071	0,072
Total	7,998	7,998	7,998	8,005	7,997	8,002	8,005	8,006	7,999	8,005	8,005	8,005
Almandine	69,00	68,43	68,34	68,38	67,98	67,71	67,27	67,14	66,77	66,08	65,94	65,95
Andradite	0,12	0,34	0,22	0,47	0,06	0,18	0,26	0,72	0,19	0,57	0,58	0,89
Grossular	2,03	1,97	2,01	1,65	2,18	1,98	2,02	1,53	1,95	1,73	1,79	1,52
Pyrope	26,59	27,08	27,24	27,31	27,49	27,87	28,23	28,41	28,93	29,47	29,51	29,58
Spessartine	2,27	2,18	2,20	2,19	2,28	2,26	2,22	2,20	2,17	2,15	2,18	2,06
Uvarovite	0,00	0,00	0,00	0,00	0,00	0,00	0,00	0,00	0,00	0,00	0,00	0,00
X_{Mg}	0,27	0,28	0,28	0,28	0,28	0,28	0,29	0,29	0,30	0,30	0,30	0,30
X_{Ca}	0,02	0,02	0,02	0,02	0,02	0,02	0,02	0,02	0,02	0,02	0,02	0,02

Rock	LowAl meta	LowAl meta	LowAl meta	LowAl meta	highAl meta	highAl meta	highAl meta	highAl meta	highAl meta	highAl meta	highAl meta	highAl meta
SiO_2	38,70	38,60	38,73	38,99	38,00	37,94	37,98	38,31	38,85	38,81	38,24	38,33
TiO_2	0,01	0,01	0,00	0,00	0,07	0,00	0,01	0,00	0,00	0,00	0,00	0,00
Al_2O_3	21,89	21,69	21,81	21,94	21,55	21,27	21,43	21,42	21,66	21,48	21,54	21,40
Cr_2O_3					0,02	0,03	0,09	0,03	0,07	0,00	0,13	0,10
FeO	30,27	30,61	30,92	30,76	29,09	29,17	30,84	31,17	31,71	31,97	32,79	32,72
MnO	0,98	0,94	1,01	0,97	0,48	0,52	0,61	0,61	0,75	0,66	0,74	0,72
MgO	7,76	7,64	7,69	7,66	8,13	8,23	7,40	7,18	6,81	6,67	5,78	5,71
CaO	0,87	0,87	0,89	0,90	1,39	1,31	1,14	1,05	0,89	0,90	0,96	0,89
Na_2O	0,01	0,00	0,01	0,01	0,02	0,00	0,02	0,02	0,02	0,04	0,00	0,00
K_2O	0,02	0,00	0,00	0,01	0,01	0,00	0,00	0,01	0,01	0,00	0,00	0,02
Total	100,51	100,36	101,06	101,24	98,75	98,47	99,53	99,81	100,77	100,53	100,18	99,89
O=12												
Si	3,000	3,001	2,993	3,005	2,988	2,992	2,986	3,004	3,018	3,027	3,007	3,019
Ti	0,001	0,001	0,000	0,000	0,004	0,000	0,001	0,000	0,000	0,000	0,000	0,000
Al(IV)	0,000	0,000	0,007	0,000	0,012	0,008	0,014	0,000	0,000	0,000	0,000	0,000
Al(VI)	2,001	1,989	1,982	1,993	1,986	1,971	1,973	1,981	1,985	1,975	1,998	1,991
Cr	0,000	0,000	0,000	0,000	0,001	0,002	0,006	0,002	0,004	0,000	0,008	0,006
Fe(III)	0,000	0,009	0,016	0,002	0,008	0,024	0,019	0,011	0,000	0,000	0,000	0,000
Fe(II)	1,965	1,982	1,982	1,981	1,905	1,900	2,009	2,033	2,070	2,089	2,173	2,177
Mn	0,064	0,062	0,066	0,063	0,032	0,035	0,041	0,041	0,049	0,043	0,049	0,048
Mg	0,897	0,886	0,886	0,880	0,953	0,967	0,867	0,839	0,789	0,775	0,678	0,670
Ca	0,072	0,072	0,074	0,074	0,117	0,110	0,096	0,088	0,074	0,075	0,081	0,075
Total	7,999	8,001	8,006	7,998	8,006	8,009	8,010	8,000	7,990	7,986	7,995	7,988
Almandine	65,53	65,94	65,73	65,99	63,12	62,84	66,37	67,61	69,41	69,83	72,90	73,29
Andradite	0,00	0,43	0,81	0,10	0,40	1,21	0,93	0,57	0,00	0,00	0,00	0,00
Grossular	2,41	1,99	1,65	2,39	3,45	2,39	2,00	2,30	2,27	2,54	2,30	2,22
Pyrope	29,91	29,57	29,60	29,41	31,89	32,32	29,04	28,07	26,46	26,17	22,73	22,56
Spessartine	2,15	2,07	2,21	2,12	1,07	1,15	1,37	1,36	1,65	1,46	1,66	1,61
Uvarovite	0,00	0,00	0,00	0,00	0,07	0,08	0,28	0,08	0,21	0,00	0,41	0,32
X_{Mg}	0,31	0,30	0,30	0,30	0,33	0,33	0,30	0,29	0,27	0,27	0,23	0,23
X_{Ca}	0,02	0,02	0,02	0,02	0,04	0,04	0,03	0,03	0,02	0,03	0,03	0,03

Garnets in both high-Al and low-Al metapelites are pyrope-almandine solid solutions, with minor grossular and spessartine components (Table 4.1). Pyrope and almandine contents of the high-Al metapelite respectively range from 23 to 32 mol% and 63 to 73 mol% (Table 4.1). In comparison, the pyrope and almandine contents of the low-Al metapelite are slightly lower, and respectively range from 27 to 30 mol% and 66 to 69 mol% (Table 4.1). X_{Mg}^{Grt} [= $Mg/(Mg+Fe^{2+}+Mn)$] of high-Al metapelite ranges from 0.23 to 0.33, while that of low-Al metapelite is slightly lower, and ranges from 0.27 to 0.31 (Fig. 4.2). X_{Ca}^{Grt} [= $Ca/(Ca+Mg+Fe^{2+}+Mn)$] of high-Al metapelite ranges from 0.02 to 0.04, while that of low-Al metapelite is lower at 0.02 (Fig. 4.2). Mn content [atoms per formula unit (apfu)] of garnet is lower in the high-Al metapelite (0.03-0.05 apfu) than the low-Al metapelite (0.06-0.07 apfu) (Fig. 4.2).

Garnets occurring both locally within the Verbaard granitoid and associated leucocratic vein (Fig. 4.3) have similar compositions and are pyrope-almandine solid solutions, with minor grossular and spessartine components (Table 4.2). Pyrope and almandine contents of these garnets respectively range from 27 to 29 mol% and 65 to 67 mol% (Table 4.2). They differ slightly in the grossular content, with garnet in the leucocratic vein ranging from 1 to 4 mol%, while that of garnet occurring locally within the Verbaard granitoid is slightly lower at 1 to 2 mol%. Both X_{Mg}^{Grt} [0.28-0.30 (within leucocratic vein); 0.30 (within granitoid)] and X_{Ca}^{Grt} [0.03-0.06 (within leucocratic vein); 0.03-0.06 (within granitoid)] are comparable for both garnet occurrences (Fig. 4.2). Mn content is also similar for both garnet occurrences [0.02-0.03 apfu (within leucocratic vein); 0.02-0.03 apfu (within granitoid)] (Fig. 4.2).

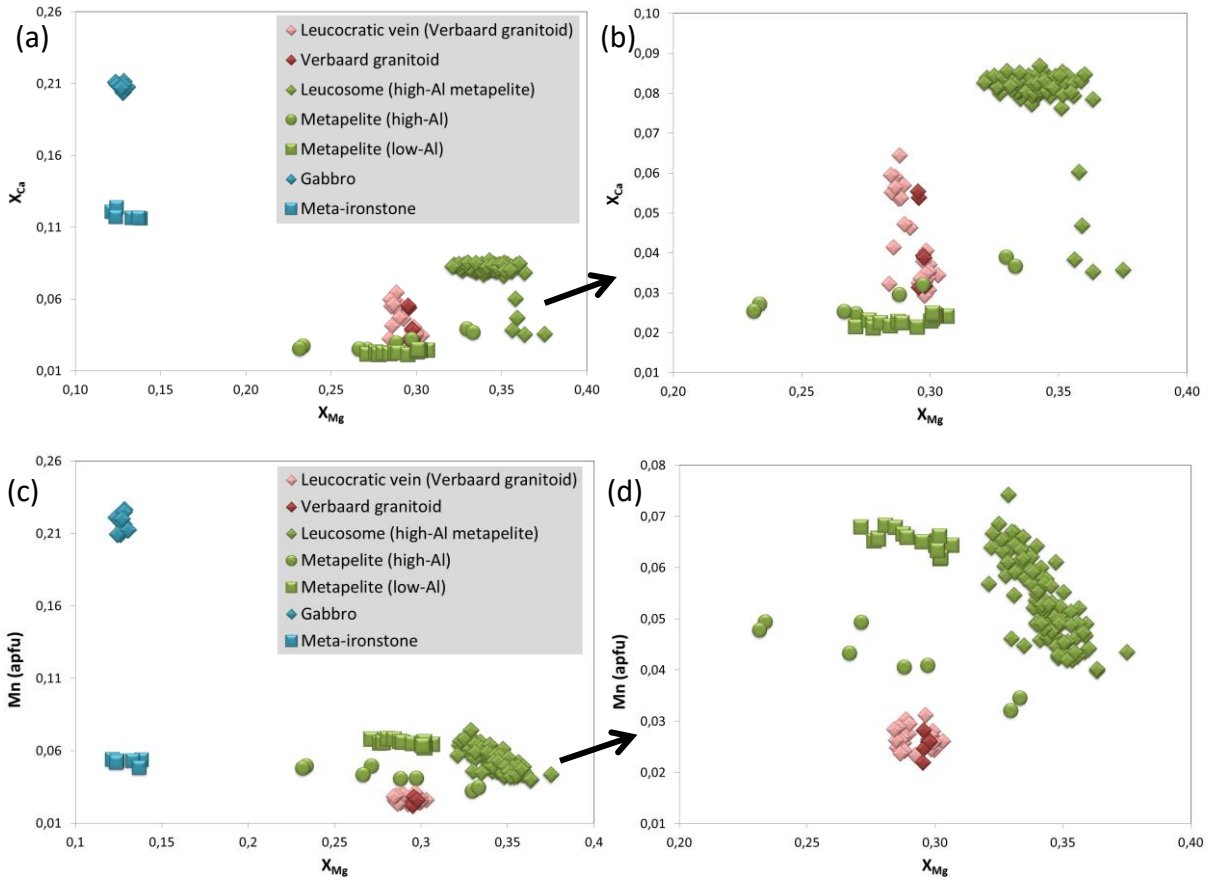


Figure 4.2. Mineral chemistry based diagrams illustrating the compositional variation observed in garnet from the studied rocks. Garnet from gabbro and meta-ironstone are also shown for comparison. **(a, b)** X_{Mg} vs X_{Ca}; **(c, d)** X_{Mg} vs Mn (apfu). (b) and (d) respectively are enlarged views of the lower right corners (indicated by arrowed lines) of (a) and (c).

Leucosomes associated with the high-Al metapelite at the O6-19 outcrop preserves the largest garnets in the study area (see Figs. 2.6, 3.7, 4.1c). Like the case of metapelites, Verbaard granitoid and associated leucocratic vein, garnet occurring in the O6-19 leucosome is also a pyrope-almandine solid solution, with minor grossular and spessartine components (Appendix 4.1). But the individual contents are slightly different from the other rocks. Pyrope and grossular contents respectively ranges from 30 to 38 mol% and 2 to 8 mol%, and are the largest among the different rocks. On the other hand, almandine content is the lowest

among the different rocks, ranging from 56 to 60 mol%. X_{Mg}^{Grt} (0.33-0.38) and X_{Ca}^{Grt} (0.04-0.08) of O6-19 leucosome (Appendix 4.1) are higher than that of other rocks (Fig. 4.2). Mn content of leucosome garnet varies from 0.04 to 0.07 apfu (Fig. 4.2).

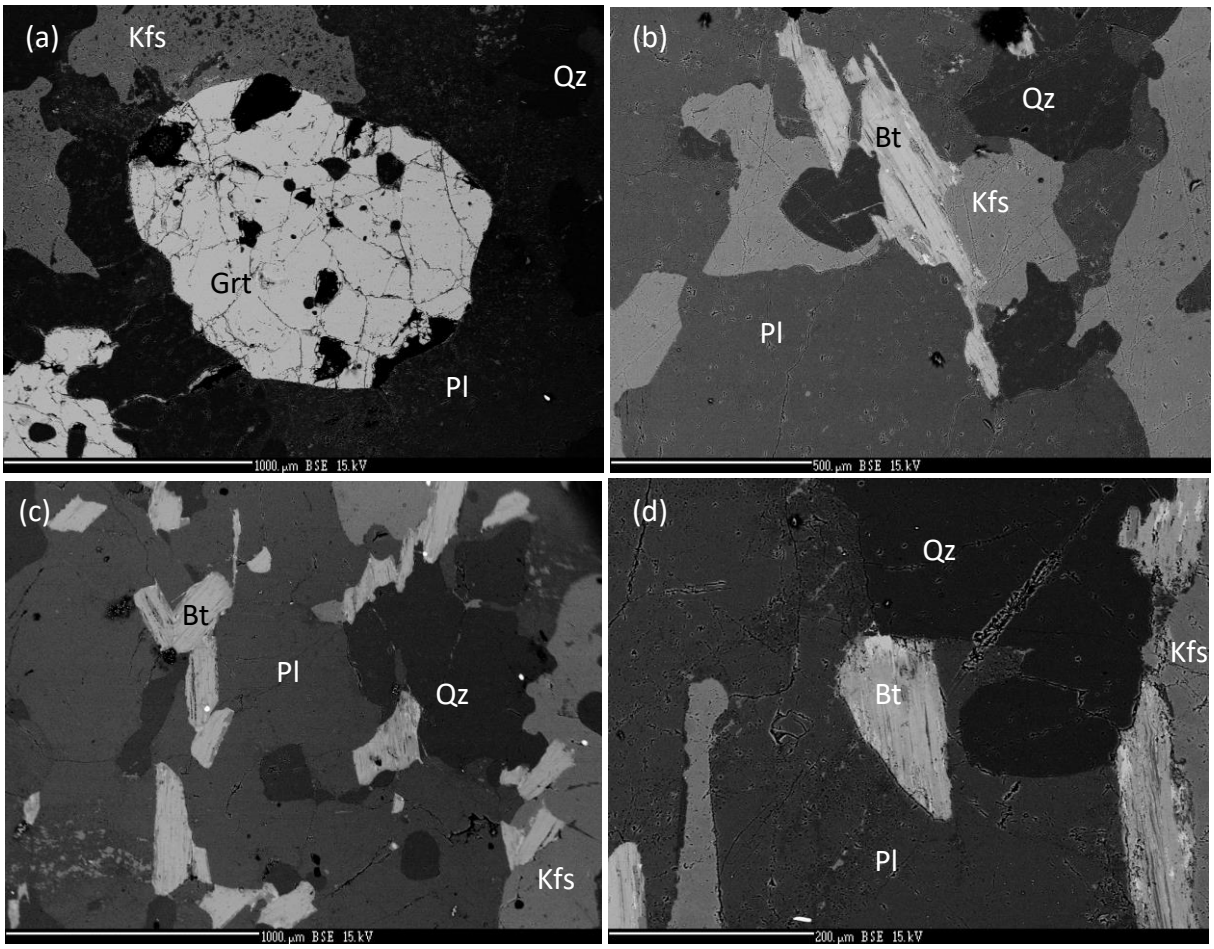


Figure 4.3. Representative BSE images illustrating the occurrence of minerals in the Verbaard granitoid and associated leucocratic vein. Garnet occurs locally in the Verbaard granitoid.

Garnet in gabbro and meta-ironstone from the study area has a different composition to that from other rocks (high-Al metapelite and associated leucosome, low-Al metapelite, Verbaard granitoid, leucocratic vein associated with Verbaard granitoid) in the study area (Figs. 4.2a, c). The different contents of garnet in gabbro include 10 mol% pyrope, 61 mol%

almandine, 16 to 18 mol% grossular and 7 mol% spessartine (Table 4.3). X_{Mg}^{Grt} varies from 0.12 to 0.13, while X_{Ca}^{Grt} varies from 0.20 to 0.21 (Figs. 4.2a, c). Mn content of garnet in gabbro varies from 0.21 to 0.23 apfu (Figs. 4.2a, c). In comparison, garnet in meta-ironstone have higher pyrope (11-12 mol%), almandine (74-75 mol%) and lower grossular (9-11 mol%) and spessartine (1-2 mol%) (Table 4.3). At similar X_{Mg}^{Grt} (0.12-0.14), garnet within the meta-ironstone has lower X_{Ca} (0.12) and Mn (0.05 apfu) than gabbro (Figs. 4.2a, c).

Table 4.2. Representative mineral chemical data of garnet occurring locally within the Verbaard granitoid (Verbaard granitoid) and those occurring within the leucocratic veins associated with the Verbaard granitoid (Leuocratic vein VG) from the study area.

	Verbaard	Verbaard	Verbaard	Verbaard	Verbaard	Verbaard	Leucocratic	Leucocratic	Leucocratic	Leucocratic	Leucocratic
Rock	**granitoid**	**granitoid**	**granitoid**	**granitoid**	**granitoid**	**granitoid**	**vein VG**	**vein VG**	**vein VG**	**vein VG**	**vein VG**
SiO_2	38,43	38,10	38,34	38,23	38,01	38,23	38,04	38,09	38,09	37,43	37,91
TiO_2	0,00	0,00	0,01	0,00	0,00	0,02	0,00	0,03	0,03	0,02	0,02
Al_2O_3	21,70	21,42	21,51	21,34	21,41	21,29	21,47	21,37	21,40	21,11	20,62
Cr_2O_3	0,00	0,00	0,00	0,03	0,01	0,01					
FeO	30,95	30,87	30,54	30,73	31,15	30,96	31,77	31,27	31,45	31,61	31,45
MnO	0,39	0,40	0,37	0,33	0,42	0,39	0,39	0,41	0,38	0,42	0,39
MgO	7,40	7,36	7,21	7,20	7,36	7,40	7,51	7,45	7,47	7,35	7,51
CaO	1,42	1,39	1,93	1,99	1,12	1,14	1,07	1,20	1,22	1,16	1,23
Na_2O	0,01	0,00	0,04	0,01	0,01	0,03	0,01	0,00	0,01	0,02	0,01
K_2O	0,01	0,00	0,00	0,00	0,01	0,01	0,00	0,01	0,02	0,01	0,01
Total	100,30	99,53	99,95	99,86	99,50	99,47	100,26	99,83	100,07	99,13	99,15
O=12											
Si	2,993	2,992	2,997	2,994	2,989	3,004	2,973	2,985	2,980	2,964	2,995
Ti	0,000	0,000	0,000	0,000	0,000	0,001	0,000	0,002	0,002	0,001	0,001
Al(IV)	0,007	0,008	0,003	0,006	0,011	0,000	0,027	0,015	0,020	0,036	0,005
Al(VI)	1,986	1,976	1,980	1,966	1,975	1,973	1,954	1,962	1,957	1,939	1,921
Cr	0,000	0,000	0,000	0,002	0,000	0,001	0,000	0,000	0,000	0,000	0,000
Fe(III)	0,012	0,021	0,017	0,029	0,022	0,019	0,041	0,032	0,037	0,053	0,069
Fe(II)	2,004	2,006	1,979	1,984	2,027	2,015	2,036	2,018	2,022	2,040	2,009
Mn	0,026	0,026	0,025	0,022	0,028	0,026	0,026	0,027	0,025	0,028	0,026
Mg	0,859	0,861	0,841	0,840	0,862	0,867	0,875	0,870	0,871	0,868	0,884
Ca	0,118	0,117	0,162	0,167	0,094	0,096	0,090	0,101	0,102	0,098	0,104
Total	8,006	8,008	8,004	8,009	8,009	8,001	8,021	8,012	8,016	8,027	8,015
Almandine	66,49	66,43	65,72	65,64	67,05	66,92	66,69	66,56	66,49	66,46	66,00
Andradite	0,61	1,06	0,86	1,45	1,09	0,96	2,05	1,60	1,84	2,70	3,48
Grossular	3,34	2,85	4,54	4,03	2,05	2,21	0,96	1,77	1,59	0,62	0,01
Pyrope	28,69	28,79	28,05	28,06	28,85	29,01	29,43	29,16	29,23	29,27	29,64
Spessartine	0,87	0,88	0,82	0,73	0,94	0,87	0,87	0,91	0,85	0,95	0,87
Uvarovite	0,00	0,00	0,01	0,09	0,02	0,03	0,00	0,00	0,00	0,00	0,00
X_{Mg}	0,30	0,30	0,30	0,30	0,30	0,30	0,30	0,30	0,30	0,30	0,30
X_{Ca}	0,04	0,04	0,05	0,06	0,03	0,03	0,03	0,03	0,03	0,03	0,03

Table 4.2. continued. Representative mineral chemical data of garnet occurring within the leucocratic veins associated with the Verbaard granitoid (Leucocratic vein VG) from the study area.

	Leucocratic	Leucocratic	Leucocratic	Leucocratic	Leucocratic	Leucocratic	Leucocratic	Leucocratic	Leucocratic	Leucocratic	Leucocratic	Leucocratic	Leucocratic
Rock	**vein VG**	**vein VG**	**vein VG**	**vein VG**	**vein VG**	**vein VG**	**vein VG**	**vein VG**	**vein VG**	**vein VG**	**vein VG**	**vein VG**	**vein VG**
SiO_2	38,16	38,18	37,82	38,05	37,94	37,95	37,74	37,60	37,53	37,64	37,44	36,71	37,40
TiO_2	0,00	0,03	0,02	0,04	0,04	0,04	0,01	0,00	0,03	0,04	0,04	0,05	0,04
Al_2O_3	21,43	21,47	21,31	21,42	21,25	21,39	21,27	21,23	21,35	21,31	21,14	21,51	21,35
Cr_2O_3												0,01	0,02
FeO	31,58	31,61	31,49	31,65	31,47	31,54	31,26	31,58	31,87	31,74	31,78	30,77	31,32
MnO	0,39	0,41	0,37	0,37	0,37	0,40	0,42	0,40	0,39	0,39	0,41	0,46	0,35
MgO	7,53	7,49	7,47	7,51	7,42	7,42	7,44	7,44	7,48	7,50	7,44	7,29	7,18
CaO	1,11	1,18	1,26	1,34	1,46	1,37	1,21	1,05	1,14	1,28	1,25	1,19	1,66
Na_2O	0,02	0,00	0,02	0,00	0,00	0,03	0,01	0,00	0,00	0,02	0,02	0,01	0,02
K_2O	0,01	0,01	0,01	0,01	0,00	0,00	0,00	0,01	0,01	0,02	0,02	0,01	0,02
Total	100,23	100,38	99,77	100,39	99,95	100,14	99,36	99,31	99,80	99,94	99,54	98,01	99,36
O=12													
Si	2,981	2,979	2,971	2,970	2,974	2,970	2,975	2,969	2,952	2,956	2,954	2,938	2,955
Ti	0,000	0,002	0,001	0,002	0,002	0,002	0,001	0,000	0,002	0,002	0,002	0,003	0,002
Al(IV)	0,019	0,021	0,029	0,030	0,026	0,030	0,025	0,031	0,048	0,044	0,046	0,062	0,045
Al(VI)	1,958	1,956	1,947	1,944	1,941	1,948	1,954	1,948	1,936	1,933	1,926	1,969	1,947
Cr	0,000	0,000	0,000	0,000	0,000	0,000	0,000	0,000	0,000	0,000	0,000	0,001	0,001
Fe(III)	0,038	0,038	0,046	0,047	0,050	0,044	0,040	0,046	0,055	0,057	0,064	0,025	0,044
Fe(II)	2,026	2,025	2,023	2,018	2,013	2,020	2,020	2,039	2,041	2,027	2,033	2,035	2,026
Mn	0,026	0,027	0,025	0,024	0,025	0,027	0,028	0,027	0,026	0,026	0,027	0,031	0,023
Mg	0,877	0,871	0,875	0,874	0,867	0,866	0,874	0,876	0,877	0,878	0,875	0,870	0,846
Ca	0,093	0,099	0,106	0,112	0,123	0,115	0,102	0,089	0,096	0,108	0,106	0,102	0,141
Total	8,016	8,017	8,023	8,023	8,021	8,022	8,020	8,024	8,033	8,032	8,034	8,034	8,030
Almandine	66,60	66,53	66,16	65,98	65,90	66,09	66,23	66,61	66,15	65,78	65,87	65,86	65,83
Andradite	1,90	1,89	2,30	2,40	2,52	2,24	2,03	2,33	2,81	2,91	3,24	1,26	2,23
Grossular	1,22	1,42	1,27	1,38	1,61	1,62	1,41	0,66	0,45	0,73	0,34	2,18	2,46
Pyrope	29,42	29,24	29,44	29,42	29,15	29,15	29,39	29,50	29,71	29,70	29,62	29,60	28,62
Spessartine	0,87	0,91	0,83	0,82	0,83	0,89	0,94	0,90	0,88	0,88	0,93	1,06	0,79
Uvarovite	0,00	0,00	0,00	0,00	0,00	0,00	0,00	0,00	0,00	0,00	0,00	0,03	0,06
X_{Mg}	0,30	0,30	0,30	0,30	0,30	0,30	0,30	0,30	0,30	0,30	0,30	0,30	0,29
X_{Ca}	0,03	0,03	0,04	0,04	0,04	0,04	0,03	0,03	0,03	0,04	0,03	0,03	0,05

	Leucocratic	Leucocratic	Leucocratic	Leucocratic	Leucocratic	Leucocratic	Leucocratic	Leucocratic	Leucocratic	Leucocratic	Leucocratic	Leucocratic
Rock	**vein VG**	**vein VG**	**vein VG**	**vein VG**	**vein VG**	**vein VG**	**vein VG**	**vein VG**	**vein VG**	**vein VG**	**vein VG**	**vein VG**
SiO_2	36,95	37,41	37,20	37,15	37,60	37,29	37,28	37,25	36,93	36,82	37,27	36,92
TiO_2	0,04	0,07	0,00	0,04	0,01	0,01	0,00	0,01	0,00	0,04	0,00	0,02
Al_2O_3	21,11	21,23	21,36	21,26	21,24	21,25	21,10	21,27	21,06	21,45	21,05	21,07
Cr_2O_3	0,03	0,00	0,00	0,03	0,00	0,02	0,00	0,03	0,06	0,00	0,02	0,00
FeO	30,80	30,81	30,58	30,68	30,81	30,66	30,86	30,84	30,88	31,69	31,77	32,10
MnO	0,38	0,41	0,40	0,45	0,37	0,39	0,36	0,39	0,35	0,44	0,43	0,42
MgO	6,93	7,00	6,92	6,97	6,88	6,88	6,91	6,85	6,88	7,15	7,03	7,04
CaO	1,90	2,03	1,94	1,91	1,96	2,10	2,30	2,12	2,00	1,70	1,48	1,15
Na_2O	0,02	0,02	0,03	0,03	0,02	0,03	0,03	0,02	0,00	0,03	0,01	0,02
K_2O	0,00	0,01	0,00	0,01	0,00	0,01	0,00	0,03	0,00	0,01	0,01	0,00
Total	98,16	98,99	98,43	98,53	98,89	98,64	98,84	98,81	98,16	99,33	99,07	98,74
O=12												
Si	2,956	2,964	2,963	2,959	2,980	2,966	2,961	2,960	2,955	2,919	2,959	2,945
Ti	0,002	0,004	0,000	0,002	0,001	0,001	0,000	0,001	0,000	0,002	0,000	0,001
Al(IV)	0,044	0,036	0,037	0,041	0,020	0,034	0,039	0,040	0,045	0,081	0,041	0,055
Al(VI)	1,949	1,951	1,971	1,957	1,967	1,961	1,941	1,956	1,945	1,928	1,934	1,931
Cr	0,002	0,000	0,000	0,002	0,000	0,001	0,000	0,002	0,004	0,000	0,001	0,000
Fe(III)	0,041	0,040	0,026	0,034	0,028	0,033	0,052	0,037	0,046	0,061	0,058	0,060
Fe(II)	2,019	2,002	2,012	2,009	2,014	2,006	1,998	2,013	2,021	2,040	2,052	2,082
Mn	0,026	0,028	0,027	0,030	0,025	0,026	0,024	0,026	0,024	0,030	0,029	0,028
Mg	0,826	0,827	0,822	0,827	0,813	0,816	0,818	0,812	0,821	0,845	0,832	0,837
Ca	0,163	0,172	0,166	0,163	0,166	0,179	0,196	0,181	0,171	0,144	0,126	0,098
Total	8,029	8,023	8,023	8,026	8,015	8,023	8,029	8,026	8,031	8,051	8,031	8,038
Almandine	65,66	65,36	65,77	65,50	66,30	65,58	64,94	65,60	65,62	65,09	66,65	67,27
Andradite	2,10	2,04	1,29	1,73	1,43	1,68	2,66	1,87	2,31	3,16	2,93	3,05
Grossular	3,32	3,78	4,30	3,68	4,15	4,29	3,96	4,13	3,30	1,79	1,26	0,29
Pyrope	27,96	27,89	27,73	27,97	27,28	27,50	27,63	27,41	27,77	28,95	28,12	28,42
Spessartine	0,87	0,93	0,91	1,03	0,83	0,89	0,82	0,89	0,80	1,01	0,98	0,96
Uvarovite	0,10	0,00	0,00	0,10	0,00	0,06	0,00	0,10	0,19	0,00	0,06	0,00
X_{Mg}	0,29	0,29	0,29	0,29	0,29	0,29	0,29	0,28	0,29	0,29	0,29	0,28
X_{Ca}	0,05	0,06	0,05	0,05	0,06	0,06	0,06	0,06	0,06	0,05	0,04	0,03

Mineral chemical profiles from rim to rim through core of large garnets from the leucocratic vein associated with the Verbaard granitoid, low-Al metapelite and leucosome associated with the high-Al metapelite (O6-19) were carried out (Fig. 4.4). Garnets from the low-Al metapelite and those occurring within the leucocratic vein associated with the Verbaard granitoid have similar pattern and show very little zoning for X_{Mg} [0.28-0.31 (low-Al metapelite), 0.29-0.30 (Verbaard granitoid-leucocratic vein) and X_{Ca} [0.02 (low-Al metapelite), 0.03-0.04 (Verbaard granitoid-leucocratic vein)] (Figs. 4.4a to d). In comparison, large garnet from leucosome associated with the high-Al metapelite (O6-19) (see Appendix 4.1) shows variation in X_{Mg} and X_{Ca}, and the results were slightly different from the other two types of garnet described above. X_{Mg}^{Grt} shows slight increase from 0.32 in core to 0.36 in both rims, whereas X_{Ca}^{Grt} is stable throughout most of the grain and drastically decreases in rims (from 0.08 to 0.04) (Figs. 4.4e, f).

4.3. Biotite

Biotite is a prominent mafic mineral defining the fabric in the high-Al and low-Al metapelites (Fig. 4.5). It's the main mafic rock-forming mineral in the Verbaard granitoid (Fig. 4.3). Biotite in the high-Al metapelite is Mg-rich with X_{Mg} (= Mg/(Mg+Fe)) of 0.52 to 0.57, and compositional ranges of 0.53 to 0.74 atoms per formula unit (apfu) Ti, 2.90 to 3.02 apfu Al, and 1.73 to 1.83 apfu K (Fig. 4.6; Table 4.4). In comparison to the high-Al metapelite, biotite in the low-Al metapelite has a higher X_{Mg} (0.54-0.68) and Al (2.85-3.17 apfu), and lower Ti (0.18-0.56 apfu) and K (1.28-1.73 apfu) (Fig. 4.6; Table 4.5). Together with their petrographic

characteristics, the difference in mineral chemical characteristics between biotite in the low-Al and high-Al metapelites could indicate the possibility of two generations of biotite.

Table 4.3. Representative mineral chemical data of garnet in gabbro and meta-ironstone (MIS) from the study area. In both cases, mineral chemical analyses focused on small garnet grains occurring within the respective rocks, for comparison with smaller garnet grains occurring within the Verbaard granitoid.

Rock	Gabbro	Gabbro	Gabbro	Gabbro	Gabbro	Gabbro	Gabbro	Gabbro	Gabbro	Gabbro	MIS	MIS	MIS	MIS	MIS	MIS
SiO_2	37,05	37,47	36,64	37,02	37,33	37,15	37,74	37,47	37,53	37,68	38,11	37,35	38,01	37,12	37,53	37,83
TiO_2	0,05	0,01	0,00	0,05	0,05	0,02	0,03	0,00	0,02	0,00	0,03	0,04	0,06	0,04	0,04	0,04
Al_2O_3	20,09	20,36	19,59	19,89	20,07	20,11	20,11	20,48	20,40	20,22	20,96	20,40	20,79	20,31	20,85	20,95
Cr_2O_3	0,08	0,06	0,25	0,28	0,15	0,09	0,20	0,04	0,03	0,05						
FeO	28,76	28,71	28,73	28,56	28,52	28,82	28,67	28,35	28,31	28,71	34,04	34,37	34,37	34,85	34,14	34,50
MnO	3,09	3,08	3,28	3,22	3,14	3,17	3,09	3,13	3,31	3,24	0,80	0,79	0,79	0,78	0,71	0,77
MgO	2,53	2,51	2,53	2,44	2,54	2,55	2,47	2,60	2,55	2,53	3,11	2,68	2,99	2,75	3,06	2,77
CaO	7,25	7,33	7,37	7,33	7,25	7,12	7,33	7,26	7,33	7,26	4,11	4,21	4,11	4,35	4,10	4,12
Na_2O	0,02	0,02	0,00	0,03	0,01	0,04	0,02	0,00	0,00	0,00	0,02	0,04	0,02	0,02	0,00	0,02
K_2O	0,01	0,00	0,00	0,00	0,00	0,00	0,01	0,01	0,01	0,00	0,01	0,01	0,01	0,01	0,01	0,00
Total	98,92	99,55	98,40	98,81	99,05	99,08	99,65	99,33	99,48	99,69	101,19	99,89	101,15	100,23	100,44	101,00
O=12																
Si	2,996	3,006	2,985	2,999	3,010	3,000	3,024	3,008	3,010	3,018	3,016	3,008	3,014	2,985	2,997	3,007
Ti	0,003	0,001	0,000	0,003	0,003	0,001	0,002	0,000	0,001	0,000	0,002	0,002	0,004	0,002	0,002	0,002
Al(IV)	0,004	0,000	0,015	0,001	0,000	0,000	0,000	0,000	0,000	0,000	0,000	0,000	0,000	0,000	0,000	0,000
Al(VI)	1,916	1,929	1,874	1,904	1,912	1,918	1,904	1,942	1,932	1,913	1,957	1,940	1,946	1,916	1,961	1,965
Cr	0,005	0,004	0,016	0,018	0,010	0,006	0,012	0,003	0,002	0,003						
Fe(III)	0,068	0,053	0,097	0,067	0,058	0,066	0,051	0,042	0,049	0,059	0,023	0,045	0,033	0,072	0,032	0,023
Fe(II)	1,877	1,873	1,860	1,868	1,865	1,880	1,870	1,861	1,850	1,864	2,230	2,270	2,246	2,271	2,248	2,271
Mn	0,211	0,210	0,227	0,221	0,214	0,217	0,209	0,213	0,225	0,220	0,054	0,054	0,053	0,053	0,048	0,052
Mg	0,305	0,300	0,308	0,294	0,305	0,307	0,295	0,311	0,305	0,303	0,367	0,322	0,353	0,330	0,364	0,328
Ca	0,628	0,630	0,643	0,637	0,626	0,616	0,629	0,624	0,630	0,623	0,348	0,363	0,349	0,375	0,351	0,351
Total	8,013	8,006	8,025	8,011	8,004	8,012	7,997	8,004	8,003	8,002	7,996	8,003	7,997	8,020	8,007	7,999
Almandine	61,60	61,65	60,56	61,29	61,31	61,71	61,52	61,42	60,94	61,24	74,08	75,13	74,51	74,62	74,49	75,46
Andradite	3,40	2,69	4,87	3,38	2,93	3,33	2,61	2,13	2,45	2,98	1,16	2,25	1,67	3,64	1,61	1,14
Grossular	17,40	18,33	15,86	17,10	17,72	17,07	18,11	18,72	18,66	17,94	10,58	9,98	10,11	8,92	10,11	10,65
Pyrope	10,24	10,10	10,30	9,89	10,31	10,32	10,01	10,45	10,27	10,24	12,36	10,83	11,92	11,04	12,17	11,02
Spessartine	7,09	7,05	7,59	7,43	7,24	7,27	7,11	7,15	7,58	7,44	1,81	1,81	1,79	1,78	1,61	1,74
Uvarovite	0,26	0,18	0,81	0,91	0,49	0,29	0,64	0,14	0,10	0,15	0,00	0,00	0,00	0,00	0,00	0,00
X_{Mg}	0,13	0,13	0,13	0,12	0,13	0,13	0,12	0,13	0,13	0,13	0,14	0,12	0,13	0,12	0,14	0,12
X_{Ca}	0,21	0,21	0,21	0,21	0,21	0,20	0,21	0,21	0,21	0,21	0,12	0,12	0,12	0,12	0,12	0,12

Biotite in the Verbaard granitoid can be quite altered (Fig. 4.3). The least altered biotite is Mg-rich with X_{Mg} of 0.48 to 0.50, and compositional ranges of 0.71 to 0.81 apfu Ti, 2.81 to

3.06 apfu Al, and 1.76 to 1.85 apfu K (Fig. 4.6; Table 4.6). In comparison to the metapelites, the biotite in the Verbaard granitoid has lower X_{Mg} (Fig. 4.6).

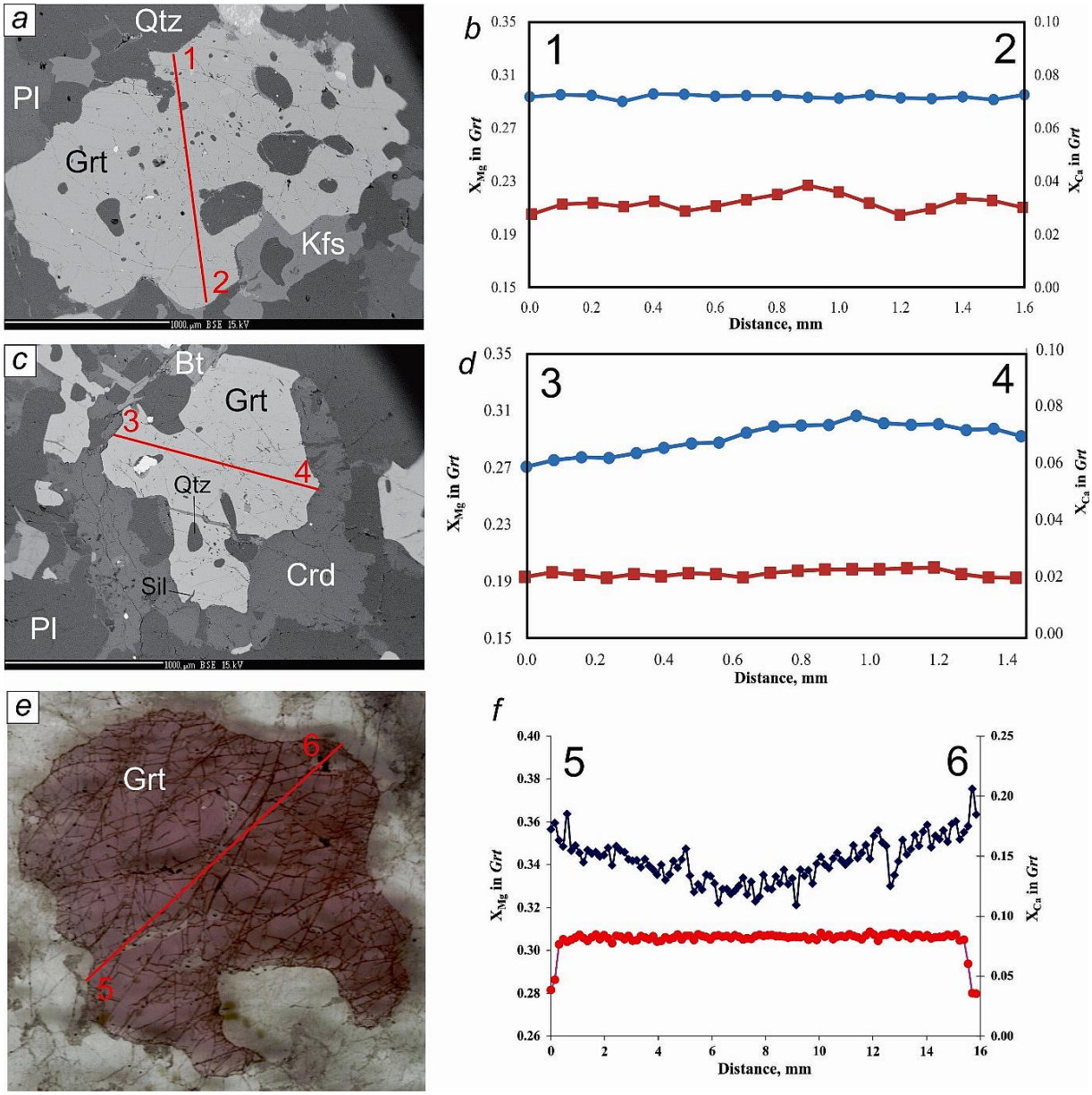


Figure 4.4. BSE and optical images of large garnets and corresponding mineral chemical profiles (indicated by numbered red lines) in terms of X_{Mg} (red) and X_{Ca} (blue) from the leucocratic vein associated with the Verbaard granitoid **(a, b)**, low-Al metapelite **(c, d)**, and leucosome associated with the high-Al metapelite at O6-19 **(e, f)**. The corresponding data set for the Verbaard granitoid is given in Table 4.2, while that of low-Al metapelite is given in Table 4.1, and that of the leucosome associated with the high-Al metapelite at O6-19 is given in Appendix 4.1.

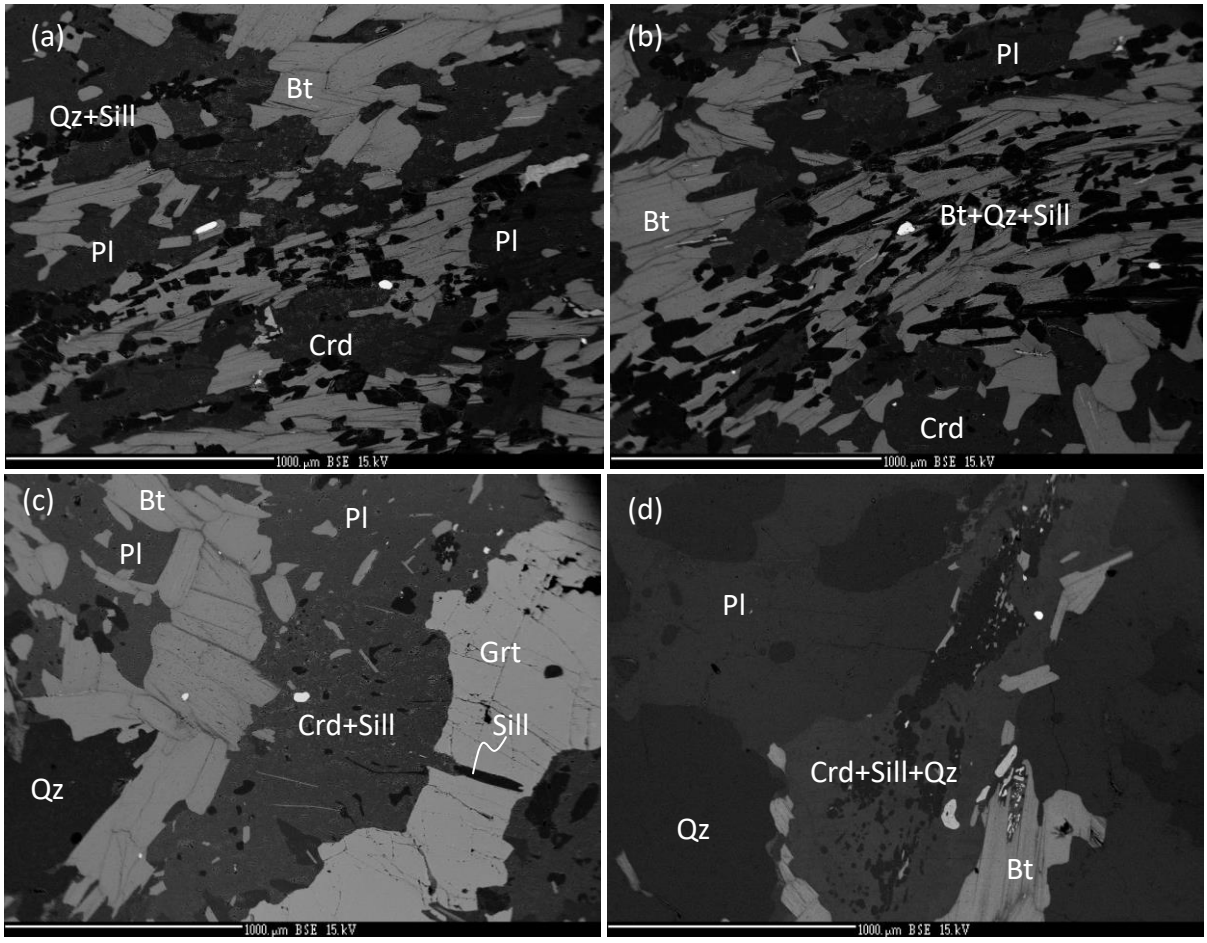


Figure 4.5. Representative BSE illustrating the mode of occurrence of the prominent minerals (biotite, cordierite, sillimanite, garnet, quartz, plagioclase) defining the fabric in the metapelites.

4.4. Feldspars

Anorthite [An (=Ca/Ca+Na+K)] contents of plagioclase in the metapelites (An_{21}-An_{24}) and Verbaard granitoid (An_{22}-An_{24}) are broadly similar (Tables 4.7, 4.8). The corresponding albite content varies from 74 to 77 mol% in the metapelites, and 73 to 75 mol% in the Verbaard granitoid (Tables 4.7, 4.8). K-feldspar composition in the metapelites is in the range of Or_{83} to Or_{93}, while that of the Verbaard granitoid is at higher orthoclase content (Or_{93-97}) (Tables 4.7, 4.8).

Table 4.4. Representative mineral chemical data of biotite in high-Al metapelite (HighAl meta) from the study area.

Rock	HighAl meta	HighAl meta	HighAl meta	HighAl meta	HighAl meta	HighAl meta	HighAl meta	HighAl meta
SiO_2	34,79	34,35	34,57	34,88	35,04	35,52	35,38	35,22
TiO_2	5,08	5,22	5,32	5,36	5,32	4,67	6,51	6,09
Al_2O_3	16,50	16,42	16,50	16,77	16,37	16,71	16,43	16,08
FeO	16,92	16,45	16,65	16,49	16,40	15,24	16,47	15,89
MnO	0,00	0,02	0,02	0,00	0,00	0,04	0,05	0,02
MgO	10,52	10,25	10,28	10,05	10,16	11,17	9,83	9,85
CaO	0,01	0,03	0,00	0,00	0,00	0,00	0,00	0,04
Na_2O	0,20	0,21	0,13	0,18	0,16	0,16	0,13	0,15
K_2O	8,95	8,70	8,97	9,38	9,29	9,29	9,56	9,10
Total								
O=22								
Si	5,339	5,345	5,337	5,324	5,360	5,382	5,322	5,386
Ti	0,586	0,610	0,618	0,616	0,612	0,532	0,736	0,700
Al(IV)	2,661	2,655	2,663	2,676	2,640	2,618	2,678	2,614
Al(VI)	0,324	0,356	0,341	0,341	0,311	0,366	0,234	0,286
Fe	2,172	2,141	2,150	2,105	2,098	1,932	2,071	2,032
Mn	0,000	0,003	0,002	0,000	0,000	0,005	0,006	0,003
Mg	2,406	2,376	2,365	2,286	2,317	2,522	2,205	2,246
Ca	0,001	0,004	0,000	0,000	0,000	0,000	0,000	0,007
Na	0,060	0,065	0,039	0,054	0,047	0,046	0,036	0,043
K	1,753	1,726	1,767	1,826	1,812	1,795	1,834	1,775
Total	15,303	15,281	15,281	15,228	15,196	15,197	15,124	15,091

4.5. Cordierite and sillimanite

As shown in chapter 3 (petrography), cordierite in the metapelite samples are prominently altered. The only fresh cordierite grains were found in low-Al metapelite. Its X_{Mg} ranges between 0.77 and 0.82 depending how far the analytical spots are situated from garnet (closer to garnet – higher X_{Mg}, away from garnet – lower X_{Mg}) (Table 4.9). Sillimanite analyses were obtained from large grains in the low-Al metapelite. Sillimanite is near pure Al_2SiO_5, with Fe (<0.6 wt.%) and Cr (<0.2 wt.%) being the impurities (Table 4.9).

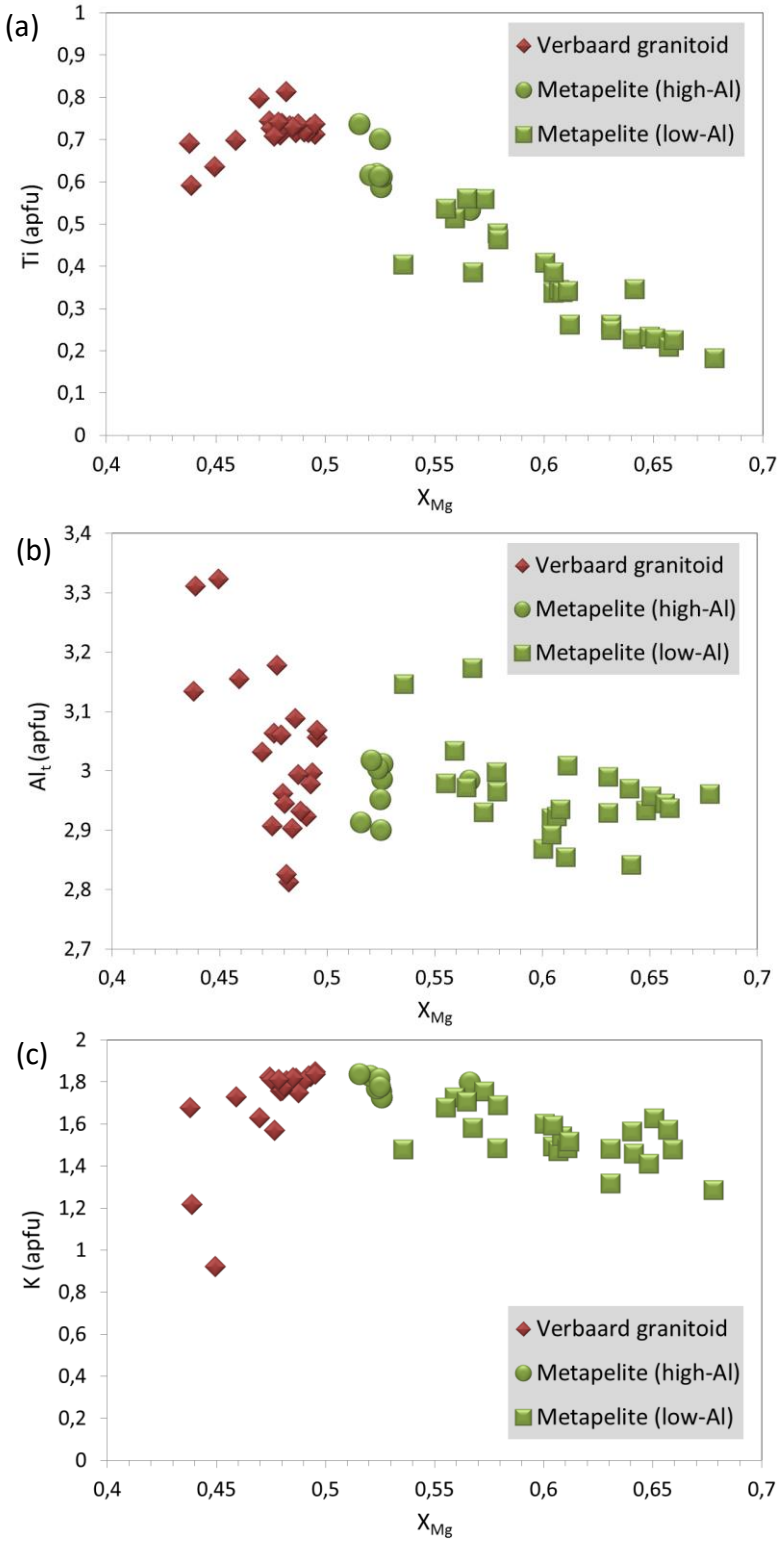


Figure 4.6. Mineral chemistry-based diagrams comparing the composition of biotite in the high-Al metapelite, low-Al metapelite and the Verbaard granitoid.

Table 4.5. Representative mineral chemical data of biotite in low-Al metapelite (LowAl meta) from the study area.

Rock	LowAl meta	LowAl meta	LowAl meta	LowAl meta	LowAl meta	LowAl meta	LowAl meta	LowAl meta	LowAl meta	LowAl meta	LowAl meta	LowAl meta
SiO_2	37,33	37,82	36,04	38,32	37,27	37,99	38,13	37,49	38,15	38,89	38,20	37,19
TiO_2	3,05	3,17	2,95	3,16	3,70	3,56	3,17	2,06	2,42	2,34	2,15	2,07
Al_2O_3	16,86	17,21	16,33	16,90	16,62	17,06	16,65	17,21	17,29	17,97	17,31	17,06
FeO	15,62	15,96	14,84	15,77	15,68	15,60	14,35	14,48	15,17	15,34	14,62	14,13
MnO	0,01	0,03	0,03	0,04	0,00	0,07	0,02	0,02	0,01	0,03	0,03	0,04
MgO	13,39	13,82	12,95	13,90	13,23	13,37	14,41	14,49	14,54	14,70	15,13	14,78
CaO	0,06	0,02	0,32	0,04	0,04	0,03	0,02	0,10	0,03	0,05	0,04	0,08
Na_2O	0,20	0,16	0,21	0,21	0,16	0,15	0,15	0,21	0,21	0,10	0,24	0,23
K_2O	7,96	7,99	7,92	8,12	8,56	8,67	7,90	8,37	8,08	7,31	7,69	8,67
F	0,58	0,53	0,47	0,58	0,61	0,58	0,73	0,55	0,65	0,73	0,61	0,69
Cl	0,12	0,12	0,13	0,13	0,13	0,14	0,11	0,12	0,11	0,11	0,11	0,12
Total	94,48	96,18	91,59	96,46	95,26	96,50	94,80	94,43	95,90	96,73	95,41	94,25
O=22												
Si	5,484	5,449	5,494	5,490	5,456	5,464	5,520	5,487	5,483	5,488	5,491	5,468
Ti	0,337	0,343	0,338	0,341	0,407	0,385	0,345	0,227	0,262	0,248	0,232	0,229
Al(IV)	2,516	2,551	2,506	2,510	2,544	2,536	2,480	2,513	2,517	2,512	2,509	2,532
Al(VI)	0,403	0,371	0,428	0,344	0,324	0,356	0,361	0,456	0,412	0,478	0,423	0,424
Fe	1,919	1,923	1,892	1,890	1,920	1,877	1,737	1,772	1,823	1,811	1,757	1,737
Mn	0,001	0,004	0,004	0,005	0,000	0,009	0,002	0,002	0,001	0,004	0,004	0,005
Mg	2,932	2,968	2,943	2,969	2,887	2,867	3,110	3,161	3,115	3,093	3,242	3,239
Ca	0,009	0,003	0,052	0,006	0,006	0,005	0,003	0,016	0,005	0,008	0,006	0,013
Na	0,057	0,045	0,062	0,058	0,045	0,042	0,042	0,060	0,059	0,027	0,067	0,066
K	1,492	1,468	1,540	1,484	1,598	1,591	1,459	1,563	1,481	1,316	1,410	1,626
F	0,269	0,241	0,227	0,263	0,282	0,264	0,334	0,255	0,295	0,326	0,277	0,321
Cl	0,030	0,029	0,034	0,032	0,032	0,034	0,027	0,030	0,027	0,026	0,027	0,030
Total	15,450	15,396	15,519	15,391	15,502	15,428	15,421	15,542	15,479	15,336	15,445	15,690

Rock	LowAl meta	LowAl meta	LowAl meta	LowAl meta	LowAl meta	LowAl meta	LowAl meta	LowAl meta	LowAl meta	LowAl meta	LowAl meta	LowAl meta
SiO_2	37,71	39,01	39,20	38,20	36,36	36,90	35,52	36,87	37,05	38,34	37,61	37,44
TiO_2	1,90	1,71	2,12	2,43	4,58	4,86	3,56	5,07	5,10	3,60	4,41	4,25
Al_2O_3	17,15	17,77	17,72	17,82	17,29	17,25	17,70	16,99	17,27	18,93	17,69	17,36
FeO	14,01	13,67	14,10	15,67	15,77	16,27	17,72	15,71	15,72	15,79	16,16	15,86
MnO	0,00	0,03	0,03	0,01	0,02	0,03	0,06	0,03	0,01	0,00	0,01	0,04
MgO	15,07	16,15	15,31	13,86	11,24	11,40	11,48	11,82	11,45	11,63	12,47	12,25
CaO	0,08	0,09	0,02	0,00	0,03	0,04	0,00	0,00	0,02	0,02	0,01	0,02
Na_2O	0,22	0,20	0,22	0,18	0,10	0,10	0,07	0,13	0,14	0,14	0,16	0,11
K_2O	8,46	7,12	8,24	8,29	9,09	8,97	7,68	9,39	9,15	8,71	8,09	9,13
F	0,79	0,75	0,65	0,40	0,35	0,38	0,42	0,39	0,38	0,41	0,69	0,52
Cl	0,11	0,09	0,08	0,15	0,14	0,12	0,09	0,11	0,12	0,13	0,1	0,09
Total	94,60	95,75	96,96	96,46	94,48	95,82	93,79	96,01	95,91	97,16	96,61	96,46
O=22												
Si	5,493	5,513	5,512	5,470	5,411	5,405	5,355	5,394	5,409	5,451	5,406	5,423
Ti	0,208	0,182	0,224	0,262	0,513	0,535	0,404	0,558	0,560	0,385	0,477	0,463
Al(IV)	2,507	2,487	2,488	2,530	2,589	2,595	2,645	2,606	2,591	2,549	2,594	2,577
Al(VI)	0,438	0,473	0,449	0,478	0,443	0,384	0,500	0,324	0,381	0,623	0,403	0,387
Fe	1,707	1,616	1,658	1,877	1,963	1,993	2,234	1,922	1,919	1,878	1,943	1,921
Mn	0,000	0,004	0,004	0,001	0,003	0,004	0,008	0,004	0,001	0,000	0,001	0,005
Mg	3,272	3,402	3,209	2,959	2,493	2,489	2,580	2,578	2,492	2,465	2,672	2,645
Ca	0,012	0,014	0,003	0,000	0,005	0,006	0,000	0,000	0,003	0,003	0,002	0,003
Na	0,062	0,055	0,060	0,050	0,029	0,028	0,020	0,037	0,040	0,039	0,045	0,031
K	1,572	1,283	1,478	1,514	1,725	1,676	1,477	1,752	1,704	1,580	1,483	1,687
F	0,364	0,335	0,289	0,181	0,165	0,176	0,200	0,180	0,175	0,184	0,314	0,238
Cl	0,027	0,022	0,019	0,036	0,035	0,030	0,023	0,027	0,030	0,031	0,024	0,022
Total	15,662	15,384	15,392	15,358	15,373	15,322	15,446	15,382	15,305	15,188	15,362	15,403

Table 4.6. Representative mineral chemical data of biotite in Verbaard granitoid from the study area.

	Verbaard	Verbaard	Verbaard	Verbaard	Verbaard	Verbaard	Verbaard	Verbaard	Verbaard	Verbaard	Verbaard
Rock	granitoid	granitoid	granitoid	granitoid	granitoid	granitoid	granitoid	granitoid	granitoid	granitoid	granitoid
SiO_2	35,41	35,28	35,41	35,43	35,76	35,58	35,61	35,27	35,35	36,13	36,58
TiO_2	6,41	6,28	6,34	6,32	6,39	6,29	6,48	6,54	7,13	6,60	6,70
Al_2O_3	16,84	17,19	16,90	16,77	16,60	16,74	16,40	16,32	15,75	16,78	17,06
FeO	17,04	16,94	17,63	17,36	17,77	18,05	17,93	18,30	17,73	17,73	17,90
MnO	0,04	0,01	0,06	0,02	0,03	0,02	0,01	0,00	0,02	0,01	0,01
MgO	9,30	9,33	9,38	9,45	9,60	9,33	9,43	9,27	9,27	9,47	9,28
CaO	0,00	0,00	0,00	0,00	0,04	0,02	0,02	0,01	0,02	0,02	0,02
Na_2O	0,11	0,12	0,14	0,08	0,10	0,15	0,15	0,08	0,12	0,07	0,10
K_2O	9,48	9,60	9,48	9,51	9,47	9,17	9,33	9,45	9,34	9,25	9,42
Total	94,62	94,74	95,34	94,94	95,76	95,35	95,36	95,24	94,73	96,06	97,07
O=22											
Si	5,345	5,321	5,319	5,337	5,341	5,340	5,348	5,329	5,355	5,355	5,356
Ti	0,727	0,712	0,717	0,717	0,718	0,710	0,732	0,743	0,812	0,736	0,738
Al(IV)	2,655	2,679	2,681	2,663	2,659	2,660	2,652	2,671	2,645	2,645	2,644
Al(VI)	0,341	0,377	0,313	0,315	0,264	0,302	0,251	0,235	0,168	0,286	0,301
Fe	2,150	2,136	2,215	2,188	2,220	2,266	2,252	2,312	2,246	2,198	2,192
Mn	0,005	0,002	0,008	0,003	0,004	0,003	0,001	0,000	0,003	0,001	0,001
Mg	2,092	2,098	2,100	2,122	2,138	2,087	2,111	2,088	2,093	2,092	2,026
Ca	0,000	0,000	0,000	0,000	0,006	0,003	0,003	0,002	0,003	0,003	0,003
Na	0,033	0,035	0,040	0,024	0,029	0,044	0,044	0,023	0,035	0,020	0,028
K	1,824	1,847	1,816	1,827	1,804	1,756	1,787	1,821	1,805	1,749	1,759
Total	15,173	15,206	15,208	15,195	15,183	15,170	15,182	15,224	15,165	15,085	15,049

	Verbaard	Verbaard	Verbaard	Verbaard	Verbaard	Verbaard	Verbaard	Verbaard	Verbaard	Verbaard	Verbaard
Rock	granitoid	granitoid	granitoid	granitoid	granitoid	granitoid	granitoid	granitoid	granitoid	granitoid	granitoid
SiO_2	35,72	35,00	33,67	34,36	34,33	30,86	34,47	33,49	33,34	33,71	31,28
TiO_2	6,43	6,50	6,85	6,28	6,31	4,87	6,43	5,93	5,85	6,14	5,32
Al_2O_3	15,88	17,28	16,63	16,91	17,05	17,43	16,95	17,12	16,94	17,59	17,78
FeO	18,06	17,09	18,11	17,80	17,34	21,95	17,54	18,56	19,60	18,82	21,39
MnO	0,02	0,03	0,05	0,01	0,00	0,06	0,06	0,00	0,02	0,07	0,02
MgO	9,40	9,42	9,01	9,05	9,17	9,63	9,04	8,84	8,57	9,62	9,80
CaO	0,04	0,04	0,88	0,00	0,01	0,07	0,03	0,01	0,03	0,10	1,18
Na_2O	0,09	0,18	0,13	0,15	0,12	0,05	0,17	0,14	0,14	0,17	0,08
K_2O	9,23	9,56	8,25	9,23	9,28	5,92	9,27	8,67	8,38	8,02	4,55
Total	94,87	95,10	93,58	93,79	93,61	90,84	93,96	92,76	92,87	94,24	91,40
O=22											
Si	5,392	5,272	5,206	5,280	5,275	4,973	5,280	5,236	5,232	5,166	4,959
Ti	0,730	0,736	0,797	0,726	0,729	0,590	0,741	0,697	0,690	0,708	0,634
Al(IV)	2,608	2,728	2,794	2,720	2,725	3,027	2,720	2,764	2,768	2,834	3,041
Al(VI)	0,217	0,341	0,237	0,344	0,363	0,284	0,340	0,390	0,365	0,343	0,282
Fe	2,280	2,153	2,342	2,288	2,228	2,958	2,247	2,427	2,572	2,412	2,836
Mn	0,003	0,004	0,007	0,001	0,000	0,008	0,008	0,000	0,003	0,009	0,003
Mg	2,115	2,115	2,077	2,073	2,101	2,313	2,064	2,060	2,005	2,198	2,316
Ca	0,006	0,006	0,146	0,000	0,002	0,012	0,005	0,002	0,005	0,016	0,200
Na	0,026	0,053	0,039	0,045	0,036	0,016	0,050	0,042	0,043	0,051	0,025
K	1,777	1,837	1,627	1,809	1,819	1,217	1,811	1,729	1,677	1,568	0,920
Total	15,155	15,245	15,271	15,286	15,278	15,398	15,266	15,347	15,361	15,305	15,216

Table 4.7. Representative mineral chemical data of feldspars in metapelites from the study area.

Rock	Metapelite	Metapelite	Metapelite	Metapelite	Metapelite	Metapelite	Metapelite	Metapelite
Mineral	Pl	Pl	Pl	Pl	Pl	Pl	Kfs	Kfs
SiO_2	62,65	62,38	62,14	62,34	62,50	62,74	61,823	64,006
TiO_2	0,00	0,01	0,08	0,02	0,06	0,00	0	0,03
Al_2O_3	23,45	23,54	23,53	23,35	23,07	23,09	17,487	18,441
FeO	0,04	0,00	0,05	0,00	0,04	0,05	0	0,109
MnO	0,03	0,02	0,00	0,00	0,01	0,02	0,03	0
MgO	0,00	0,00	0,01	0,00	0,00	0,00	0	0
CaO	4,78	4,81	4,97	4,97	4,63	4,72	2,032	0,136
Na_2O	8,51	8,69	8,68	8,54	8,99	9,03	0,743	0,641
K_2O	0,26	0,29	0,17	0,17	0,14	0,15	14,44	15,17
Total	99,71	99,74	99,62	99,39	99,44	99,80	96,56	98,53
O=8								
Si	2,779	2,770	2,763	2,775	2,783	2,784	2,967	2,991
Al	1,226	1,232	1,234	1,225	1,210	1,208	0,989	1,016
Fe(II)	0,002	0,000	0,002	0,000	0,002	0,002	0,000	0,004
Ca	0,227	0,229	0,237	0,237	0,221	0,225	0,104	0,007
Na	0,732	0,748	0,749	0,737	0,776	0,777	0,069	0,058
K	0,015	0,016	0,010	0,009	0,008	0,008	0,884	0,904
Total	4,980	4,995	4,994	4,984	5,000	5,004	5,014	4,980
Or	1,50	1,65	0,97	0,96	0,77	0,83	83,58	93,30
Ab	75,19	75,30	75,25	74,93	77,25	76,94	6,54	5,99
An	23,31	23,04	23,78	24,11	21,98	22,23	9,88	0,70

Table 4.8. Representative mineral chemical data of feldspars in the Verbaard granitoid.

	Verbaard	Verbaard	Verbaard	Verbaard	Verbaard	Verbaard	Verbaard	Verbaard	Verbaard	Verbaard	Verbaard	Verbaard	Verbaard
Rock	granitioid	granitioid	granitioid	granitioid	granitioid	granitioid	granitioid	granitioid	granitioid	granitioid	granitioid	granitioid	granitioid
Mineral	Kfs	Kfs	Kfs	Pl	Pl	Pl	Pl	Pl	Pl	Pl	Pl	Pl	Kfs
SiO_2	64,19	63,51	64,21	61,89	62,03	62,09	61,31	61,17	67,24	65,64	61,58	60,90	62,99
TiO_2	0,00	0,00	0,07	0,03	0,00	0,00	0,02	0,00	0,00	0,00	0,00	0,00	0,06
Al_2O_3	18,15	18,06	17,79	23,17	23,18	23,36	23,17	23,08	21,62	22,27	24,51	24,72	19,41
FeO	0,11	0,06	0,19	0,03	0,00	0,03	0,03	0,04	0,39	0,01	0,00	0,02	0,00
MnO	0,00	0,03	0,00	0,00	0,00	0,00	0,01	0,01	0,00	0,01	0,03	0,00	0,00
MgO	0,00	0,00	0,03	0,00	0,00	0,00	0,02	0,00	0,01	0,00	0,00	0,00	0,02
CaO	0,08	0,22	0,01	5,00	5,00	5,04	4,71	4,90	0,94	2,11	5,28	5,63	0,05
Na_2O	0,60	0,61	0,26	8,64	8,49	8,46	8,77	8,71	8,27	9,12	6,87	7,29	1,56
K_2O	15,40	15,31	15,91	0,47	0,48	0,48	0,35	0,29	0,09	0,11	0,36	0,36	14,22
Total	98,52	97,80	98,47	99,22	99,18	99,46	98,39	98,20	98,56	99,27	98,63	98,92	98,31
O=8													
Si	3,002	2,996	3,011	2,769	2,773	2,768	2,764	2,764	2,953	2,888	2,751	2,723	2,942
Al	1,000	1,004	0,983	1,222	1,222	1,228	1,231	1,229	1,119	1,155	1,290	1,303	1,069
Fe(II)	0,004	0,002	0,007	0,001	0,000	0,001	0,001	0,002	0,014	0,000	0,000	0,001	0,000
Ca	0,004	0,011	0,001	0,239	0,239	0,241	0,228	0,237	0,044	0,099	0,253	0,270	0,003
Na	0,054	0,056	0,024	0,749	0,736	0,732	0,766	0,763	0,704	0,778	0,595	0,632	0,141
K	0,919	0,921	0,952	0,027	0,027	0,028	0,020	0,017	0,005	0,006	0,021	0,021	0,847
Total	4,984	4,989	4,978	5,007	4,997	4,997	5,011	5,011	4,841	4,926	4,909	4,950	5,002
Or	94,02	93,27	97,52	2,63	2,71	2,75	2,01	1,67	0,67	0,70	2,36	2,23	85,49
Ab	5,55	5,62	2,41	73,79	73,41	73,16	75,56	75,00	93,46	88,04	68,53	68,53	14,26
An	0,43	1,11	0,07	23,58	23,88	24,09	22,43	23,33	5,87	11,26	29,11	29,25	0,25

Table 4.9. Representative mineral chemical data of cordierite (Crd) and sillimanite (Sill) in the low-Al metapelite from the study area.

Rock	LowAl meta	LowAl meta	LowAl meta	LowAl meta	LowAl meta	LowAl meta	LowAl meta	LowAl meta	LowAl meta	LowAl meta
Mineral	Crd	Crd	Crd	Crd	Crd	Crd	Crd	Crd	Crd	Crd
SiO_2	50,33	50,04	50,03	50,24	50,10	49,92	49,73	49,80	49,95	50,37
TiO_2	0,00	0,00	0,03	0,00	0,00	0,00	0,00	0,00	0,00	0,01
Al_2O_3	33,25	33,20	33,21	33,07	33,14	33,23	33,08	33,14	33,02	33,29
Cr_2O_3										
FeO	4,36	4,53	4,91	5,05	5,03	5,08	5,06	5,44	5,40	4,77
MnO	0,04	0,03	0,04	0,05	0,05	0,04	0,05	0,05	0,05	0,02
MgO	11,21	11,00	10,82	10,66	10,57	10,58	10,36	10,33	10,32	10,87
CaO	0,00	0,02	0,01	0,02	0,02	0,00	0,02	0,02	0,01	0,00
Na_2O	0,20	0,23	0,21	0,18	0,15	0,17	0,16	0,15	0,17	0,14
K_2O	0,00	0,01	0,01	0,01	0,00	0,00	0,01	0,01	0,01	0,00
Total	99,39	99,06	99,27	99,28	99,06	99,02	98,47	98,94	98,93	99,47
O=18										
Si	5,030	5,030	5,020	5,040	5,040	5,030	5,030	5,030	5,040	5,040
Ti	0,000	0,000	0,000	0,000	0,000	0,000	0,000	0,000	0,000	0,000
Al	3,920	3,930	3,930	3,910	3,930	3,940	3,950	3,940	3,930	3,920
Cr										
Fe	0,360	0,380	0,410	0,420	0,420	0,430	0,430	0,460	0,460	0,400
Mn	0,000	0,000	0,000	0,000	0,000	0,000	0,000	0,000	0,000	0,000
Mg	1,670	1,650	1,620	1,590	1,580	1,590	1,560	1,550	1,550	1,620
Ca	0,000	0,000	0,000	0,000	0,000	0,000	0,000	0,000	0,000	0,000
Na	0,040	0,040	0,040	0,040	0,030	0,030	0,030	0,030	0,030	0,030
K	0,000	0,000	0,000	0,000	0,000	0,000	0,000	0,000	0,000	0,000
Total	11,030	11,030	11,030	11,020	11,010	11,020	11,010	11,020	11,010	11,010
X_{Mg}	0,82	0,81	0,8	0,79	0,79	0,79	0,78	0,77	0,77	0,8

Rock	LowAl meta	LowAl meta	LowAl meta	LowAl meta	LowAl meta	LowAl meta	LowAl meta	LowAl meta	LowAl meta
Mineral	Crd	Crd	Crd	Crd	Crd	Crd	Sill	Sill	Sill
SiO_2	50,30	49,99	49,94	49,78	49,90	50,27	37,14	37,06	36,83
TiO_2	0,00	0,00	0,00	0,00	0,00	0,00			
Al_2O_3	33,30	33,07	33,19	33,20	33,19	33,38	62,00	62,32	62,08
Cr_2O_3							0,18	0,15	0,21
FeO	4,97	4,98	5,41	5,47	5,36	5,39	0,32	0,28	0,59
MnO	0,03	0,06	0,04	0,01	0,05	0,05	0,00	0,02	0,00
MgO	10,73	10,63	10,31	10,33	10,30	10,38	0,00	0,00	0,02
CaO	0,00	0,01	0,01	0,00	0,02	0,03	0,01	0,00	0,00
Na_2O	0,14	0,12	0,13	0,13	0,10	0,11	0,01	0,01	0,00
K_2O	0,00	0,00	0,00	0,00	0,00	0,00	0,02	0,01	0,00
Total	99,47	98,86	99,03	98,92	98,92	99,61	99,68	99,85	99,73
O=18							O=5		
Si	5,040	5,040	5,030	5,020	5,030	5,040	1,007	1,003	1,000
Ti	0,000	0,000	0,000	0,000	0,000	0,000			
Al	3,930	3,930	3,940	3,950	3,940	3,940	1,981	1,988	1,986
Cr							0,004	0,003	0,005
Fe	0,420	0,420	0,460	0,460	0,450	0,450	0,007	0,006	0,013
Mn	0,000	0,010	0,000	0,000	0,000	0,000	0,000	0,000	0,000
Mg	1,600	1,600	1,550	1,550	1,550	1,550	0,000	0,000	0,001
Ca	0,000	0,000	0,000	0,000	0,000	0,000	0,000	0,000	0,000
Na	0,030	0,020	0,030	0,030	0,020	0,020	0,001	0,001	0,000
K	0,000	0,000	0,000	0,000	0,000	0,000	0,001	0,000	0,000
Total	11,010	11,010	11,010	11,010	11,000	11,000	3,001	3,002	3,005
X_{Mg}	0,79	0,79	0,77	0,77	0,77	0,77			

Chapter 5

Whole-rock geochemical characteristics

5.1. Introduction

This chapter presents whole rock characteristics of the two types of metapelites (referred as Verbaard metapelites in geochemistry based figures), leucosome associated with the high-Al metapelite, and the Verbaard granitoid and associated leucocratic vein from the study area. For each rock type, separating a representative sample was challenging, especially to avoid contamination (e.g., Verbaard granitoid without garnet, leucosome without metapelite portion; Fig. 5.1). Each of the rock samples for powdering was carefully selected, after making sure of least contamination (through petrographic examination of thin section from the same sample). The biggest challenge faced was to sample the biotite-bearing Verbaard granitoid *sensu stricto* rock with no garnet. A mixed Verbaard granitoid (with visible garnet-bearing leucocratic vein and metapelitic material) was sampled close to the contact with metapelite (see Fig. 2.9b), and was also included for geochemical analyses to understand the effect of contamination and for comparison purpose. Major, trace and rare-earth element data obtained for all the rock samples are given in Tables 5.1 and 5.2.

5.2. Major element characteristics

High-Al metapelite was sampled from the O6-19 outcrop for whole-rock geochemistry. It is represented by sample O6-19M in Fig. 5.1, and is characterized by SiO_2 contents of 54.09

wt.%, TiO_2 of 1.44 wt.%, Al_2O_3 of 22.48 wt.%, Fe_2O_3 of 8.03 wt.%, MgO of 5.04 wt.%, CaO of 0.75 wt.%, Na_2O of 0.46 wt.%, and K_2O of 4.26 wt.% (Table 5.1). Mg# and total Fe+MgO+TiO_2 (Fe_t+Mg+Ti) of the high-Al metapelite are respectively 56.2 and 14.5.

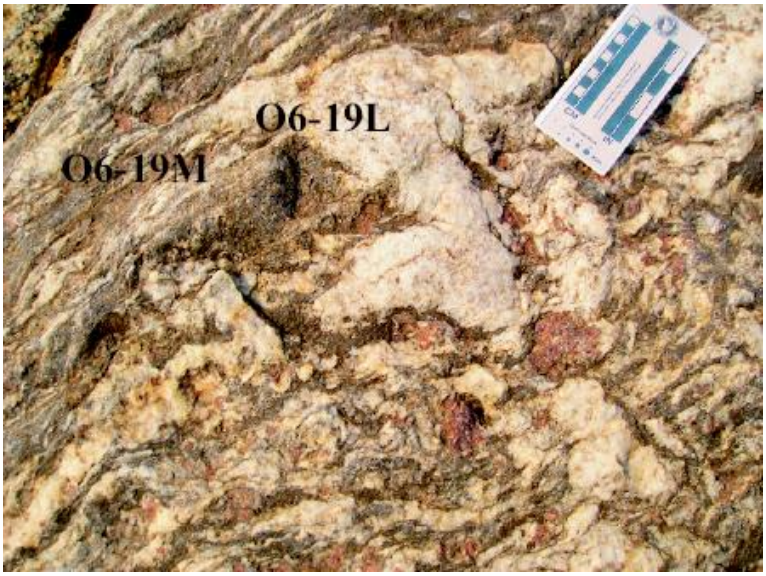


Figure 5.1. Field photograph illustrating the high-Al metapelite (sample O6-19M) and associated leucosome (O6-19L) sampled for whole-rock geochemistry.

In comparison, the low-Al metapelite (sample MT10) is characterized by higher SiO_2 (73.19 wt.%), Na_2O (0.66 wt.%) and K_2O (5.72 wt.%) contents, and lower TiO_2 of 0.31 wt.%, Al_2O_3 of 11.9 wt.%, Fe_2O_3 of 3.68 wt.%, MgO of 2.12 wt.%, CaO of 0.35 wt.%, Mg# (54.1) and (Fe_t+Mg+Ti) (6.1) (Table 5.1). The major element geochemical characteristics of O6-19M and MT10 are respectively similar to that of high-Al and low-Al metapelites reported by Boryta and Condie (1990) from the Musina area (Fig. 5.2). Comparing the major element contents of the metapelite samples from the study area indicates a clear progression from O6-19M to MT10, with the high silica sample characterized by more "felsic" elements and low silica sample with more "mafic" elements (Fig. 5.2).

Table 5.1. Representative major and trace element data for rocks from the study area.

Sample No	VG8a	VG8b	VG8c	VG8d	VG8e	VG8fg	VGL8f	O6-19L	O6-19M	MT10
Rock type	Verbaard granitoid	Verbaard granitoid	Verbaard granitoid	Verbaard granitoid	Verbaard granitoid	Verbaard granitoid (contaminated)	leucosome low-Al migm metapelite	leucosome high-Al migm metapelite	High-Al migm metapelite	Low-Al migm metapelite
SiO_2	72,77	72,32	72,41	71,30	72,89	71,56	73,83	72,83	54,09	73,19
TiO_2	0,30	0,30	0,28	0,29	0,31	0,41	0,08	0,02	1,44	0,31
Al_2O_3	14,89	15,02	14,96	14,58	14,74	15,17	14,79	16,06	22,48	11,90
Fe_2O_3*	1,57	1,64	1,68	2,10	1,61	3,18	1,13	0,26	8,03	3,68
MnO	0,01	0,01	0,01	0,01	0,01	0,03	0,03		0,07	0,03
MgO	0,47	0,52	0,52	0,53	0,54	1,86	0,29	0,03	5,04	2,12
CaO	2,32	2,33	2,30	2,08	2,26	1,32	3,65	4,13	0,75	0,35
Na_2O	4,18	3,79	3,86	3,49	3,89	2,64	3,77	4,06	0,46	0,66
K_2O	2,57	3,23	3,09	3,19	2,91	2,24	0,76	0,88	4,26	5,72
P_2O_5	0,05	0,06	0,06	0,08	0,05	0,02	0,02	0,03	0,01	0,04
LOI	0,70	0,60	0,70	1,30	0,60	1,30	0,80	0,85	1,90	0,85
Total	99,83	99,82	99,87	98,95	99,81	99,73	99,15	99,15	98,53	98,85
ASI	1,08	1,08	1,08	1,13	1,08	1,66	1,08	1,06	3,34	1,51
Na+K-Ca	4,43	4,69	4,65	4,60	4,54	3,56	0,88	0,81	3,97	6,03
Fe/Fe+Mg	0,77	0,76	0,76	0,80	0,75	0,63	0,80	0,90	0,61	0,63
K_2O/Na_2O	0,61	0,85	0,80	0,91	0,75	0,85	0,20	0,22	9,26	8,67
Mg#	38,02	39,38	38,81	34,08	40,73	54,51	34,46	19,12	56,25	54,14
Fe_t+Mg+Ti	2,34	2,46	2,48	2,92	2,46	5,45	1,50	0,31	14,51	6,11
Na_2O/K_2O	1,63	1,17	1,25	1,09	1,34	1,18	4,96	4,61	0,11	0,12
Quartz (Q)**	33,09	32,31	32,60	33,77	33,62	42,09	40,80	37,04	26,02	43,66
Corundum(C)	1,13	1,20	1,23	1,80	1,20	6,05	1,18	0,99	15,77	4,08
Orthoclase(Or)	15,19	19,09	18,26	18,85	17,20	13,24	4,49	5,20	25,18	33,80
Albite(Ab)	35,37	32,07	32,66	29,53	32,92	22,34	31,90	34,35	3,89	5,58
Anorthite(An)	11,18	11,17	11,02	9,80	10,89	6,42	17,98	20,29	3,66	1,48
Cr (ppm)	164,2	109,5	95,8	205,3	95,8	478,9	205,3	68,4	865,4	342,1
Ni	<20	<20	<20	6,4	<20	78	4,5	2	48,9	15,4
Ba	520	693	672	777	664	680	151,1	158,7	876,2	1359
Ga	21,7	20,3	21	23,5	20	18,9	17,6	15,7	33,5	14,9
Hf	4,6	4,2	4	6,8	4,7	3,9	6,2	6,1	14,3	13,1
Nb	3	2,4	2,6	1,9	2	5,8	3,4	3,4	16,6	6,7
Rb	51	61,4	59,6	72,5	59,5	56,9	27	14,6	156,9	140,5
Sr	218,2	225	233	220,7	230,5	116,2	217,2	166	60,9	79,1
Th	19,3	13,9	14,5	25	25,3	18	7,4	5	3,5	3
U	1,8	1,6	1,8		1,9	1,2				
V	33	35	32	24,9	29	94	14,7	8,6	174,7	46,9
Zr	153,7	151,7	143	165,7	159	126	84,2	58,8	270	77,5
Y	2,1	2,1	2,5	2,5	2,8	5,5	8,9	2,8	24,6	7,3
La	36,3	33	36,7	26,9	39,9	45,4	20,8	24,9	13,4	14,4
Ce	59,5	56,3	63,2	81,8	69,2	84,4	42,1	46,6	77,3	102,3
Rb/Ba	0,10	0,09	0,09	0,09	0,09	0,08	0,18	0,09	0,18	0,10
Rb/Sr	0,23	0,27	0,26	0,33	0,26	0,49	0,12	0,09	2,58	1,78
Sr/Y	103,90	107,14	93,20	88,28	82,32	21,13	24,40	59,29	2,48	10,84
Nb/Zr	0,02	0,02	0,02	0,01	0,01	0,05	0,04	0,06	0,06	0,09
Zr/Hf	33,41	36,12	35,75	24,37	33,83	32,31	13,58	9,64	18,88	5,92

*total Fe as Fe_2O_3; ASI - Aluminium saturation index; Na+K-Ca - Na_2O+K_2O-CaO; Fe/Fe+Mg - total Fe/total Fe+MgO; Fe+Mg+Ti - total Fe+MgO+TiO_2; ** CIPW norm; migm - migmatitic

Leucosome (sample O6-19L) associated with the high-Al metapelite O6-19M is characterized by SiO_2 contents of 72.83 wt.%, Al_2O_3 of 16.06 wt.%, Fe_2O_3 of 0.26 wt.%, CaO of 4.13 wt.%, Na_2O of 4.06 wt.%, K_2O of 0.88 wt.%, Mg# of 19.1 and (Fe_t+Mg+Ti) of 0.3 (Table

5.1). It falls in the field of tonalite in the normative An-Ab-Or triplot (Fig. 5.3a), is peraluminous in terms of aluminium saturation index [ASI = molar Al/(Ca – 1.67P + Na + K = 1.06] (Shand, 1943) (Fig. 5.3b) and corundum normative (0.99 vol.%) (Table 5.1), ferroan in terms of Fe-number [total Fe/ (total Fe+MgO)] (Fig. 5.3c) and calcic in terms of the modified alkali index (MALI; Na_2O+K_2O-CaO) (Fig. 5.3d).

The Verbaard granitoid (samples VG8a to VG8e; visibly no garnet or contamination) is characterized by SiO_2 contents of 71.3 to 72.89 wt.%, TiO_2 of 0.28 to 0.31 wt.%, Al_2O_3 of 14.58 to 15.02 wt.%, Fe_2O_3 of 1.57 to 2.1 wt.%, MgO of 0.47 to 0.54 wt.%, CaO of 2.08 to 2.33 wt.%, Na_2O of 3.49 to 4.18 wt.%, K_2O of 2.57 to 3.23 wt.%, Mg# of 34.1 to 40.7 and (Fe_t+Mg+Ti) of 2.34 to 2.92 (Table 5.1). They fall in the field of granodiorite in the normative An-Ab-Or triplot (Fig. 5.3a), peraluminous in terms of aluminium saturation index (ASI = 1.08-1.13; Fig. 5.3b) and corundum normative (1.13-1.8 vol.%) (Table 5.1), magnesian in terms of Fe-number (Fig. 5.3c) and calcic in terms of the modified alkali index (Fig. 5.3d).

Sample VG8fg represents a "contaminated" Verbaard granitoid, with visible garnet bearing leucocratic vein and metapelitic material (sampled near the contact with metapelite; see Fig. 2.9b), and is characterized by SiO_2 contents of 71.56 wt.%, TiO_2 of 0.41 wt.%, Al_2O_3 of 15.17 wt.%, Fe_2O_3 of 3.18 wt.%, MgO of 1.86 wt.%, CaO of 1.32 wt.%, Na_2O of 2.64 wt.%, K_2O of 2.24 wt.%, Mg# of 54.5 and (Fe_t+Mg+Ti) of 5.5 (Table 5.1). It has higher Ti, Al, Fe and Mg, and lower Ca, Na and K, than Verbaard granitoid *sensu stricto* samples (Fig. 5.1). The strongly peraluminous (ASI = 1.66) (Fig. 5.3b) and corundum normative (6 vol.%) compositions indicate the abundance of garnet in sample VG8fg (Table 5.1).

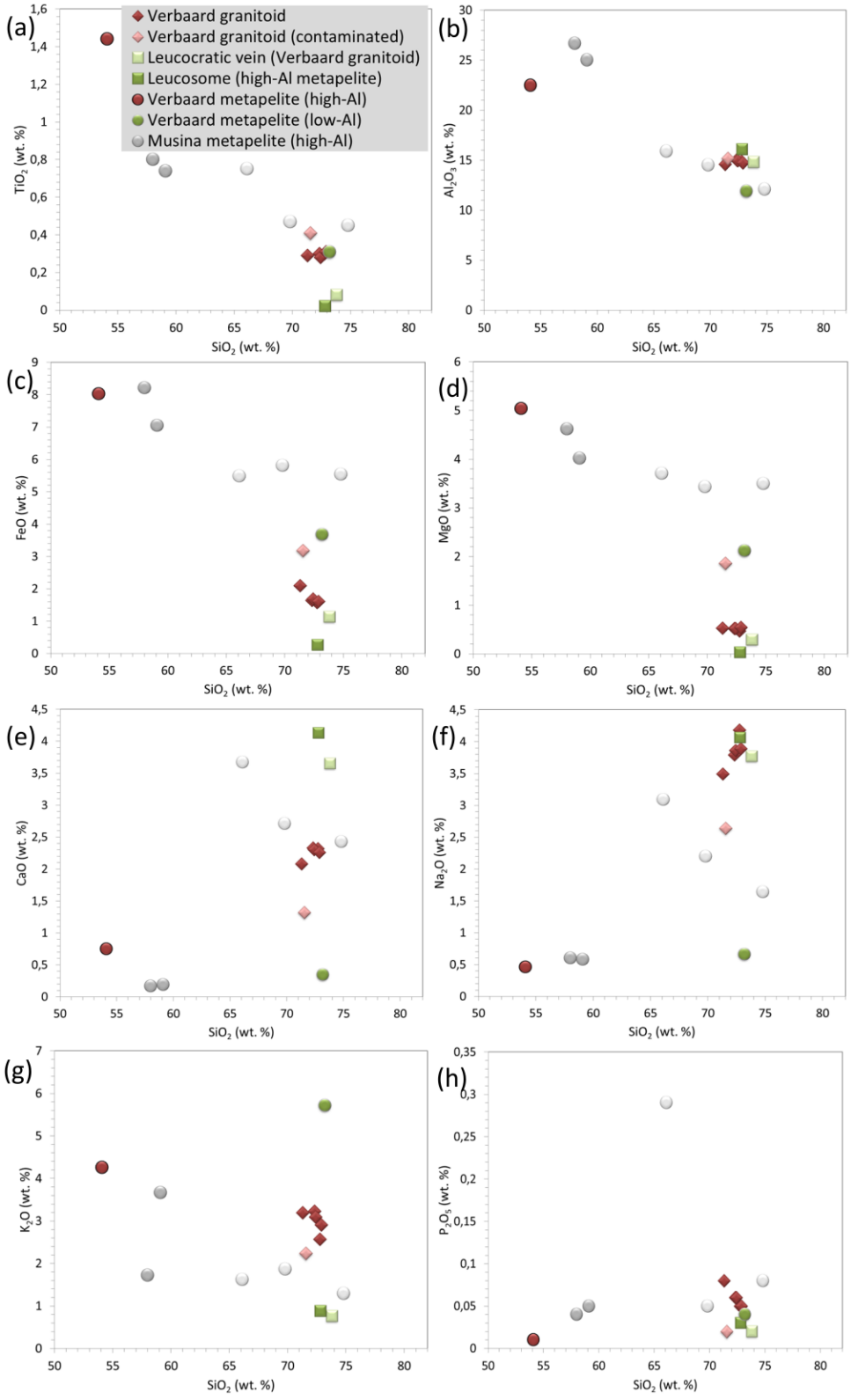


Figure 5.2. Major element Harker variation diagrams for the rocks from the study area. Data on high-Al and low-Al metapelite from Musina (Musina metapelite) is from Boryta and Condie (1990).

The leucocratic vein (sample VGL8f – no garnet occurs in the sample) associated with the Verbaard granitoid is characterized by SiO_2 contents of 73.83 wt.%, Al_2O_3 of 14.79 wt.%, Fe_2O_3 of 1.13 wt.%, MgO of 0.29 wt.%, CaO of 3.65 wt.%, Na_2O of 3.77 wt.%, K_2O of 0.76 wt.%, Mg# of 34.5 and (Fe_t+Mg+Ti) of 1.5 (Table 5.1). It falls in the field of tonalite in the normative An-Ab-Or triplot (Fig, 5.3a), is peraluminous in terms of aluminium saturation index (ASI = 1.08; Fig. 5.3b) and corundum normative (1.18 vol.%) (Table 5.1), magnesian in terms of Fe-number (Fig. 5.3c) and calcic in terms of the modified alkali index (Fig. 5.3d).

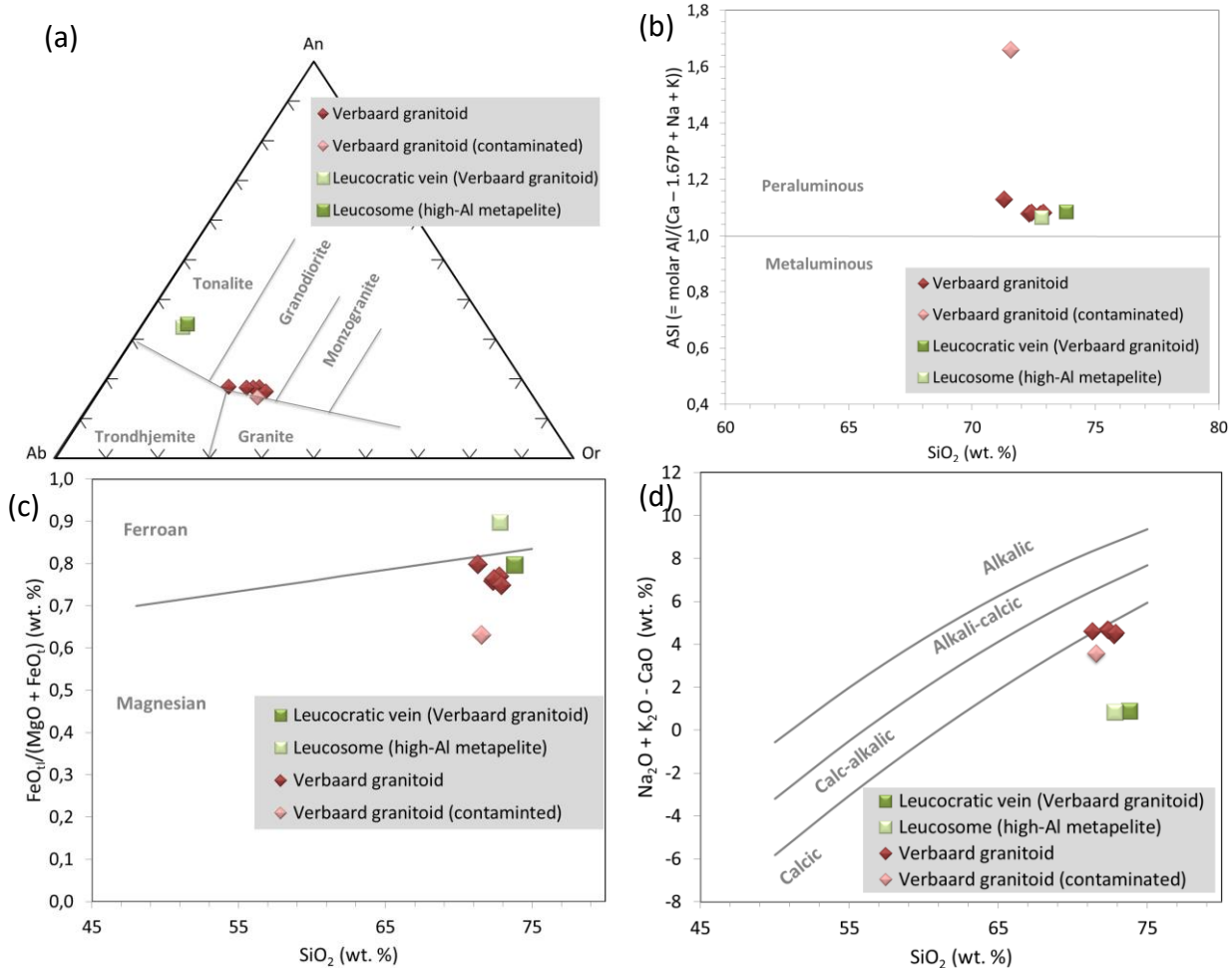


Figure 5.3. The felsic rocks from the study area in terms of the normative An-Ab-Or classification diagram of O'Connor (1965) modified by Barker (1979 **(a)**, aluminium saturation index (ASI) vs. SiO_2 plot **(b)**, FeO_t/(MgO + FeO_t) vs. SiO_2 plot **(c)**, and Na_2O + K_2O-CaO vs. SiO_2 plot **(d)**.

To understand which mineral phases control the composition of the Verbaard granitoid, average compositions of prominent rock-forming minerals were plotted together with the whole-rock content (Fig. 5.4). Based on petrography, minerals in equilibrium were connected by tie lines in these plots (Fig. 5.4). It follows that the composition of the Verbaard granitoid is mainly controlled by felsic minerals plagioclase, quartz and K-feldspar (Fig. 5.4). When considering the "mafic" elements, biotite also plays a prominent role in controlling the composition of the Verbaard granitioid (Fig. 5.4). The good correlation between mineral chemical data and whole-rock geochemical data supports petrographic observations, arguing for the general preservation of primary magmatic compositions in the studied Verbaard granitoid.

5.3. Trace and rare earth element characteristics

The metapelites are characterized by high contents of Cr, Ni, V and Nb, with high-Al metapelite (Cr = 865.4 ppm; Ni = 48.9 ppm; V = 174.7 ppm; Nb = 16.6 ppm) having higher contents than the low-Al metapelite (Cr = 342.1 ppm; Ni = 15.4 ppm; V = 46.9 ppm; Nb = 6.7 ppm) (Table 5.1; Fig. 5.5). The felsic rocks have lower Cr, Ni, V and Nb contents, with the Verbaard granitoid having 95.8 to 205.3 ppm Cr, 6.4 to <20 ppm Ni, 24.9 to 35 ppm V and 2 to 3 ppm Nb, leucocratic vein associated with the Verbaard granitoid having 205.3 ppm Cr, 5 ppm Ni, 14.7 ppm V and 3.4 ppm Nb, and the leucosome associated with high-Al metapelite having 68.4 ppm Cr, 2 ppm Ni, 8.6 ppm V and 3.4 ppm Nb (Table 5.1; Fig. 5.5).

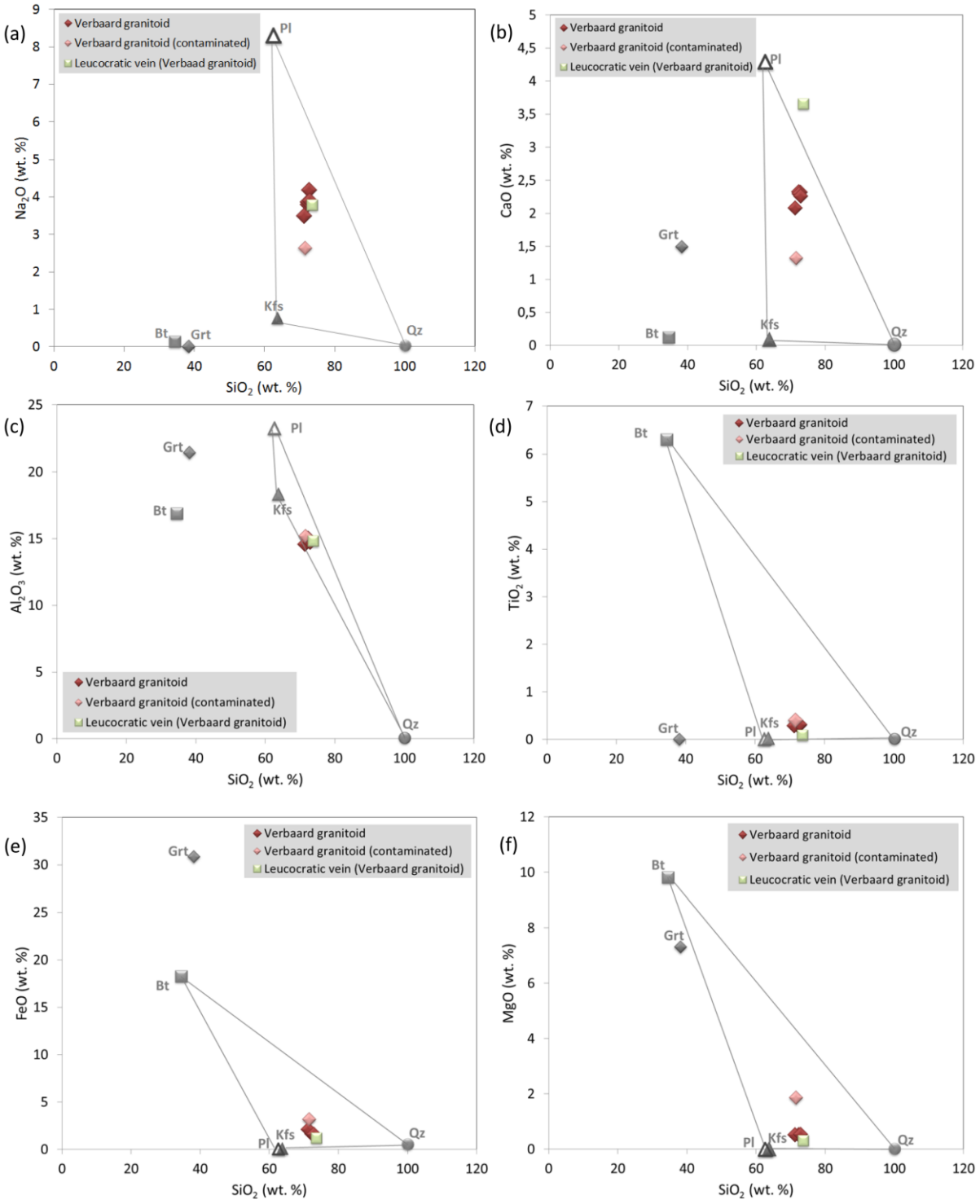


Figure 5.4. (a to **f)** Major element Harker variation diagrams comparing the whole-rock compositions of the Verbaard granitoid from the study area, with average compositions of prominent minerals from the rock. The leucocratic vein associated with the Verbaard granitoid is also plotted for comparison. Tie lines are connected between minerals in equilibrium and are based on petrography.

The contaminated Verbaard granitoid sample has higher Cr (478.9 ppm), Ni (78 ppm), and V (94 ppm) than Verbaard granitoid *sensu stricto* samples (Table 5.1).

The Na-rich nature of the felsic rocks are characterized by high contents of Sr, with the Verbaard granitoid having the highest (218.2-233 ppm), followed by leucocratic vein associated with the Verbaard granitoid (217.2 ppm) and the leucosome associated with high-Al metapelite (166 ppm) (Table 5.1). The metapelites have lower Sr contents (high-Al metapelite: 60.9 ppm; low-Al metapelite: 79.1) (Table 5.1; Fig. 5.5). The contaminated Verbaard granitoid also has lower Sr (116 ppm) content.

Ba and Rb contents correlate with the K contents of the rocks. The metapelites with biotite abundance have high contents with low-Al metapelite having higher contents (Ba = 1359 ppm; Rb = 140.5 ppm), than the high-Al metapelite (Ba = 876.2 ppm; Rb = 156.9 ppm) (Table 5.1; Fig. 5.5). The Verbaard granitoid, where biotite is the main mafic rock-forming mineral, also have high Ba and Rb contents (Ba = 520-777 ppm; Rb = 51 to 72.5 ppm). The contaminated Verbaard granitoid has comparable Ba (680 ppm) and Rb (57 ppm) contents (Table 5.1). The leucosome (Ba = 158.7 ppm; Rb = 14.6 ppm) and leucocratic vein (Ba = 151.1 ppm; Rb = 27 ppm) have the lowest Ba and Rb contents (Table 5.1; Fig. 5.5).

Like the major element contents, comparing the trace element contents of the metapelite samples from the study area indicates a progression from O6-19M (low silica) to MT10 (high silica) (Fig. 5.5).

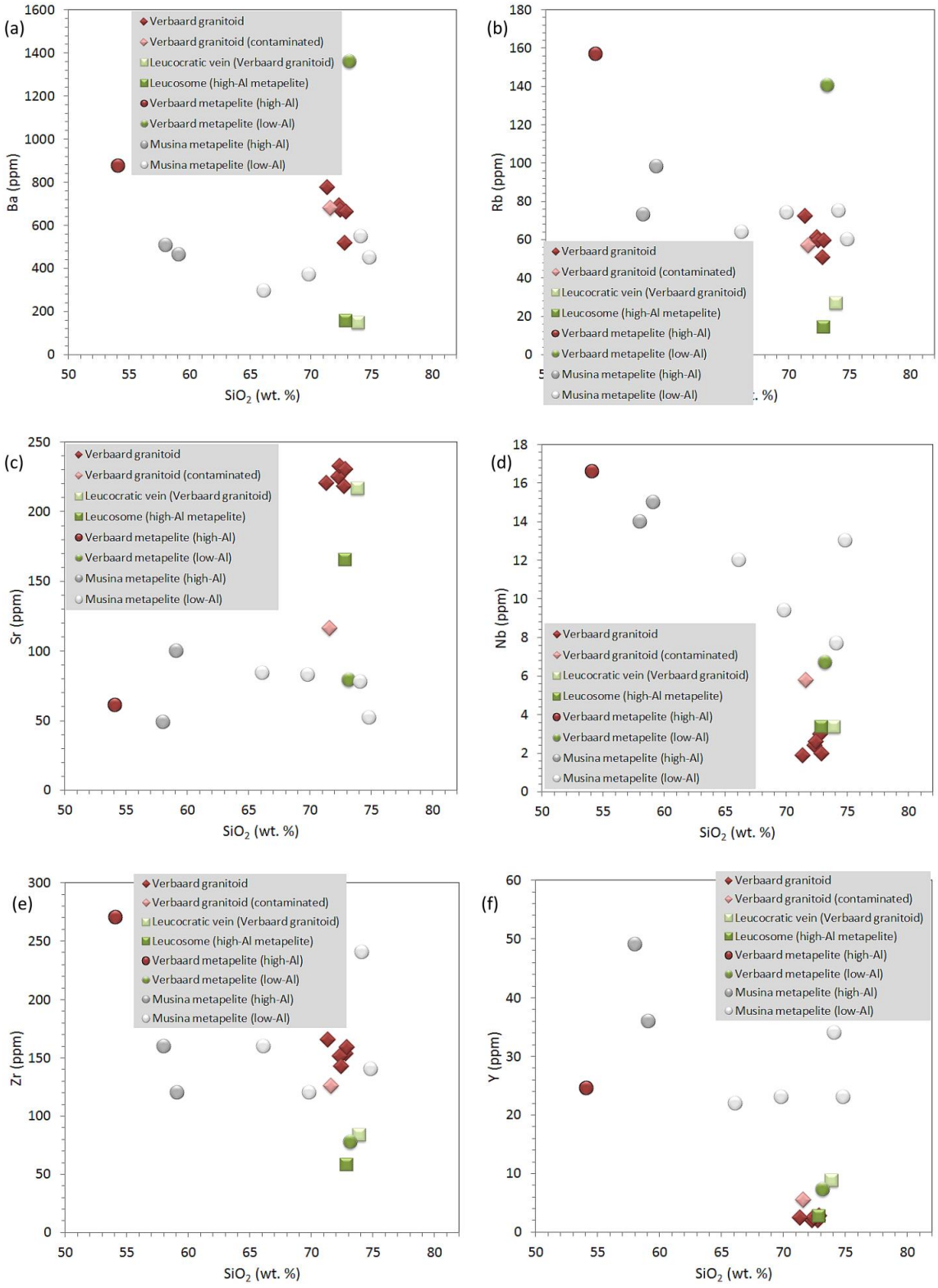


Figure 5.5. Trace element Harker variation diagram for the rocks from the study area. Data on high-Al and low-Al metapelite from Musina (Musina metapelite) is from Boryta and Condie (1990).

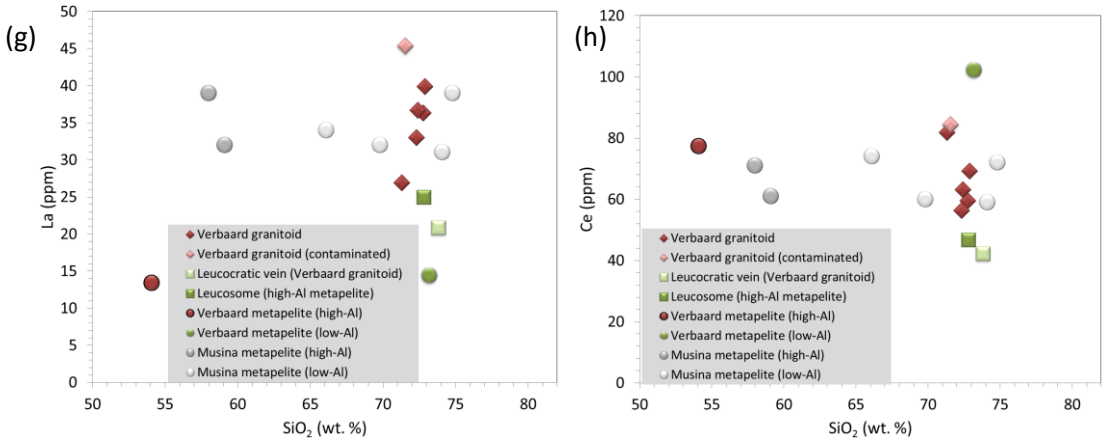


Figure 5.5. continued. Trace element Harker variation diagram for the rocks from the study area.

In terms of trace element ratios, metapelites (high-Al metapelite: 2.6; low-Al metapelite: 1.8) have higher Rb/Sr than the felsic rocks (Verbaard granitoid: 0.23-0.33; contaminated Verbaard granitoid: 0.49; leucocratic vein associated with Verbaard granitoid: 0.12; leucosome associated with high-Al metapelite: 0.09) (Table 5.1). In contrast, the Sr/Y (Verbaard granitoid: 82-107; leucocratic vein associated with Verbaard granitoid: 24; leucosome associated with high-Al metapelite: 59) and Zr/Hf (Verbaard granitoid: 24-36; leucocratic vein associated with Verbaard granitoid: 14; leucosome associated with high-Al metapelite: 10) ratios are higher in the felsic rocks than the metapelites [high-Al metapelite: 2.5 (Sr/Y), 19 (Zr/Hf); low-Al metapelite: 11 (Sr/Y), 6 (Zr/Hf)] (Table 5.1). The contaminated Verbaard granitoid has a Sr/Y ratio of 21.1 and Zr/Hf ratio of 32.3.

In the primitive-mantle normalized (Sun and McDonough, 1989) multi-element spider gram, the Verbaard granitoid *sensu stricto* and contaminated Verbaard granitoid show similar large ion lithophile element (LILE) enrichment, with high-field strength element (HFSE) depleted pattern (Fig. 5.6a), and negative Nb, Ta, P and Ti anomalies (Fig. 5.6a).

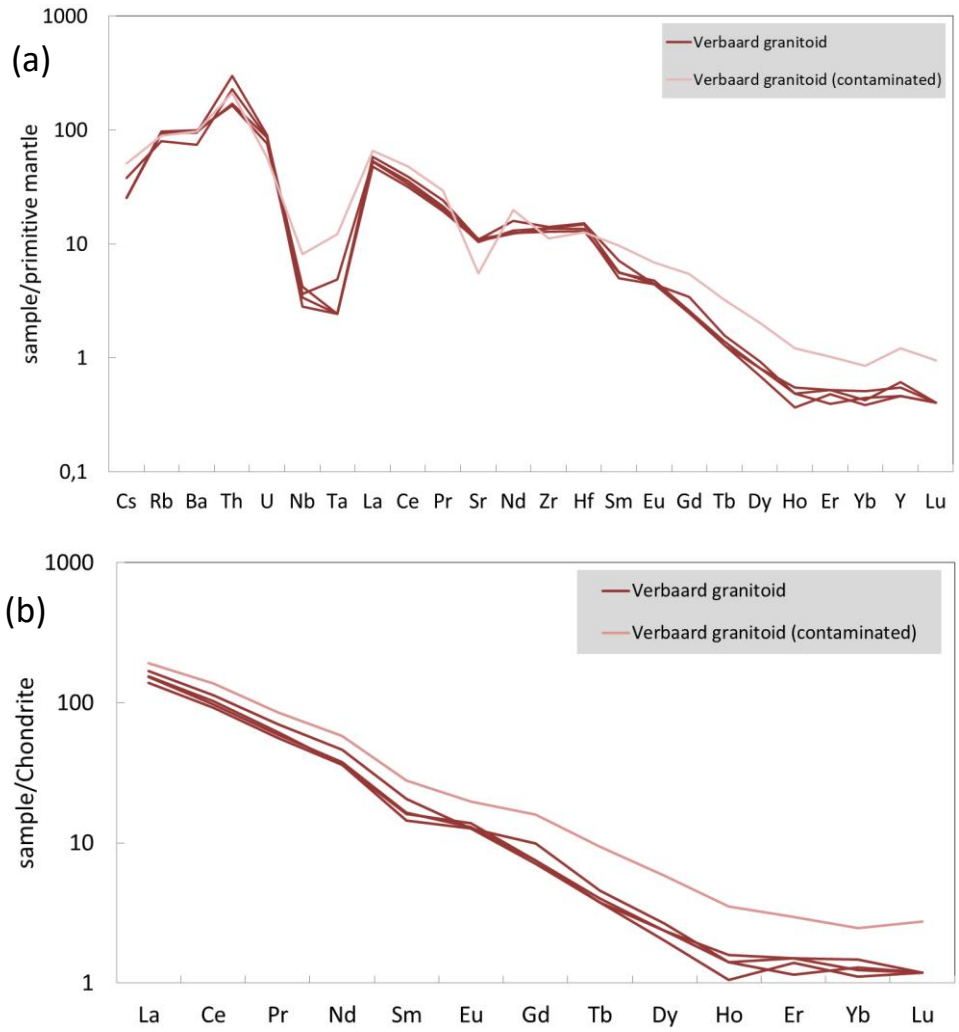


Figure 5.6. Primitive mantle-normalized (Sun and McDonough, 1989) trace element spider gram **(a)** and chondrite-normalized (Sun and McDonough, 1989) REE diagram **(b)** of the Verbaard granitoid *sensu stricto* and contaminated Verbaard granitoid from the study area.

The chondrite-normalized (Sun and McDonough, 1989) REE patterns of the rocks also show similar pattern with enrichment of light REE (LREE, e.g., La) relative to middle REE (MREE, e.g., Sm) [$(La/Sm)_N$ – Verbaard granitoid *sensu stricto*: 8.2-9.6; contaminated Verbaard granitoid: 6.8], depletion of heavy REE (HREE, e.g., Yb) [$(Gd/Yb)_N$ – Verbaard granitoid *sensu stricto*: 1.6-2.2; contaminated Verbaard granitoid: 2.4] and variable Eu

anomalies [(Eu/Eu*) – Verbaard granitoid *sensu stricto*: 0.8-1.2; contaminated Verbaard granitoid: 0.9] (Fig. 5.6b; Table 5.2).

Table 5.2. Representative REE data of Verbaard granitoid samples from the study area.

Sample No	VG8a	VG8b	VG8c	VG8e	VG8fg
Rock type	Verbaard granitoid	Verbaard granitoid	Verbaard granitoid	Verbaard granitoid	Verbaard granitoid (with grt)
La (ppm)	36,3	33	36,7	39,9	45,4
Ce	59,5	56,3	63,2	69,2	84,4
Pr	5,64	5,32	5,91	6,7	8,14
Nd	17,7	16,8	16,9	21,7	27
Sm	2,52	2,22	2,47	3,16	4,29
Eu	0,75	0,74	0,8	0,74	1,15
Gd	1,54	1,46	1,54	2,03	3,26
Tb	0,14	0,14	0,15	0,17	0,35
Dy	0,6	0,51	0,6	0,68	1,49
Ho	0,08	0,06	0,09	0,08	0,2
Er	0,19	0,23	0,25	0,25	0,49
Tm	0,02	0,02	0,02	0,02	0,06
Yb	0,22	0,19	0,25	0,21	0,42
Lu	0,03	0,03	0,03	0,03	0,07
La/Sm_N	9,30	9,60	9,59	8,15	6,83
Dy/Yb_N	1,83	1,80	1,61	2,17	2,37
Eu/Eu*	1,08	1,18	1,17	0,84	0,90
La/Yb_N	118,35	124,58	105,30	136,29	77,54

Except the contaminated sample, the rest of the Verbaard granitoid samples form a coherent group in the different major, trace and REE plots, and can be used for petrogenetic characterization purposes. After establishing the provenance of garnet found associated with the Verbaard granitoid and understanding its implications, detailed petrogenetic characterization is attempted in chapter 6, as part of discussion of the results.

Chapter 6

Discussion

6.1. Introduction

This chapter primarily focuses on two aspects related to the Verbaard granitoid – provenance of garnet associated with it and petrogenetic characterization. Discussion on metapelites from the Musina area, related high-grade events and compositional variation of garnet serves the earlier purpose, while the later on petrogenesis is done in comparison to other related Neoarchean granitoids from the Central Zone. Relevant background material from published literature is included to help put forward the case argued here.

6.2. Are the two groups of metapelites an artifact of the extent of partial melting?

Although Boryta and Condie (1990) recognized two groups of metapelite in the Musina area (including the Verbaard area) based on their whole-rock Al content (see Figs. 5.2, 5.5), they do not present any field, petrographic or mineral chemical characteristics of the high-Al and low-Al metapelites. The present study carried out a detailed field, petrographic and mineral chemical characterization of high-Al and low-Al metapelites from the Verbaard area (summary of characteristic features given in Fig. 6.1).

From the field (see chapter 2), the main difference between the two types of metapelite is the darker appearance of the high-Al metapelite with more restitic domains and lesser volume of leucosomic material (see Figs. 2.3, 2.5, 6.1a), and the lighter appearance of the

low-Al metapelite due to the higher volume of leucosomic material (see Figs. 2.4, 6.1b). Biotite-rich melanocratic layers typically occur along the margins of the leucosomic material in both metapelites (Figs. 6.1a, b). The occurrence of garnet is conspicuous in both metapelites (Figs. 6.1a, b), with increase of garnet grain size from the restitic domain to the leucosomic material. The irregular outline of leucosomic material associated with the metapelites argues for *in situ* partial melting.

From petrography (see chapter 3), a conspicuous feature of metapelites is the sillimanite-cordierite±biotite-dominant layers, which is thicker and prominent in the darker high-Al metapelite (see Figs. 3.1, 3.2, 6.1c), while the layers/patches in the low-Al metapelite are thinner and almost devoid of biotite (see Figs. 3.10, 6.1d). In contrast, quartzofeldspathic material with lobate rounded grain margins, typical of anatectic origin (Figs. 6.1e, f), occurs in both metapelites, with a prominence in the low-Al metapelite. The lesser modal proportion of biotite and prominence of quartzofeldspathic material can be interpreted in terms of progression of biotite dehydration melting, resulting in the formation of garnet.

In terms of mineral chemistry (see chapter 4), garnets in both high-Al and low-Al metapelites are pyrope-almandine solid solutions, with minor grossular and spessartine components (Table 4.1). The garnets in both metapelites have comparable compositions (see Figs. 4.2, 6.1g), indicating that they likely belong to the same generation (see also section 6.3). Similarly, biotite mineral chemical compositions in both metapelites are comparable (see Fig. 4.6).

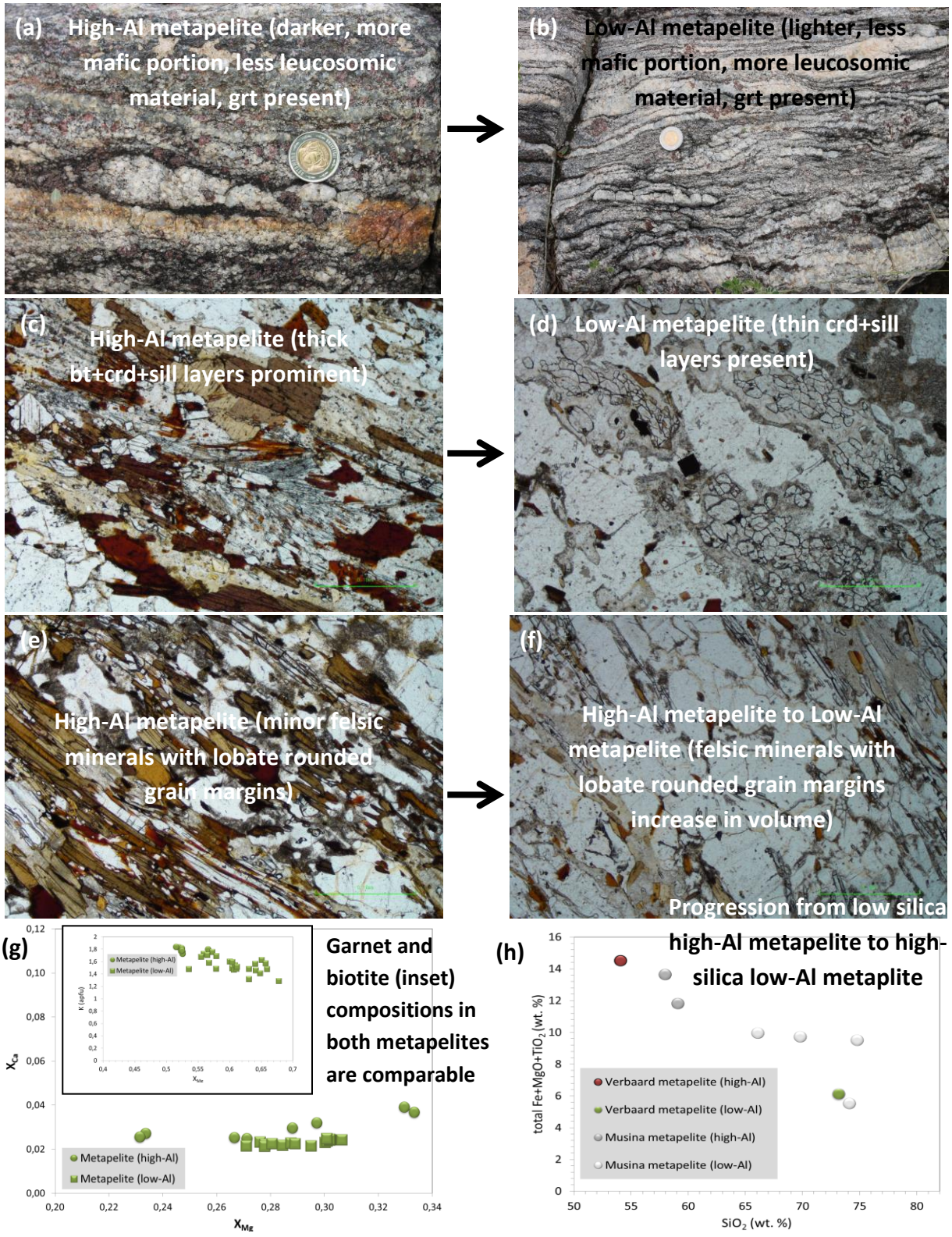


Figure 6.1. Comparison of characteristic field **(a, b)**, petrographic **(c** to **f)**, mineral chemical **(g)** and whole-rock geochemical **(h)** features of high-Al and low-Al metapelites from the study area.

In terms of whole-rock geochemistry (see chapter 5), a progression can be seen between the major and trace element concentrations from low-silica high-Al metapelite to high-silica low-Al metapelite (see Figs. 5.2, 5.6, 6.1h). This progression correlates well with the presence of more leucosomic material and less restitic domain in the low-Al metapelite than the high-Al metapelite. Thus it is suggested that the distinction of the two groups of metapelite – high-Al and low-Al – is an artifact of the extent of partial melting, with the high-Al metapelite preserving more of the restitic domains, while the low-Al metapelite preserving more of the leucosomic material. Such an argument is further supported by the similar chondrite normalized REE and primitive mantle normalized multielement patterns in Fig. 6.2. Hence there is no need to distinguish two groups of Beit Bridge Group metapelites, and the two groups recognized by earlier studies is just an artifact of the extent of partial melting preserved within the metapelite at a particular location. Instead, focus should be on the number of melting event(s) related to the high-grade event(s) on the metapelite.

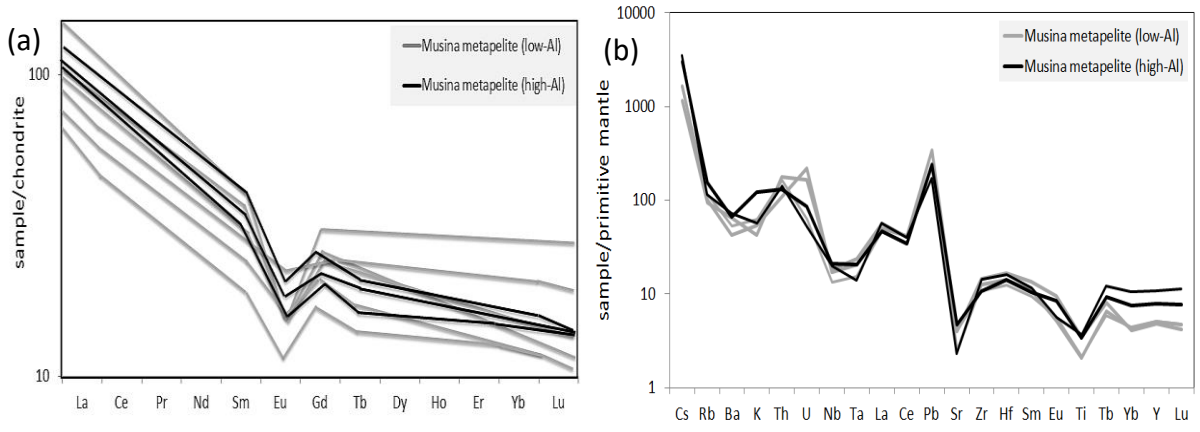


Figure 6.2. Chondrite normalized REE **(a)** and primitive mantle normalized multielement spider **(b)** diagrams of low-Al and high-Al metapelites from the Musina area [from Boryta and Condie (1990)].

6.3. Timing of high-grade event(s) and related melting of the metapelites

Previous studies from the Musina area recognized two high-grade events and related melting of the metapelites (Jaeckel et al., 1997; Holzer et al., 1998; Boshoff, 2008; Millonig et al., 2008; Van Reenen et al., 2008).

Holzer et al. (1998) obtained a Pb–Pb sillimanite–garnet isochron age of 2521 ± 4 Ma from a metapelite enclave within the Neoarchean Bulai pyroxene-bearing granitoid, in the northern part of the Musina area (see Fig. 1.10). Millonig et al. (2008) obtained U–Pb monazite ages of 2644 ± 8 Ma (monazite enclosed in garnet) and 2639 ± 8 Ma (matrix monazite) from another metapelite enclave within the ~2.61 Ga Bulai pyroxene-bearing granitoid (Figs. 6.3a, b). They correlated the ~2.64 Ga to the metamorphic overprint of the metapelite by the intruding ~2.65 Ga Singelele leucogranite in the area (see Figs. 6.4a, b). These and other studies pointed out the absence of any Paleoproterozoic high-grade event within the Bulai pluton, in the northern part of the Musina area. The metapelite inclusions were likely shielded from the Paleoproterozoic event by the Bulai pluton.

Boshoff (2008) studied the metapelite at the O6-19 outcrop (same outcrop as in the present study) from southwest of Musina. U-Pb data for zircon and monazite from the leucosome (O6-19L) associated with the metapelite at O6-19 was presented by Boshoff (2008) and Van Reenen et al. (2008). Of the strongly discordant zircons, one cluster of four grains closer to the Concordia defined a mean $^{207}Pb/^{206}Pb$ age of 2011 ± 11 Ma, while another cluster of four <1% discordant grains defined a concordant age of 2610.3 ± 8.5 Ma (Fig. 6.3d). All the monazite data yielded a combined mean $^{207}Pb/^{206}Pb$ age of 2017.1 ± 2.8

Ma (Fig. 6.3c). Thus the metapelite at O6-19, southwest of Musina, records evidence for two high-grade events (Boshoff, 2008; Van Reenen et al., 2008). Application of the Pb–Pb stepwise leaching (PbSL) geochronologic method on garnet from the darker restitic domain (O6-19M) and the composite leucosome (O6-19L) from O6-19 gave errorchron ages of 2310 ± 43 Ma and 2103 ± 820 Ma, interpreted as mixed ages that reflect the effect of the Palaeoproterozoic overprint onto the Neoarchaean Pb-Pb isotopic signature of the minerals (Boshoff, 2008).

Jaeckel et al. (1997) presented U-Pb zircon data on metapelites and associated garnet-bearing leucosomes from the Causeway locality, north of the O6-19 outcrop (southeast of Musina). Here the metapelites occur infolded with the ~3·31-3·28 Ga Sand River granitoid gneiss, with the garnet-bearing leucosome occurring as an in situ melt patch in the metapelite. They reported mean $^{207}Pb/^{206}Pb$ ages of 2027.8 ± 4.7 Ma and 2026.8 ± 0.5 Ma from the metapelite, and 2026 ± 8 Ma from the garnet-bearing leucosome (Figs. 6.3e, f). Although the Paleoproterozoic ages have been interpreted as peak metamorphic, the possibility of an earlier Neoarchean high-grade event cannot be discounted. This is supported by field evidence of intrusion of the Neoarchean Singelele leucogranite into metapelite at the Causeway locality (Figs. 6.4c, d). Later studies from the Causeway locality on the Sand River granitoid gneiss indicated the prominence of two high-grade metamorphic events – ~2.65 and 2.02 Ga (Gerdes and Zeh, 2009; Zeh et al., 2010). Further, the overwhelming nature of the Paleoproterozoic event at the Causeway locality has been pointed out by a number of studies (Jaeckel et al., 1997; Rajesh et al., 2014).

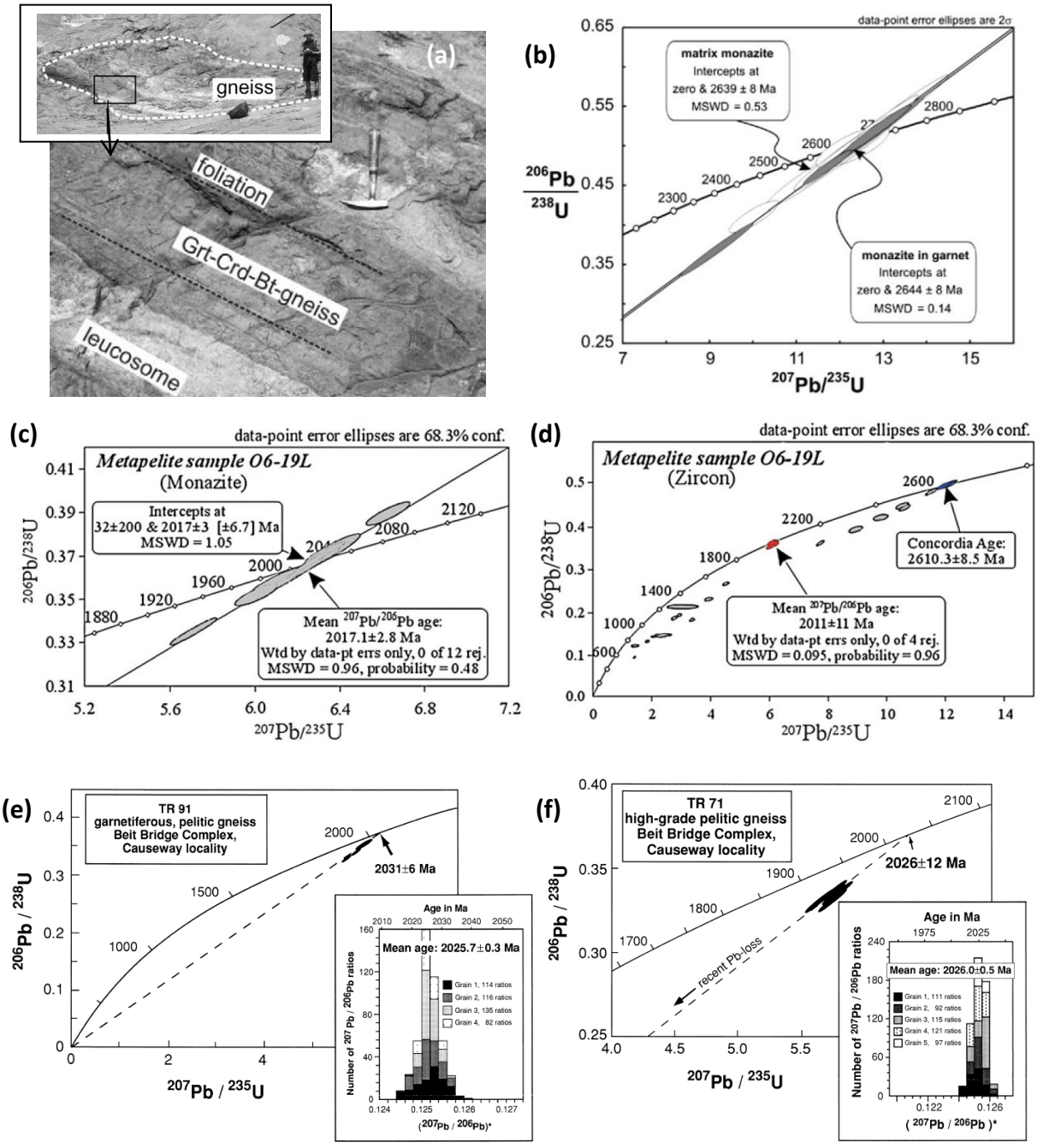


Figure 6.3. (a) Field photograph illustrating the garnet (Grt)–cordierite (Crd)–biotite (Bt)-bearing metapelite and associated leucosome studied by Millonig et al. (2008). It occurs as an inclusion within the Bulai porphyritic granitoid (see inset). **(b)** U – Pb Concordia diagram showing the results of monazite dating from the metapelite shown in (a) [from Millonig et al. (2008)]. U – Pb concordia diagrams of the monazite **(c)** and zircon **(d)** analyses of the leucocratic material (O6-19L) from the metapelite at O6-19 (from Van Reenen et al., 2008). U-Pb Concordia diagrams of zircons from garnetiferous metapelite **(e)** and associated garnet-bearing in situ leucosome **(f)** from the Causeway locality. Inset in both (e) and (f) shows histogram for radiogenic Pb isotope ratios and the mean age [from Jaeckel et al. (1997)].

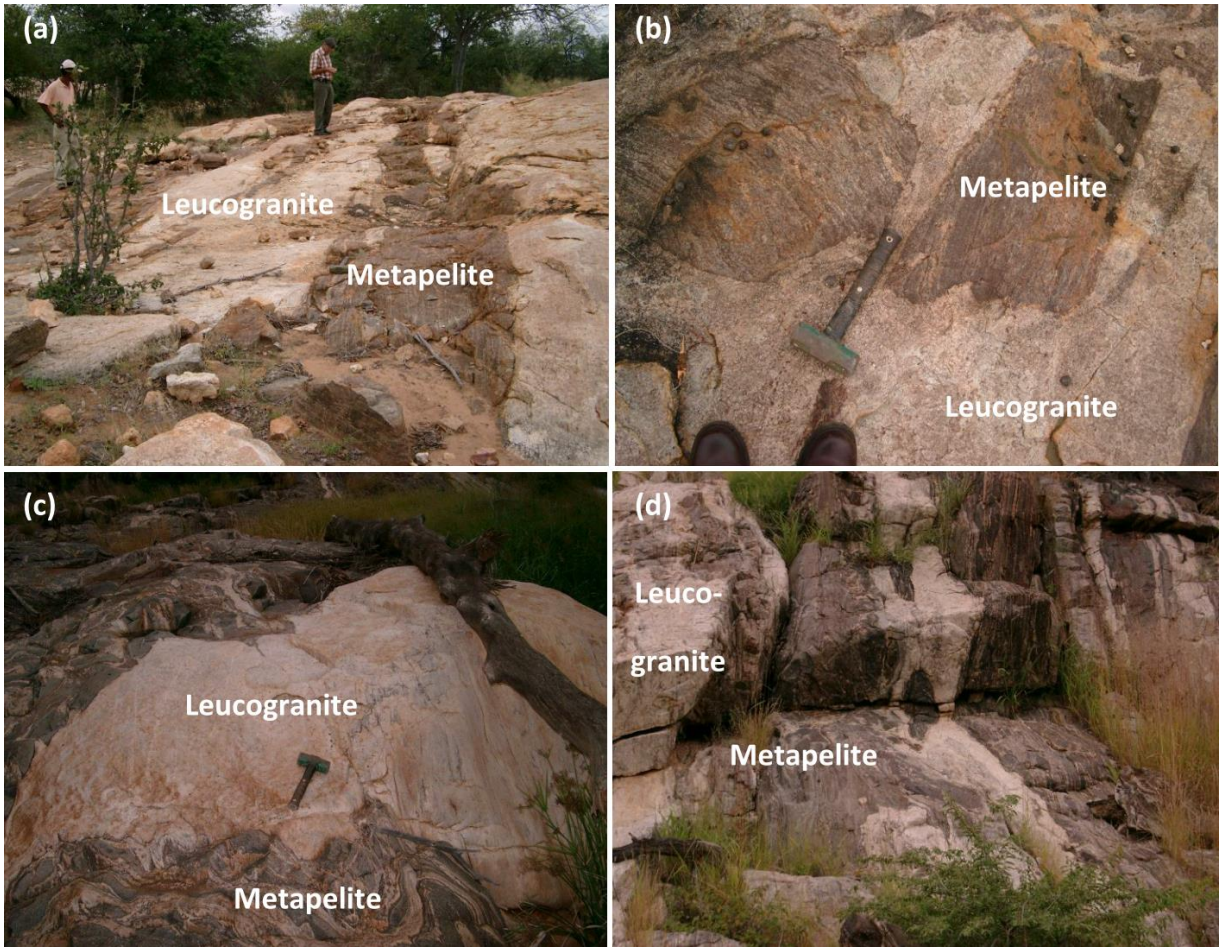


Figure 6.4. Field photographs illustrating the prominent intrusive relation between the Neoarchean Singelele leucogranite and the older metapelite. **(a)** and **(b)** – within the Bulai pluton, in the northern part of the Musina area. **(c)** and **(d)** – from the Causeway locality, to the southeast of Musina.

Thus, except within the Bulai pluton, a typical metapelite from the Musina area has likely undergone two high-grade events (Jaeckel et al., 1997; Holzer et al., 1998; Boshoff, 2008; Millonig et al., 2008; Van Reenen et al., 2008). The earlier high-grade event is related to the intrusion of the Neoarchean granitoids. Both the events likely resulted in accompanying melting (Jaeckel et al., 1997; Holzer et al., 1998; Boshoff, 2008; Millonig et al., 2008; Van Reenen et al., 2008).

6.4. Compositional variation of garnet in metapelites

Rim-core-rim profiles of garnets in metapelites from the Musina area were presented by Zeh et al. (2004), Millonig et al. (2008), Perchuk et al. (2008) and this study. The three metapelites studied by Zeh et al. (2004) are closer to the present study area (Fig. 6.5a). In terms of the mineral assemblage, the metapelite at PA and KA are comparable to the one studied from the Verbaard area. Garnet (garnet A in Fig. 6.5b) in metapelite from PA preserve a relic prograde zonation, characterized by increasing Xprp contents towards the rim (~0.35 to 0.38; Zeh et al., 2004). Xgrs of the same garnet shows a decrease towards the rim (~0.08 to 0.04) (Fig. 6.5b). Garnet in metapelite from KA has a more or less constant Xgrs (~0.04-0.03), similar to the rim composition of PA (Fig. 6.5b). The decreasing Xprp of garnet A (in metapelite PA) at its margins is due to retrograde diffusive Fe-Mg exchange with matrix minerals (Zeh et al., 2004).

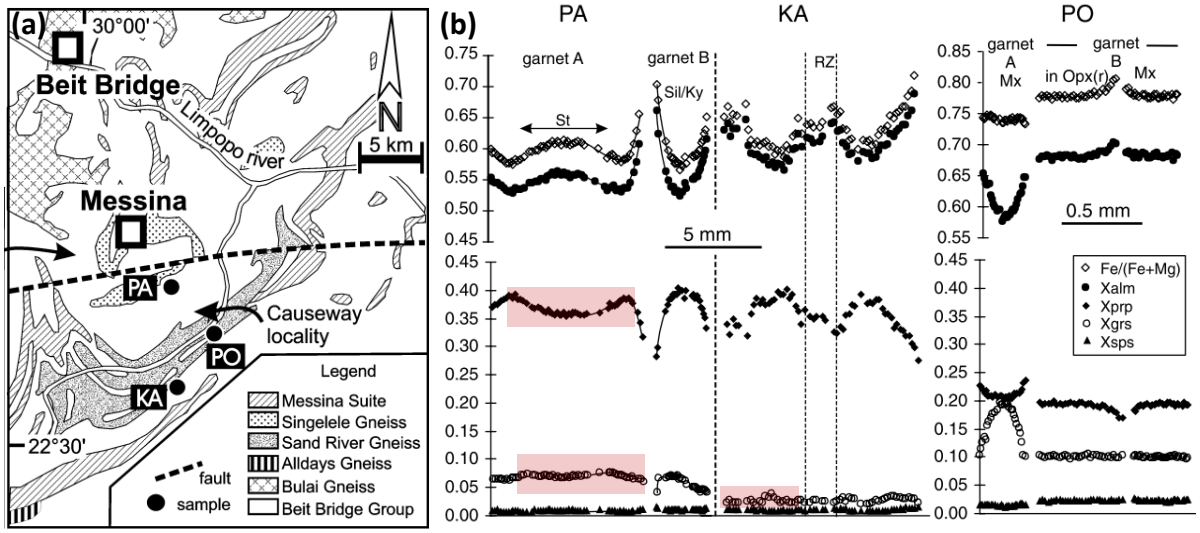


Figure 6.5. (a) Geologic map of the Musina area showing metapelites (PA, KA, PO) studied by Zeh et al. (2004). **(b)** Rim-core-rim garnet profiles from metapelites PA, KA and PO [from Zeh et al. (2004)]. The Xprp and Xgrs profiles discussed in the text are highlighted. As the data set was not included with Zeh et al. (2004), no plotting as part of the present study (e.g., X_{Mg} vs X_{Ca}; Fig. 6.8) was carried out.

Although no geochronologic data is available, Zeh et al. (2004) considered all the garnets in the three metapelites to be related to the Paleoproterozoic event. But as has been suggested by later studies, metapelites in the Musina area preserves evidence for two high-grade events. Hence, the rim-core-rim garnet profile in metapelites studied by Zeh et al. (2004) need to re-interpreted. They could be relics of different stages of the Neoarchean event, or a combination of Neoarchean relic and Paleoproterozoic events.

Millonig et al. (2008) presented rim-core-rim profiles of garnets in metapelite inclusions within the Bulai pluton (Fig. 6.6). These garnets are clearly related to the Neoarchean metamorphic event (~2.64 Ga; Millonig et al., 2008). They have not been affected by the Paleoproterozoic event. The high Xprp contents of garnets (e.g., MP1: ~0.40) from these metapelites stay constant in the core and decreases towards the rims (~0.40 to 0.30) (Fig. 6.6b). Xgrs is low (~0.03-0.04) and more or less constant (Fig. 6.6b).

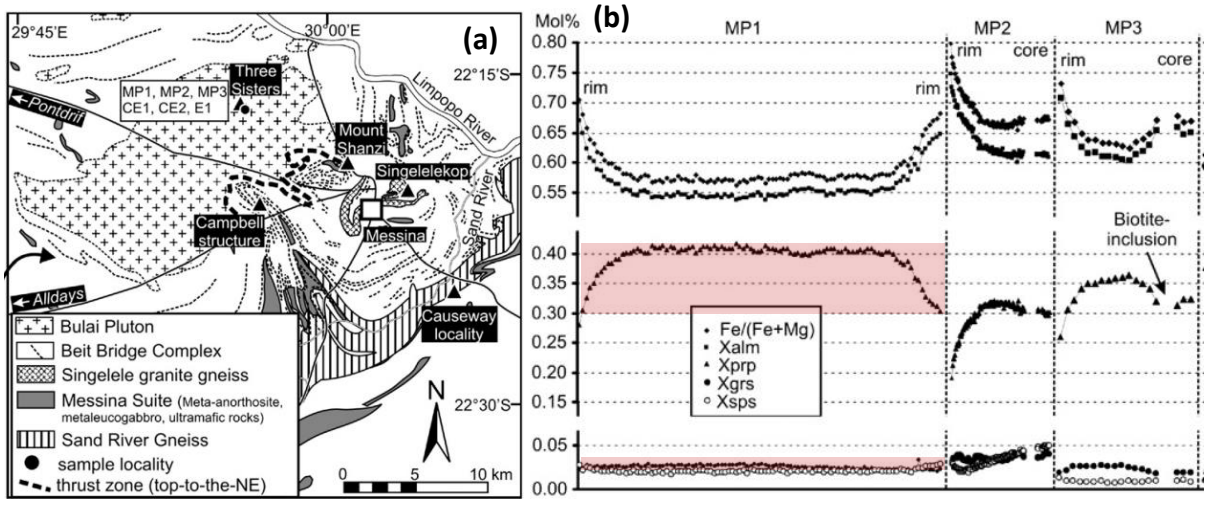


Figure 6.6. (a) Geologic map of the Musina area showing metapelites (MP1, MP2, MP3) studied by Millonig et al. (2008) which occur within the Bulai pluton. **(b)** Rim-core-rim garnet profiles from metapelites MP1, MP2, MP3 [from Millonig et al. (2008)]. The Xprp and Xgrs profiles discussed in the text are highlighted. Representative average data given in Millonig et al. (2008) is included in the X_{Mg} vs X_{Ca} plot (Fig. 6.8).

Based on the association with retrograde cordierite and biotite, Perchuk et al. (2008) interpreted the dominant garnet present in metapelite at O6-19 to have formed during the retrograde stage of the Neoarchean high-grade event. Representative rim-core-rim profile of garnet indicates more or less constant X_{Mg} in core and decrease at the rims (~0.28 to 0.25) (Fig. 6.7). Perchuk et al. (2008) also pointed out the presence of rare relics of earlier garnet in metapelite at O6-19, and likely represents relic of an earlier stage of the Neoarchean event. This is indicated in the X_{Mg} vs X_{Ca} plot in Fig. 6.8, where a lone data sits at high X_{Ca} (~0.08). X_{Ca} of garnets related to the retrograde stage is lower (~0.05-0.03) (Fig. 6.8).

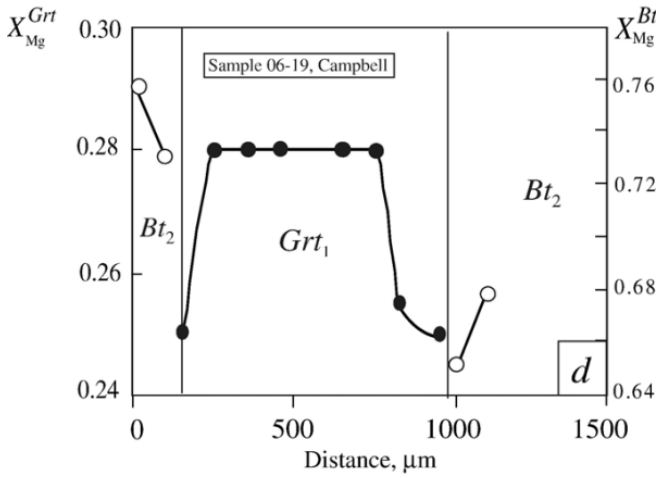


Figure 6.7. Representative rim-core-rim X_{Mg} profile of garnet and adjacent biotite in metapelite at O6-19 [from Perchuk et al. (2008)].

The present study characterized a wider set of metapelite samples from the Verbaard area, including a set of samples [different from that of Perchuk et al. (2008)] from O6-19. Garnets in the metapelites show low uniform X_{Mg} (~0.23-0.33) and X_{Ca} (~0.03-0.04) compositions (Fig. 6.8). Importantly, the low X_{Ca} garnet from the metapelite show typical

association (surrounded by) with retrograde cordierite (e.g., see Fig. 4.4c). This texture indicate the reaction Grt + Sil + Qtz = Crd, which reflects decompression of the rocks.

Regarding the timing of this event, geochronologic data on metapelites from the larger Musina area consistently showed evidence for a Neoarchean high-grade event. For e.g., Millonig et al. (2008) obtained U–Pb monazite ages of 2644 ± 8 Ma (monazite enclosed in garnet) and 2639 ± 8 Ma (matrix monazite) from another metapelite enclave within the ~2.61 Ga Bulai pyroxene-bearing granitoid. No Paleoproterozoic overprint ages were reported from these metapelites. Absence of Paleoproterozoic ages from the metapelites were recently confirmed by Kröner et al. (2018), who also reported only a Neoarchean age (~2.61 Ga) for the high-grade event. In the Verbaard area (present study area), Van Reenen et al. (2008) presented U-Pb zircon ages, which indicated of two high-grade events – the earlier at 2610 ± 8 Ma and the later at 2011 ± 11 Ma – for the migmatitic metapelite that hosts garnet-bearing leucosome at O6-19 outcrop. Application of the Pb-Pb stepwise leaching (PbSL) method on garnet from the restitic domain (O6-19M) and the composite leucosome (O6-19L) from the O6-19 outcrop gave errorchron ages of 2310 ± 43 Ma and 2103 ± 820 Ma, interpreted as mixed ages that reflect the effect of the Palaeoproterozoic overprint onto the Neoarchaean Pb-Pb isotopic signature of the minerals (Boshoff, 2008). This indicates that the formation of garnet in the metapelite and associated leucosome are related to the Neoarchean event, and not be related to the Paleoproterozoic event. Thus it is argued that the prominent low X_{Ca} garnets belong to the retrograde stage of the Neoarchean

event that affected metapelites in the Verbaard area. No relic of earlier garnet was found in the metapelites, supporting their rarity as pointed out by earlier studies.

In addition to the metapelites, large garnet (see Fig. 3.7) occurring in wider leucosome associated with the metapelite at O6-19 was also characterized in this study. Geochronologic studies indicate that the wider leucosomes associated with metapelites in the Musina are related to the Paleoproterozoic event (Jaeckel et al., 1997; Boshoff, 2008; Van Reenen et al., 2008). Rim-core-rim mineral chemical profile of large garnet in wider leucosome indicates that X_{Ca} is high and nearly constant (~0.08) in the core of garnet porphyroblast (see Figs. 4.4e, f, 6.8). But X_{Ca} decreases from 0.08 down to 0.03 along the rim of the garnet porphyroblast (see Figs. 4.4e, f, 6.8).

Based on its similarity to the high X_{Ca} (~0.08) rare relic garnet reported by Perchuk et al. (2008), it is argued that the near constant high X_{Ca} (~0.08) core of the garnet prophyroblast in wider leucosome represents relic of earlier garnet from the associated metapelite. Together with its higher X_{Mg} (~0.32-0.36), and the general corollary that high X_{Ca}-X_{Mg} in garnet is achieved under higher pressure conditions (Spear, 1993), the core portion of garnet in wider leucosome is inferred to represent relic of an earlier higher pressure stage of the Neoarchean event that affected the metapelite.

In contrast, based on its similarity to the lower X_{Ca} (~0.05-0.03) of garnets from the retrograde stage reported by Perchuk et al. (2008), it is argued that the lower X_{Ca} rims of the garnet porphyroblast in wider leucosome represents retrograde diffusion of the earlier relic garnet from the associated metapelite. Thus the wider leucosomes associated with

metapelite in the Verbaard area (including O6-19) are important sites of preservation of garnet formed in the metapelite during the Neoarchean high-grade event.

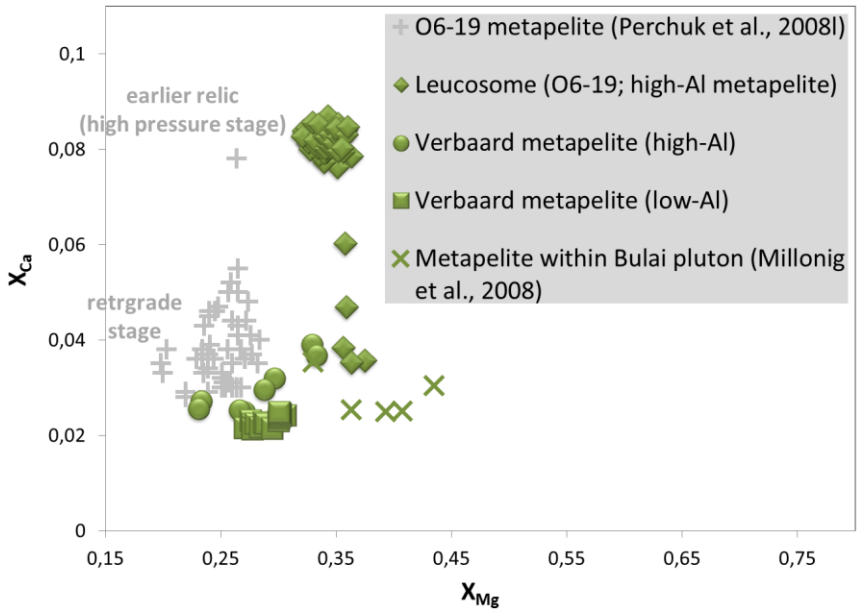


Figure 6.8. X_{Mg} vs X_{Ca} mineral chemistry based diagram comparing the compositional variation observed in garnets in metapelites from the Musina area. Data on garnet in metapelite inclusions within the Bulai pluton is from Millonig et al. (2008). Data on garnet in metapelite at O6-19 reported by Perchuk et al. (2008) is also shown. The likely compositional characteristics of the earlier relic high-pressure and later retrograde stage related to the Neoarchean high-grade event is indicated.

6.5. Provenance of garnet in the Verbaard granitoid

There are two mode of occurrence of garnet within the Verbaard granitoid. The prominent one is the conspicuous network of anatectic garnet-bearing leucocratic veins (see Figs. 2.10 to 2.13). Unlike the irregular outlined garnet-bearing leucosomes associated with the metapelite (see Fig. 2.6), and indicative of *in situ* partial melting, the leucocratic veins associated with the Verbaard granitoid have more or less straight outline. Further, there are no biotite-bearing melanocratic layers along the margins of the leucocratic veins, indicating that they formed *elsewhere* by partial melting (e.g., Sawyer, 1999; White and Powell, 2010;

Jost et al., 2018), and then segregated away from the source region overprinting on to the adjacent rocks.

Petrographically, the mode of occurrence of large garnet porphyroblasts with inclusions and their lobate rounded irregular grain margins with the adjacent felsic minerals (see Fig. 3.18; e.g., Sawyer, 1999; White and Powell, 2010; Jost et al., 2018) in the leuocratic veins associated with the Verbaard granitoid are supportive of an anatectic origin. A similar relationship between large garnet porphyroblasts with inclusions and associated felsic minerals is seen in the leucosomic portion associated with the metapelites (see Figs. 3.8, 3.12, 3.13). Although their mode of occurrence is different (garnet is prominent in the metapelites, while they occur in leucocratic veins overprinting the Verbaard granitoid), the mineral chemical profiles of garnet porphyroblasts from the Verbaard granitoid and metapelite (see Figs. 4.4a to d) are similar. Thus garnets in both rock types likely had a similar origin.

Significantly, X_{Ca} of garnet grains associated with the Verbaard granitoid (both within the granitoid and in leucocratic veins associated with the granitoid) exhibit a decrease from ~0.06 to 0.03 (Fig. 6.9). This trend of decreasing X_{Ca} at more or less constant X_{Mg} is exactly similar to that observed for the lower X_{Ca} rims of the garnet porphyroblast in wider leucosome associated with the metapelite at O6-19 (Fig. 6.9). The range of lower X_{Ca} is also similar to that of garnets in metapelite related to the retrograde stage reported by Perchuk et al. (2008) (Fig. 6.8). Both rocks exhibit rare occurrence of high X_{Ca}-X_{Mg} garnet. Such high X_{Ca}-X_{Mg} in garnet is generally achieved under higher pressure conditions (Spear, 1993). In

contrast, the low X_{Ca} garnets in the metapelites are consistently surrounded by retrograde cordierite. The formation of such retrograde cordierite is typically associated with a decrease of pressure conditions (Spear, 1993). Together with the available ages, it is likely that the studied garnets and their chemical compositions represent different stages of the Neoarchean high-grade event. Thus the garnets found in leucocratic veins overprinting the Verbaard granitoid represent relics of garnet in metapelite formed during the Neoarchean high-grade event. Here the leucocratic veins represent segregated melt from the source region (metapelite).

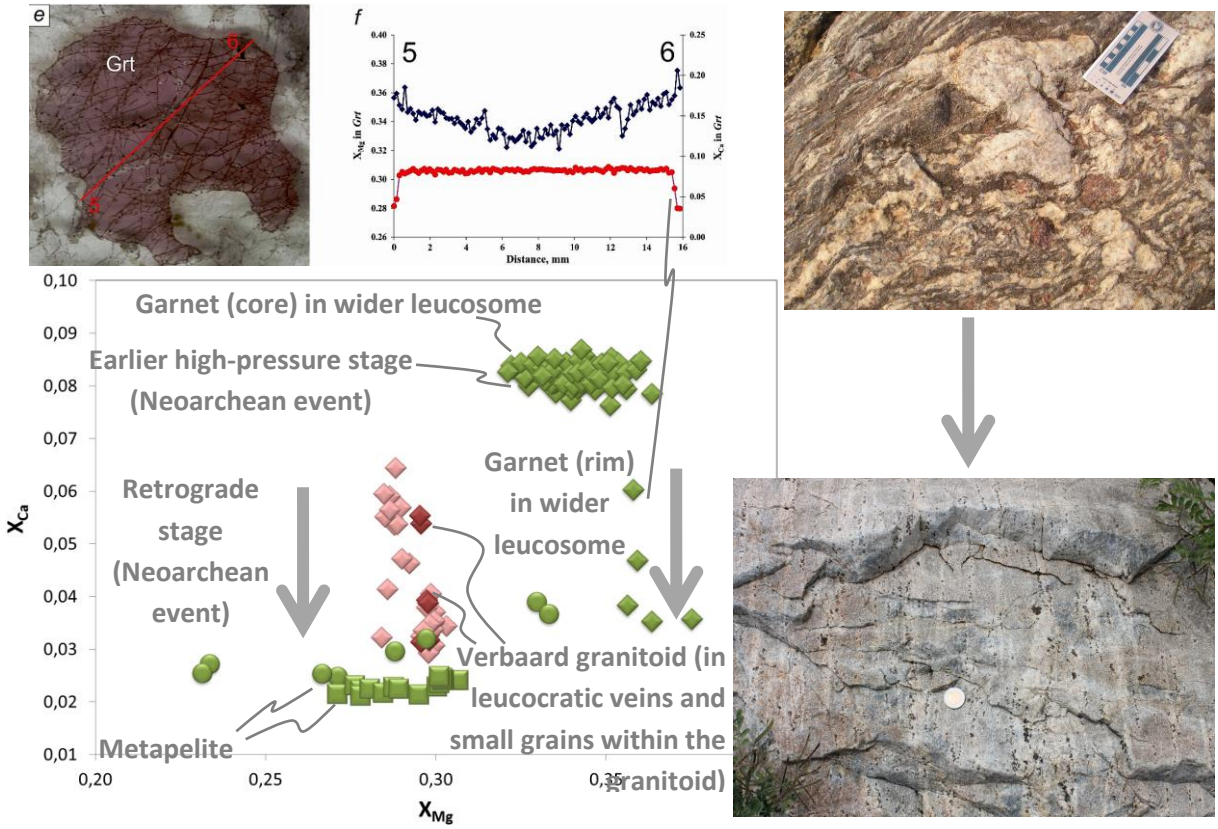


Figure 6.9. X_{Mg} vs X_{Ca} garnet mineral chemistry diagram summarizing the concept of provenance of garnet in the Verbaard granitoid with respect to adjacent metapelites and associated large garnet-bearing wider leucosomes. The arrowed lines indicate the change in garnet composition discussed in the text. Insets are representative images from chapters 2 and 4. See text for more details.

The (less prominent) second mode of occurrence is the small garnet grains occurring locally within the Verbaard granitoid. Unlike the uniformly distributed biotite, the locally occurring garnet is certainly not a rock-forming mineral in the Verbaard granitoid.

As the Verbaard grantioid occur in a high-grade terrane, there is also the possibility that the garnet associated with the granitoid is related to assimilation of metapelitic country rocks. It is certainly a process to consider. In general, minerals like garnet related to assimilation tend to occur closer (concentrated near) to the supracrustal inclusion in granitoids from Archean high-grade terranes (e.g., see Fig. 1.6). In the present study, no supracrustal inclusion occurs within the Verbaard granitoids. Also garnet occurs conspicuously associated with leucocratic veins overprinting the granitoids. Hence they are related to the anatectic overprint. Regarding the small garnet grains occurring locally in the Verbaard grantioid, as shown by mineral chemical characterization, these garnets have exactly similar composition as the ones in the overprinting leucocratic veins. In addition, the possible effect of contamination of metapelitic material was addressed by sampling a granitoid sample from its contact with surrounding metapelite (in process deliberately including metapelitic material). The geochemical characteristics detailed in chapter 5 argue against any form of contamination or assimilation of garnet from the metapelitic rocks.

Local occurrence of small garnet grains are not restricted to the Verbaard granitoid in the study area. They also occur in gabbro and meta-ironstone (see Figs. 3.19, 3.20). But unlike the occurrence in the Verbaard granitoid, the small garnet grains occurring within the gabbro and meta-ironstone do not exhibit any (preferential) association with

quartzofeldspathic melt-related (with lobate rounded grain margins) material. Petrographic studies indicate that the small garnet grains in gabbro and meta-ironstone occur along the margin of pyroxene (see Figs. 3.19, 3.20). Further, mineral chemical characteristics of these garnets are different (e.g., lower X_{Mg}; see Fig. 4.2) from that of small garnet grains occurring within the Verbaard granitoid. Hence it is likely that the small garnet grains occurring locally within the gabbro and meta-ironstone are related to an overprint different from that seen in the Verbaard granitoid. The small garnet grains occurring within the Verbaard granitoid and those associated with leucocratic veins have overlapping mineral chemical characteristics (Fig. 6.9), indicating that both were related to the anatectic event which overprinted the granitoid. Thus for the petrogenetic characterization of the Neoarchean Verbaard granitoid, it is important to use granitoid samples with least or no effect of the anatectic overprint.

6.6. Petrogenetic characterization of the Neoarchean Verbaard granitoid

The petrogenetic characterization of the Verbaard granitoid is carried out in a comparative way, with respect to other Neoarchean granitoid events in the Central Zone. These include:

- ~2.73-2.64 Ga Alldays biotite±amphibole-bearing granitoid
- ~2.68-2.62 Ga Singelele garnet-bearing leucogranite
- ~2.65 Ga Avoca biotite-amphibole-bearing granite
- ~2.63 Ga Avoca pyroxene-bearing granitoid
- ~2.61-2.58 Ga Bulai pyroxene-bearing and pyroxene-absent granitoid

Of these the Alldays granitoid and the Singelele leucogranite are the most voluminous and are widely distributed within the Central Zone. The Avoca rocks are localized as a small pluton to the northwest of the Alldays area, while the Bulai granitoid constitutes a composite batholith in the northern part of the Musina area (see Fig. 1.10). Jaeckel et al. (1997), Hofmann et al. (1998) and Kröner et al. (1998) suggested the existence of a new Neoarchean granitoid variant – the ~2.65-2.62 Ga Verbaard granitoid – within the Central Zone. One of the main reasons pointed out by these studies for the Verbaard granitoid to be considered as a separate Neoarchean granitoid variant is its different appearance in the field, with the conspicuous association with a network of garnet-bearing leucocratic veins. But, as shown by the present study, these garnet-bearing leucocratic veins are related to the anatectic overprint event that affected the Verbaard area. Without the garnet-bearing leucocratic veins, it is simply a biotite-bearing granitoid. It could be that the so-called Verbaard granitoid is a manifestation of some other Neoarchean granitoid event in the Verbaard area. Except for the ~2.61-2.58 Ga Bulai granitoid, all the other granitoid events are possible candidates for comparison with the ~2.65-2.62 Ga Verbaard granitoid.

In terms of association with overprinting garnet-bearing anatectic leucocratic material, the Singelele leucogranite is comparable. To evaluate this further, a comparative exercise was carried out with garnet mineral chemical composition from adjacent leucosome overprinted and non-overprinted Singelele leucogranite (Fig. 6.10a) at the Causeway locality. The composition of primary magmatic garnet from the non-overprinted and coarser garnet from the overprinted portions of leucocratic veins in the Singelele leucogranite is different

from those of garnet in the Verbaard granitoid, metapelites and associated leucosomes (Fig. 6.10b). Further, biotite, which is also a rock forming mineral in the Singelele leucogranite, has compositional characteristics different from that of biotite in the Verbaard granitoid (Figs. 6.10c to f). In terms of whole-rock geochemical characteristics, the Singelele samples are granites in the normative An-Ab-Or composition (Fig. 6.11a), marginally peraluminous as indicated by the ASI ratios of 1.04 to 1.11 (Fig. 6.11b) and corundum normative (0.45-1.1 vol.%), ferroan in terms of Fe-number (Fig. 6.11c) and calcic to alkalic in terms of modified alkali lime index (Fig. 6.11d). Although both overprinted and non-overprinted Singelele leucogranite from the Causeway locality are characterized by similar LREE contents, the (visibly) leucosome overprinted leucogranite (with coarse garnet) has higher HREE contents than the non-leucosome overprinted one (Fig. 6.12). The higher HREE contents are likely due to the presence of garnet. In comparison, the Verbaard granitoid has different compositional characteristics (Figs. 6.11a to d). Although the REE pattern is different, the feature of contaminated Verbaard granitoid having higher HREE contents than the non-contaminated Verbaard granitoid is comparable to that observed for the overprinted and non-overprinted Singelele leucogranite (Fig. 6.12a). As the composition of the source plays an important role in determining the chemistry of the melt, primary melts generated from common crustal sources may be distinguished using appropriate major-element plots (e.g., Figs. 6.11e, f; Montel and Vielzeuf, 1997; Patiño Douce, 1999; Gerdes et al., 2000; Altherr and Siebel, 2002).

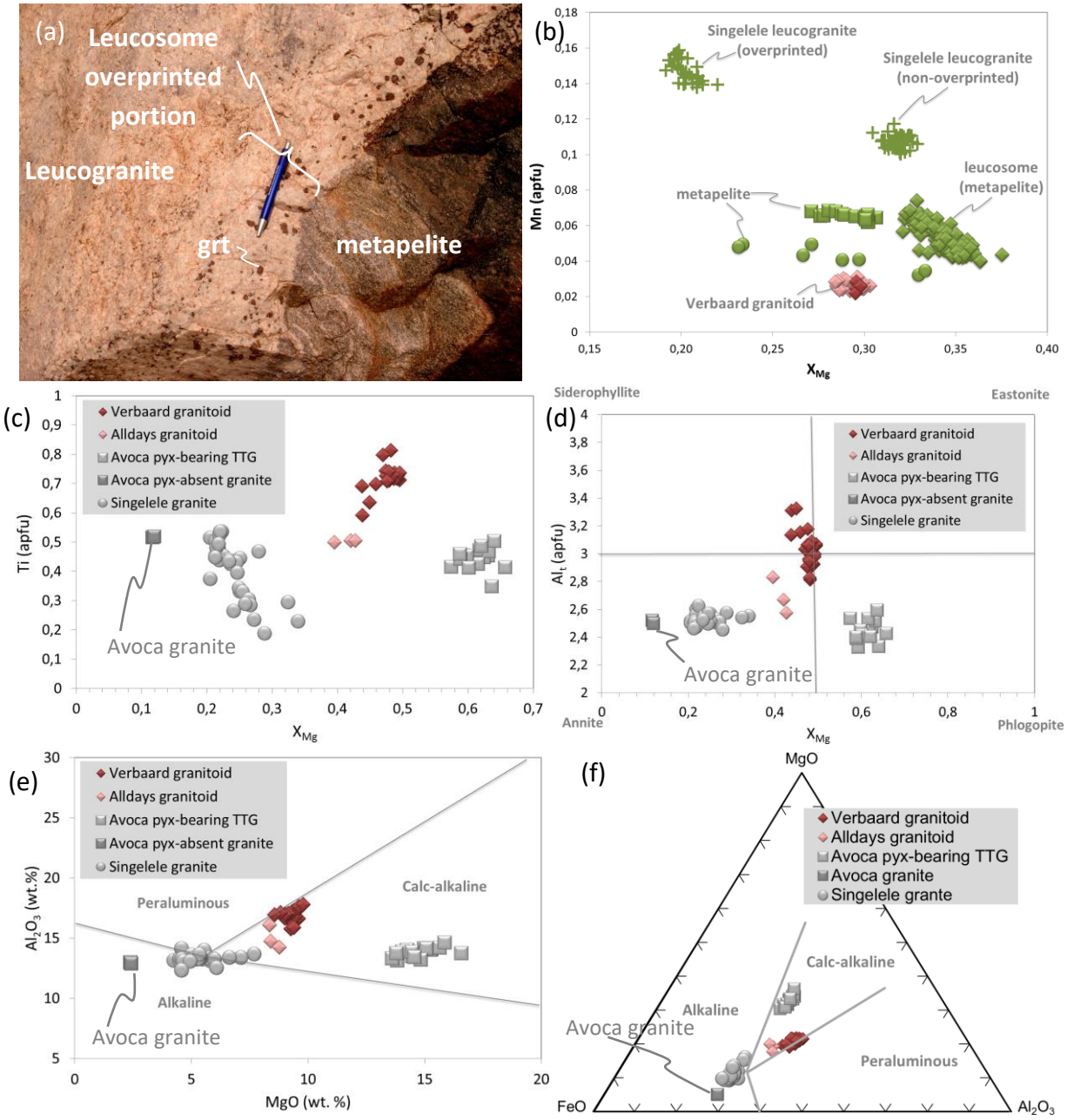


Figure 6.10. (a) Representative field photograph of the Singelele leucogranite illustrating the local overprint by leucosome vein, with garnet grains coarser in the overprinted portions, relative to the non-overprinted ones. Mineral chemistry based diagrams comparing the composition of garnet **(b)** and biotite **(c** to **f)** in the Verbaard granitoid studied here with other Neoarchean granitoids in the Central Zone. The data for other Neoarchean granitoids are from Rajesh et al. (2018), and Rajesh (unpublished data). The fields in (e) and (f) are from Abdel-Rahman (1994).

Comparison of the bulk composition of the Singelele leucogranite with experimental melts produced from pelites, greywackes, and metabasalts reviewed by Patiño Douce (1999) is given in Figs. 6.11e, f. The Singelele leucogranite samples exhibit a close match with experimental melts of greywacke (Figs. 6.11e, f), supporting the general contention that the peraluminous composition of leucogranites is indicative of the magma containing a significant component of supracrustal rocks (Chappell and White, 1974, Miller, 1985; Patiño Douce, 1999). In contrast, the Verbaard granitoid samples exhibit a close match with metabasalt (amphibolite) experimental melts (Figs. 6.11e, f). Hence, the Verbaard granitoid cannot be an equivalent of the Singelele leucogranite. Instead, Na-rich TTG granitoids like the Avoca and Alldays granitoids are suitable for comparison.

With pyroxene forming a prominent rock-forming mineral in the Avoca TTG, the Alldays TTG is a better candidate for comparison with the Verbaard granitoid. This inference is supported by the biotite mineral chemical characteristics, with the Verbaard granitoid falling closer to the Alldays granitoid and different from the Avoca rocks (Figs. 6.10c to f). Significantly, the biotite compositions fall in the calc-alkaline field in the biotite discrimination diagrams of Abdel-Rahman (1994) (Figs. 6.10e, f).

Together with the tonalitic variant dated by Jaeckel et al. (1997) (the lone sample falling in the tonalite field in Fig. 6.11a), the studied Verbaard granitoid samples (which are granodioritic) are comparable to the Alldays TTG which is dominated by tonalites and granodiorites (Fig. 6.11a). This is different from the Avoca TTG which is dominated by trondhjemites (Fig. 6.11a).

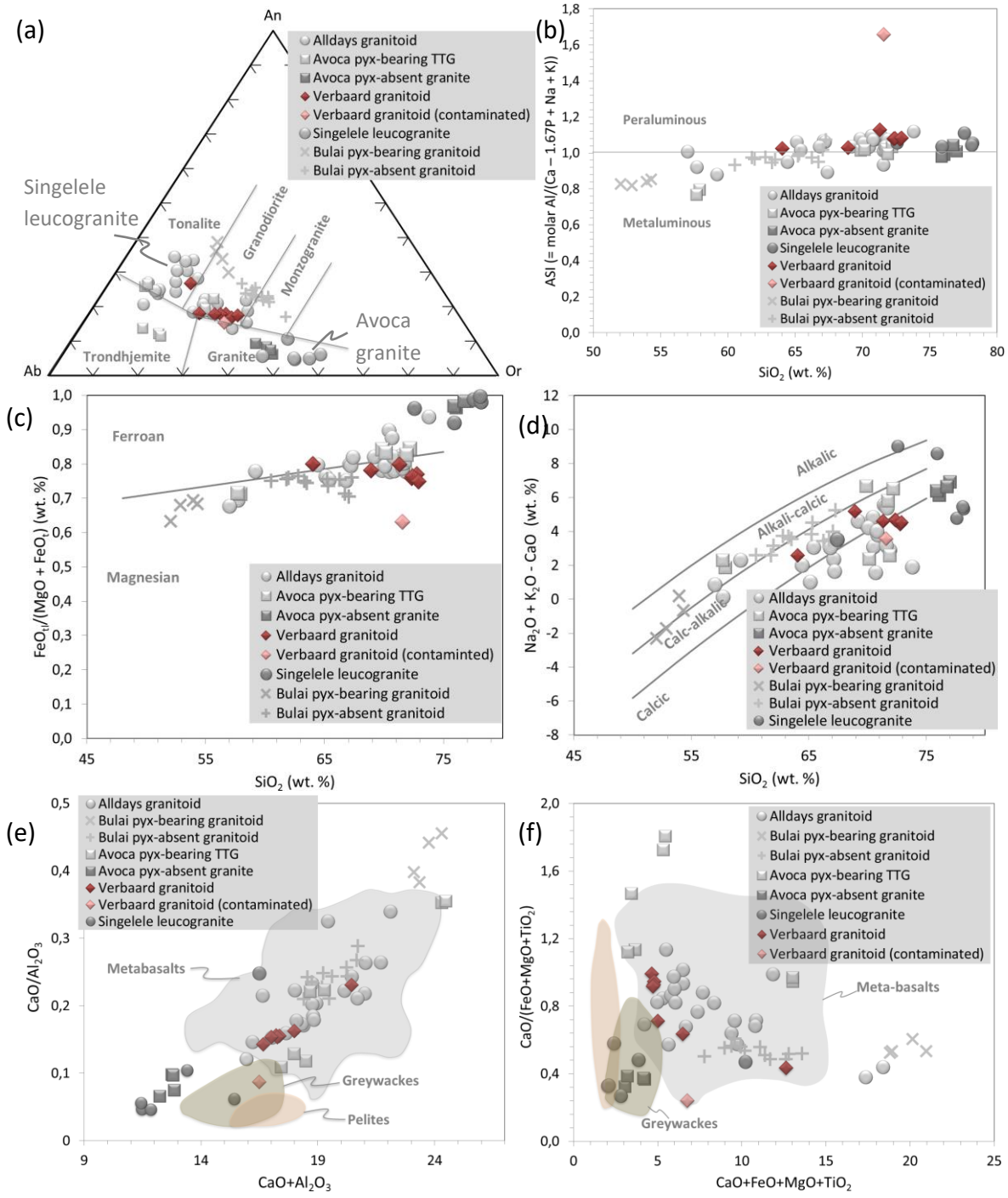


Figure 6.11. Representative whole-rock geochemistry based diagrams comparing the Verbaard granitoid samples studied here with other Neoarchean granitoids from the Central Zone. The tonalitic and granodioritic Verbaard granitoid samples dated by Jaeckel et al. (1997) are also included in the different plots. Data for the Neoarchean granitoids, except Bulai granitoid, is from Rajesh et al. (2018), and Rajesh (unpublished data). Data for Bulai granitoid is from Laurent et al. (2011). Fields in (c) and (d) are from Frost et al. (2001). The experimental melt compilation given in (e) and (f) are from Patiño Douce (1999).

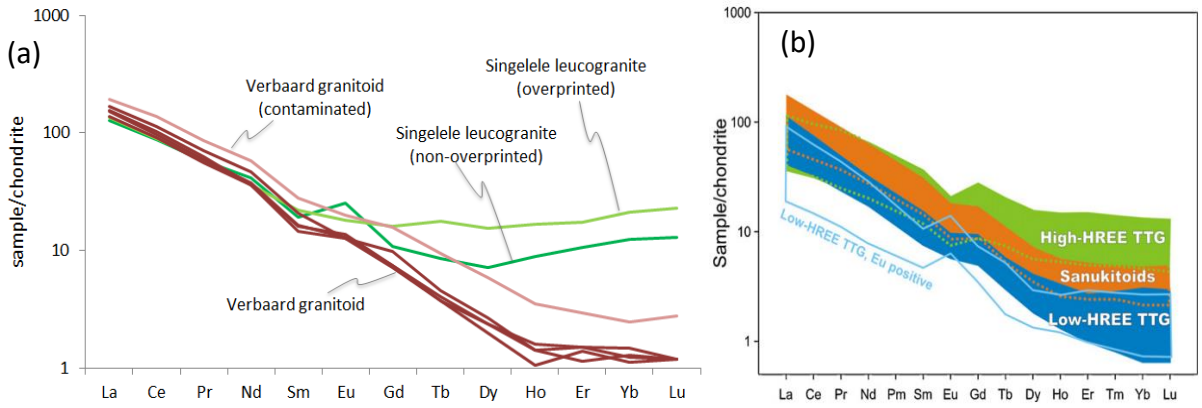


Figure 6.12. (a) Chondrite-normalized (Sun and McDonough, 1989) REE pattern of the Verbaard granitoid *sensu stricto* and contaminated Verbaard granitoid compared with that of leucosome overprinted and non-overprinted Singelele leucogranite from the Causeway locality, north of the O6-19 outcrop. Data on Singelele leucogranite is from Rajesh et al. (2018). Both the contaminated and overprinted samples contain prominent garnet accounting for the higher HREE content. **(b)** Chondrite-normalized (Taylor and McLennan, 1985) REE patterns of Archean granitoids demonstrating their division into high- and low-HREE TTG and medium-HREE sanukitoid groups [from Halla et al. (2009)].

While the Alldays TTG is metaluminous to mildly peraluminous, the Verbaard granitoid samples are mildly peraluminous (Fig. 6.11b). The contaminated Verbaard granitoid (with prominent garnet) is strongly peraluminous (Fig. 6.11b). Both the Alldays TTG and Verbaard granitoid are magnesian to slightly ferroan and calcic to calc-alkalic (Figs. 6.11c, d).

Comparison with experimental melts indicates that the Na-rich rocks – Avoca TTG, Alldays TTG and Verbaard granitoid – are similar to amphibolite-derived melts (Figs. 6.11e, f). This is in line with the general assertion that amphibolite-derived melts are depleted in alkalis, enriched in CaO, and are commonly tonalitic-trondhjemitic-granodioritic (Beard and Lofgren, 1991; Rapp et al., 1991; Patiño Douce, 1999). On the other hand, K-rich granites like the Singelele leucogranite fall towards the fields of melts of supracrustal rocks (Figs. 6.11e, f).

The contaminated Verbaard granitoid shows the effect of the presence of contaminated supracrustal material (Figs. 6.11e, f).

Thus the Neoarchean biotite-bearing Verbaard granitoid (including both the tonalitic and granodioritic variants) is an Archean TTG, with typical geochemical characteristics, generally attributed to derivation from a metabasaltic source (e.g., Fig. 6.11; Barker and Arth, 1976; Rapp et al., 1991; Martin, 1994; Smithies, 2000; Foley et al., 2002; Moyen, 2011). Like the Alldays granitoid, the geochemical characteristics of the Verbaard granitoid are comparable to the low-HREE group of Archean TTG recognized by Halla et al. (2009) (Figs. 6.12b, 6.13a). Except for the overprinting garnet-bearing leucocratic veins, the features of the Verbaard granitoid is comparable to those of the Alldays granitoid (e.g., Figs. 6.10, 6.11). Although garnet occurs locally in the Alldays granitoid, this is assimilated from the supracrustal metapelite inclusions within it (Brandl, 2002). As shown in the present study, the overprinting garnet-bearing leucocratic veins associated with the Verbaard granitoid are a local feature, restricted to the Verbaard area and surroundings. Thus the Verbaard granitoid likely represents the manifestation of Alldays granitoid magmatism in the Verbaard area.

Halla et al. (2009) pointed out that the Archean TTG garnitoids are diverse (Figs. 6.12b, 6.13a). Moyen (2011), expanding upon the work of Halla et al. (2009), pointed out the existence of three groups of TTGs in terms of their depth of origin (translated to pressure conditions) – low-pressure TTG, medium-pressure TTG and high-pressure TTG. Using the compilation of whole-rock geochemical data given in Moyen (2011), an exercise was carried out to delineate potential trend lines associated with the low-pressure, medium-pressure

and high-pressure TTGs. After delineating the trend lines, they were compared with geochemical data from the Alldays, Avoca and Verbaard granitoids from the Central Zone (Figs. 6.13c to f). A parallel whole-rock geochemical study (Rajesh et al., 2018) identified that the ~2.73-2.64 Ga Alldays granitoid consists of two groups – an older ~2.73-2.72 Ga low-K group and a younger ~2.65-2.64 Ga medium-K group (Fig. 6.13b). When these two groups of Alldays granitoids were compared with the trend lines delineated from Moyen (2011), a significant trend emerges – the older ~2.73-2.72 Ga group is similar to low-pressure TTGs, while the younger ~2.65-2.64 Ga group is similar to medium-pressure TTGs (Figs. 6.13c to f). Significantly, the ~2.65-2.62 Ga Verbaard granitoid samples are closely comparable to the medium-pressure TTGs in Figs. 6.13c to d. In comparison, the ~2.63 Ga Avoca pyroxene-bearing granitoid is similar to high-pressure TTGs (Figs. 6.13c to d).

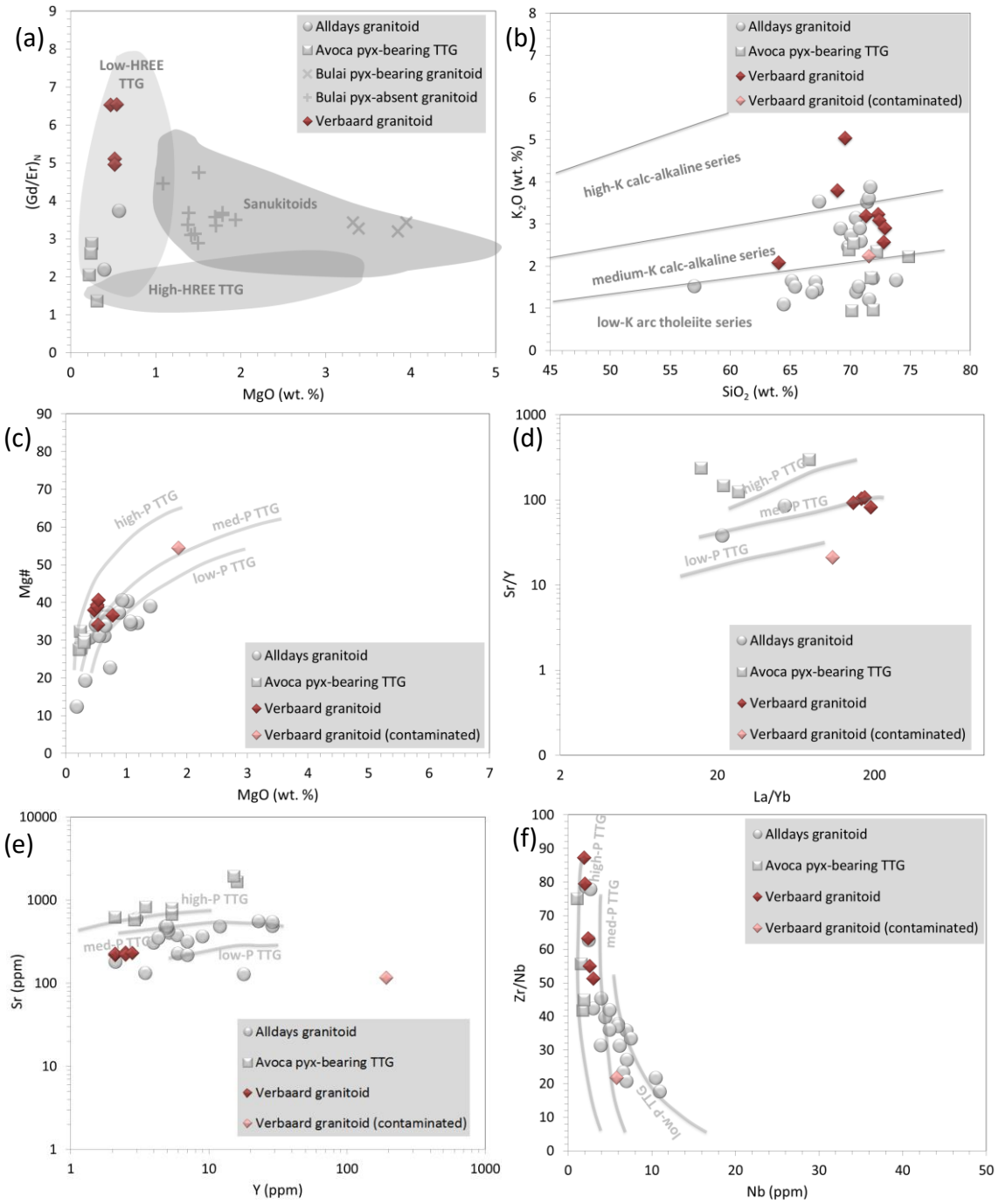


Figure 6.13. Representative geochemistry based diagrams comparing Verbaard, Alldays and Avoca granitoids with that of the different groups of Archean TTGs. The different groups of Archean granitoids in (a) is from Halla et al. (2009). Approximate trends of high-pressure, medium-pressure and low-pressure TTGs in (c to f) are drawn based on respective fields as well as compilations from Moyen (2011). Bulai granitoids, considered as sanukitoids (Laurent et al., 2011), is included in (a) for comparison. Data for Alldays and Avoca granitoids is from Rajesh et al. (2018), while that of the Bulai granitoid is from Laurent et al. (2011).

Chapter 7

Concluding remarks

- The Verbaard area, southwest of Musina, exposes all the prominent rock types – Beit Bridge Group supracrustals, Messina layered mafic to ultramafic intrusion, Neoarchean granitoids, Paleoproterozoic anatectic rocks – of the Central Zone of the Limpopo Complex high-grade terrane.

- Of the different Beit Bridge Group supracrustals, metapelites are dominantly exposed in the study area. Two types of migmatitic garnet-biotite-sillimanite-cordierite-bearing metapelites – high-Al and low-Al metapelite – occur. It is argued that the distinction between the two groups of metapelite is an artifact of the extent of partial melting, with the darker high-Al metapelite preserving more of the restitic domains, while the lighter low-Al metapelite preserve more of the melt-bearing leucosomic material.

- The prominent low X_{Ca} garnets in the metapelites are interpreted to be part of the retrograde stage of the Neoarchean high-grade event that affected these rocks. In comparison, no relic of earlier garnet is preserved in the metapelites. Instead, cores of large garnets in leucosomes associated with the metapelites have higher X_{Ca}-X_{Mg} composition, interpreted to represent relics of an earlier high-pressure stage of the Neoarchean event. The lower X_{Ca} of rims of these garnet porphyroblasts are similar to the retrograde stage garnets in the metapelites. Thus the wider leucosomes

associated with metapelites are potential sites of preservation of different stages of garnet formation in metapelites during the Neoarchean high-grade event.

- The Neoarchean Verbaard granitoid, which is intrusive into the metapelites, is characterized by a conspicuous network of garnet-bearing leucocratic veins. Unlike the wider leucosomes associated with the metapelites, these leucocratic veins are characterized by more or less straight boundaries without any biotite-bearing melanocratic margin, indicating that they formed *elsewhere* by partial melting, and then segregated away from the source region overprinting the adjacent rocks.

- Mineral chemical characteristics of garnet porphyroblasts from the Verbaard granitoid, metapelite and associated wider leucosomes are comparable, arguing for a common origin. Thus the garnet found in leucocratic veins overprinting the Verbaard granitoid are sourced from the metapelites. The leucocratic veins represent segregated melt from the source region (metapelite).

- The non-contaminated Verbaard granitoid samples are mildly peraluminous, magnesian to slightly ferroan and calcic to calc-alkalic. These whole-rock geochemical characteristics are similar to those of low-HREE Archean TTGs. Comparison with experimental melts of a variety of source rocks indicate that the Verbaard granitoid are likely melts of metabasalts.

- A comparative mineral chemical and whole-rock geochemical exercise with other geochronologically comparable Neoarchean granitoids in the Central Zone indicate

that the closest correlatives of the Verbaard granitoid are the Alldays and Avoca granitoids. Unlike the Avoca granitoid, which is dominated by trondhjemites, the compositional characteristics of the Verbaard granitoid are comparable with that of the Alldays granitoid, which is dominated by tonalites and granodiorites. Of the two groups of Alldays granitoids, the Verbaard granitoid is closely comparable to the younger medium-pressure TTG group.

- In summary, it is argued that the Verbaard granitoid represents a manifestation of the Alldays TTG granitoid magmatism in the Verbaard area. Hence, there is no need to consider it as a *separate* Neoarchean granitoid variant in the Central Zone.

- Finally, as an extension of the results of the present study, it is important to point out some important strategies that could minimize misinterpretation(s) when studying Neoarchean (or Archean in general) granitoids in high-grade terranes.

    - When studying overprinted granitoids, it is important to carry out careful sampling of non-overprinted portions and compare with results from overprinted/contaminated portions (e.g., contaminated Verbaard granitoid vs Verbaard granitoid *sensu stricto*).

    - Evaluate the compositional (mineral chemical, whole-rock geochemical) characteristics of the studied granitoid with respect to those of other granitoid events that happened before and after it (e.g., Verbaard granitoid compared to Alldays, Avoca, Singelele and Bulai granitoids).

- Carefully evaluate the spatial distribution of voluminous (widespread) granitoids, and acknowledge the possibility that the same granitoid exposed in different parts of a high-grade terrane can exhibit effects of local overprint event(s) (e.g., Alldays granitoid showing a network of garnet-bearing leucocratic veins only in the Verbaard area).

- Understand the provenance of the mineral considered to have formed during the overprint of the granitoid. Microprobe profiling (mineral chemical profile) of the overprinting mineral from the granitoid and associated/adjacent rocks can help the provenance exercise (e.g., mineral chemical profiles of garnet from metapelite, associated leucosome and the Verbaard granitoid).

REFERENCES

Abdel-Rahman, A.M., 1994. Nature of biotite from alkaline, calc-alkaline and peraluminous magmas. Journal of Petrology 35, 525-541.

Almeida, J.A.C., Dall'Agnol, R., Dias, S.B., Althoff, F.J., 2010. Origin of the Archean leucogranodiorite-granite suites: Evidence from the Rio Maria terrane and implications for granite magmatism in the Archean. Lithos 120, 235-257.

Altherr, R., Siebel, W., 2002. I-type plutonism in a continental back-arc setting: Miocene granitoids and monzonite from the central Aegean Sea, Greece. Contributions to Mineralogy and Petrology 143, 397-415.

Bahnemann, K.P., 1973. The origin of the Singelele granite gneiss near Messina, northern Transvaal. In: Lister, L.A. (Ed.), symposium on granites, gneisses and related rocks. Special Publication. Special Publication of the Geological Society of South Africa 3, 235-244.

Barbarin, B., 1996. Genesis of the two main types of peraluminous granitoids. Geology 24, 295-298.

Barker, F., 1979. Trondhjemite: Definition, environment and hypothesis of origin. Development in Petrology 6, 1-12.

Barker, F., Arth, J.G., 1976. Generation of trondhjemitic-tonalite liquids and Archean bimodal trondhjemite-basalt suites. Geology 4 (10), 596-600.

Barton, J.M., Jr., Holzer, L., Kamber, B., Doig, R., Kramers, J.D., Nyfeler, D., 1994. Discrete metamorphic events in the Limpopo Belt, southern Africa: Implications for the application of P-T paths in complex metamorphic terranes. Geology 22, 1035-1038.

Beard, J.S., Lofgren, G.E., 1991. Dehydration melting and water-saturated melting of basaltic and andesitic greenstones and amphibolites at 1, 3 and 6.9 kb. Journal of Petrology 32, 365-401.

Belyanin, G.A., Rajesh, H.M., Sajeev, K., Van Reenen, D.D., 2012. Orthopyroxene + sillimanite predating sapphirine + quartz: A rare case of ultrahigh-temperature metamorphism from the Central Zone, Limpopo Complex, South Africa. Canadian Mineralogist 50, 1153-1163.

Berger, M., Kramers, J.D., Nagler, T.F., 1995. Geochemistry and geochronology of charnoenderbites in the Northern Marginal Zone of the Limpopo Belt, southern Africa, and genetic models. Schweizerische Mineralogische and Petrographische Mitteilungen 75, 17-42.

Bibikova, E,V., Petrova, A., Claesson, S., 2005. The temporal evolution of sanukitoids in the Karelian Craton, Baltic Shield: An ion microprobe U-Th-Pb isotopic study of zircons. Lithos 79, 129-145.

Blenkinsop, T.G., 2011. Archaean magmatic granulites, diapirism, and Proterozoic reworking in the Northern Marginal Zone. In: D.D. Van Reenen, J. D. Kramers, S. McCourt, L. L. Perchuk (Eds.) Origin and evolution of Precambrian high-grade gneiss terranes, with special emphasis on the Limpopo Complex of southern Africa. Geological Society of America Memoir 207, 245-268.

Bohlender, F., van Reenen, D.D., Barton Jr., J.M., 1992. Evidence for metamorphic and igneous charnokites in the Southern Marginal Zone of the Limpopo Belt. Precambrian Research 55, 429-449.

Boryta, M.D., Condie, K.C., 1990. Geochemistry and origin of the Archean Beit Bridge Complex, Limpopo Belt, South Africa. Journal of Geological Society of London 147, 229-239.

Boshoff, R., 2004. Formation of major fold types during distinct geological events in the Central Zone of the Limpopo Belt, South Africa: New structural, metamorphic and geochronologic data. MSc Thesis, Rand Afrikaans University, Johannesburg, 121p.

Boshoff, R., 2008. The Neoarchean to Palaeoproterozoic evolution of the polymetamorphic Central Zone of the Limpopo high-grade terrain in South Africa. PhD thesis, University of Johannesburg, 216p.

Boshoff, R., Van Reenen, D.D., Smit, C.A., Perchuk, L.L., Kramers, J.D., Armstrong, R., 2006. Geologic history of the Central Zone of the Limpopo Complex: The western Alldays area. The Journal of Geology 114, 699-716.

Brandl, G., 2002. The geology of the Alldays area. Council for Geoscience, South Africa 71p.

Buick, I.S., Hermann, J., Williams, I.S, Gibson, R.L, Rubatto, D., 2006. A SHRIMP U-Pb and LA-ICP-MS trace elements study of the petrogenesis of garnet-cordierite-orthoamphibole gneisses from the Central Zone of the Limpopo Belt, South Africa. Lithos 88, 150-172.

Buick, I.S., Williams I.S., Gibson, R.L., Cartwright, I., Miller, J.A., 2003. Carbon and U-Pb evidence for a Palaeoproterozoic crust component in the Central Zone of the Limpopo Belt, South Africa. Journal of the Geological Society London 160, 601-612.

Champion, D.C., Sheraton, J.W., 1997. Geochemistry and Nd isotope systematic of Archean granites of the Eastern Goldfields, Yilgarn craton, Australia: Implications for crustal growth processes. Precambrian Research 83, 109-132.

Champion, D.C., Smithies, R.H., 2003. Archean granites. In: Blevin, P.L., Chappell, B.W., Jones, M. (Eds.), Magmas to Mineralization: The Ishihara Symposium. AGSO Geoscience Australia pp. 19-24 (Record 2003/14).

Chappell, B.W., White, A.J.R., 1974. Two contrasting granite type. Pacific Geology 8, 173-174.

Chudy, T.C., Zeh, A., Gerdes, A., Barton Jr., J.M., 2008. Palaeoarchaean (3.3 Ga) mafic magmatism and Palaeoproterozoic (2.02 Ga) amphibolite-facies metamorphism in the Central Zone of the Limpopo Belt: New geochronological, petrological and geochemical constraints from metabasic and metapelitic rocks from the Venetia area. South African Journal of Geology 111, 387-406.

Condie, K.C., 2005.TTG and adakites: Are they both slab melts? Lithos 80, 33-44.

Condie, K.C., Aster, R.C., 2010. Episodic age spectra of orogenic granitoids: The supercontinent connection and continental growth. Precambrian Research 180, 227-236.

Condie, K.C., Belousova, E., Griffin, W.L., Sircombe, K.N., 2009. Granitoid events in space and time: Constraints from igneous and detrical zircon age spectra. Gondwana Research 15, 228-242.

Dall'Agnol, R., Cunhu, I.R.V., Guimaraes, F.V., Oliveira, D.C., Teixeira, F.B.T., Feio, G.R., Lamarao, C.N., 2017. Mineralogy, geochemistry and petrology of Neoarchean ferroan to magnesian granites of Carajas Province, Amazonian craton: The origin of hydrated granites associated with charnockites. Lithos 277, 3-32.

Davis, W.J., Gariepy, C., Sawyer, E.W., 1994. Pre- 2.8 Ga crust in the Opatica gneiss belt: A potential source of detrital zircons in the Abitibi and Pontiac Sub province, Superior Province, Canada. Geology 22, 1111-1114.

Day, W.C., Weiblen, P.W., 1986. Origin of the late Archean granite: Geochemical evidence from the Vermolion Granite Complex of northern Minnesota. Contribution to Mineralogy and Petrology 93, 283- 296.

Dey, S., Nandy, J., Choudhary, A.K., Liu, Y., Zong, K., 2014. Origin and evolution of granitoids associated with the Kadiri Greenstone Belt, eastern Dharwar craton: A history of orogenic to anorogenic magmatism. Precambrian Research 246, 64-90.

Dey, S., Pandey, U.K., Rai, A.K., Chaki, A., 2012. Geochemical and Nd isotope constraints on petrogenesis of granitoids from the NW part of the eastern Dharwar craton: Possible implication for late Archean crustal accretion. Journal of Asian Earth Science 45, 40-56.

England, P.C., Thompson, A., 1986. Some thermal and tectonic models for crustal melting in continental collision zones. Geological Society, London, Special Publication 19, 83-94.

Farina, F., Albert, C., Lana, C., 2015. The Neoarchean transition between medium- and high-K granitoids: Clues from the Southern Sao Francisco craton, Brazil. Precambrian Research 266, 375-394.

Feio, G.R.L., Dall'Agnol, R., Dantas, E.L., Macambira, M.J.B., Santos, J.O.S., Althoff, F.J., Soares, J.E.B., 2013. Archean granitoid magmatism in the Canaa dos Carajas area: Implications for crustal evolution of the Carajas Province, Amazonian craton, Brazil. Precambrian Research 227, 157-185.

Feng, R., Kerrich, R., 1992. Geochemical evolution of granitoids from the Archean Abitibi southern volcanic zone and the Pontiac Subprovince, Superior Province, Canada: Implications for tectonic history and source regions. Chemical Geology 98, 23-70.

Foley, S., Tiepolo, M., Vannucci, R., 2002. Growth of early continental crust controlled by melting of amphibolites in subduction zones. Nature 417, 837-840.

Fripp, R.E.P., 1983.The Precambrian geology of the area around the Sand River near Messina, Central Zone, Limpopo Mobile Belt. In: Van Beiljon, W.J., Legg, J.H. (Eds.), the Limpopo Mobile Belt. Special Publication of the Geological Society of South Africa 8, 89- 102.

Fripp, R.E.P., Lilly, P.A., Barton, J.M., Jr 1979. The structure and the origin of the Singelele gneiss at the type locality near Messina, South Africa. Transactions of the Geological Society of South Africa, 82, 161-167.

Frost, B.R Barnes, C.G., Collins, W.J., Arcules, R.J., Ellis, D.J., Frost, C.D., 2001. A geochemical classification for granitic rocks. Journal of Petrology 42, 2033-2048.

Frost, B.R., Frost, C.D., Hulsebosch, T.P., Swapp, S. M., 2000. Origin of the charnockites of the Louis Lake Batholith, Wind River Range, Wyoming. Journal of Petrology 41, 1759-1776.

Frost, C.D., Frost, B.R., 2011. On ferroan (A-type) granitoids: Their compositional variability and modes of origin. Journal of Petrology 52, 39-53.

Frost, C.D., Frost, B.R., Kirkwood, R., Chamberlain, K.R., 2006. The tonalite- trondhjemite-granodiorite (TTG) to granodiorite-granite (GG) transition in the late Archean plutonic rocks of the central Wyoming Province. Canadian Journal of Earth Sciences 43, 1419-1444.

Frost, C.D., Swapp, S.M., Frost, B.R., Finley-Blasi, L., Fitz-Gerald, D.B., 2016. Leucogranites of the Teton Range, Wyoming: A record of Archean collisional orogeny. Geochimica et Cosmochimica Acta 185, 528–549.

Gerdes, A., Rner, G.W., Henk, A., 2000. Post-collision granite generation and HT-LP metamorphism by radiogenic heating. The Variscan South Bohemian Batholith. Journal of the Geological Society of London 157, 577-587.

Gerdes, A., Zeh, A., 2009. Zircon formation versus zircon alteration-new insights from combined U-Pb and Lu-Hf-situ LA-ICP-MS analyses, and consequences for the interpretation of Archean zircon from the Central Zone of the Limpopo Belt. Chemical Geology 261, 230-243.

Gerya, T.V., Perchuk, L.L., 1994. A new thermodynamic database for thermobarometry. International mineralogy association, 16th general meeting, Abstract, Pisa, p. 142.

Gromet, L.P., Dymek, R.F., Haskin, L.A., Korotev, R.L., 1984. The “north American shale composite”: Its compilation, major and trace elements characteristics. Geochimica et Cosmochimica Acta 48, 2469-2482.

Halla, J., van Hunen, J., Heilimo, E., Holtta, P., 2009. Geochemical and numerical constraints on Neoarchean plate tectonics. Precambrian Research 174, 155-162.

Halla, J., Whitehouse, M.J., Ahmad, T., Bagai, Z., 2017. Archean granitoids: An overview and significance from a tectonic perspective. Geological Society, London, Special Publication 449, 1-18.

Heilimo, E., Halla, J., Holtta, P., 2010. Discrimination and origin of the sanukitoid series: Geochemical constraints from the Neoarchean western Karelian Province, Finland. Lithos 115, 27-39.

Henry, D.L., Guidotti, C.V., and Thompson, J.A., 2005. The Ti- saturation surface for low-to-medium pressure metapelite biotite: Implications for geothermometry and Ti-substitution mechanisms. American Mineralogist 90, 316-328.

Hoffman, A., Kroner, A., Brandl, G., 1998. Field relationships of mid- to late Archean high-grade gneisses of igneous and sedimentary parentage in the Sand River, Central Zone of the Limpopo Belt, South Africa. South African Journal of Geology 101, 185-200.

Holzer, L., 1995. The magmatic petrology of the Bulai Pluton and the tectono-metamorphic overprint at 2.0 Ga in the Central Zone of the Limpopo Belt (Messina- Beit Bridge area, southern Africa). Unpublished Diploma thesis, University of Berne, Berne, Swizerland.

Holzer, L., Frei, R., Barton Jr., J.M., Kramers, J.D., 1998. Unraveling the record of successive high-grade events in the Central Zone of the Limpopo Belt using Pb single phase dating of metamorphic minerals. Precambrian Research 87, 87-115.

Horrocks, P.C., 1980. Ancient Archean supracrustal rocks from the Limpopo Belt. Nature 286, 596-599.

Horrocks, P.C., 1983. A corundum and sapphirine paragenesis from the Limpopo Mobile Belt, southern Africa. Journal of Metamorphic Geology 1, 13-23.

Huang, X.L., Niu, Y.L., Xu, Y.G., Yang, Q.J., Zhong, J.W., 2010. Geochemistry of TTG and TTG-like gneisses from Lushan- Taihua Complex in the southern North China craton: Implications for late Archean crustal accretion. Precambrian Research 182, 43-56.

Ichihashi, T., Miyano, T., 1995. A unique P-T trajectory of the Limpopo Central Zone with tectonic setting deeper to the marginal zones, northeast Beit Bridge, Zimbabwe, Centennial Congress (1995). Geological Society of South Africa Extended abstract 2, 178-180.

Jaeckel, P., Kröner, A., Kamo, S.L., Brandl, G., Wendt, J.I., 1997. Late Archaean to early Proterozoic granitoid magmatism and high-grade metamorphism in the central Limpopo Belt, South Africa. Journal of the Geological Society of London 154, 25-44.

Jahn, B.M., Glikson, A.Y., Peucat, J.J., Hickman, A.H., 1981. REE geochemistry and isotope data of Archean silicic volcanics and granitoids from the Pilbara Block, western Australia: Implications for the early crustal evolution. Geochimica et Cosmochimica Acta 45, 1633-1652.

Jayananda, M., Chardon, D., Peucat, J.-J., Capdevila, R., 2006. 2.61 Ga potassic granites and crustal reworking in the western Dharwar craton, southern India: Tectonic, geochronologic and geochemical constraints. Precambrian Research 150 (1-2), 1-26.

Jayananda, M., Janardhan, A.S., Sivasubramanian, P., Peucat, J.J., 1995. Geochronologic and isotopic constraints on the granulite formation in the Kodaikanal area, southern India. Journal of the Geological Society of India 34, 373-390.

Jost, B.M., Webb, M., White, L.T., 2018 The Mesozoic and Palaeozoic granitoids of north-western New Guinea. Lithos 312–313, 223–243.

Kampunzu, A.B., Tombale, A.R., Zhai, M., Bagai, Z., Majaule, T., Modisi, M.P., 2003. Major and trace elements geochemistry of plutonic rocks from Francistown, NE Botswana: Evidence for a Neoarchean continental active margin in the Zimbabwe craton. Lithos 71, 431-460.

Keeditse, M., 2017. Hydrous conditions in the Archean mantle as evidenced from the meta-ultramafic to -mafic remnants of the Messina layered intrusion, Limpopo Complex, southern Africa. Unpublished MSc thesis, BIUST, 106p.

Kemp, A.I.S., Hawkesworth, C.J., 2003. Granitic perspectives on the generation and secular evolution of the continental crust. In: Rudnick, R.L., (Ed.), the crust. Treatise on Geochemistry. Elsevier-Pergamon, Oxford, pp. 349-410.

Key, R.M., 1977. The geological history of the Limpopo Mobile Belt based on the field mapping of the Botswana Geological Survey. In: Ermanovics, I.F., Key, R.M., (Eds.), the proceeding of a seminar pertaining to the Limpopo Mobile Belt. Geological survey department. Bulletin 12, 41-60.

Kramers, J.D., McCourt, S., Roering, C., Smit, C.A., Van Reenen, D.D., 2011. Tectonic models proposed for the Limpopo Complex: Mutual compatibilities and constraints. Geological Society of America Memoir 207, 311-324.

Kröner, A., Jaechel, P., Brandl, G., Nemchin, A.A., Pidgeon, R.T., 1999. Single zircon ages for granitoids gneisses in the Central Zone of the Limpopo belt, southern Africa and geodynamic significance. Precambrian Research 93, 299-337.

Kröner, A., Nemchin, A.A., Jaeckel, P., Hofmann, A., Brandl, G., Pidgeon, R.T., 1998. Field relationship and age of supracrustal Beit Bridge Complex and associated granitoid gneisses in the Central Zone of the Limpopo Belt, South Africa. South African Journal of Geology 101, 201-213.

Laurent, O., Martin, H., Doucelance, R., Moyen, J.-F., Paquette, J.-J., 2011. Geochemistry and petrogenesis of high-K “sanukitoids” from the Bulai Pluton, Central Limpopo Belt, South Africa: Implications for geodynamic changes at the Archean-Proterozoic boundary. Lithos 123, 73-91.

Laurent, O., Martin, H., Moyen, J.F., Doucelance, R., 2014. The diversity and evolution of late-Archean granitoids: Evidence for the onset of “modern-style” plate tectonics between 3.0 and 2.5 Ga. Lithos 205, 208–235.

Lobach-Zhuchenko, S.B., Rollinson, H., Chekulaev, V.P., Savatenkov, V.M., Kovalenko, A.V., Martin, H., Guseva, H.S., Arestova, N.A., 2008. Petrology of a late Archean, highly potassic, sanukitoid pluton from the basaltic shield: Insight into late Archean mantle metasomatism. Journal of Petrology 49 (3), 393-420.

Manya, S., Maboko, M.A.H., Nakamura, E., 2007. Geochemistry and Nd isotopic composition of potassic magmatism in the Neoarchean Musoma-Mara greenstone belt, northern Tanzania. Precambrian Research 159, 231-240.

Martin, H., 1994. The Archean grey gneisses and the genesis of the continental crust. In: Condie, K.C. (Ed.), Archean crustal evolution, development in Precambrian geology. Elsevier, Amsterdam pp. 205-260.

Martin, H., Chauval, C., Jahn, B.M., 1983. Major and trace elements geochemistry and crustal evolution of granodioritic Archean rocks from eastern Finland. Precambrian Research 21, 159-180.

Martin, H., Moyen, J.-F., Rapp, R., 2010. The sanukitoid series: magmatism at the Archean-Proterozoic transition. Earth and environmental sciences transactions of the Royal Society of Edinburgh 100, 15-33.

Martin, H., Smithies, R.H., Moyen, J.F., Champion, D., 2005. An overview of adakite, tonalite-trondhjemite-granodiorite (TTG), and sanukitoid: Relationships and some implications for crust evolution. Lithos 79, 1-24.

Mikkola, P., Huhma, H., Heilima, E., Whitehouse, M., 2011. Archean crustal evolution of the Suomussalmi district as part of the Kianta Complex, Karelia: Constraints from geochemistry and isotopes of granitoids. Lithos 125, 287-307.

Mikkola, P., Lauri, L.S., Kapyaho, A., 2012. Neoarchean leucogranitoids of the Kianta Complex, Karelian Province, Finland: Source characteristics and processes responsible for the observed heterogeneity. Precambrian Research 206- 207, 72-68.

Milidragovic, D., Francis, D., 2014. Ferropicrite-driven reworking of the Ungava craton and the genesis of Neoarchean pyroxene granitoids. Earth and Planetary Science Letters 386, 138- 148.

Miller, C.F., 1985. Are strongly peraluminous magmas derived from pelitic sedimentary sources? Journal of Geology 93, 673-689.

Millonig, L., Zeh, A., Gerdes, A., Klemd, R., 2008. Neoarchean high-grade metamorphism in the Central Zone of the Limpopo Belt (South Africa): Combined petrological and geochronological evidence from the Bulai pluton. Lithos 103, 333-351.

Montel, J.M., Vielzeuf, D., 1997. Partial melting of metagreywackes, Part II. Compositions of minerals and melts. Contribution Mineral Petrology 128, 176-196.

Moreno, J.A., Baldim, M.R., Semprich, J., Oliveira, E.P., Verma, S.K., Teixeira, W., 2017. Geochronological and geochemical evidences for extension-related Neoarchean granitoids in the southern São Francisco Craton, Brazil. Precambrian Research 294, 322–343.

Mouri, H., Whitehouse, M.J., Brandl, G., Rajesh, H.M., 2009. A magmatic age and four successive metamorphic events recorded in zircons from a single meta-anorthosite sample in the Central Zone of the Limpopo Belt, South Africa. Journal of the Geological Society of London 166, 827-830.

Moyen, J.F., 2011.The composite Archean grey gneisses: Petrological significance, and evidence for a non- unique tectonic setting for Archean crustal growth. Lithos 123, 21-36.

Moyen, J.F., Martin, H., Jayananda, M., Auvray, B., 2003. Late Archean granites: A typology based on the Dharwar craton (India). Precambrian Research 127, 103-123.

O'Connor, J.T., 1965. A classification for quartz-rich igneous rocks based on feldspar ratio. US geological survey, professional papers 525-B, 79-84.

Patino Douce, A.E., 1999. What do experiments tell us about the relative contribution of crust and mantle to the origin of granitic magmas? In: Castro, A., Fernandez, C., Vigneresse, J.L., (Eds), understanding granites: Integrating new and classical techniques. Special Publication of the Geological Society of London., vol. 168, pp.55-75.

Perchuk, L.L., Van Reenen, D.D., Varlamov, D.A., Tabatabaeimanesh, Van Kal, S.M., Boshoff, R., 2008. P-T record of two high-grade metamorphic events in the Central Zone of the Limpopo Complex, South Africa. Lithos 103, 70-105.

Percival, J.A., Mortensen, J.K., 2002. Water-deficient calc-alkaline plutonic rocks of northeasten Superior Province, Canada: Significance of charnockitic magmatism. Journal of Petrology 43, 1617-1650.

Rajesh, H.M., 2012. A geochemical perspective on charnockite magmatism in Peninsular India. Geoscience Frontiers 3, 773-788.

Rajesh, H.M., Belyanin, G.A., Van Reenen, D.D., 2018. Three tier transition of Neoarchean TTG-sanukitoid magmatism in the Beit Bridge Complex, Southern Africa. Lithos 296, 431-451.

Rajesh, H.M., Safonov, O.G., Belyanin, G.A., Kramers, J.D., 2014. Monazite-fluorapatite characteristics as evidence for interplay between ~2.04 Ga fluid-induced dehydration and melting of the Sand River Gneiss, Limpopo Complex, South Africa. South African Journal of Geology 117, 237-254.

Rapp, R., Norman, M., Laporte, D., Yaxley, G., Martin, H., Foley, S., 2010. Continent formation in the Archean and chemical evolution of the cratonic lithosphere: Melt-rock reaction experiments at 3-4 GPa and petrogenesis of Archean Mg-diorites (sanukitoids). Journal of Petrology 51, 1237-1266.

Rapp, R.P., Watson, E.B., Miller, C.F., 1991. Partial melting of amphibolites/eclogites and the origin of Archean trondhjemites and tonalites. Precambrian Research 51, 1-25.

Regan, S.P., Williams, M., Mahan, K.H., Dumond, G., Jercinovic, M.J., Orlandini, O., 2017. Neoarchean arc magmatism and subsequent collisional orogenesis along the eastern Rae domain, western Churchill Province: Implications for the early growth of Laurentia. Precambrian Research 294, 151-174.

Retief, E.A., Compston, W., Armstrong, R.A., Williams, I.S., 1990. Characteristics and preliminary U-Pb ages of zircon from Limpopo Belt lithologies. Extended abstracts, the Limpopo Belt. A field workshop on granulites and deep crustal tectonics, June 21- July 1, 1990, Rand Afrikaans University (now University of Johannesburg).

Rigby, M.J., Basson, I.J., Kramers, J.D., Graser, P., Mavimbela, P.K., 2011. The structural, metamorphic and temporal evolution of the country rocks surrounding Venetia mine, Limpopo Belt, South Africa: Evidence for a single Palaeoproterozoic tectono-metamorphic events with implications for a tectonic model. Precambrian Research 186, 51-69.

Rigby, M.J., Mouri, H., Brandl, G., 2008. P-T conditions and the origin of quartzofeldspathic veins in metasyenites from the Central Zone of the Limpopo Belt, South Africa. South African Journal of Geology 111, 313-332.

Rudnick, R.L., Gao, S., 2004.Composition of the continental crust. In: Holland, H.D., Turekian, K.K. (Ed.), Treatise of Geochemistry. Elsevier, Amsterdam, pp. 1-64.

Sage, R.P., Lightfoot, P.C., Doherty, W., 1996. Geochemical characteristics of granitoid rocks from within the Archean Michipicoten greenstone belt, Wawa Subprovince, Superior Province, Canada: Implications for source regions and techtonic evolution. Precambrian Research 76, 155-190.

Sawyer, E.W., 1999. Criteria for the recognition of partial melting. Physics Chemistry Earth Sciences (A) 24, 269-279.

Shand, S.J., 1943. The eruptive rocks. 2nd Edition, John Wiley, New York 444p.

Shang, C.K., Satir, M., Nsifa, E.N., Liegeois, J.P., Siebel, W., Taubald, H., 2007. Archean high-K granitoids produced by remelting of the earlier tonalite-trondhjemite-granodiorite (TTG) in the Sangmelima region of the Ntem Complex of the Congo craton, southern Cameroon. International Journal Earth Sciences 96, 817-842.

Shirey, S.B., Hanson, G.N., 1984. Mantle- derived Archean monzodiorites and trachyandesites. Nature 310, 222-224.

Smit, C.A., van Reenen, D.D., Roering, C., Boshoff, R., Perchuk, L. L., 2011. Neoarchean to Paleoproterozoic evolution of the polymetamorphic Central Zone of the Limpopo Complex. The Geological Society of America Memoir 207, 213-244.

Smithies, R.H., 2000. The Archaean tonalite–trondhjemite–granodiorite (TTG) series is not an analogue of Cenozoic adakite. Earth and Planetary Science Letters 182, 115–125.

Sohnge, P.G., 1946. The geology of the Messina copper mines and surrounding country. Memoir Geological Survey of South Africa 40, 280 p.

Spear, F. S., 1993. Metamorphic Phase Equilibria and Pressure-Temperature-Time Paths. Mineralogical Society of America. Washington DC 799p.

Stern, R.A., Hanson, G.N., 1991. Archean high-Mg granodiorites: A derivative of light rare earth enriched monzodiorite of mantle origin. Journal of Petrology 32, 201-238.

Stevenson, R., Henry, P., Gariepy, C., 1999. Assimilation-fractional crystallization origin of Archean sanukitoid suites: Western Superior Province, Canada. Precambrian Research 96, 83-99.

Sun, S.S., McDonough, W.E., 1989. Chemical and isotopic systematics of oceanic basalts: Implications for mantle composition and processes. In: Saunders, A. D., Norry, M.J. (Eds.), magmatism in the ocean basins: Geological Society of London, Special Publication 42, pp. 313–345.

Sylvester, P.J., 1994. Archean granite plutons. In: Condie, K.C. (Ed.), Archean crustal evolution. Developments in Precambrian Geology, vol.11. Elsevier, Amsterdam, pp 261-314.

Taylor, R.S., McLennan, S.M., 1985. The continental crust: Its composition and evolution. Blackwell, Oxford 312 pp.

Tsunogae, T., Van Reenen, D.D., 2006. Corundum+quartz and Mg-staurolite bearing granulite from the Limpopo Belt, southern Africa: Implications for a P-T path. Lithos 92, 576-587.

Tsunogae, T., Van Reenen, D.D., 2011. High-pressure and ultrahigh-temperature granulite-facies metamorphism of Precambrian high-grade terranes: Case study of the Limpopo Complex. In: D.D. Van Reenen, J.D. Kramers, S. McCourt, L.L. Perchuk (Eds.) origin and evolution of Precambrian high-grade gneiss terranes, with special emphasis on the Limpopo Complex of Southern Africa. Geological Society of America Memoir 207, 107-124.

Tsunogae, T., Yurimoto, H., 1995. Single zircon U-Pb geochronology of the Limpopo Belt by secondary ion mass spectrometry. Geochemical Journal 29, 197-205.

Van Reenen, D.D., Boshoff, R., Smit, C.A., Perchuk, L. L., Kramers, J. D., McCourt, S. M., Armstrong, R. A., 2008. Geochronological problems in the Limpopo Complex, South Africa. Gondwana Research 14, 644-662.

Van Reenen, D.D., Perchuk, L.L., Smit, C.A., Varlamov, D.A., Boshoff, R., Huizenga, J.M., Gerya, T.V., 2004. Structural and P-T evolution of a major cross fold in the Central Zone of the Limpopo high-grade terrane, South Africa. Journal of Petrology 45, 1413-1439.

Van Reenen, D.D., Smit, C.A., Perchuk, L. L., Roering, C., Boshoff, R., 2011. Thrust exhumation of the Neoarchaen ultrahigh-temperature Southern Marginal Zone, Limpopo Complex: Convergence of decompression-cooling paths in the hanging wall and prograde P-T paths in the footwall. Geological Society of America Memior 207, 189-212.

Vijaya Kumar, K., Ernst, W.G., Leelanandam, C., Wooden, J.L., Grove, M.J., 2011. Origin of ~2.5 Ga potassic granite from the Nellore Schist Belt, SE India: Textural, cathodoluminescence, and SHRIMP U-Pb data. Contributions to Mineralogy and Petrology 162, 867-888.

Wang, Y., Zhang, Y., Zhao, G., Fan, W., Xia, X., Zhang, A., 2009. Zircon U-Pb geochronological and geochemical constraints on the petrogenesis of Taishan sanukitoids (Shandong):

Implications for Neoarchean subduction in the eastern block, north China craton. Precambrian Research 174, 273-286.

Watkeys, M.K., Light, M.P.R., Broderick, T.J., 1983. A retrospective of the Central Zone of the Limpopo Belt, Zimbabwe. In: The Limpopo Belt. Special Publication 8 (Eds. Van Biljon, W.J., Legg, J.H.), Geological Society of South Africa 8, 65-80.

Watkins, J.M., Clemens, J.D., Treloar, P.J., 2007. Archean TTGs as sources of younger granitic magmas: Melting of sodic metatonalites at 0.6-1.2 GPa. Contributions to Mineralogy and Petrology 154, 91-110.

Weaver, B.L., Tarney, J., 1981. Lewisian gneiss geochemistry and Archean crustal development model. Earth and Planetary Science Letters 55, 171-180.

Whalen, J.B., Percival, J.A., McNicoll, V.J., Longstaffe, F.J., 2004. Geochemical and isotopic (Nd-O) evidence bearing on the origin of late-to post-orogenic high-K granitoid rocks in the western Superior Province: Implication for late-Archean tectonomagmatic processes. Precambrian Research 132, 303-326.

White, R.W., Powell, R., 2010. Retrograde melt–residue interaction and the formation of near-anhydrous leucosomes in migmatites. Journal of Metamorphic Geology 28, 579-597.

Zeh, A., Gerdes, A., Barton Jr, J., Klemd, R., 2010. U-Th and Lu-Hf systematics of zircon from TTGs, leucosomes, meta-anorthosites and quartzites of the Limpopo Belt (South Africa): Constraints for the formation, recycling and metamorphism of Palaeoarchaean crust. Precambrian Research 179, 50-68.

Zeh, A., Gerdes, A., Barton, J.M., Jr., 2009. Archean accretion and crustal evolution of the Kalahari craton: The zircon age and Hf isotope record of granitoid rocks from Barberton/Swaziland to the Francistown Archean Journal of Petrology 50, 933-966.

Zeh, A., Gerdes, A., Klemd, R., Barton Jr., J.M., 2007. Archaean to Proterozoic crustal evolution in the Central Zone of the Limpopo Belt (South Africa/Botswana): Constraints

from combined U–Pb and Lu–Hf isotope analyses of zircon. Journal of Petrology 48, 1605–1639.

Zeh, A., Holland, T.J.B., Klemd, R., 2005. Phase relationships in grunerite–garnet-bearing amphibolites in the system CFMASH, with applications to metamorphic rocks from the Central Zone of the Limpopo Belt, South Africa. Journal of Metamorphic Geology 23, 1–17.

Zeh, A., Klemd, R., Buhlmann, S., Barton, J.M., 2004. Pro- and retrograde P-T evolution of granulites of the Beit Bridge Complex, Limpopo Belt, South Africa: Constraints from quantitative phase diagrams and geotectonic implications. Journal of Metamorphic Geology 22, 79-95.

Appendix

Mineral chemical data of microprobe profiling of large garnet in wider leucosome associated with the high-Al metapelite (leucosome highAl meta) O6-19 from the study area. The data is given continuously from 5 to 6 in the trend line shown in Fig. 4.4e.

	leucosome	leucosome	leucosome	leucosome	leucosome	leucosome	leucosome	leucosome	leucosome	leucosome	leucosome	leucosome
Rock	highAl meta	highAl meta	highAl meta	highAl meta	highAl meta	highAl meta	highAl meta	highAl meta	highAl meta	highAl meta	highAl meta	highAl meta
SiO_2	38,67	37,26	38,24	38,22	37,87	39,17	38,53	37,93	39,53	38,00	39,13	38,17
TiO_2	0,00	0,01	0,01	0,01	0,00	0,01	0,04	0,00	0,02	0,00	0,01	0,02
Al_2O_3	21,43	21,93	21,47	21,35	22,45	21,98	21,66	21,25	21,17	21,44	21,34	21,48
Cr_2O_3	0,07	0,08	0,04	0,04	0,05	0,05	0,03	0,04	0,06	0,00	0,01	0,00
FeO	27,99	28,51	27,35	27,55	27,42	27,63	27,41	27,28	27,00	27,06	26,63	27,30
MnO	0,79	0,74	0,75	0,64	0,61	0,76	0,70	0,70	0,70	0,70	0,75	0,78
MgO	8,86	8,97	8,40	8,29	8,86	8,39	8,34	8,13	8,05	8,19	8,12	8,19
CaO	1,38	1,71	2,75	2,90	2,89	2,94	2,97	3,02	2,92	2,83	2,94	3,04
Na_2O												
K_2O												
Total	99,19	99,21	99,01	99,00	100,15	100,93	99,68	98,35	99,45	98,22	98,93	98,98
O=12												
Si	3,010	2,915	2,986	2,987	2,924	2,998	2,988	2,985	3,062	2,991	3,044	2,984
Ti	0,000	0,001	0,001	0,001	0,000	0,001	0,002	0,000	0,001	0,000	0,001	0,001
Al(IV)	0,000	0,085	0,014	0,013	0,076	0,002	0,012	0,015	0,000	0,009	0,000	0,016
Al(VI)	1,967	1,942	1,965	1,957	1,970	1,983	1,970	1,960	1,933	1,981	1,958	1,966
Cr	0,004	0,005	0,002	0,002	0,003	0,003	0,002	0,002	0,004	0,000	0,001	0,000
Fe(III)	0,017	0,047	0,028	0,035	0,024	0,012	0,023	0,034	0,000	0,017	0,000	0,029
Fe(II)	1,805	1,818	1,758	1,766	1,747	1,757	1,755	1,762	1,750	1,764	1,737	1,756
Mn	0,052	0,049	0,050	0,042	0,040	0,049	0,046	0,047	0,046	0,047	0,049	0,052
Mg	1,028	1,046	0,978	0,966	1,020	0,957	0,964	0,954	0,930	0,961	0,942	0,954
Ca	0,115	0,143	0,230	0,243	0,239	0,241	0,247	0,255	0,242	0,239	0,245	0,255
Total	7,998	8,051	8,012	8,013	8,042	8,003	8,009	8,014	7,968	8,008	7,977	8,013
Almandine	59,90	57,51	57,89	58,12	55,58	58,38	57,93	57,95	58,08	58,33	57,90	57,75
Andradite	0,83	2,42	1,42	1,76	1,24	0,62	1,15	1,69	0,00	0,85	0,00	1,47
Grossular	2,81	2,24	6,16	6,24	6,78	7,28	7,02	6,72	8,15	7,13	8,32	7,07
Pyrope	34,49	35,89	32,75	32,33	34,88	31,94	32,27	31,95	32,00	32,13	32,07	31,99
Spessartine	1,75	1,68	1,66	1,42	1,36	1,64	1,54	1,56	1,58	1,56	1,68	1,73
Uvarovite	0,22	0,25	0,12	0,12	0,16	0,15	0,09	0,13	0,19	0,00	0,03	0,00
X_{Mg}	0,36	0,36	0,35	0,35	0,36	0,35	0,35	0,35	0,34	0,35	0,35	0,35
X_{Ca}	0,04	0,05	0,08	0,08	0,08	0,08	0,08	0,08	0,08	0,08	0,08	0,08

	leucosome	leucosome	leucosome	leucosome	leucosome	leucosome	leucosome	leucosome	leucosome	leucosome	leucosome	leucosome
Rock	highAl meta	highAl meta	highAl meta	highAl meta	highAl meta	highAl meta	highAl meta	highAl meta	highAl meta	highAl meta	highAl meta	highAl meta
SiO_2	38,36	38,32	38,58	38,70	37,74	38,63	38,51	38,95	37,76	38,14	38,14	38,43
TiO_2	0,03	0,02	0,00	0,01	0,01	0,03	0,02	0,00	0,02	0,03	0,03	0,01
Al_2O_3	21,45	21,57	21,91	21,58	21,76	21,82	22,12	21,24	21,71	21,50	21,83	22,01
Cr_2O_3	0,00	0,06	0,01	0,08	0,05	0,03	0,00	0,10	0,00	0,07	0,04	0,04
FeO	27,41	27,17	27,41	27,80	27,11	27,54	26,91	27,23	27,30	27,42	27,48	26,85
MnO	0,70	0,70	0,74	0,75	0,76	0,77	0,81	0,82	0,80	0,88	0,79	0,78
MgO	8,16	8,15	8,35	8,15	8,27	8,32	8,26	8,11	8,11	8,14	8,06	8,13
CaO	2,90	3,02	2,96	2,80	3,01	3,02	2,92	3,00	2,85	2,87	3,01	2,96
Na_2O												
K_2O												
Total	99,01	99,01	99,96	99,87	98,71	100,16	99,55	99,45	98,55	99,05	99,38	99,21
O=12												
Si	2,997	2,992	2,983	2,999	2,959	2,983	2,983	3,026	2,968	2,982	2,973	2,987
Ti	0,002	0,001	0,000	0,001	0,001	0,002	0,001	0,000	0,001	0,002	0,002	0,001
Al(IV)	0,003	0,008	0,017	0,001	0,041	0,017	0,017	0,000	0,032	0,018	0,027	0,013
Al(VI)	1,973	1,979	1,982	1,973	1,972	1,971	2,005	1,946	1,980	1,966	1,980	2,005
Cr	0,000	0,004	0,001	0,005	0,003	0,002	0,000	0,006	0,000	0,004	0,002	0,002
Fe(III)	0,022	0,014	0,016	0,019	0,021	0,022	0,000	0,019	0,017	0,025	0,014	0,000
Fe(II)	1,768	1,760	1,757	1,783	1,757	1,756	1,751	1,750	1,777	1,768	1,777	1,757
Mn	0,046	0,046	0,048	0,049	0,050	0,050	0,053	0,054	0,053	0,058	0,052	0,051
Mg	0,950	0,949	0,963	0,942	0,967	0,958	0,954	0,939	0,950	0,949	0,937	0,942
Ca	0,243	0,253	0,245	0,233	0,253	0,250	0,242	0,250	0,240	0,240	0,251	0,247
Total	8,005	8,006	8,011	8,004	8,024	8,012	8,007	7,991	8,019	8,013	8,015	8,005
Almandine	58,63	58,30	57,89	59,14	57,08	57,83	58,12	57,94	58,10	58,17	58,29	58,49
Andradite	1,10	0,73	0,78	0,98	1,09	1,12	0,00	0,97	0,84	1,25	0,73	0,00
Grossular	7,00	7,53	7,41	6,54	7,30	7,17	8,12	7,17	7,24	6,59	7,61	8,13
Pyrope	31,72	31,70	32,26	31,45	32,67	32,11	31,97	31,78	32,02	31,82	31,50	31,54
Spessartine	1,55	1,55	1,62	1,64	1,71	1,69	1,78	1,83	1,79	1,95	1,75	1,72
Uvarovite	0,00	0,19	0,03	0,25	0,16	0,09	0,00	0,31	0,00	0,22	0,12	0,12
X_{Mg}	0,34	0,34	0,35	0,34	0,35	0,35	0,35	0,34	0,34	0,34	0,34	0,34
X_{Ca}	0,08	0,08	0,08	0,08	0,08	0,08	0,08	0,08	0,08	0,08	0,08	0,08

	leucosome	leucosome	leucosome	leucosome	leucosome	leucosome	leucosome	leucosome	leucosome	leucosome	leucosome	leucosome
Rock	**highAl meta**	**highAl meta**	**highAl meta**	**highAl meta**	**highAl meta**	**highAl meta**	**highAl meta**	**highAl meta**	**highAl meta**	**highAl meta**	**highAl meta**	**highAl meta**
SiO_2	38,19	37,74	38,25	37,91	37,44	38,25	37,88	37,78	37,86	37,95	38,10	38,43
TiO_2	0,00	0,00	0,02	0,01	0,00	0,01	0,01	0,01	0,04	0,01	0,00	0,03
Al_2O_3	21,70	21,77	21,65	21,89	21,21	21,78	21,77	21,71	21,72	22,22	21,65	21,41
Cr_2O_3	0,10	0,04	0,05	0,02	0,02	0,05	0,04	0,05	0,07	0,04	0,00	0,07
FeO	27,25	27,62	27,67	27,69	27,75	27,74	27,90	27,56	26,95	27,32	27,31	27,53
MnO	0,81	0,86	0,88	0,83	0,91	0,94	0,91	0,90	0,87	0,93	0,90	0,91
MgO	8,06	8,03	8,00	8,14	7,83	8,03	8,20	8,04	8,10	8,35	7,91	7,73
CaO	2,90	3,00	2,84	2,87	2,94	2,92	2,98	3,05	2,88	3,05	3,00	2,86
Na_2O												
K_2O												
Total	99,01	99,06	99,36	99,36	98,10	99,72	99,69	99,10	98,49	99,87	98,87	98,97
O=12												
Si	2,985	2,956	2,984	2,959	2,966	2,974	2,950	2,958	2,974	2,943	2,985	3,009
Ti	0,000	0,000	0,001	0,001	0,000	0,001	0,001	0,001	0,002	0,001	0,000	0,002
Al(IV)	0,015	0,044	0,016	0,041	0,034	0,026	0,050	0,042	0,026	0,057	0,015	0,000
Al(VI)	1,985	1,968	1,976	1,974	1,950	1,972	1,952	1,964	1,986	1,976	1,985	1,976
Cr	0,006	0,002	0,003	0,001	0,001	0,003	0,002	0,003	0,004	0,002	0,000	0,004
Fe(III)	0,008	0,026	0,018	0,022	0,043	0,021	0,040	0,029	0,006	0,018	0,013	0,008
Fe(II)	1,774	1,784	1,787	1,785	1,795	1,783	1,777	1,776	1,765	1,754	1,776	1,795
Mn	0,054	0,057	0,058	0,055	0,061	0,062	0,060	0,060	0,058	0,061	0,060	0,060
Mg	0,939	0,938	0,930	0,947	0,925	0,931	0,952	0,938	0,949	0,965	0,924	0,902
Ca	0,243	0,252	0,237	0,240	0,250	0,243	0,249	0,256	0,242	0,253	0,252	0,240
Total	8,009	8,027	8,011	8,025	8,025	8,016	8,032	8,026	8,013	8,031	8,010	7,996
Almandine	58,61	57,83	58,92	58,03	58,35	58,44	57,27	57,61	58,01	56,51	58,61	59,68
Andradite	0,38	1,32	0,89	1,09	2,19	1,07	2,05	1,46	0,31	0,94	0,66	0,40
Grossular	7,44	7,07	6,91	6,96	6,16	6,95	6,26	7,04	7,62	7,55	7,78	7,43
Pyrope	31,46	31,72	31,18	32,01	31,18	31,29	32,27	31,72	31,89	32,80	30,95	30,25
Spessartine	1,80	1,93	1,95	1,85	2,06	2,08	2,03	2,02	1,95	2,08	2,00	2,02
Uvarovite	0,31	0,13	0,16	0,06	0,06	0,16	0,13	0,16	0,22	0,13	0,00	0,22
X_{Mg}	0,34	0,34	0,34	0,34	0,33	0,34	0,34	0,34	0,34	0,35	0,33	0,33
X_{Ca}	0,08	0,08	0,08	0,08	0,08	0,08	0,08	0,08	0,08	0,08	0,08	0,08

	leucosome	leucosome	leucosome	leucosome	leucosome	leucosome	leucosome	leucosome	leucosome	leucosome	leucosome	leucosome
Rock	highAl meta	highAl meta	highAl meta	highAl meta	highAl meta	highAl meta	highAl meta	highAl meta	highAl meta	highAl meta	highAl meta	highAl meta
SiO_2	38,36	38,18	38,45	38,23	38,54	38,72	38,09	38,63	38,55	37,83	38,00	38,13
TiO_2	0,00	0,00	0,04	0,01	0,03	0,01	0,02	0,01	0,00	0,02	0,00	0,00
Al_2O_3	21,63	21,75	21,51	21,47	21,40	21,37	21,71	21,51	21,84	21,62	22,24	21,90
Cr_2O_3	0,04	0,09	0,04	0,04	0,07	0,09	0,00	0,05	0,03	0,05	0,07	0,04
FeO	27,45	27,48	27,72	27,39	27,26	27,77	27,07	27,83	27,65	27,94	27,83	27,86
MnO	0,99	0,99	0,88	0,92	1,01	0,97	0,95	0,93	0,96	0,88	1,02	0,97
MgO	7,83	7,78	7,98	7,92	7,81	7,61	7,72	7,81	7,77	7,77	7,93	8,01
CaO	3,05	3,00	2,98	2,88	2,99	3,01	2,95	3,01	2,94	3,02	3,01	2,92
Na_2O												
K_2O												
Total	99,35	99,27	99,60	98,86	99,11	99,55	98,51	99,78	99,74	99,13	100,10	99,83
O=12												
Si	2,992	2,983	2,992	2,995	3,011	3,016	2,992	3,002	2,995	2,965	2,948	2,964
Ti	0,000	0,000	0,002	0,001	0,002	0,001	0,001	0,001	0,000	0,001	0,000	0,000
Al(IV)	0,008	0,017	0,008	0,005	0,000	0,000	0,008	0,000	0,005	0,035	0,052	0,036
Al(VI)	1,982	1,986	1,967	1,979	1,971	1,963	2,003	1,972	1,996	1,965	1,983	1,973
Cr	0,002	0,006	0,002	0,002	0,004	0,006	0,000	0,003	0,002	0,003	0,004	0,002
Fe(III)	0,014	0,007	0,025	0,016	0,010	0,013	0,000	0,020	0,002	0,027	0,011	0,022
Fe(II)	1,777	1,788	1,779	1,779	1,770	1,797	1,783	1,789	1,795	1,805	1,795	1,789
Mn	0,065	0,066	0,058	0,061	0,067	0,064	0,063	0,061	0,063	0,058	0,067	0,064
Mg	0,910	0,906	0,926	0,925	0,910	0,884	0,904	0,905	0,900	0,908	0,917	0,928
Ca	0,255	0,251	0,248	0,242	0,250	0,251	0,248	0,251	0,245	0,254	0,250	0,243
Total	8,006	8,010	8,008	8,005	7,996	7,994	8,003	8,003	8,003	8,022	8,028	8,022
Almandine	58,87	59,01	58,82	59,01	58,81	59,64	59,38	59,32	59,67	58,86	58,13	58,32
Andradite	0,68	0,37	1,27	0,78	0,53	0,64	0,00	1,01	0,10	1,36	0,56	1,11
Grossular	7,71	7,77	6,91	7,17	7,66	7,54	8,30	7,21	7,98	7,03	7,71	6,98
Pyrope	30,43	30,38	30,94	30,88	30,54	29,75	30,21	30,26	30,05	30,62	31,11	31,32
Spessartine	2,19	2,20	1,94	2,04	2,24	2,15	2,11	2,05	2,11	1,97	2,27	2,15
Uvarovite	0,12	0,28	0,12	0,12	0,22	0,28	0,00	0,15	0,09	0,16	0,22	0,12
X_{Mg}	0,33	0,33	0,34	0,33	0,33	0,32	0,33	0,33	0,33	0,33	0,33	0,33
X_{Ca}	0,08	0,08	0,08	0,08	0,08	0,08	0,08	0,08	0,08	0,08	0,08	0,08

	leucosome	leucosome	leucosome	leucosome	leucosome	leucosome	leucosome	leucosome	leucosome	leucosome	leucosome	leucosome
Rock	**highAl meta**	**highAl meta**	**highAl meta**	**highAl meta**	**highAl meta**	**highAl meta**	**highAl meta**	**highAl meta**	**highAl meta**	**highAl meta**	**highAl meta**	**highAl meta**
SiO_2	38,39	37,83	38,69	37,91	37,82	38,10	38,90	38,03	38,08	37,72	38,06	38,39
TiO_2	0,04	0,03	0,03	0,01	0,00	0,01	0,01	0,01	0,02	0,01	0,03	0,00
Al_2O_3	21,41	21,96	21,26	21,56	21,51	21,40	21,29	21,46	21,54	22,36	21,58	21,53
Cr_2O_3	0,08	0,00	0,08	0,03	0,05	0,09	0,05	0,03	0,07	0,04	0,01	0,06
FeO	27,80	27,41	27,84	27,51	27,40	27,76	28,00	27,07	27,25	27,13	27,17	27,47
MnO	0,99	0,97	1,01	1,03	0,94	1,12	0,93	0,99	0,97	0,94	0,82	0,96
MgO	7,73	7,89	7,63	7,65	7,91	7,80	7,81	7,86	7,80	8,05	7,77	7,91
CaO	2,93	2,91	2,99	3,02	2,99	3,02	3,04	2,97	2,98	3,00	2,92	2,97
Na_2O												
K_2O												
Total	99,37	99,00	99,53	98,72	98,62	99,30	100,03	98,42	98,71	99,25	98,36	99,29
O=12												
Si	2,998	2,963	3,016	2,981	2,974	2,980	3,015	2,992	2,990	2,943	2,996	2,996
Ti	0,002	0,002	0,002	0,001	0,000	0,001	0,001	0,001	0,001	0,001	0,002	0,000
Al(IV)	0,002	0,037	0,000	0,019	0,026	0,020	0,000	0,008	0,010	0,057	0,004	0,004
Al(VI)	1,970	1,991	1,955	1,980	1,970	1,956	1,948	1,984	1,984	2,000	1,998	1,977
Cr	0,005	0,000	0,005	0,002	0,003	0,006	0,003	0,002	0,004	0,002	0,001	0,004
Fe(III)	0,020	0,006	0,020	0,015	0,024	0,033	0,030	0,012	0,009	0,000	0,000	0,017
Fe(II)	1,796	1,789	1,795	1,794	1,778	1,783	1,785	1,769	1,779	1,775	1,789	1,776
Mn	0,065	0,064	0,067	0,069	0,063	0,074	0,061	0,066	0,065	0,062	0,055	0,063
Mg	0,900	0,921	0,887	0,897	0,927	0,910	0,902	0,922	0,913	0,936	0,912	0,920
Ca	0,245	0,244	0,250	0,254	0,252	0,253	0,252	0,250	0,251	0,251	0,246	0,248
Total	8,004	8,019	7,995	8,012	8,017	8,016	7,998	8,006	8,006	8,028	8,001	8,005
Almandine	59,56	58,50	59,46	59,08	58,25	58,50	59,01	58,62	58,92	57,55	59,52	58,88
Andradite	1,00	0,31	1,02	0,76	1,20	1,68	1,50	0,62	0,48	0,00	0,00	0,85
Grossular	6,94	7,93	7,14	7,68	7,12	6,53	6,85	7,66	7,69	8,40	8,19	7,26
Pyrope	30,06	31,09	29,87	30,08	31,18	30,52	30,42	30,81	30,53	31,81	30,43	30,71
Spessartine	2,19	2,17	2,25	2,30	2,11	2,49	2,06	2,21	2,16	2,11	1,82	2,12
Uvarovite	0,25	0,00	0,25	0,09	0,16	0,28	0,15	0,09	0,22	0,13	0,03	0,19
X_{Mg}	0,33	0,33	0,32	0,32	0,33	0,33	0,33	0,33	0,33	0,34	0,33	0,33
X_{Ca}	0,08	0,08	0,08	0,08	0,08	0,08	0,08	0,08	0,08	0,08	0,08	0,08

	leucosome	leucosome	leucosome	leucosome	leucosome	leucosome	leucosome	leucosome	leucosome	leucosome	leucosome	leucosome
Rock	highAl meta	highAl meta	highAl meta	highAl meta	highAl meta	highAl meta	highAl meta	highAl meta	highAl meta	highAl meta	highAl meta	highAl meta
SiO_2	39,25	37,78	37,97	38,58	38,32	37,64	37,86	37,92	38,37	38,47	37,80	38,30
TiO_2	0,01	0,03	0,00	0,01	0,00	0,03	0,03	0,02	0,02	0,03	0,02	0,03
Al_2O_3	20,89	21,50	21,58	21,44	21,53	21,94	21,73	21,61	21,25	21,48	21,92	21,29
Cr_2O_3	0,05	0,08	0,03	0,06	0,06	0,01	0,04	0,03	0,02	0,02	0,02	0,06
FeO	27,69	26,95	27,55	27,22	27,13	26,63	27,06	27,60	27,06	26,92	27,01	26,88
MnO	0,86	0,85	0,93	0,90	0,89	0,83	0,87	0,97	0,89	0,86	0,85	0,78
MgO	7,53	7,92	7,93	7,99	7,79	8,01	8,12	8,10	7,94	8,10	8,20	8,02
CaO	2,94	2,93	2,99	2,88	2,92	2,85	3,09	2,99	3,01	2,89	2,98	2,97
Na_2O												
K_2O												
Total	99,22	98,04	98,98	99,08	98,64	97,94	98,80	99,24	98,56	98,77	98,80	98,33
O=12												
Si	3,062	2,983	2,975	3,011	3,006	2,967	2,967	2,964	3,011	3,008	2,961	3,010
Ti	0,001	0,002	0,000	0,001	0,000	0,002	0,002	0,001	0,001	0,002	0,001	0,002
Al(IV)	0,000	0,017	0,025	0,000	0,000	0,033	0,033	0,036	0,000	0,000	0,039	0,000
Al(VI)	1,922	1,985	1,971	1,973	1,991	2,007	1,976	1,958	1,967	1,981	1,985	1,973
Cr	0,003	0,005	0,002	0,004	0,004	0,001	0,002	0,002	0,001	0,001	0,001	0,004
Fe(III)	0,012	0,007	0,025	0,010	0,000	0,000	0,018	0,035	0,017	0,007	0,011	0,010
Fe(II)	1,795	1,773	1,781	1,767	1,781	1,768	1,755	1,770	1,758	1,754	1,758	1,756
Mn	0,057	0,057	0,062	0,060	0,059	0,055	0,058	0,064	0,059	0,057	0,056	0,052
Mg	0,876	0,932	0,926	0,930	0,911	0,941	0,949	0,944	0,929	0,944	0,957	0,940
Ca	0,246	0,248	0,251	0,241	0,245	0,241	0,259	0,250	0,253	0,242	0,250	0,250
Total	7,971	8,009	8,017	7,996	7,997	8,014	8,019	8,024	7,997	7,996	8,021	7,996
Almandine	59,42	58,53	58,35	58,71	59,37	58,30	57,34	57,54	58,30	58,31	57,31	58,33
Andradite	0,61	0,36	1,24	0,49	0,00	0,00	0,91	1,75	0,88	0,36	0,55	0,53
Grossular	7,70	7,69	7,11	7,41	8,02	8,08	7,71	6,61	7,56	7,70	7,84	7,68
Pyrope	30,16	31,25	31,13	31,21	30,45	31,72	31,97	31,84	31,21	31,66	32,34	31,53
Spessartine	1,96	1,91	2,07	2,00	1,98	1,87	1,95	2,17	1,99	1,91	1,90	1,74
Uvarovite	0,16	0,25	0,09	0,19	0,19	0,03	0,13	0,09	0,06	0,06	0,06	0,19
X_{Mg}	0,32	0,34	0,33	0,34	0,33	0,34	0,34	0,34	0,34	0,34	0,35	0,34
X_{Ca}	0,08	0,08	0,08	0,08	0,08	0,08	0,09	0,08	0,08	0,08	0,08	0,08

	leucosome	leucosome	leucosome	leucosome	leucosome	leucosome	leucosome	leucosome	leucosome	leucosome	leucosome	leucosome
Rock	**highAl meta**	**highAl meta**	**highAl meta**	**highAl meta**	**highAl meta**	**highAl meta**	**highAl meta**	**highAl meta**	**highAl meta**	**highAl meta**	**highAl meta**	**highAl meta**
SiO_2	38,58	37,66	37,80	37,96	38,49	37,59	37,93	37,38	37,90	37,79	38,27	38,35
TiO_2	0,02	0,02	0,00	0,00	0,00	0,02	0,00	0,02	0,01	0,00	0,00	0,00
Al_2O_3	21,36	21,69	21,90	21,52	21,75	22,15	21,67	21,63	21,84	21,74	21,66	20,19
Cr_2O_3	0,01	0,07	0,07	0,08	0,05	0,05	0,03	0,06	0,01	0,07	0,12	0,02
FeO	26,99	27,10	26,98	27,19	27,10	26,99	26,49	27,03	26,59	26,74	26,61	26,71
MnO	0,74	0,79	0,79	0,73	0,72	0,74	0,72	0,77	0,74	0,83	0,75	0,68
MgO	7,99	8,06	8,29	8,10	8,22	8,31	7,99	8,36	8,45	8,28	8,22	7,50
CaO	2,94	3,04	3,01	2,95	2,90	3,03	3,09	3,04	2,85	3,02	3,02	2,96
Na_2O												
K_2O												
Total	98,63	98,43	98,84	98,53	99,23	98,88	97,92	98,29	98,39	98,47	98,65	96,41
O=12												
Si	3,021	2,964	2,959	2,982	2,996	2,942	2,989	2,945	2,973	2,967	2,995	3,072
Ti	0,001	0,001	0,000	0,000	0,000	0,001	0,000	0,001	0,001	0,000	0,000	0,000
Al(IV)	0,000	0,036	0,041	0,018	0,004	0,058	0,011	0,055	0,027	0,033	0,005	0,000
Al(VI)	1,972	1,977	1,980	1,976	1,992	1,986	2,003	1,957	1,992	1,980	1,992	1,908
Cr	0,001	0,004	0,004	0,005	0,003	0,003	0,002	0,004	0,001	0,004	0,007	0,001
Fe(III)	0,005	0,015	0,014	0,017	0,004	0,009	0,000	0,034	0,006	0,014	0,000	0,016
Fe(II)	1,762	1,768	1,753	1,769	1,760	1,758	1,752	1,747	1,738	1,742	1,741	1,773
Mn	0,049	0,053	0,052	0,049	0,047	0,049	0,048	0,051	0,049	0,055	0,050	0,046
Mg	0,933	0,946	0,967	0,948	0,954	0,970	0,939	0,982	0,988	0,969	0,959	0,896
Ca	0,247	0,256	0,252	0,248	0,242	0,254	0,261	0,257	0,240	0,254	0,253	0,254
Total	7,990	8,020	8,023	8,012	8,003	8,030	8,005	8,033	8,014	8,019	8,003	7,967
Almandine	58,58	57,67	57,00	58,24	58,51	56,74	58,26	56,20	57,05	56,91	57,87	58,56
Andradite	0,25	0,78	0,69	0,86	0,21	0,44	0,00	1,73	0,29	0,69	0,01	0,85
Grossular	8,03	7,64	7,62	7,22	7,71	8,04	8,64	6,79	7,74	7,65	8,07	7,89
Pyrope	31,45	31,90	32,69	31,81	31,84	32,95	31,40	33,34	33,24	32,66	32,02	31,03
Spessartine	1,66	1,78	1,77	1,63	1,58	1,67	1,61	1,74	1,65	1,86	1,66	1,60
Uvarovite	0,03	0,22	0,22	0,25	0,15	0,16	0,09	0,19	0,03	0,22	0,37	0,07
X_{Mg}	0,34	0,34	0,35	0,34	0,35	0,35	0,34	0,35	0,36	0,35	0,35	0,33
X_{Ca}	0,08	0,08	0,08	0,08	0,08	0,08	0,09	0,08	0,08	0,08	0,08	0,09

	leucosome	leucosome	leucosome	leucosome	leucosome	leucosome	leucosome	leucosome	leucosome	leucosome	leucosome	leucosome
Rock	highAl meta	highAl meta	highAl meta	highAl meta	highAl meta	highAl meta	highAl meta	highAl meta	highAl meta	highAl meta	highAl meta	highAl meta
SiO_2	38,63	38,25	38,28	38,49	39,04	38,23	38,49	38,13	37,99	38,58	38,20	38,56
TiO_2	0,00	0,04	0,02	0,00	0,02	0,01	0,00	0,01	0,04	0,03	0,00	0,00
Al_2O_3	20,55	21,61	22,06	21,42	20,68	22,03	21,25	21,68	21,96	21,53	21,70	21,52
Cr_2O_3	0,05	0,04	0,08	0,07	0,02	0,05	0,03	0,03	0,07	0,07	0,05	0,08
FeO	27,35	26,94	26,81	27,31	26,50	27,25	26,69	26,93	26,60	27,00	27,20	26,74
MnO	0,67	0,74	0,66	0,80	0,67	0,64	0,74	0,70	0,66	0,65	0,74	0,69
MgO	7,78	8,05	8,36	8,18	8,07	8,48	8,18	8,45	8,52	8,25	8,44	8,32
CaO	3,01	2,95	3,09	3,00	2,87	3,07	3,00	2,97	3,03	2,92	2,98	2,96
Na_2O												
K_2O												
Total	98,04	98,62	99,36	99,27	97,87	99,76	98,38	98,90	98,87	99,03	99,31	98,87
O=12												
Si	3,047	2,997	2,974	2,999	3,070	2,962	3,018	2,978	2,965	3,007	2,974	3,008
Ti	0,000	0,002	0,001	0,000	0,001	0,001	0,000	0,001	0,002	0,002	0,000	0,000
Al(IV)	0,000	0,003	0,026	0,001	0,000	0,038	0,000	0,022	0,035	0,000	0,026	0,000
Al(VI)	1,913	1,993	1,994	1,968	1,918	1,976	1,965	1,975	1,986	1,979	1,967	1,979
Cr	0,003	0,002	0,005	0,004	0,001	0,003	0,002	0,002	0,004	0,004	0,003	0,005
Fe(III)	0,032	0,002	0,000	0,025	0,009	0,018	0,013	0,020	0,006	0,007	0,026	0,007
Fe(II)	1,772	1,764	1,743	1,755	1,735	1,748	1,737	1,739	1,730	1,753	1,745	1,738
Mn	0,045	0,049	0,043	0,053	0,045	0,042	0,049	0,046	0,044	0,043	0,049	0,046
Mg	0,915	0,940	0,968	0,950	0,946	0,980	0,956	0,984	0,991	0,959	0,979	0,967
Ca	0,254	0,248	0,257	0,250	0,242	0,255	0,252	0,249	0,253	0,244	0,249	0,247
Total	7,982	8,001	8,012	8,005	7,966	8,022	7,993	8,015	8,017	7,997	8,018	7,997
Almandine	58,41	58,72	57,33	58,14	57,36	56,91	57,64	57,06	56,55	58,27	57,06	57,78
Andradite	1,65	0,09	0,00	1,23	0,45	0,92	0,66	1,02	0,33	0,38	1,34	0,35
Grossular	6,90	8,05	8,40	6,92	7,85	7,53	7,74	7,23	8,00	7,58	6,87	7,69
Pyrope	31,34	31,37	32,56	31,73	32,73	33,07	32,21	33,04	33,43	32,12	32,94	32,40
Spessartine	1,53	1,64	1,46	1,76	1,54	1,42	1,66	1,56	1,47	1,44	1,64	1,53
Uvarovite	0,16	0,12	0,25	0,22	0,06	0,16	0,09	0,09	0,22	0,22	0,16	0,25
X_{Mg}	0,33	0,34	0,35	0,34	0,35	0,35	0,35	0,36	0,36	0,35	0,35	0,35
X_{Ca}	0,09	0,08	0,09	0,08	0,08	0,08	0,08	0,08	0,08	0,08	0,08	0,08

	leucosome	leucosome	leucosome	leucosome	leucosome	leucosome	leucosome	leucosome	leucosome
Rock	**highAl meta**	**highAl meta**	**highAl meta**	**highAl meta**	**highAl meta**	**highAl meta**	**highAl meta**	**highAl meta**	**highAl meta**
SiO_2	38,11	38,35	37,91	38,61	38,22	37,84	38,30	37,29	38,07
TiO_2	0,00	0,00	0,01	0,01	0,03	0,00	0,00	0,02	0,02
Al_2O_3	21,79	21,56	22,11	21,61	22,01	22,05	22,14	22,58	21,96
Cr_2O_3	0,05	0,06	0,05	0,09	0,06	0,00	0,09	0,01	0,03
FeO	27,50	27,66	27,08	26,23	27,47	27,55	27,10	27,89	28,07
MnO	0,65	0,69	0,71	0,67	0,64	0,66	0,72	0,66	0,61
MgO	8,55	8,39	8,62	8,50	8,47	8,56	8,74	9,52	9,12
CaO	3,01	3,07	3,03	3,04	2,90	2,93	2,18	1,31	1,28
Na_2O									
K_2O									
Total	99,66	99,78	99,52	98,76	99,80	99,59	99,27	99,28	99,16
O=12									
Si	2,959	2,976	2,945	3,009	2,962	2,942	2,973	2,903	2,965
Ti	0,000	0,000	0,001	0,001	0,002	0,000	0,000	0,001	0,001
Al(IV)	0,041	0,024	0,055	0,000	0,038	0,058	0,027	0,097	0,035
Al(VI)	1,956	1,951	1,971	1,985	1,974	1,965	2,000	1,976	1,982
Cr	0,003	0,004	0,003	0,006	0,004	0,000	0,006	0,001	0,002
Fe(III)	0,036	0,041	0,022	0,000	0,018	0,032	0,000	0,019	0,013
Fe(II)	1,749	1,754	1,737	1,710	1,762	1,760	1,767	1,796	1,815
Mn	0,043	0,045	0,047	0,044	0,042	0,043	0,047	0,044	0,040
Mg	0,990	0,970	0,998	0,987	0,979	0,992	1,011	1,105	1,059
Ca	0,250	0,255	0,252	0,254	0,241	0,244	0,181	0,109	0,107
Total	8,027	8,020	8,031	7,995	8,021	8,035	8,013	8,052	8,019
Almandine	56,65	57,29	55,95	56,95	57,42	56,50	58,29	56,68	59,33
Andradite	1,84	2,05	1,13	0,00	0,92	1,61	0,00	1,00	0,67
Grossular	6,46	6,34	7,28	8,22	7,03	6,69	5,82	2,73	2,84
Pyrope	33,44	32,61	33,90	33,07	33,04	33,72	34,02	38,06	35,71
Spessartine	1,44	1,52	1,59	1,48	1,42	1,48	1,59	1,50	1,36
Uvarovite	0,16	0,19	0,16	0,28	0,19	0,00	0,28	0,03	0,09
X_{Mg}	0,36	0,35	0,36	0,36	0,35	0,35	0,36	0,38	0,36
X_{Ca}	0,08	0,08	0,08	0,08	0,08	0,08	0,06	0,04	0,04